UNIVERSITAT DE BARCELONA

Climate variability predictions for the wind energy industry: a climate services perspective

Llorenç Lledó Ponsatí

PhD thesis

Climate variability predictions for the wind energy industry: a climate services perspective

Llorenç Lledó Ponsati

Supervisors:
Francisco Javier Doblas Reyes
Albert Soret Miravet

Universitat de Barcelona

Programa de doctorat en física

Climate variability predictions for the wind energy industry: a climate services perspective

Memòria presentada per optar al grau de doctor
per la Universitat de Barcelona.

Autor:	Llorenç Lledó Ponsati
Directors:	Francisco-Javier Doblas Reyes Albert Soret Miravet
Tutor:	Joan Bech Rustullet

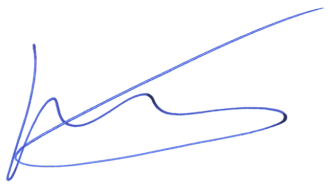

UNIVERSITAT DE BARCELONA

The research leading to this PhD thesis has been carried out at the Earth Sciences department of the Barcelona Supercomputing Center-Centro Nacional de Supercomputación (BSC-CNS).

Aknowledgments

The Barcelona Supercomputing Center-Centro Nacional de Supercomputación (BSC-CNS) has supported the development of this PhD thesis by providing invaluable technical, scientific, logistic and financial resources.

The research leading to these results has received funding from the EU H2020 and FP7 Framework Programmes under projects S2S4E (H2020 GA 776787) and EUPORIAS (FP7 GA 308291). The research leading to these results has been in part developed under the Copernicus Climate Change Service (C3S) Framework Agreement number C3S_441_Lot2_CEA (CLIM4ENERGY), a programme being implemented by the European Centre for Medium-Range Weather Forecasts (ECMWF) on behalf of the European Commission. The research leading to these results has received funding from the Ministerio de Ciencia, Innovación y Universidades as part of the RESILIENCE project (CGL2013-41055-R). The research leading to these results has received co-funding from the H2020 ERA-net ERA4CS (GA 690462) as part of the projects INDECIS and MEDSCOPE.

The writing of this thesis could not have been possible without the collaboration of many people. In the first place I want to thank the supervisors, Albert Soret and Francisco-Javier Doblas-Reyes for guiding the work and creating the necessary conditions for developing this research. To both I owe gratitude for their trust and exigency level. The Earth Sciences department of the BSC has been the breeding ground to carry out the investigations. Thanks to all members of the department that helped me during this time and made working in this place an enriching experience. The innumerable scientific discussions held within the Earth System Services group have been key to set goals, define methods, interpret results and overcome many difficulties. I want to thank Isadora Jiménez, Nube González-Reviriego, Nicola Cortesi, Marta Terrado, Andrea Manrique, Lluís Palma, Ilaria Vigo, Raül Marcos and very specially Verónica Torralba and Jaume Ramon for those fruitful interactions. I want to thank Kim Serradell and the Computational Earth Sciences group for providing technical assistance and specialized tools, and for setting up an efficient framework for collaborative work. Pierre-Antoine Bretonnière, Margarida Samsó and Julia Giner deserve a special mention for their assistance with the downloading and curation of datasets. I also want to thank Omar Bellprat, Irene Cionni, Louis-Philippe Caron, Dragana Bojović, Asun Lera St Clair, Rodrigo Manzanas and Daniel San Martín for their contributions to the publications that compose this work, as well as the constructive comments of all the anonymous reviewers that provided feedback to the published material.

This PhD has also benefited from many discussions held within the framework of research projects with scientists from other institutions such as IPSL, MeteoFrance, ENEA, University of Reading, ECMWF or SMHI, and with industrial partners from energy companies such as EDPR, EnBW, Nnergix, Iberdrola, EDF or E.ON among others. I want to thank Joan Bech for providing an easy link with the Universitat de Barcelona and Luciana Marques and Aina Ribera from the the BSC administration staff for receiving me with a smile every time I needed their assistance.

Last but not least, this thesis could not have been possible without the support of my family and friends. Marta, Xevi, Dídac, Tom and Anna, thanks for your company in the mountains during this four years, where all the everyday worries vanished. To my mother, brothers and extended family, thanks for being my role model and inspiring me perseverance and commitment during hard times. I want to mention specially three women that have been a guide to me: Eulàlia, Clara and Montserrat, thanks for your examples of life. To the GAC choir members for the fresh air of the

Sunday's rehersals. To my political family, Mar, Judith and Josep thanks for making me feel at home in Girona. To the Mosqueroles bunch for the lovely times. Anna, I cannot thank you enough in this lines. Thanks for your vitality, complicity and absolute support to carry out this work.

Contents

List of Figures

List of Tables

Acronyms

AEP Annual Energy Production.

AMV Atlantic Multidecadal Variability.

C3S Copernicus Climate Change Service.

CMIP Coupled Model Intercomparison Project.

CORDEX Coordinated Regional climate Downscaling Experiment.

CRPSS Continuous Ranked Probability Skill Score.

DCPP Decadal Climate Prediction Project.

EA East Atlantic.

EAWR East Atlantic/Western Russia.

ECMWF European Center for Medium-Range Weather Forecasts.

EDGAR Emission Database for Global Atmospheric Research.

ENSO El Niño/Southern Oscillation.

ESM Earth System Model.

GFCS Global Framework for Climate Services.

GHG Greenhouse Gas.

IOD Indian Ocean Dipole.

IRENA International Renewable Energy Agency.

JRC Joint Research Center of the European Commission.

MJO Madden-Julian Oscillation.

NAO North Atlantic Oscillation.

NPM North Pacific Mode.

NREL National Renewable Energy Laboratory.

NWP Numerical Weather Prediction.

O&M Operations and Maintenance.

PDO Pacific Decadal Oscillation.

QBO Quasi-Biennial Oscillation.

RPSS Ranked Probability Skill Score.

S2S Sub-seasonal to Seasonal.

S2S2D Sub-seasonal to Seasonal to Decadal.

SCA Scandinavian Pattern.

SST Sea Surface Temperature.

TSO Transmission System Operator.

WCRP World Climate Research Program.

WMO World Meteorological Organization.

WRA Wind Resource Assessment.

Abstract

In order to mitigate the climate change effects, the world is undergoing an energy transition from polluting sources towards renewable energies. This transition is turning the electricity system more dependent on atmospheric conditions and more prone to suffer the effects of climate variability. The atmospheric circulation is changing in certain aspects due to increasing concentrations of greenhouse gases in the atmosphere, but it also varies from year to year due to natural variability processes occurring in the Earth system at timescales of weeks, months and years. The atmosphere interacts with other components of the Earth System —such as the ocean, the cryosphere or the continental surface— that evolve more slowly than the atmosphere and drive the low-frequency variability. The natural climate oscillations that occur at those timescales impact wind speed and wind power generation. Therefore a better knowledge of how the wind resource varies at sub-seasonal, seasonal and decadal time scales is key to understand the risks that the electricity system is facing.

Anticipating this variability would also be helpful to many stakeholders in the energy sector to take precautionary actions. Forecasts at sub-seasonal, seasonal and decadal timescales are starting to be possible recently thanks to advances in climate modelling capabilities. Because climate variability is partly driven by coupled physical processes occurring in the Earth, numerical models that represent the interaction between different components of the Earth system can be employed to produce forecasts at these scales. The science of climate prediction deals with the challenge of producing predictions beyond meteorological timescales (i.e. weeks, months and years ahead) although not reaching the centennial timescales, which are studied with scenario-based climate projections. Climate predictions employ the current state of the atmosphere, the ocean, the cryosphere, and the land surface to produce numerical integrations of each component and the forcings and interactions between them to model the evolution of the Earth system as a whole.

However, the usage of climate predictions in the wind power sector —or more generally in any specific decision-making context— poses a series of difficulties due to many complex aspects of this type of predictions. The efforts devoted in many initiatives to bring the needs of the users to the center of the discussion have given rise to the field of climate services. In order to assist decision-making, it is not only desirable to have the best predictions available but also to tailor them to the specific needs of each user. To achieve this goal, a dialogue with stakeholders needs to be established, and a trans-disciplinary approach needs to be set up to take advantage of the developments in many research fields regarding knowledge transfer and communication.

The work presented in this dissertation advances the knowledge required to produce and successfully apply climate predictions to decision-making in the wind power sector and deals with the three aforementioned challenges: a) understanding the impact of climate oscillations at sub-seasonal and seasonal timescales on wind resource; b) developing methods to produce

forecasts of wind speed and wind power generation at this scales; and c) facilitating the uptake of those predictions by means of a climate-services-based approach.

Resum

Per tal de mitigar els efectes del canvi climàtic, tots els països del món estan duent a terme una transició energètica de fonts contaminants cap a energies renovables. Aquesta transició està incrementant la sensibilitat del sistema elèctric a les condicions atmosfèriques i fent-lo més vulnerable als efectes de la variabilitat climàtica. La circulació atmosfèrica està canviant en certs aspectes com a conseqüència de l'increment dels gasos d'efecte hivernacle a l'atmosfera, però una part important de les variacions que es registren entre anys consecutius es deuen a processos de variabilitat naturals que tenen lloc al sistema Terra a escales de setmanes, mesos i anys. L'atmosfera interacciona amb altres components del sistema Terra — com l'oceà, la criosfera o la superfície continental— que evolucionen més lentament que l'atmosfera i que en condicionen la seva variabilitat a baixa freqüència. Les oscil·lacions naturals que tenen lloc a aquestes escales temporals impacten el vent i la generació d'energia eòlica. Per tant és indispensable tenir un millor coneixement de com varia el recurs eòlic a escales sub-estacionals, estacionals i decadals per tal d'anticipar els riscs a què el sistema elèctric està sotmès.

Anticipar aquesta variabilitat seria de gran utilitat a diversos actors del sistema energètic per tal de prendre mesures de prevenció. Gràcies a múltiples avenços en les capacitats de modelització climàtica, les prediccions sub-estacionals, estacionals i decadals comencen a ser possibles avui en dia. El fet que la variabilitat climàtica estigui condicionada per processos físics acoblats que tenen lloc al nostre planeta possibilita l'ús de models numèrics que representen les interaccions entre les diferents components del sistema Terra a aquestes escales de temps. La disciplina científica de la predicció climàtica aborda el repte de produir pronòstics més enllà de l'escala meteorològica (és a dir, a setmanes, mesos i anys vista) però sense arribar a les escales centenals que s'estudien mitjançant projeccions basades en escenaris d'emissions. Les prediccions climàtiques es valen de l'estat actual de l'atmosfera, l'oceà, la criosfera i el subsòl per produir integracions numèriques de cadascuna de les components del sistema i representar les seves interaccions per tal de modelar l'evolució del sistema Terra en el seu conjunt.

Malgrat aquests avenços, l'ús de les prediccions climàtiques en el sector de l'energia eòlica —i en general en qualsevol context de presa de decisions— presenta una sèrie de dificultats degut a les complexitats d'aquest tipus de previsions. De l'esforç de diverses iniciatives de posar les necessitats dels usuaris al centre de la discussió n'ha sorgit la disciplina dels serveis climàtics. Per tal d'assistir la presa de decisions, no només és necessari disposar de les millors prediccions possibles sinó que cal també ajustar-les a les necessitats específiques de cada ús. Aquest objectiu només es pot assolir amb un diàleg constant i transdisciplinari entre els científics i les parts interessades que integri els avenços en diferents àmbits respecte la transferència de coneixement i la comunicació.

El material presentat en aquesta tesi avança el coneixement necessari per tal de produir i

aplicar prediccions climàtiques a la presa de decisions per part de la indústria eòlica, abordant tres reptes: a) avaluar l'impacte d'oscil·lacions climàtiques sub-estacionals i estacional en el recurs eòlic; b) desenvolupar mètodes per produir prediccions de vent o de generació eòlica a aquestes escales; i c) facilitar l'adopció d'aquestes previsions mitjançant una aproximació basada en els serveis climàtics.

Chapter 1

Introduction

1.1 Climate and energy

1.1.1 The bi-directional links between climate and energy

The energy sector is the biggest contributor to Greenhouse Gas (GHG) emissions worldwide (see figure 1.1) (Crippa et al., 2019), which are responsible for the climate change our planet is currently experiencing (Intergovernmental Panel on Climate Change, 2014). In order to try to limit the magnitude and the effects of this climate change, the majority of the World's countries have signed international treaties such as the Kyoto protocol (1997) and the Paris agreement (2015). In order to comply with those legal obligations, many countries and international institutions are embracing a gradual phase out of polluting sources (coal, oil, gas, but also nuclear power in many cases) and a transition towards renewable energy sources like wind, solar and hydro power. For instance, European institutions are putting in place a new climate strategy known as the new European green deal (European Commission, 2019), which aims at becoming climate neutral by 2050 and reducing GHG emissions to at least a 50% of 1990 levels in 2030.

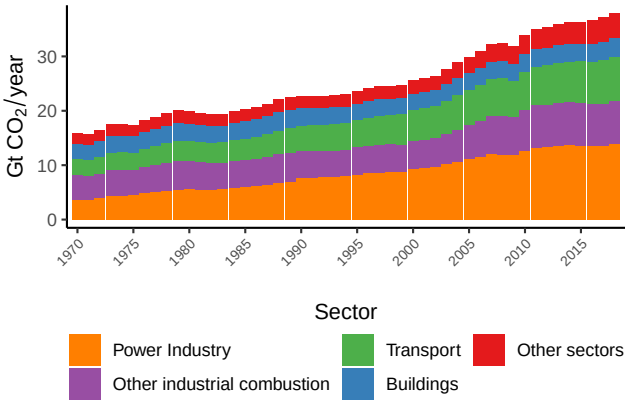

Figure 1.1: Fossil CO_2 emissions by sector and year. Data source: JRC EDGAR.

These goals can only be achieved through a decarbonisation of the energy sector and a massive penetration of renewable energies. Among those, solar and wind energy are the sources that are experiencing the biggest growth worldwide (figure 1.2). However, in most renewable energy conversion systems like wind or solar the fuel cannot be directly controlled nor stored for later usage. The power output from these plants depends almost exclusively on meteorological factors such as wind or irradiation, and is thus intermittent and non-dispatchable (i.e. cannot be turned on and off at discretion of the plant operator). With higher integration of renewables in the electricity mix, the energy system becomes more dependent on atmospheric conditions (Bloomfield et al., 2016; De Felice et al., 2020). Therefore, understanding atmospheric variability becomes crucial to many actors in the energy sector: from ensuring a secure power supply to anticipating energy sales or operating power plants.

Indeed, both energy demand and supply are affected by atmospheric conditions at several time scales, from small-scale turbulence through meteorological phenomena, seasonal anomalies and up to climate change impacts (Dubus et al., 2018). Wind power generation relies heavily on wind speed conditions. Solar power generation has solar angle as its most important factor, but cloudiness, humidity and air turbidity have also a strong

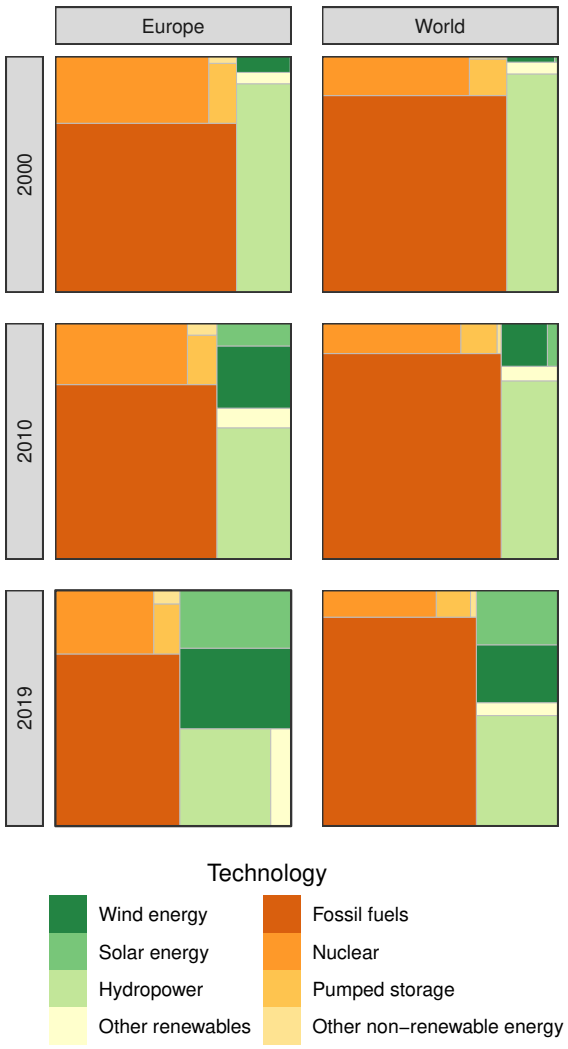

Figure 1.2: Installed capacity of renewable and non-renewable energy sources in Europe and the world in 2000, 2010 and 2019, expressed as a percentage of the total installed capacity. Data source: IRENA.

impact in modulating surface solar radiation. Hydropower generation relies on the availability of water in the dams, which depends largely on precipitation and snow melt in the preceding days. On the other side, energy demand is sensitive to temperature variations in many countries that use electricity for cooling or heating (Valor et al., 2001; Bessec and Fouquau, 2008). To a much lesser extent, non-renewable energy is also impacted by atmospheric phenomena. Extreme events can pose risks to conventional generation sources and electricity transport. For instance, high temperatures can be a limiting factor for power plants that use river water as cooling due to environmental constraints (van Vliet et al., 2016); low water levels in some European rivers can affect navigability and disrupt the supply chain of fuel (Jonkeren et al., 2013); or freezing rain can damage power lines (Makkonen, 1998).

1.1.2 Usage of weather and climate information in the wind energy industry

The development of large-scale wind energy during the last 40 years (Kaldellis and Zafirakis, 2011) has entailed an increasing interest —and a considerable amount of invested resources— in better understanding and characterizing wind speed conditions near the surface, where wind turbines are installed.

Thanks to the efforts devoted to improve mesoscale modelling and statistical model output correction techniques, nowadays weather forecasts of wind speed up to 10 days ahead are routinely used in every operational wind farm of the world in order to sell energy in the daily markets with some anticipation or to schedule maintenance tasks, for instance (Giebel and Kariniotakis, 2017).

Another aspect that was crucial since the beginning for the deployment of wind power was selecting the best locations and the most suitable turbine designs in order to maximize return over investment. That gave rise to the field of Wind Resource Assessment (WRA), which studies the climate of wind speed conditions at heights between 30 and 200 m above ground, where the hubs and blades of the turbines are installed (Brower, 2012). Although the goal of WRA is to anticipate the wind speed conditions and the total electricity generation during the lifetime of a wind farm, all state-of-the-art resource assessment studies actually investigate the wind speed conditions in the past 20 to 30 years and assume that future conditions will be similar to past conditions.

WRA studies are typically made by combining short records of on-site observations close to hub heights with longer records from reanalysis

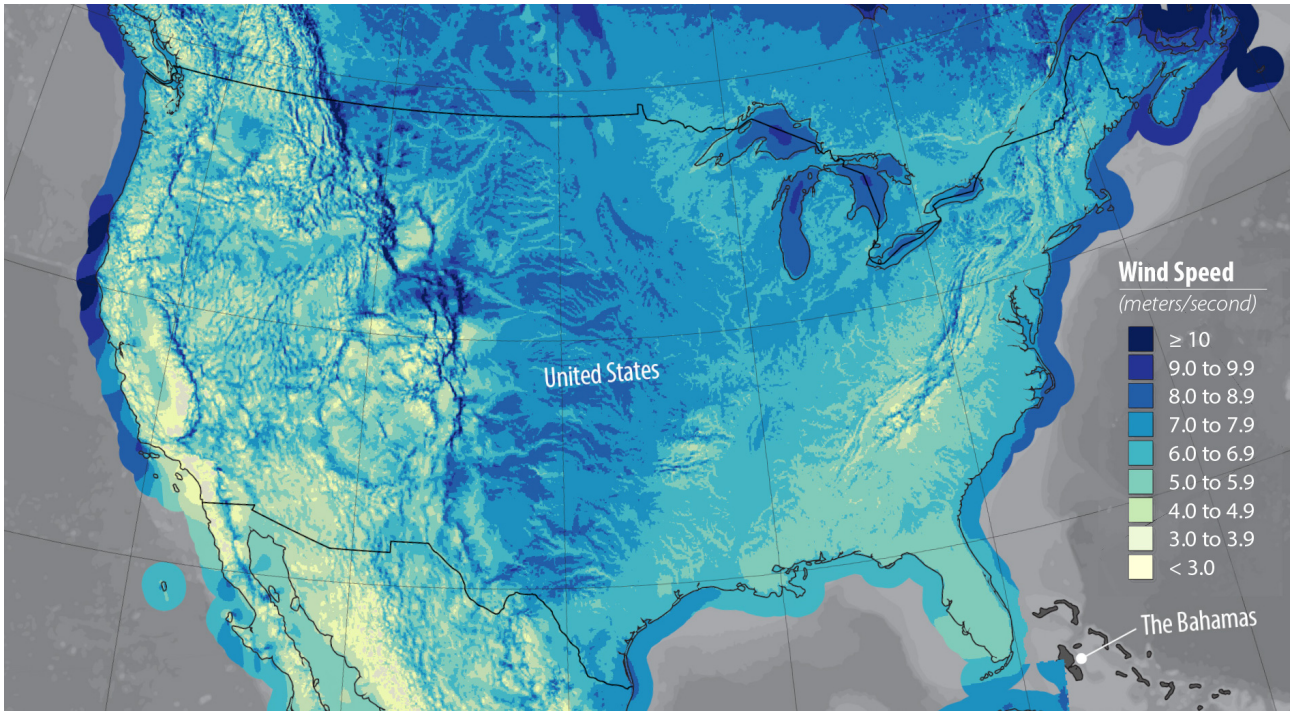

Figure 1.3: Mean wind speed conditions 100m above ground in the US during 2012, estimated from a global reanalysis that has been downscaled with a mesoscale model to a resolution of 2 km. Source: NREL (Draxl et al., 2015).

datasets which are downscaled to the local scale of the wind farm (see figure 1.3). WRA studies investigate not only climatological mean wind speed estimates but also the whole distribution of wind speed values, that is used to derive Annual Energy Production (AEP) estimates. Analyzing the annual cycle is also important in order to understand how wind generation and revenues will be spread across the year and produce monthly budgets. Another key concept in WRA studies is the interannual variability of the resource (i.e. the standard deviation of annual mean wind speed across several years). The higher this value is the more risk exists that for one particular year the AEP is low (Brower et al., 2013).

Boundary layer meteorology and fluid dynamics have also received the impulse of wind energy research (Peña et al., 2015). Understanding turbulence, vertical wind shear, wakes or maximum wind gusts that can be expected in a wind turbine are key elements to anticipate electricity losses or structural loads and fulfill safety design criteria during pre-construction stages. The ice accretion is another atmospheric phenomena that causes energy losses in cold climates, and has also been further investigated in the last years (Makkonen et al., 2001; Yirtici et al., 2016; Son and Kim, 2020).

Another topic that has received the attention of wind farm owners is that of monthly, seasonal or annual wind speed anomalies, which drive the revenues of their assets. Reanalysis datasets are again employed in forensic (ex-post) studies to understand the recent performance of operating plants compared to that expected in the climatology-based budgets (see figure 1.4). This helps understanding good and bad periods for the business. In order to understand the drivers of those anomalies, sometimes they are accompanied by descriptions of the global atmospheric circulation such as the strength of teleconnection indices or the occurrence of specific weather regimes. However, scientific analyses of specific events that affected wind energy production are scarce.

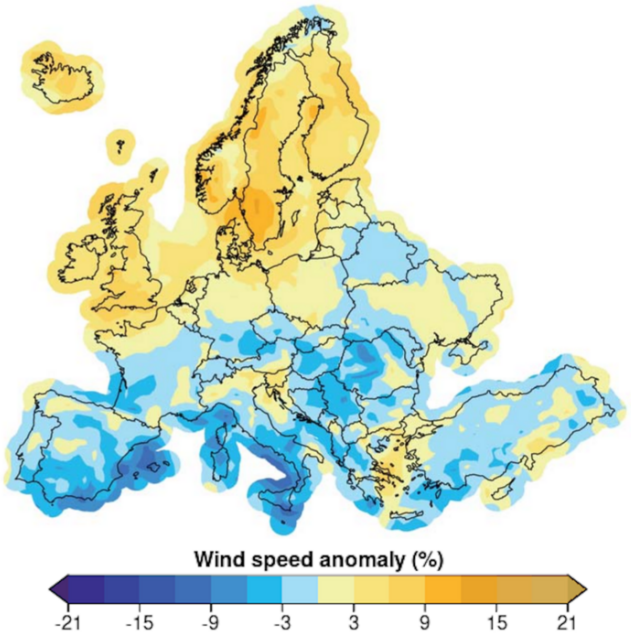

Figure 1.4: Percentual wind speed anomalies at 100 m above ground in Europe during 2015 with respect to the 1988–2014 average, obtained from a combination of CFSR, MERRA and ERA-Interim reanalyses. Source: AWS Truepower Wind Trends bulletin.

1.1.3 Going beyond state-of-the-art: potential uses of climate predictions in the wind energy sector

Observed climate conditions in the recent past from reanalysis datasets and meteorological forecasts up to 10 days ahead from numerical weather prediction models are trusted and routinely employed by the energy industry to optimize the extraction of the kinetic energy contained in the wind. The latest advances in climate modelling are starting to make forecasts at longer timescales available.

Under the current context of climate change, atmospheric circulation patterns are changing and will continue to change in the coming decades. Therefore wind speed conditions for the future 20 or 30 years will not necessarily resemble climatologies of the previous 30 years. Future climate projections from climate models that employ different GHG emission scenarios (e.g. simulations from CMIP and CORDEX experiments) have been available for a long time now. While the impact of GHG-induced climate change has been especially studied in terms of temperature and precipitation changes at the middle and end of the 21st century, the impact of climate change on wind resource has received much less attention so far (Tobin et al., 2016; Gonzalez et al., 2019). Those future climate projections have many uncertainties and shortcomings, but they provide useful information that has not been assimilated by the industry yet. Most wind resource assessment studies only incorporate this information as an additional risk or uncertainty, at most (Ebinger, 2011).

On top of long-term climate change, the conditions for a particular week, month, season or year might differ substantially from mean climate conditions for that period (see figure 1.5). This climate variability at timescales between weather and long-term climate change affects the wind industry in many ways and can now be partially anticipated thanks to recent advances in climate prediction (Merryfield et al., 2020).

There are several situations in which forecasts of future wind speed or wind power generation more than 15 days ahead would benefit many stakeholders in the wind energy sector (see table 1.1) (Buontempo, 2018). For instance, Operations and Maintenance (O&M) teams —which cannot perform their activities during strong winds for safety reasons and also to avoid generation losses as far as possible— need to plan their maintenance activities weeks ahead. Similarly, wind farm owners need to anticipate monthly total generation and revenues of their assets. This can help them minimize problems with shortage of cash flow or put in place hedging strategies. The energy trading business makes money from anticipating electricity prices at different time scales. While intra-daily and day-ahead markets are very well informed by Numerical Weather Prediction (NWP) services, trading operations at weekly, monthly or seasonal scales are also impacted by atmospheric variability among other factors. Transmission System Operator (TSO) need to constantly guarantee a balance between electricity supply and demand. Having estimates of renewable generation weeks and months ahead can help to schedule alternative power supply sources. At even longer time scales,

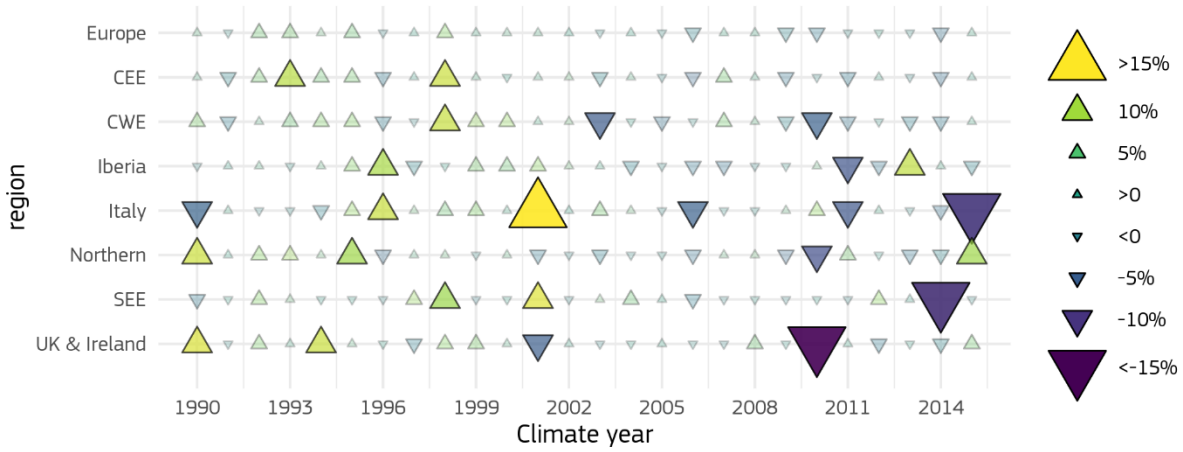

Figure 1.5: Year-to-year variations of wind speed conditions in several regions of Europe. CEE stands for Central Eastern Europe, CWE for Central Western Europe and SEE for South Eastern Europe. Source: De Felice et al. (2020). See figure 2 therein for the region definitions.

developers of new wind farm projects have to estimate future wind resource during the lifetime of the wind farm (20 or 30 years), and policy makers have to plan the installation of new capacity and electricity mix of different energy sources.

1.2 Wind speed variability at sub-seasonal, seasonal and decadal time scales

1.2.1 The scales of atmospheric variability

The atmospheric circulation varies naturally at different time scales, and near-surface wind speeds, which are driven by surface pressure gradients, necessarily reflect those circulation changes. The physical processes that shape the atmospheric state are typically classified according to its scales of motion into microscale processes (e.g. turbulence and boundary layer thermals), mesocale processes (e.g land-sea breezes, mountain-valley flows or cloud phenomena), synoptic scale processes (movement of high and low pressure areas or tropical cyclones) and planetary scale motions (e.g. the position and strength of the the polar and subtropical jets, the Hadley, Ferrel and polar cells or the intertropical convergence zone).

This classification is however bounded spatially at 40 000 km (the Earth's circumference), while the time dimension is not bounded. Therefore, for studying low-frequency variability (i.e all variations that occur at timescales longer than 15 days) a classification that relies only on time scales is more suitable and commonly employed. All the processes that occur on a timescale of 2 to 6 weeks are classified as sub-seasonal processes, those that occur between 1 and 12 months are referred to as seasonal and processes that span between 1 and 10 years as decadal.

Centennial or millennial timescales cover even longer period processes. At this long climate scales variations are known to be caused both by human factors such as GHG emissions or land use changes and by natural processes such as volcanic activity or astronomic variations in the Earth's orbit.

1.2.2 The atmosphere within the Earth system

Atmospheric variations at Sub-seasonal to Seasonal to Decadal (S2S2D) scales are not just the outcome of random concatenation of different weather events, but they are often driven by phys-

Table 1.1: Details of the needs of different user profiles regarding forecasts of wind and wind power generation.

User profile	Forecast use cases	Variables of interest	Time horizon	Spatial scale
O&M manager	(i) operate under safety conditions and (ii) minimize production losses	wind speed, wind power generation	days, weeks and months ahead	site level
Wind farm owner	(iii) anticipate monthly or annual revenues	wind power generation	months and years ahead	site or portfolio level
Energy trader	(iv) anticipate electricity prices	renewable generation, electricity demand, electricity prices	hours, days, weeks and months ahead	country level
TSO	(v) guarantee balance between supply and demand and (vi) schedule alternative power sources	renewable generation, electricity demand	hours, days, weeks and months ahead	country or region level
Project developer	(vii) estimate annual energy production and its variability	wind speed and wind power generation	years and decades ahead	site level
Policy maker	(viii) plan future electricity mix	wind power generation, renewable generation, electricity demand	years and decades ahead	country level

ical processes that occur on the Earth at slower timescales than meteorological phenomena. The Earth system is a complex system composed of many components that interact between them. At S2S2D timescales, the ocean circulation, the sea ice extent, the snow cover or the soil moisture interact bi-directionally with the atmosphere. Those components evolve much more slowly than the atmosphere, and modify (or force) it at those time scales (see figure 1.6). For instance, soil moisture conditions or snow cover do not change from one day to another as weather conditions do, and it takes a few weeks or months to substantially modify sea surface temperatures or the polar sea ice extent.

The chaotic nature of the atmosphere does not allow to anticipate its exact evolution more than 10 or 15 days ahead, i.e. when integrating the equations of motion of the atmosphere, even small uncertainties in the knowledge of the current state of the atmosphere (also known as initial conditions) will grow dramatically with time and make any forecast totally uncertain after a few days. However, the low-frequency variations that the other components of the Earth system impart to it (known as boundary condition forcings) can be obtained by studying longer-period averages and filtering out all the weather-related variability. In this sense, different types of atmospheric predictability can be obtained from initial conditions than from boundary conditions (Meehl et al., 2009).

For example, the Arctic sea ice extent has declined dramatically in the past decade, reaching minimum values never witnessed in our recent records. This has profound implications for the radiative energy budget of the planet: with less sea ice, the solar radiation that was previously reflected to the space and lost is now being absorbed by the oceans and modifies (forces) the global atmospheric circulation and the position of the storm tracks. Indeed some anomalous sea ice extent episodes have already been associated to atmospheric extreme events (Navarro et al., 2019). Similarly, anomalies in soil moisture availability can exacerbate droughts (Prodhomme et al., 2015), while changes in Sea surface Temperature can modify convection in the tropics and modify the whole global atmospheric circulation (Stan et al., 2017; Liu and Alexander, 2007).

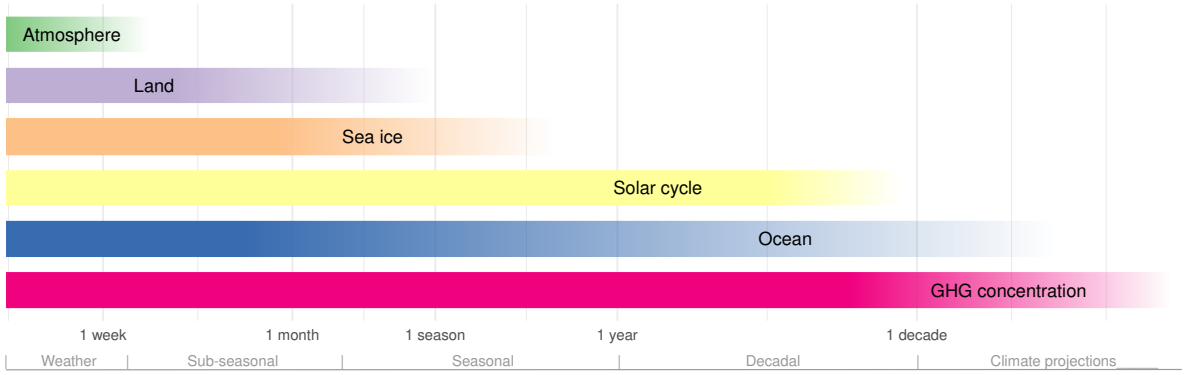

Figure 1.6: Predictability of the different components of the Earth System that force the atmosphere at longer timescales.

1.2.3 The impact of climate phenomena on wind power generation at S2S2D scales

It is not only the slower evolution of these components, but also the occurrence of coupled physical processes and teleconnective mechanisms that allows to better understand the forcings that those components exert on the atmosphere. This is, variability at S2S2D timescales follows some recurrent patterns known as natural modes of variability or climate oscillations. For instance, at sub-seasonal timescales (i.e. few weeks ahead), the Madden-Julian Oscillation (MJO) is a coupled sea surface temperature/convection/wind propagating wave that circulates along the equator and completes a lap to the Earth in around 40 days. At seasonal timescales El Niño/Southern Oscillation (ENSO) is the most important source of variability and represents a change in the Walker cell circulation coupled to oceanic processes. In Europe, the North Atlantic Oscillation (NAO) shapes the circulation of storm tracks at seasonal timescales, although other teleconnection indices such as the East Atlantic (EA) or the Scandinavian Pattern (SCA) are also relevant. At decadal timescales the Atlantic Multidecadal Variability (AMV) and Pacific Decadal Oscillation (PDO) reflect very slow changes in the ocean temperature in the Pacific and Atlantic oceans related to the thermohaline circulation. The stratosphere, although being part of the atmosphere, also displays some structured low-frequency variability that influences the troposphere at S2S2D scales, such as the strength of the polar vortex or the Quasi-Biennial Oscillation (QBO). For its simplicity, the QBO has been illustrated in figure 1.7 as an example of a climate oscillation.

Although the aforementioned climate oscillations take place in specific regions of the globe (e.g. the equator or the poles), its effects can reach very distant places and impact many different surface parameters, hence the name of teleconnections. In some regions and periods of the year those climate oscillations or natural modes of variability can have a detectable impact on near-surface wind conditions when overlapped with higher-frequency weather variability. This is possible only if the amount of low-frequency variability is of a comparable magnitude to the high-frequency atmospheric variability. This is usually studied in terms of signal-to-noise ratios where the climate forcing signals are compared to the weather-scale variability.

The impact of many teleconnections on surface conditions has been studied for temperature and precipitation in the scientific literature, but not much has been done for near-surface wind speed yet (see Brayshaw et al. (2011) for an example). One way to study the impact that natural climate oscillations have on wind speed and wind power generation is analyzing historical records. Estimates of near-surface wind speed (Ramon et al., 2019) and wind power generation (González-Aparicio et al., 2017) in the last decades

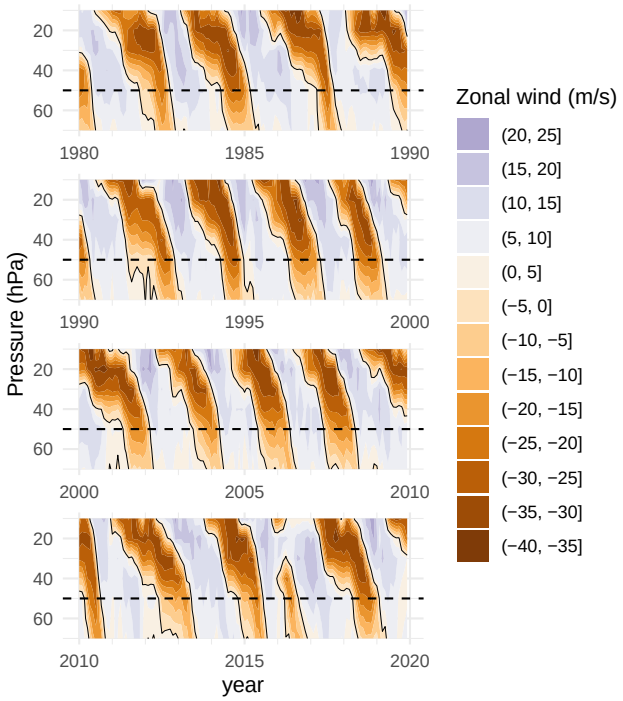

Figure 1.7: Illustration of the Quasi-Biennial Oscillation: the monthly-mean evolution of the zonal wind speed in a cross-section of the equatorial stratosphere shows that at 50 hPa the wind oscillates from westerly to easterly approximately every 13 months and completes a whole cycle every two years approximately. Data source: Freie Universität Berlin.

can be obtained from multiple reanalysis datasets. Similarly, teleconnection indices that represent the phase and intensity of the climate oscillations can be obtained directly from observational records or from reanalyses. Techniques such as linear correlation or stratifications (also known as composite maps) allow to analyze the impact that a climate oscillation or teleconnection index has on the mean wind speed. Identifying key variability drivers in each region of the world is the first step towards understanding how low-frequency atmospheric variability can affect wind power generation at S2S2D scales. Unveiling the role of specific climate oscillations in shaping particular events that disrupted the business-as-usual procedures is also a powerful way to highlight the importance of climate variability and the need to better understand the climate system (Lledó et al., 2018).

1.3 Climate prediction

1.3.1 Sources of predictability and coupled Earth System Models

Climate oscillations, feedbacks and teleconnections act as sources of predictability of the Earth system at S2S2D scales. Atmospheric variability at these scales is driven by physical processes occurring in the whole Earth system, and this brings the possibility of forecasting it. Climate prediction deals with the challenge of providing operational forecasts at these horizon ranges (e.g. see Kumar et al. (2020)). Those forecasts are often referred to as initialized climate predictions, because they use the same climate models employed for long-term climate projections, but they are initialised with the current state of the atmosphere/ocean/land/ice conditions. Climate predictions are in turn subdivided into sub-seasonal (Mariotti et al., 2018), seasonal (Doblas-Reyes et al., 2013) and decadal predictions (Kirtman and Power, 2013; Smith et al., 2019) according to the length of the simulation (see the time axis in figure 1.6).

Climate prediction systems employ an Earth System Model (ESM) to represent physical phenomena in the atmosphere, the ocean, the land surface and the sea ice. Indeed an ESM consists of separate numerical models for each of the components, which are then coupled together to simulate interactions between them (i.e. there is an exchange of information at regular time intervals that transfers forcings of any kind between the different components). As said before, correctly representing climate oscillations and coupled phenomena in climate predictions is a key element to ensure predictability. However, representing teleconnection pathways correctly is also necessary in order to obtain skillful predictions of wind speed or other surface variables far from the places where the physical process take place.

Thanks to sustained advances in the field of climate modeling, nowadays many national meteorological centers, international institutions and research centers produce climate predictions regularly. For instance, the World Climate Research Program (WCRP) Sub-seasonal to

Seasonal (S2S) prediction project provides access to 11 diferent subseasonal prediction systems; the Copernicus Climate Change Service (C3S) gathers seasonal predictions from 6 different centers (`https://climate.copernicus.eu/seasonal-forecasts`); and the WCRP Decadal Climate Prediction Project (DCPP) coordinates the production of decadal predictions to contribute to the 6^{th} phase of the Coupled Model Intercomparison Project (CMIP) (Boer et al., 2016).

1.3.2 The need for ensemble prediction

The climate system as a whole is a dynamical system with a chaotic behaviour. This means that even if an ESM was able to model the Earth system processes perfectly, slightly different initial conditions would produce totally different trajectories after some integration time, i.e. the slightest uncertainty in the initial conditions will propagate in time producing very different results. Climate prediction systems deal with this challenge employing an ensemble of predictions. Several integrations are produced from slightly different but equally plausible initial conditions. Some prediction systems also employ slight variations of model parameters. Then the results for each of the ensemble members (or realizations) will follow different trajectories. In the hypothetical case of a perfect model and an infinite sample of realizations, the actual trajectory of the Earth System after some integration time would resemble only one of the realizations (that one with the *right* initial conditions). As the *right* initial conditions are not known a priori, it does not seem very useful to have one correct prediction and many other wrong. However, as the slowly-varying components of the Earth System can still be predicted to a certain degree from its initial conditions, the forcings that those impart to the atmosphere will be similar in all the realizations. Although all the trajectories might be different regarding the atmospheric state (and indeed none of them actually matches the observed trajectory due to the limited number of ensemble members), when looking at the other Earth system components all the trajectories are closer. Therefore all the atmospheric trajectories receive a similar forcing from the slowly-varying and predictable components. This offers the opportunity to compare the distribution of values to a climatological distribution for the same period and analyze deviations from it. To obtain the forcing results the values have to be averaged to the time scale of the forcing signal.

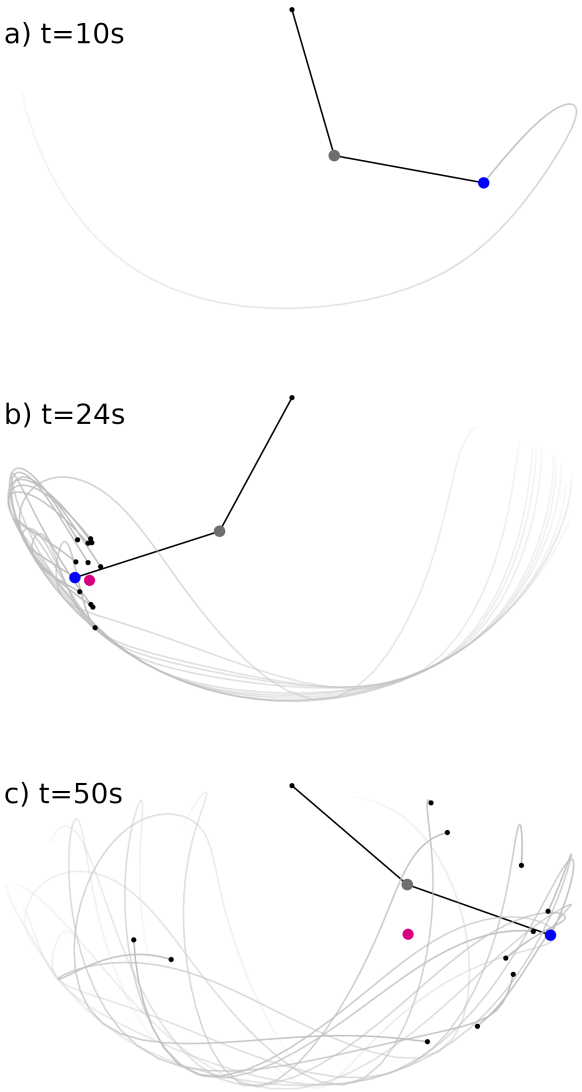

Figure 1.8: A double pendulum displaying chaotic behaviour, at three different integration times of the equations that describe its dynamics. An ensemble simulation is performed with 11 members (black dots) initialized with a slightly different initial position. The magenta dot represents the ensemble mean, and the grey lines depict the recent trajectories of the ensemble members and the actual pendulum.

The strategy to obtain information from an en-

semble of predictions has been exemplified in figure 1.8 with a simpler chaotic system (Richter and Scholz, 1984). A double pendulum consists of one mass attached with a wire to a fixed point, and a second mass attached with another wire to the first mass. From an initial position (initial conditions) the pendulum is let free to oscillate. The equations that describe the movement of the two masses is perfectly known, but as the Earth, this system displays a chaotic behaviour, and a slight error in measuring the initial conditions derives in large errors after some time. An ensemble of slightly different initial conditions (black dots) have been employed to understand how the different members behave after some time. At the beginning of the simulation (panel a, $t = 10\,\mathrm{s}$) all the members match the actual pendulum (blue dot, which is hiding all the black dots). After some more time (panel b, $t = 24\,\mathrm{s}$) the different members start to diverge, but they are still close to the blue point. The ensemble mean (magenta dot) is a good representative of any ensemble member. At time $t = 50\,\mathrm{s}$ (panel c) the ensemble members have diverged significantly. While some members are still close to the actual value (blue dot) many others are far away. The ensemble mean (magenta dot) is not a good representative of the ensemble members anymore. However, we can use the distribution of the ensemble members to produce some probabilistic forecasts. In this case, only two members lie to the left of the fixed point, while 9 are on the right side, i.e. there is more probability of being on the right than on the left side. Although in this simplified example there are no boundary conditions, we could imagine that a similar situation to panel c could occur when there is an external forcing to the system, for instance if an horizontal force is pushing softly the pendulum masses to the right.

1.3.3 Bias adjustment

Climate models represent physical processes in the Earth system in a simplified way, and therefore are affected by systematic errors. Firstly the dynamics of the atmosphere or the ocean are computed over a discrete three-dimensional mesh and integrated over a discrete time step. For instance, current configurations employed operationally to produce seasonal predictions employ grids of around 30 km of resolution at most. Although current short-term atmosphere-only predictions can be run at much higher resolutions, the long integration times and the coupling of climate simulations require massive amounts of computing time, which is limited for operational tasks. Secondly, even at high resolution, many energy exchanges within the system need to be parametrized employing empirical relations. Therefore, all the predictions from climate models have biases due to the relatively coarse scale of its grid, the approximate integration of the dynamical equations and the simplifications in the parametrizations. For example, figure 1.9 shows the biases in sea ice concentration in the European Center for Medium-Range Weather Forecasts (ECMWF) SEAS5 seasonal prediction system in summer and autumn for the predictions made one month in advance.

Even if these biases can sometimes be of substantial magnitude, the power of climate predictions lies in the ability to detect anomalies caused by climate forcings. For any practical application of climate predictions it is essential to understand the biases and adjust the predictions to remove those biases as much as possible. To this end, all climate predictions need to be accompanied with a hindcast, i.e. a set of retrospective forecasts made with the same configuration as the real-time forecasts but for which corresponding observations are already available. From this hindcast, biases can be computed and subtracted from predictions to obtain more accurate values. Not only biases in the mean value are corrected but also differences in variability and ensemble spread can be corrected. Also, it is important to consider different corrections for each season or month of the year, and for each lead time. There are many methods available in the literature (Torralba et al., 2017; Manzanas et al., 2019), although due the short sample sizes that are typically available in the hindcasts it is advisable to employ simple methods. Bias adjustment is of special importance if those predictions are used in impact models that rely on the absolute values of the predictions, as is the case of wind power generation.

1.3.4 Forecast quality assessment

Any forecast is useless without a previous estimate of its quality. Aside of bias adjustment, hindcasts

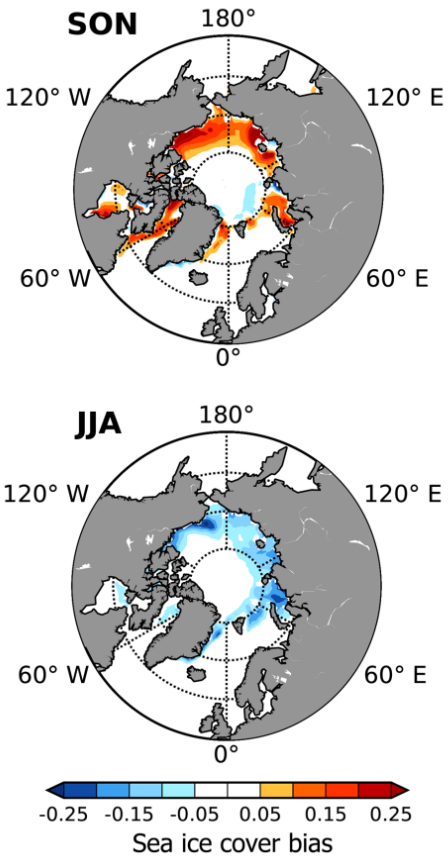

Figure 1.9: Sea ice concentration biases of the ECMWF SEAS5 seasonal predictions issued one month in advance for summer and autumn in the Arctic region according to OSI-450 observations. In summer there is a general lack of melting, while in autumn the refreezing is too slow. Adapted from Johnson et al. (2019).

are also essential to quantify the quality of climate predictions. As with bias adjustment, it is customary in the climate prediction arena to measure performance separately for each month or season and for each lead time. There exist many verification metrics, and each one is suitable to verify different aspects of the predictions (Jolliffe and Stephenson, 2011; Mason, 2018). Ensemble mean correlation is one of the most used verification metrics in climate prediction. It measures linear association between observations and the ensemble mean of the forecasts. It is a simple metric and is easily understandable. However it overlooks many important aspects of the predictions, such as its reliability. The reliability of a probabilistic prediction indicates how accurate the issued probabilities are with respect to the observed frequencies of occurrence. The probabilistic nature of climate predictions requires specific verification metrics. For instance the Continuous Ranked Probability Skill Score (CRPSS) assesses the quality of the distribution of an ensemble of members, whereas the Ranked Probability Skill Score (RPSS) measures the quality of probabilities for ordered categories.

1.3.5 Attribution experiments

Aside of producing operational climate predictions, another powerful usage of ESMs is the ability to conduct idealized experiments to investigate specific physical processes or the contribution of individual components of the Earth system on the onset of anomalous episodes (Barnston et al., 2005). For instance, attribution of extreme events to climate change is one of the most typical examples. Knowing if the occurrence of an extreme event was caused by climate change is a recurrent question in media whenever such disasters occur. Attribution experiments can unveil the contribution that GHG emissions had in the occurrence of an event by comparing the probabilities of occurrence of an event in two simulation with and without taking into account the contribution of GHG emissions. This answers the increase in likelihood that such an event occurs due to climate change. Similarly, attribution experiments at S2S2D timescales can analyze the particular role of a specific factor other than GHG emissions. For instance, the role of Sea Surface Temperature (SST), soil moisture or sea ice extent anomalies in initiating or maintaining atmospheric extreme events can be studied by comparing experiments where those components of the prediction system are modified systematically to exclude its contributions (see Prodhomme et al. (2015), Lledó et al. (2018) or Navarro et al. (2019) for some examples).

1.4 The rise of climate services

1.4.1 From data to services

With a growing knowledge of how the Earth system behaves and also with an increasingly concerned population on the perils of climate change, climate services have appeared as a tool to inform society of past, current and future

climate and its associated risks in many socio-economic sectors. While the amount of scientific data produced both by the Earth observing and modeling communities keeps growing and its associated uncertainties decrease, the uptake of this information by the society is hindered by the complexity of this type of information (Buontempo et al., 2014). Climate services need to provide that information in a way that assists decision making by individuals and organizations (i.e. actionable information).

In order to overcome the difficulties of the society at digesting climate information, the Global Framework for Climate Services (GFCS) initiative, established in 2009 during the World Climate Conference-3 by the World Meteorological Organization (WMO), is leading international efforts to develop science-based climate information services for various climate-sensitive sectors such as the energy sector (Hewitt et al., 2013). The GFCS is based on five pilars or action lines (see figure 1.10):

1. Observations and monitoring: collection and quality control of Earth observations.

2. Research, modelling and prediction: basic science required to advance understanding of the Earth system.

3. Climate services information systems: adequate infrastructure and technical means to collect and disseminate climate information.

4. User interface platforms: appropriate channels of communication between users and climate service providers to ensure that user needs are met.

5. Capacity development: the development of the right skills or practices that enable to take advantage of climate data.

This structure stresses that having the best scientific methods and observations is not enough to produce good climate services. The information needs to be converted into formats that can be trusted, understood and digested by the users. The tools that present the information need to be co-designed with the users and tailored in order to facilitate decision-making and provide relevant

Figure 1.10: The five pillars of the GFCS. Source: WMO.

content. All the information has to be accompanied with good documentation, traceability and uncertainty quantification to raise trust. Training materials, case studies and dissemination are also key to foster its utilisation. Therefore the development of climate services requires a transdisciplinary approach that goes beyond climate science itself (Christel et al., 2018).

1.4.2 Tailoring climate predictions for the energy sector

The user needs of different stakeholders aiming to use climate predictions are very diverse (Bessembinder et al., 2019). An overview of the different use cases, user profiles and their needs regarding predictions at S2S2D scales has already been briefly discussed in section 1.1.3 and summarized in table 1.1. While many of the activities outlined there can be directly informed by wind speed forecasts, wind power generation is often the final variable that is required by decision makers. Therefore the development of impact models that translate wind speed to wind power generation would be useful to many of them. A typical way forward is the production of sectoral indicators that summarize the impact of atmospheric variables on the final variable

of interest and disregard other external factors. In the wind energy industry, indicators such as the wind power density (the total kinetic energy available in the wind that goes through a wind turbine) or the capacity factor (the percentage of utilisation of a power plant) are widely known and are employed as proxies of generation potential. Therefore producing forecasts of these indicators could be very helpful.

Another important difference amongst usages of climate predictions in the energy sector is the required spatial scale of the forecast. Some use cases need the information at site level (for instance planning the maintenance of a turbine or anticipating revenues of a specific wind farm), while other uses might require information aggregated at region, or country level (e.g. anticipating total renewable generation in a country for estimating electricity prices). Providing climate predictions at the local scale is still challenging due to the coarse scale of the ESMs employed (Schwitalla et al., 2020) and the lack of sufficiently long and trustworthy observational datasets (Ramon et al., 2020). It is generally recognized that better skills can be obtained when analyzing regional averages, due to the cancelling of location errors (Chardon et al., 2016).

A third important aspect when producing predictions is the selection of specific thresholds that are useful for making a decision. Climate predictions are probabilistic in nature, and therefore provide probabilities that an event will occur or not. While an O&M operator is interested in knowing when the wind will be below a safety threshold, another user might be interested into the probability of the production being above a certain number. The variety of specific decisions is often difficult to handle, and many climate service implementations use generic categories to suit many users. For instance, predictions in the form of tercile probabilities are widely employed by many prediction centers, while predictions of extreme events are also of special interest to many stakeholders. Figure 1.11 shows an example of a visualization of a seasonal forecast of wind speed displaying probabilities for tercile categories and extreme events.

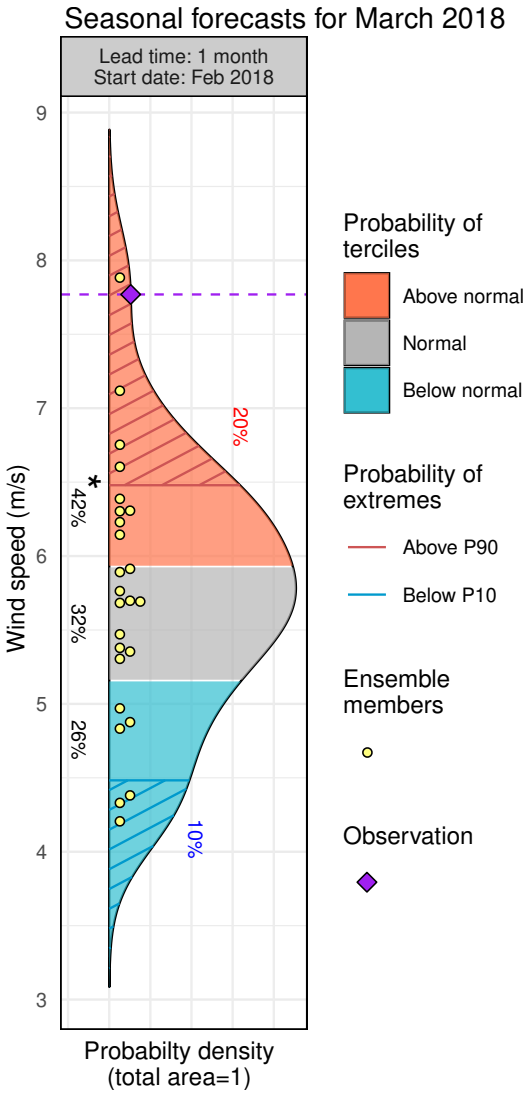

Figure 1.11: A visualization of a seasonal forecast of 10 m wind speed in the form of probabilities of tercile categories and extreme events. The forecast is for March 2018 in a location of the northwest of Spain. The probability of observing a wind speed exceeding the 90^{th} percentile of the climatological distribution was doubled. Source: S2S4E project.

The skill levels that are needed to make a climate-prediction-informed decision are also relative to the usage. Although from a verification point of view positive skill scores always reflect a benefit with respect to a climatological prediction, the skill levels at which a certain decision can lead to benefits is difficult to establish and certainly not equal for any decision, because the costs and

risks involved in each decision are different (Katz and Murphy, 1997).

In summary, the design of any climate service has to consider the specific needs of the users at which it is directed in order to produce meaningful and actionable forecasts, and has to tailor the presentation of the information to those needs.

Chapter 2

Objectives and structure of this work

The main goal of this work is to advance the knowledge of atmospheric variability at sub-seasonal and seasonal timescales affecting the wind energy sector and to foster the production of climate predictions at this scales by developing sound scientific methods that allow to anticipate wind and wind power generation conditions. There is a big gap between climate prediction science and the effective delivery of climate information to the society, and climate services aim to bridge this gap by shaping the contents and the forms of the predictions to the user needs. With the final goal of generating a corpus of knowledge that allows the production of climate services for the wind energy industry, three main objectives of this work have been set:

Objectives

(i) Characterize the impact of atmospheric variability at S2S scales on near-surface wind speed and wind power generation.

(ii) Develop methods to anticipate wind speed and wind power variability at S2S timescales.

(iii) Tailor those predictions for the provision of climate services for the wind power industry and facilitate its uptake.

This dissertation is presented in the form of a compendium of publications. The work is divided in five parts that have been published as research papers in different peer-reviewed journals. The first paper (chapter 3) investigates the drivers of an unprecedented wind drought episode in North America by means of an attribution experiment at seasonal timescales and uncovers the role of the North Pacific Mode (NPM) teleconnection in shaping the seasonal variations of wind speed in the region. The second paper (chapter 4) unveils the impact that strong MJO events have on near-surface wind speed in Europe at sub-seasonal timescales, while it signals some weaknesses of current sub-seasonal prediction systems. The third paper (chapter 5) presents a methodology to convert seasonal predictions of wind speed to forecasts of capacity factor, an indicator that is useful to anticipate wind power generation. The fourth paper (chapter 6) evaluates the skill of five seasonal prediction systems at anticipating four teleconnection indices that are relevant to define the atmospheric circulation over Europe. This work is a first step towards producing improved forecasts near the surface by employing the teleconnection forecasts as predictors in a statistical model. The fifth paper (chapter 7) draws a parallel between some very technical aspects of forecast verification and the more familiar concepts that are often used in gambling, by means of a roulette game that rep-

resents the possible outcomes of the wind speed conditions and is played with information based on climate predictions. Each chapter is preceded by a short summary of the publication and the objectives addressed. Finally chapter 8 presents the main conclusions and future directions.

Chapter 3

Investigating the effects of Pacific sea surface temperatures on the wind drought of 2015 over the United States

In this work, a widespread and persistent episode of low wind speed conditions in North America in 2015 was investigated. The American wind power sector suffered the impact of this episode, which drastically reduced energy generation and income during several months in a row. Aside of the cash flow problems originated by the mince energy generation, it also caused a devaluation of the assets of the wind farm owners. From a naive perspective, a business that has generated low revenues in the past without a credible reason that can be reverted or at least understood and quantified, will not be expected to generate good income levels in the future and will be considered risky. In order to provide at least an interpretation to why this wind drought occurred, the impact of tropical SSTs (and specifically of ENSO and NPM states) into wind speeds in North America was analyzed using historical records from a reanalysis dataset. After finding evidence that positive NPM phases —such as the one observed in 2015— produce a wind stilling in the area of study, an attribution experiment with the coupled Atmosphere-Ocean EC-Earth model was performed. This experiment confirmed that high SSTs in an area of the western tropical Pacific ocean produced Rossby wave trains that propagated towards North America impacting its wind speed.

This paper deals with objectives (i) and (iii) of this dissertation.

Lledó, L., Bellprat, O., Doblas-Reyes, F. J., and Soret, A. (2018). Investigating the effects of Pacific sea surface temperatures on the wind drought of 2015 over the United States. *Journal of Geophysical Research: Atmospheres*, 123(10):4837–4849, doi: 10.1029/2017jd028019

Journal of Geophysical Research: Atmospheres

RESEARCH ARTICLE
10.1029/2017JD028019

Investigating the Effects of Pacific Sea Surface Temperatures on the Wind Drought of 2015 Over the United States

Llorenç Lledó[1], Omar Bellprat[1], Francisco J. Doblas-Reyes[1,2], and Albert Soret[1]

[1]Barcelona Supercomputing Center, Barcelona, Spain, [2]ICREA, Pg. Lluís Companys 23, Barcelona, Spain

Key Points:
- Long-lasting low wind speed conditions reduced wind power generation in the United States in 2015
- Retrospective climate predictions confirm that anomalous SSTs in the tropical Pacific Ocean forced the event

Supporting Information:
- Supporting Information S1

Correspondence to:
L. Lledó,
llledo@bsc.es

Citation:
Lledó, L., Bellprat, O., Doblas-Reyes, F. J., & Soret, A. (2018). Investigating the effects of Pacific sea surface temperatures on the wind drought of 2015 over the United States. *Journal of Geophysical Research: Atmospheres*, *123*. https://doi.org/10.1029/2017JD028019

Received 10 NOV 2017
Accepted 9 APR 2018
Accepted article online 19 APR 2018

Abstract During the first quarter of 2015 the United States experienced a widespread and extended episode of low surface wind speeds. This episode had a strong impact on wind power generation. Some wind farms did not generate enough cash for their steady payments, and the value of some assets decreased. Although the wind industry expressed their concerns, the episode has not received much attention from the scientific community and remains weakly understood. In this paper we aim to fill this gap and advance understanding of the underlying processes at seasonal time scales. Using retrospective climate predictions, we find that high sea surface temperatures in the western tropical Pacific ocean associated with a strongly positive phase of the North Pacific Mode played a central role to establish and maintain those wind anomalies. In a more general way it has also been shown that interannual variability of wind speed over North America is not only dominated by El Niño/Southern Oscillation but also by other sea surface temperature variations in the tropical Pacific. This new knowledge can be useful for industry stakeholders to anticipate future periods of low wind speed.

1. Introduction

In order to try to limit the effects of climate change and reduce greenhouse gas emissions, a huge effort to decarbonize the energy sector is taking place in many countries all over the world. One of the pillars of this decarbonization is the adoption of renewable energies. Wind energy, in particular, is the technology that has experienced the biggest growth in recent years (Global Wind Energy Council, 2016). However, wind farm owners, operators, and project developers face the challenge of understanding variability of wind speeds at several time scales to run their business successfully. In the forthcoming years renewables will reach high penetration levels in the electricity mix (Obama, 2017). Then transmission system operators will also need to understand weather and climate oscillations that impact electricity generation in order to guarantee energy supply and dimension transmission and backup facilities.

All these stakeholders are exposed to the risks that extreme events can bring. One of such events happened in 2015 in the United States, where wind power covers approximately 5% of the total electricity demand (U.S. Energy Information Administration, 2017). During the first quarter of 2015 (January–March), surface wind speeds were well below normal in most of the contiguous United States (see Figure 1), which reduced substantially the electricity generation of most of the wind farms in the country (U.S. Energy Information Administration, 2017). The wind speed reduction was especially relevant in Texas, Oklahoma, and Kansas, where most of the biggest wind farms are concentrated. The standardized anomalies reached values of more than three standard deviations away from the 1979–2014 mean in a widespread region, revealing that this was a very infrequent event. Indeed, the wind industry did not anticipate such low wind episode. Some companies experienced financial problems due to the lack of energy production and revenues (Meyer, 2015), and there were concerns on the value of the assets. The term "wind drought" was coined, and a lot of questions arose: When would winds revert back to normal conditions? Did anthropogenic climate change have an influence on this episode? Could this episode repeat in the near future (Brower, 2015; Maverick, 2015)?

All these questions direct us to ask what caused the episode. Some informal sources argued that the event was caused by a developing El Niño/Southern Oscillation (ENSO) warm phase, which is known to reduce winter and spring wind speeds in North America (Brower, 2015; ESS-BSC Catalogue, Earth System Services, Earth Science Department, Barcelona Supercomputing Center, 2016; St. George & Wolfe, 2009). However, El Niño was only weakly expressed at the time. The confusion might have derived from alarmist interpretations of seasonal forecasts, which anticipated a strong El Niño few months before (Climate Prediction Center and International

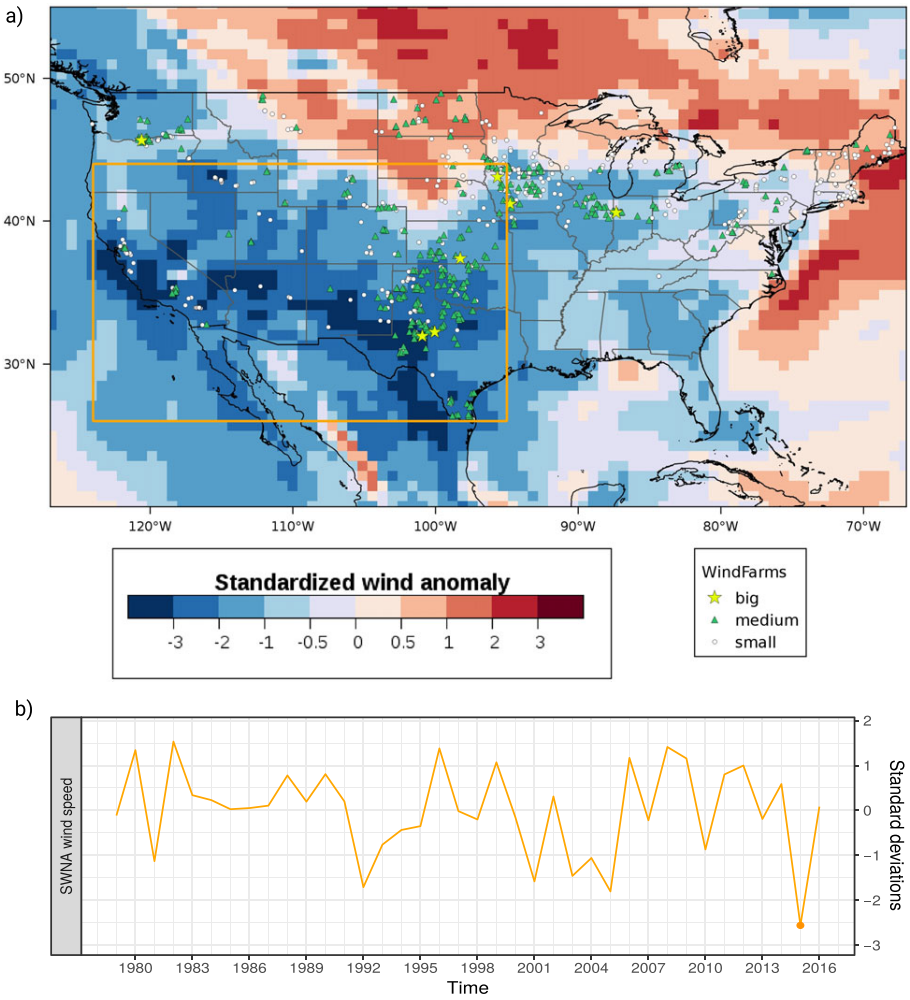

Figure 1. (a) Surface wind speed anomalies for the first quarter of 2015, expressed as the number of standard deviations away from the 1979–2014 mean for the same quarter. Values are from ERA-Interim reanalysis. The orange box delimits the region where the anomalies were more extreme (southwestern North America region, hereafter referred to as SWNA, 124°W–95°W and 26°N–44°N). The distribution of the U.S. wind farm fleet is overplotted: white dots, green triangles, and yellow stars represent small (<100 MW), medium (<400 MW), and big (>400 MW) wind farms (source: U.S. Energy Information Administration, 2016). (b) Temporal evolution of January–March mean wind speed anomalies over SWNA. 2015 is signaled with a dot. ERA = European Centre for Medium-Range Weather Forecasts Re-Analysis.

Research Institute for Climate and Society, 2014). Instead, the North Pacific Mode (NPM; Deser & Blackmon, 1995; Hartmann, 2014) was in a strongly positive phase during the event, as will be seen in section 3. The impact that NPM has on North American winter temperatures has already been studied by Hartmann (2014) and Bellprat et al. (2016) for extremely cold events. Seager et al. (2015) also related it to Californian drought in 2011–2014. In this study we analyze the role it could have played on stilling the wind in North America.

The positive phase of NPM, with high sea surface temperatures (SSTs) off the North American west coast and also in the western tropical Pacific, is thought to be favored by atmospheric variability known as North Pacific Oscillation (Baxter & Nigam, 2015; Ding et al., 2015). Alexander et al. (2010) showed how extratropical SST anomalies associated to NPM can propagate southwesterly due to the wind evaporation-SST feedback and persist on tropical Pacific waters until next winter. This teleconnection, first described by Vimont et al. (2003) and known as seasonal footprinting mechanism (SFM), explains why positive phases of NPM can trigger positive ENSO events the next winter (Di Lorenzo et al., 2010; Ding et al., 2015; Yu & Paek, 2015). However, Bond et al. (2015) already suggested that NPM impacts in North America might derive from tropical origin and not from the blob in North American shores. Indeed Stuecker (2018) very recently proved that Central Pacific

El Niño events (which are related to the tropical component of NPM) can produce in turn extratropical SST anomalies off the North America west coast. Here we will show the tropical roots of the wind drought episode by performing retrospective climate predictions with an atmosphere-only climate model where the role of SST patterns can be studied systematically.

The data sets, methods and characteristics of the atmospheric climate model used are described in section 2. In section 3 the event is analyzed. The coincidental state of the ocean during similar periods of low wind speed in the region is studied, and the role of ENSO and NPM in shaping the interannual variability of wind speed in North America is investigated. A set of sensitivity experiments using an Atmospheric General Circulation Model (AGCM) are presented in section 4. Discussion and concluding remarks follow in section 5.

2. Data and Methods

The January–March 2015 event has been analyzed using surface wind speed and SST anomalies in the European Centre for Medium-Range Weather Forecasts (ECMWF) Re-Analysis (ERA)-Interim reanalysis computed at monthly and 3-monthly time scales. ERA-Interim (Dee et al., 2011) is routinely produced at the ECMWF and provides gridded data at a spatial resolution of around 80 km (spectral resolution of T255). It is widely used in the wind industry to track anomalies. All the anomalies have been computed with respect to the 1979–2014 period, which is the period that was available when the event occurred. Moreover, the anomalies have been standardized dividing the absolute deviations by the standard deviation of the historical reference period. This helps to understand how extreme the anomalies were with respect to natural variability in the recent past.

Additionally, empirical orthogonal function analysis (EOF) and linear correlations have been employed to uncover relationships between SSTs and winds in the ERA-Interim data set. In order to achieve the largest possible sample size, the full ERA-Interim period 1979–2016 including the event was considered. The EOF patterns are normalized to 1, and the principal components (PC) have been standardized in the plots. The separation of EOF patterns has been tested with the North et al. rule of thumb (North et al., 1982; Wilks, 2005) using $n = 30$. Statistical significance for all correlations has been tested using a two-tailed t test with a confidence level of 95%.

The EC-Earth Earth-system model has been used for the AGCM experiments. EC-Earth is built using three main model components: Integrated Forecasting System for the atmosphere, Nucleus for European Modelling of the Ocean for the ocean, and Louvain-la-Neuve Sea Ice Model for the sea ice (Hazeleger et al., 2012, Prodhomme, Batté, et al., 2016). But in the present study only the atmospheric component (Integrated Forecasting System; cycle 36r) has been used, while sea ice and sea surface temperatures have been prescribed from ERA-Interim reanalysis on a daily basis. In all the experiments the spectral resolution of the atmospheric model is T255 (the same as ERA-Interim and corresponding to around 80 km) with a vertical resolution of 91 levels. For each of the experiments, a large ensemble with 100 members has been simulated. The singular vector perturbation technique (Buizza & Palmer, 1995) has been applied to the ERA-Interim observations to obtain slightly different but equally plausible initial conditions that result in diverging answers after the first few days of integrations. Then 3 months of simulations initialized on 1 January have been computed to cover the period of interest. The Autosubmit workflow manager (Manubens-Gil et al., 2016) has been used to manage efficiently the high number of simulations that were run. As AGCMs have systematic errors, a hindcast simulation for the period 1981–2010 has been prepared with 10 ensemble members to adjust the model biases. In order to identify and adjust those biases, we have followed the simple bias correction methodology described in Torralba et al. (2017), with separate adjustments for each month. This method adjusts both the bias and variance but does not inflate ensemble spread.

3. Anatomy of the Event

An analysis of the status of the ocean and atmosphere during the first quarter of 2015 (January–March, referred to as Q1) has been done to illustrate the particularities of the event. However, trying to understand cause-effect relationships from simultaneous anomalies in one event would be adventurous, and therefore similar patterns in the past records have been explored using two EOF analyses of wind speeds and SSTs from ERA-Interim reanalysis (Dee et al., 2011).

Figure 2 shows the evolution of SST and surface wind speed during Q1 2015 over the tropical and north Pacific Ocean and the United States. In the first column, a band of anomalously high SST can be seen off the

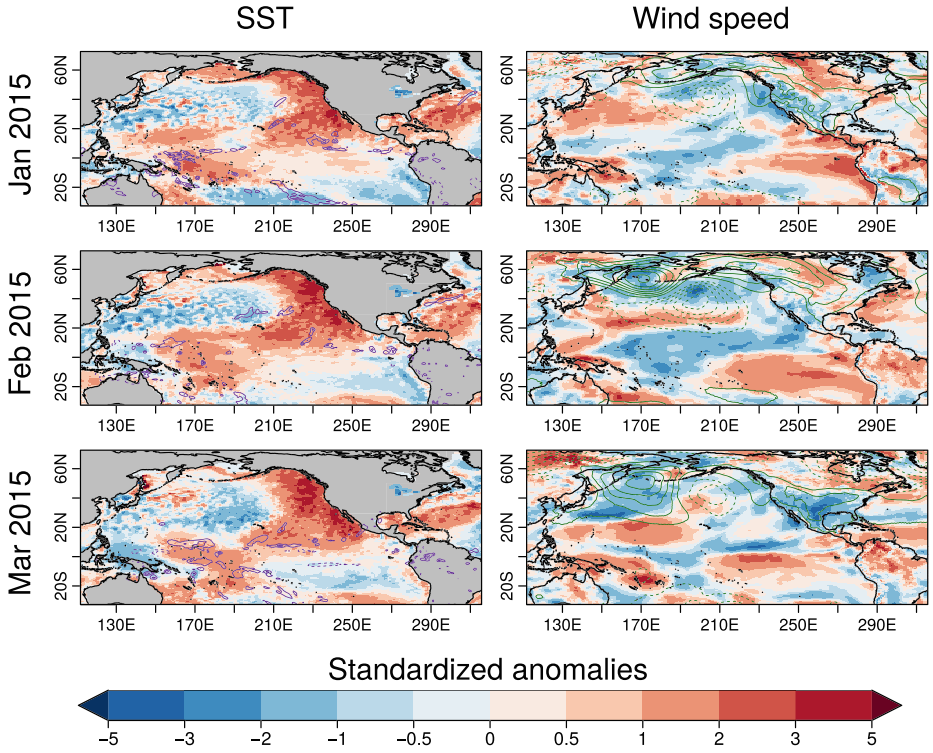

Figure 2. SST and surface wind speed anomalies for the first months of 2015, expressed as the number of standard deviations away from the 1979–2014 mean for the same month, drawn from ERA-Interim reanalysis. Purple contours show precipitation anomalies, and green contours show sea level pressure anomalies. Contour intervals are 5 mm/day and 2 hPa, respectively, with zero contour omitted. SST = sea surface temperature; ERA = European Centre for Medium-Range Weather Forecasts Re-Analysis.

western coast of North America. The western tropical Pacific also experienced remarkable positive anomalies, although not so outstanding in terms of standardized values. Those SST patterns resemble very much the anomalies associated to the positive phase of NPM (Hartmann, 2014). January and March are the months that experienced the highest wind anomalies of the period in the United States, in consistence with higher sea level pressures in the continent.

At the same time, during Q1 2015 the Arctic Oscillation (AO) was in a high phase (reaching 1.8 in March). Chen et al. (2013) showed how the AO in spring is a determinant for the SFM to be able to trigger an El Niño event next year. Interestingly, this event was followed by a strong El Niño next winter, so probably the SFM was very active during 2015.

Notice that the wind drought persisted also during the second quarter of the year (April–June) (see supporting information Figure S1), although here we will focus only on Q1. The region where the anomalies were higher during this period has been identified (see the orange box in Figure 1). We will refer to this region as southwestern North America region (SWNA, 124°W–95°W and 26°N–44°N).

To characterize the event with respect to past variability, an EOF analysis of Q1 surface winds over the United States (covering 140°W–65°W and 22°N–50°N and removing all water grid points) has been computed (see Figure 3). The first and second modes (referred to as m1 and m2 hereafter) account only for a 53% of the total variance in the EOF domain. But they correlate to 0.82 and 0.53 with the SWNA-averaged anomalies (presented in Figure 1b). Therefore, those two modes alone can reproduce a 95% of SWNA averaged anomalies. Hence, the Q1 2015 event can be decomposed into a slightly negative phase of the first mode and a strongly negative phase of the second mode (right column of Figure 3). Indeed, the second mode reached an outstanding absolute minimum in the records. This decomposition shows that the Q1 2015 anomaly is outstanding in terms of magnitude, but similar m2-shaped anomaly patterns were observed in the past, although not so strong. Analyzing those similar episodes in the historical records will help to better understand

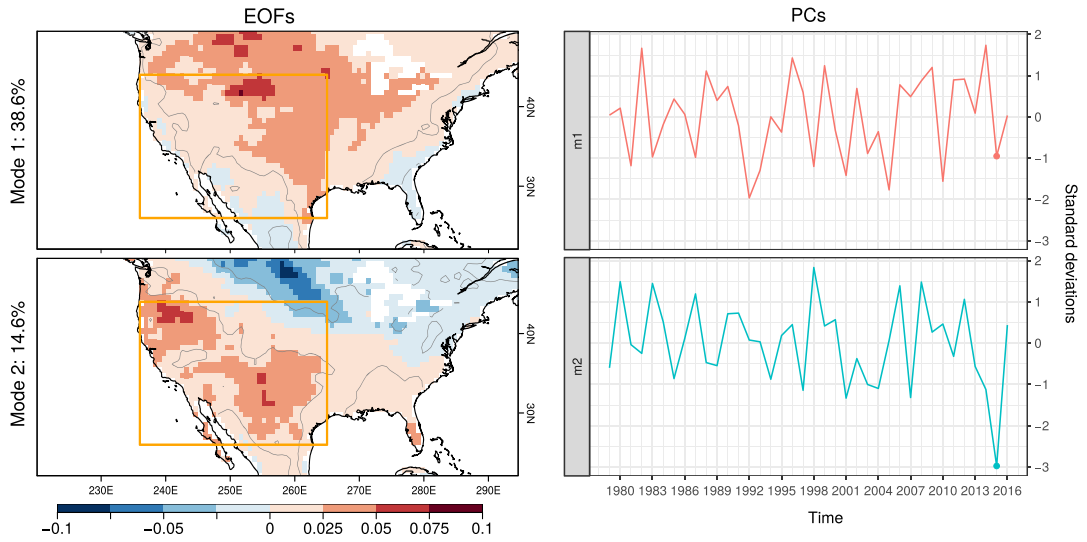

Figure 3. EOF analysis of Q1-averaged surface winds over the United States. (left column) EOF patterns. Gray contours enclose statistically significant areas. The orange box delimits the SWNA region. (right column) evolution of the normalized PCs. A dot highlights 2015 value in each time series. EOF = empirical orthogonal function; SWNA = southwestern North America region; PC = principal components.

the underlying processes. First m1 variability will be studied. Although m1 was not in a very high phase during the event, the description of the physical processes behind m1 variations, which are well known, will help to understand the processes behind m2 variability later.

Figure 4 shows the correlation coefficients between each of the two PCs and Q1 SSTs for all grid points. This plot identifies oceanic regions that could be contributing to generate those anomalies. For the first mode the pattern resembles very much the typical ENSO SST anomalies, in both the tropics and extratropics. We hypothesize that ENSO-like variations in the tropical Pacific have an influence on the strength of the first mode of U.S. wind speed. The sign of the correlations indicates that positive (warm) phases of ENSO are coincidental with negative phases of the first mode, that is, reduced wind speeds in most of the continent but specially in the north and center. For some time now, ENSO has been known to modify the general circulation patterns (Horel & Wallace, 1981) and to impart extratropical SST anomalies in both north and south Pacific oceans through the atmospheric bridge process (Alexander et al., 2002), specially during boreal winter

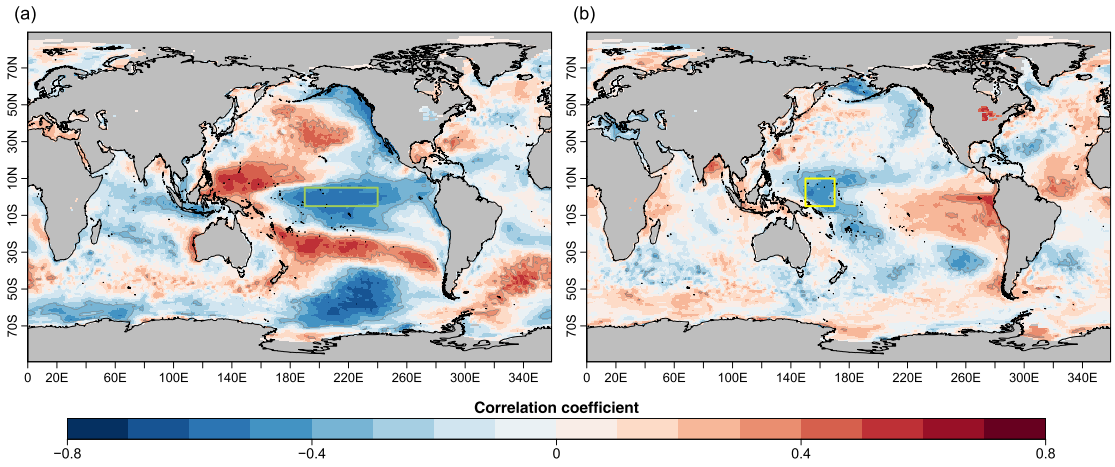

Figure 4. Correlation coefficients between Q1-averaged SSTs and the first PCs of U.S. wind speed. (a) Correlation with first mode. (b) Correlation with second mode. Two regions with high correlations are identified: the NINO3.4 region (green box, 170°W–120°W and 5°S–5°N, referred to as NINO3.4) and a western tropical Pacific region (yellow box, 150°E–170°E and 5°S–10°N, referred to as WTP). Gray contours enclose statistically significant areas. SST = sea surface temperature; PC = principal components.

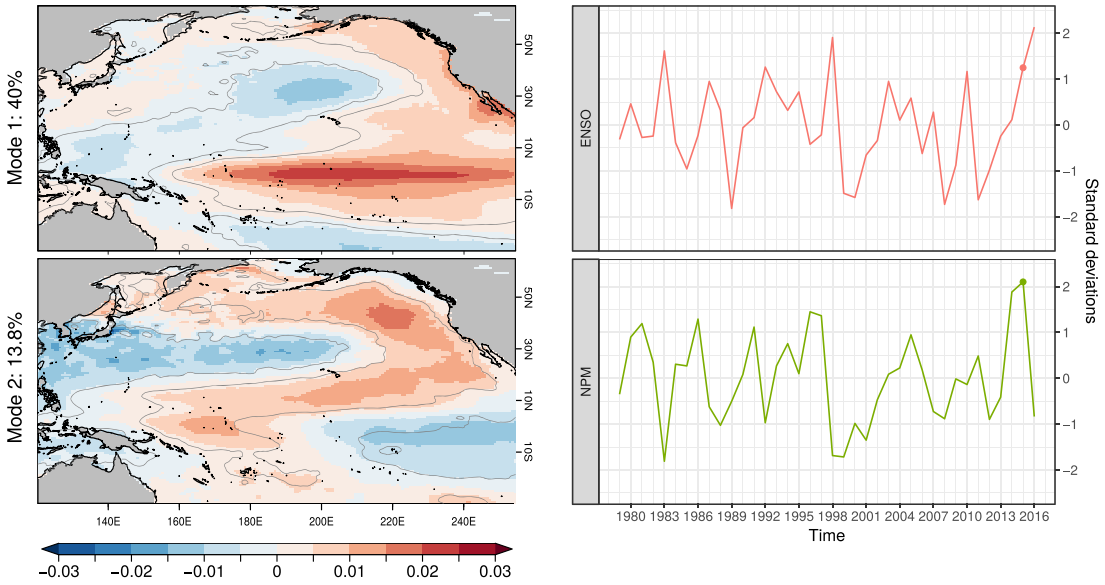

Figure 5. EOF analysis of Q1 Pacific SST. (left column) EOF patterns are drawn with color. Gray contours enclose statistically significant areas. (right column) Evolution of the normalized PCs. A dot highlights 2015 value in each time series. EOF = empirical orthogonal function; SST = sea surface temperature; PC = principal components.

and spring. Tropical SSTs are known to force midlatitudinal atmospheric circulation through warm anomalies that induce convective systems. The tropical convective motion results in midtropospheric diabatic heating and upper troposphere divergence that exert a quasi-stationary Rossby wave response and modulate the extratropical circulation (DeWeaver & Nigam, 2002; Trenberth et al., 1998). Extratropical SSTs in turn are mainly forced by wind speed variations which dominate underlying SSTs through evaporative processes: higher winds increase evaporation and reduce SSTs (Cayan, 1992). Therefore, it is plausible that whenever the atmospheric bridge is in place both extratropical SST and wind anomalies originate from tropical SST variations. With this in mind the NINO3.4 region (170°W–120°W and 5°S–5°N) has been highlighted in the map as an adequate indicator for the first mode of U.S. winds, even if higher correlations can be seen in the

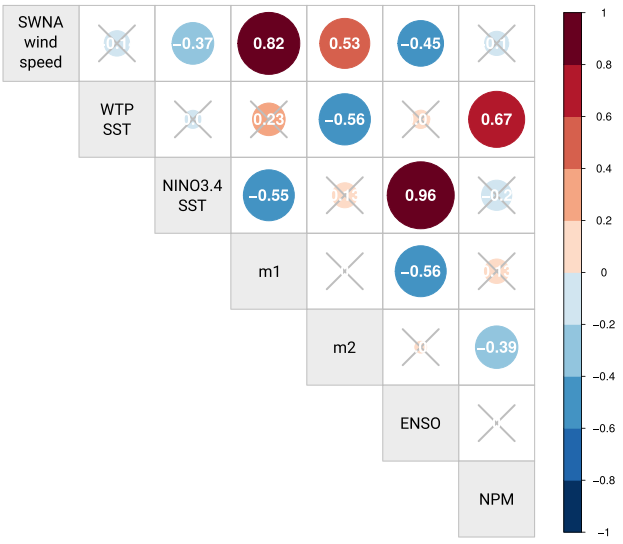

Figure 6. Linear correlation matrix including Q1 values of wind and SST anomalies and the first PCs of the two EOF analyses. A cross indicates nonsignificance at the 5% level. All the correlations can be found in the column above the corresponding label or in the row on its right. SST = sea surface temperature; PC = principal components; EOF = empirical orthogonal function.

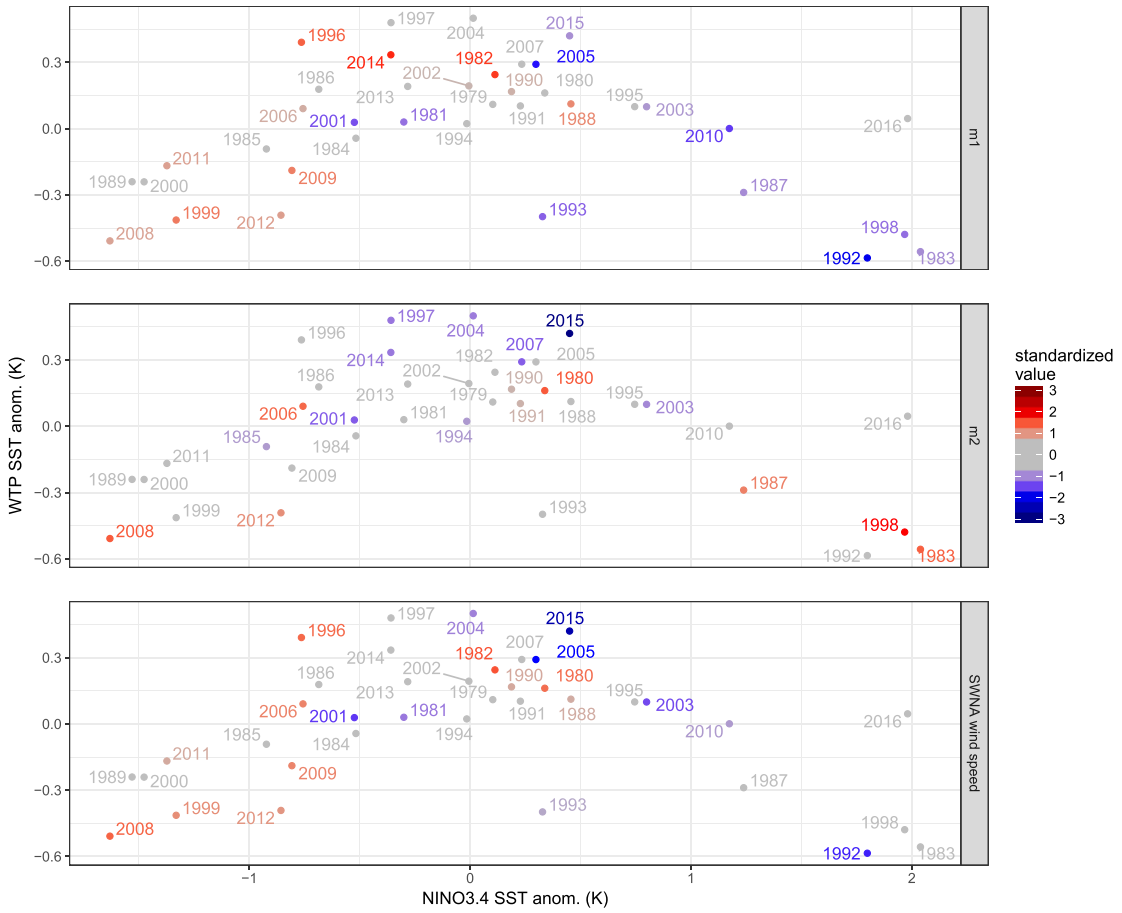

Figure 7. Scatterplot of NINO3.4 and WTP SSTs, labeled with the corresponding year and colored with standardized values of m1, m2, and SWNA wind speed in each of the panels. A strong nonlinear relationship between NINO3.4 and WTP SSTs can be seen. SST = sea surface temperature; SWNA = southwestern North America region; WTP = western tropical Pacific region.

southern Pacific ocean. A statistically significant correlation coefficient of −0.55 is obtained between Q1 NINO3.4 average SSTs and the first PC (see Figure 6).

For the second mode correlations are more modest (Figure 4b), but still two spots with moderate correlation can be identified: a region in the Western Tropical Pacific (150°E–170°E and 5°S–10°N, referred to as WTP), and another region of opposed sign in the eastern tropical Pacific. There are also spots with significance in the extratropics. A correlation of −0.56 is obtained between WTP SSTs and the second PC, suggesting that an atmospheric bridge teleconnection might be at play also in this case. The precipitation anomalies for Q1 2015 (see Figure 2) show enhanced convection in the western tropical Pacific and support this hypothesis for the 2015 event. This will be investigated further in section 4.

In order to better interpret the correlation map for the second mode, an EOF analysis of SSTs over tropical and north Pacific has been performed. The region has been set to 30°S–65°N and 120°E–105°W, following Hartmann (2014). Q1 averages for the 1979–2016 period have been employed, and the linear trend has been removed prior to analysis. Both the EOF patterns and the PC evolutions of the first two modes are shown in Figure 5. The third and fourth modes, although not relevant for the 2015 event, are shown in supporting information Figure S2. The first mode is ENSO, the dominant oscillation of global SSTs (Trenberth, 1997). The second mode corresponds to the NPM. A 1-year-lagged correlation coefficient of 0.57 between NPM and ENSO confirms it (not shown), as NPM is known to be one of the precursors of ENSO with 1 year of advance (Pegion & Alexander, 2013; Vimont et al., 2003; Wang et al., 2012). The Pacific Decadal Oscillation (Mantua et al., 1997), which is the second mode in Hartmann (2014), appears as the third mode in this decomposition.

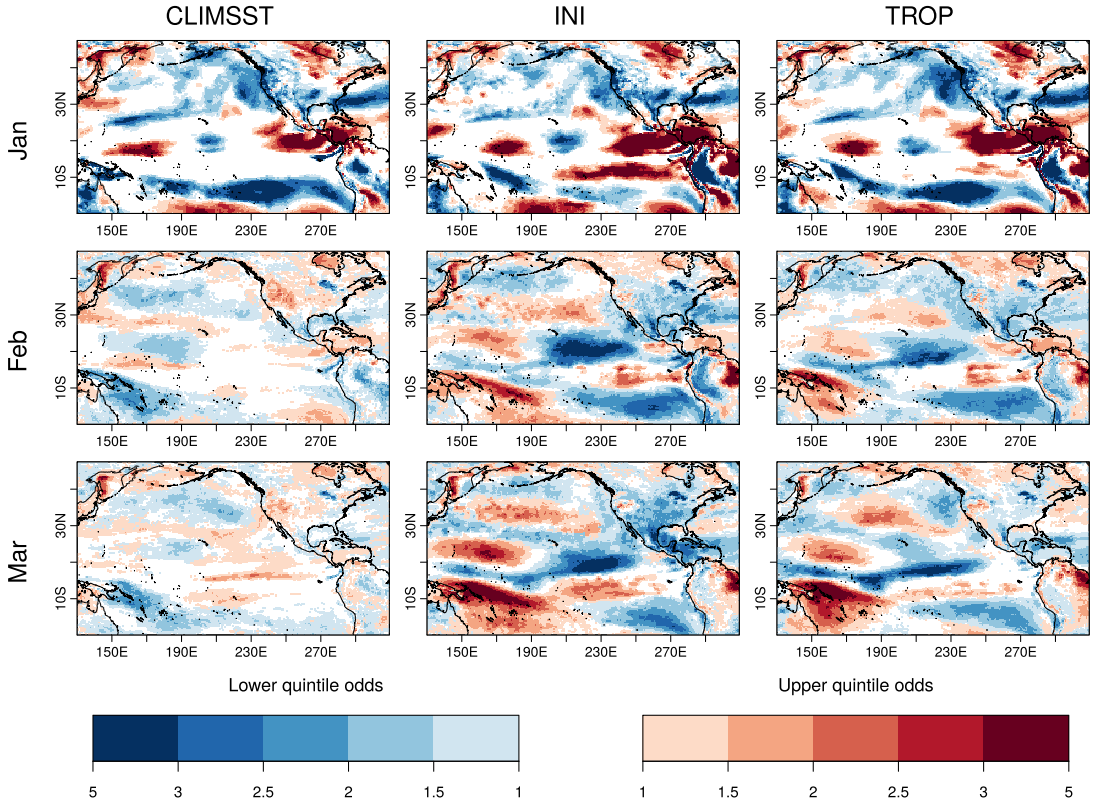

Figure 8. Odds of upper and lower quintiles of wind speed for CLIMSST (left column), INI (middle column), and TROP (right column) simulations initialized in January, for each of the three months. The odds are the ratio between the probability for the anomalies to be in the lower quintile, the interquintile range, or the upper quintile and the climatological probability of these three categories (20%, 60%, and 20%, respectively). Each grid point is colored with the category corresponding to the highest odds ratio. If the point corresponds to the interquintile range, the point is drawn in white. If the point is attributed to the lower (upper) quintile category, the corresponding odds ratio is plotted in blue (red). In January the impact of the initialization dominates the signal. In February and March the impact of different SST forcings emerges. SST = sea surface temperature.

Correlating the two U.S. wind speed PCs (m1 and m2) to the two Pacific SST PCs (ENSO and NPM), some linear relationships have been identified. Figure 6 summarizes the results in a matrix style plot. As pointed before, m1 anticorrelates with ENSO (−0.56). The m1 has also a weak positive correlation with NPM, but it is nonsignificant at 5% level. On the other hand, m2 has a significant correlation with NPM (−0.39), so that positive phases of NPM, with high SSTs in the WTP region, are related to reduced wind speeds in SWNA region, specially along the diagonal of the SWNA box. Notice that the NPM does not represent all SST variability in WTP region (see supporting information Text S1). This explains why the pattern in Figure 4b) does not match the NPM mode. Summarizing, in the past records there is a correspondence between ENSO (or NINO3.4 SSTs) and m1 events (31% of explained variance), and another correspondence between WTP SSTs (of which a portion is due to NPM) and m2 (also 31% of explained variance). From this we conclude that interannual variability of Q1 wind speed in North America is linked to NINO3.4 and WTP SST anomalies, that is, to ENSO, NPM, and any other SST variability in the WTP region.

Going back to the event under study, remember that Q1 2015 was marked by a strong negative phase of the second PC of U.S. wind speed and a slight negative phase of the first mode. Based on the PCs from EOF analysis of SST (Figure 5), during 2015 NPM was strongly positive, while ENSO was in a slightly positive phase, in accordance to the aforementioned relationships. This confirms that ENSO did not play a role in the episode, while NPM might play an important role.

In the previous paragraphs, the impact of NINO3.4 and WTP SSTs on North American wind speed has been undertaken separately. Analyzing it jointly will give a more detailed picture. Although NINO3.4 and WTP SSTs do not correlate significantly, a scatterplot (Figure 7) reveals that there is indeed a well-defined but nonlinear relationship between those SSTs, which results from ENSO nonlinearities and the antisymmetry of El Niño

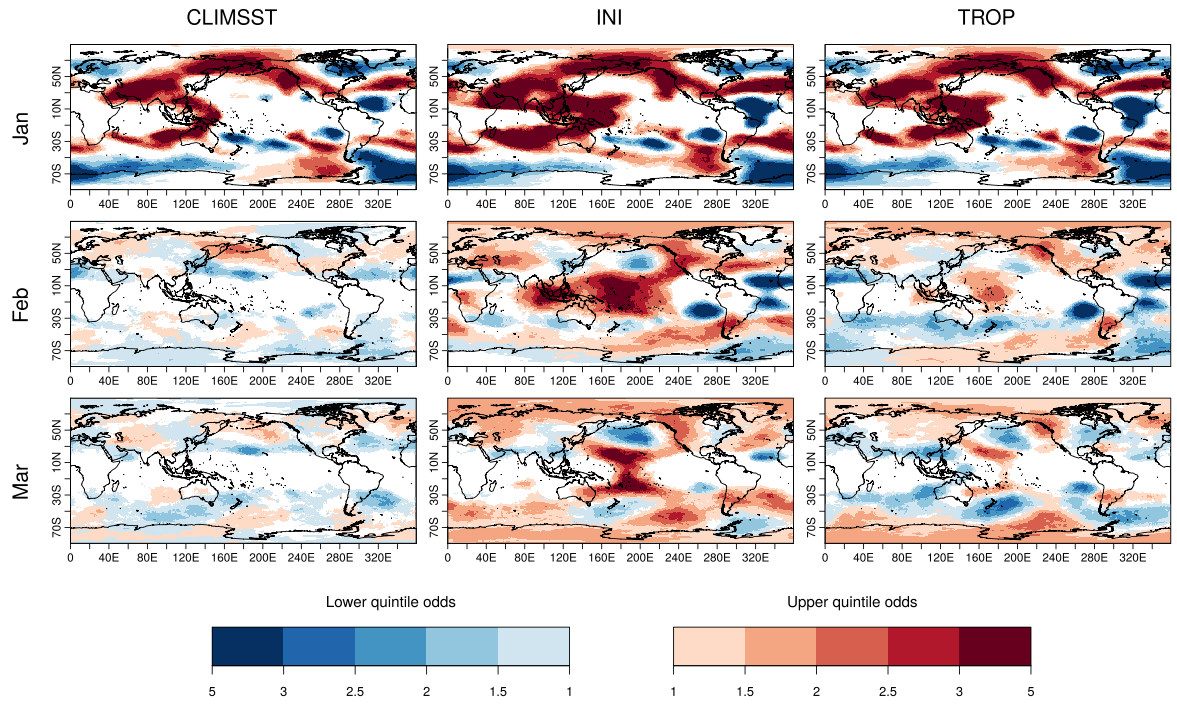

Figure 9. Same as Figure 8 but for geopotential height at 200 hPa. The Gill-type response can be seen in the INI and TROP simulations over the western Pacific. Its associated Rossby wave reaches North America.

and La Niña patterns (Monahan & Dai, 2004). Both highest and lowest NINO3.4 SSTs (i.e., strong ENSO phases) match low SSTs in WTP, with high WTP SSTs being observed only under relatively neutral ENSO conditions. Therefore, 2015-like anomalies might occur only under near-neutral ENSO states(see 1997, 2004, and 2007 in the top center of the panels). Regarding strong ENSO phases, in the first panel we see how m1 standardized value decreases from left to right, but in the second panel, m2 decreases from bottom to top. This implies that during strongly positive ENSO phases, m1 and m2 effects might compensate and moderate anomalies in SWNA (see, for instance, the strong 1983 or 1998 El Niño events on the bottom right of the panels), while under strongly negative ENSO phases m1 and m2 will contribute together to positive SWNA speed anomalies (e.g., 2008 on the bottom left).

4. Retrospective Model Predictions

To disentangle and confirm the relationships between NPM status and wind anomalies during the 2015 event uncovered in the previous section, a set of experiments using retrospective predictions with the EC-Earth forecast system have been performed (see section 2 for details). The January–March period has been simulated with different configurations, all initialized on 1 January 2015 using actual atmospheric conditions as initial conditions. The first model configuration uses January–March 2015 ERA-Interim daily SSTs as boundary conditions (referred to as INI hereafter). A second configuration uses a fixed SST climatology for January, February, and March (1981–2010) instead, to evaluate the impact of SST conditions in Q1 2015 (referred to as CLIMSST). Finally, a third simulation uses actual SST conditions only in the tropics (between 10°S and 10°N), climatological conditions north/south of 15°N/S and a transition zone in between (referred to as TROP).

Analyzing differences in the ensemble mean is not a good idea, because it is a deterministic metric and sometimes does not reflect the behavior of the distribution extremes. Instead, following Prodhomme, Doblas-Reyes, et al., (2016) we plot the odds of the INI, TROP, and CLIMSST simulations for higher and lower quintiles of wind speed (Figure 8). The probabilities for the anomalies to be in the lower quintile, the interquintile range, or the upper quintile are computed and then divided by the climatological probability of these three categories (20%, 60%, and 20%, respectively). These ratios are the odds: an odd higher than 1 indicates increased probabilities of the category. Then each grid point is colored with the category corresponding to the highest odds ratio. If the point corresponds to the interquintile range, the point is drawn in white.

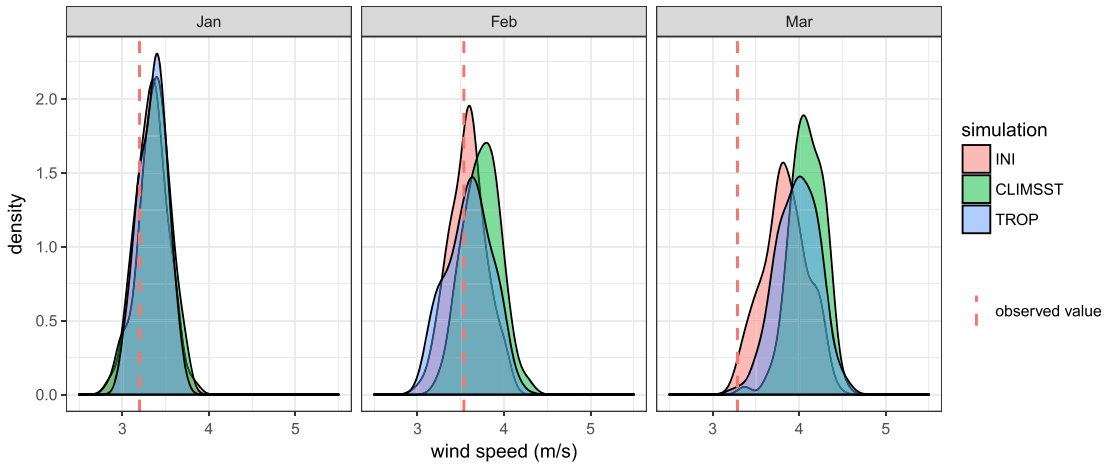

Figure 10. Probability distribution of SWNA wind speed for CLIMSST, INI and TROP simulations for January, February, and March. Dashed line indicates ERA-Interim observed value. SWNA = southwestern North America region; ERA = European Centre for Medium-Range Weather Forecasts Re-Analysis.

If the point is attributed to the lower (upper) quintile category, the corresponding odds ratio is plotted in blue (red). For this particular analysis no bias adjustment is needed because the quintile thresholds are computed from the hindcast.

The odds for January are similar for the three configurations. All of them display increased probabilities of lower quintile winds in North America, although they are more marked in the INI and TROP simulations. This implies that a large part of the anomaly signal was already present in the atmospheric initial conditions, regardless of the SSTs that have been used, as found in Bellprat et al. (2016). Therefore, the strong impact of the initialization in January does not allow to extract conclusions regarding the SST forcings. However, in February and March the effect of the different SSTs starts to emerge and the odds behave differently in each configuration. In February and March the odds for the INI simulation indicate that there exist increased probabilities of low wind speeds under this setting, which are consistent with the anomalies that were observed. Only a spot around 40°N and 120°W indicates enhanced probabilities of upper-quintile winds, in contradiction to what was observed. This might follow from biases in the exact location of pressure systems, which can appear in coarse-resolution configurations of EC-Earth or from the lack of ocean-atmosphere coupling in the experiments. Also, the odds and the anomalies do not necessarily need to match in all places. Internal atmospheric variability also plays a role, and therefore observed anomalies can deviate from the pattern with more probability to occur. Looking now at the CLIMSST simulation, the signal is reversed in February and March, and there is increased probability of winds above upper quintile (i.e., increased probability of high wind speeds). Therefore, without the observed SSTs that were prescribed in the INI simulation the wind anomalies would have been unlikely and we can affirm that SSTs contributed decisively to shape the event.

We have hypothesized in section 3 that NPM-related tropical Pacific SST anomalies observed in 2015 are responsible for imparting the wind speed anomalies recorded in North America, even if standardized anomalies were higher in the extratropical Pacific for this episode. The odds of the TROP simulation support this idea. Although climatological SSTs have been used in the extratropics, the obtained patterns resemble very much the INI simulation. This confirms the tropical roots of the episode. However, the odd ratio values for TROP are smaller than for INI in North America, specially during March. This indicates that the extratropical SST anomalies might have also contributed partially to maintain the event. The extratropical surface wind speed signal shows a clear Rossby wave response in the INI simulation, which is still visible in the TROP simulation. This suggests that the western tropical Pacific SSTs exert a quasi-stationary Rossby wave as discussed in Hartmann (2014) and illustrated in Trenberth et al. (1998). This has been confirmed analyzing geopotential heights at 200 hPa (Figure 9). The convective processes in WTP region (see supporting information Figure S3) produce diabatic heating in the midtroposphere and result in flow divergence and high pressures at 200 hPa level. In the INI and TROP simulations a Gill-type response to the anomalous SSTs can bee seen in the western

Pacific, similar to the Gill-type responses associated to ENSO events (DeWeaver & Nigam, 2002; García-Serrano et al., 2017). Therefore, we conclude that the physical mechanism that forced the event is similar to the mechanism at play during strong positive ENSO phases but located more to the west.

Finally, an analysis of the mean wind speed over SWNA for the three configurations has been made. In this case we use bias-adjusted data (see section 2), which allows comparison to ERA-Interim values. Figure 10 shows the probability distribution functions for wind speed averages over SWNA (only land points), drawn from the 100 ensemble members in each configuration. In February and March the distributions for INI and TROP simulations are shifted to lower wind speeds, therefore making the wind drought more probable. A Kolmogorov-Smirnov test confirms that those distributions differ significantly from CLIMSST distribution at 99% level. For March, when the episode was at its maximum, the observed anomaly was quite extreme even for the INI simulation and could not have been possible under climatological SST conditions. Analyzing the whole Q1 period, such a persistent low wind speed episode would have a return period of around 694 years according to ERA-Interim observations. But under the specific SSTs that were observed the return period descended to 48 years, making the event 14 times more probable (see supporting information Figure S4 for average Q1 distributions).

5. Discussion and Conclusions

It has been shown that the U.S. wind drought of Q1 2015 can be attributed to the North Pacific Mode state — and more specifically to its western tropical pacific anomalies — and holds no relationship with ENSO, although historically ENSO has dominated the interannual variability of wind speeds in North America. First an EOF analysis of wind speed over North America revealed that the second mode of variability was in a strongly negative phase during the first quarter of 2015, with drastic reductions of wind speed in the SWNA region. Similarly, an EOF analysis of tropical and North Pacific SSTs showed that at the same time the second variability mode (NPM) was in a very positive phase, with anomalously high SSTs off the North American shores and also in the western tropical Pacific. A relationship between those variability modes has been found in the observational records of the recent past (1979–2016), with a correlation of −0.39. The analysis suggests that western tropical Pacific anomalies associated to NPM state induce an atmospheric-bridge process and cause the wind speed reductions in the United States. Indeed, the SSTs in this area correlate to −0.56 with the second mode of wind speed. In a similar way it is found that the first wind speed mode correlates to −0.55 with NINO3.4 region SSTs (i.e., with ENSO phases).

A set of AGCM experiments has been produced for the Q1 2015 period to be able to understand causality relationships between Pacific SSTs and North American wind speeds. In a first AGCM experiment, a comparison of 100 ensemble members forced with observed anomalous SSTs and 100 ensemble members that used climatological SST averages revealed that such reductions of wind speed in SWNA were only possible under anomalous SST conditions. Therefore, SSTs are the main drivers for the observed wind speed anomalies.

A second experiment where the observed SSTs were only forced in the tropics confirmed that the extratropical wind speed anomalies arose from the tropical SST anomalies. The NPM-related extratropical SST anomalies contributed to the wind speed reductions to a lesser extent. The extratropical wind speed anomalies are linked to a Rossby wave train exerted by the warm western tropical SST anomalies which induce a wave-like response in the surface winds as shown in Figure 9. The SFM (Vimont et al., 2003) and AO (Chen et al., 2013) could also have played a role in the episode, but it has not been studied here. Also, the continuation of the episode during the second quarter of the year has not been explored.

Regarding the impact that such low wind speed episodes have in the renewable energy industry, it is clear from this study that not only ENSO events have to be tracked to anticipate wind droughts in the United States and North America, but also NPM status or other episodes of high SST in WTP are relevant. ENSO events will impart anomalies in the center and north of the continent, while NPM events will be impacting the southwest. This knowledge can be useful in the future for practical applications in the wind industry. Informing with some anticipation of probabilities of low wind speed conditions can help stakeholders to trigger some resilience mechanisms. Also, showing practical examples of how much climate oscillations can impact wind power generation will increase awareness of the need of a climate-informed wind resource assessment.

Acknowledgments
This work was funded by the EU projects S2S4E (GA 776787), EUCP (GA 776613), CLIM4ENERGY (C3S_441_Lot2_CEA), EUCLEIA (GA 607085), INDECIS (GA 690462), and MEDSCOPE (GA 690462). Omar Bellprat has been funded by the European Space Agency (ESA) Living Planet Fellowship Programme under the project VERITAS-CCI. We thank Daniel Cabezón for helping and informing on the wind drought episode and Javier García-Serrano for the insights on the interpretation of the physical processes. All the analyses have been performed using the statistical software R (R Core Team, 2015). The startR and s2dverification R packages have been used to read data sets, compute EOFs, and plot maps. Model output from the numerical experiments can be accessed through EUDAT facilities at the link http://doi.org/10.23728/b2share.71078a8618414e9b906cfa6bb7d2cdab. The reanalysis data and models used are listed in the references. We also acknowledge Javier Vegas and Nicolau Manubens for technical support, as well as the EC-Earth consortium for the model development.

References

Alexander, M. A., Bladé, I., Newman, M., Lanzante, J. R., Lau, N. C., & Scott, J. D. (2002). The atmospheric bridge: The influence of ENSO teleconnections on air-sea interaction over the global oceans. *Journal of Climate*, *15*(16), 2205–2231. https://doi.org/10.1175/1520-0442(2002)015<2205:TABTIO>2.0.CO;2

Alexander, M. A., Vimont, D. J., Chang, P., & Scott, J. D. (2010). The impact of extratropical atmospheric variability on ENSO: Testing the seasonal footprinting mechanism using coupled model experiments. *Journal of Climate*, *23*(11), 2885–2901. https://doi.org/10.1175/2010JCLI3205.1

Baxter, S., & Nigam, S. (2015). Key role of the North Pacific oscillation-West Pacific pattern in generating the extreme 2013/14 North American Winter. *Journal of Climate*, *28*(20), 8109–8117. https://doi.org/10.1175/JCLI-D-14-00726.1

Bellprat, O., Massonnet, F., García-Serrano, J., Fučkar, N. S., Guemas, V., & Doblas-Reyes, F. J. (2016). 8. The role of Arctic sea ice and sea surface temperatures on the cold 2015 February over North America. *Bulletin of the American Meteorological Society*, *97*(12), S36–S41. https://doi.org/10.1175/BAMS-D-16-0159.1

Bond, N. A., Cronin, M. F., Freeland, H., & Mantua, N. (2015). Causes and impacts of the 2014 warm anomaly in the NE Pacific. *Geophysical Research Letters*, *42*, 3414–3420. https://doi.org/10.1002/2015GL063306

Brower, M. (2015). The North American 'wind drought': Is it the new normal?, AWS Truepower. 9 December 2015. Retrieved from https://www.awstruepower.com/the-north-american-wind-drought/. (Last accessed: 31 July 2017).

Buizza, R., & Palmer, T. N. (1995). The singular-vector structure of the atmospheric global circulation. *Journal of the Atmospheric Sciences*, *52*(9), 1434–1456. https://doi.org/10.1175/1520-0469(1995)052<1434:TSVSOT>2.0.CO;2

Cayan, D. R. (1992). Latent and sensible heat flux anomalies over the northern oceans: Driving the sea surface temperature. *Journal of Physical Oceanography*, *22*(8), 859–881. https://doi.org/10.1175/1520-0485(1992)022<0859:lashfa>2.0.co;2

Chen, S., Chen, W., Yu, B., & Graf, H. F. (2013). Modulation of the seasonal footprinting mechanism by the boreal spring Arctic Oscillation. *Geophysical Research Letters*, *40*, 6384–6389. https://doi.org/10.1002/2013GL058628

Climate Prediction Center and International Research Institute for Climate and Society (2014). El Niño/Southern Oscillation (ENSO) diagnostic discussion. Retrieved from https://www.cpc.ncep.noaa.gov/products/analysis_monitoring/enso_disc_jul2014/ensodisc.html (Last accessed: 7 August 2017).

Dee, D. P., Uppala, S. M., Simmons, A. J., Berrisford, P., Poli, P., Kobayashi, S., et al. (2011). The ERA-Interim reanalysis: Configuration and performance of the data assimilation system. *Quarterly Journal of the Royal Meteorological Society*, *137*(656), 553–597. https://doi.org/10.1002/qj.828

Deser, C., & Blackmon, M. L. (1995). On the relationship between tropical and North Pacific sea surface temperature variations. *Journal of Climate*, *8*(6), 1677–1680. https://doi.org/10.1175/1520-0442(1995)008<1677:OTRBTA>2.0.CO;2

DeWeaver, E., & Nigam, S. (2002). Linearity in ENSO's atmospheric response. *Journal of Climate*, *15*(17), 2446–2461. https://doi.org/10.1175/1520-0442(2002)015<2446:LIESAR>2.0.CO;2

Di Lorenzo, E., Cobb, K. M., Furtado, J. C., Schneider, N., Anderson, B. T., Bracco, A., et al. (2010). Central Pacific El Niño and decadal climate change in the North Pacific Ocean. *Nature Geoscience*, *3*(11), 762–765. https://doi.org/10.1038/ngeo984

Ding, R., Li, J., Tseng, Y.-H., Sun, C., & Guo, Y. (2015). The Victoria mode in the North Pacific linking extratropical sea level pressure variations to ENSO. *Journal of Geophysical Research: Atmospheres*, *120*, 27–45. https://doi.org/10.1002/2014JD022221

ESS-BSC Catalogue, Earth System Services, Earth Science Department, Barcelona Supercomputing Center (2016). ERA-Interim seasonal Niño 3.4 impact on 10 m wind speed and 2 m temperature. Retrieved from http://www.bsc.es/ess/content/era-interim-seasonal-ni%C3%B1o-34-impact-10m-wind-speed-and-2m-temperature (Last accessed: 20 October 2017).

García-Serrano, J., Cassou, C., Douville, H., Giannini, A., & Doblas-Reyes, F. J. (2017). Revisiting the ENSO teleconnection to the tropical North Atlantic. *Journal of Climate*, *30*(17), 6945–6957. https://doi.org/10.1175/JCLI-D-16-0641.1

Global Wind Energy Council (2016). Global wind energy outlook 2016.

Hartmann, D. L. (2014). Pacific sea surface temperature and the winter of 2014. *Geophysical Research Letters*, *42*, 1894–1902. https://doi.org/10.1002/2015GL063083.Received

Hazeleger, W., Wang, X., Severijns, C., Ştefănescu, S., Bintanja, R., Sterl, A., et al. (2012). EC-Earth v2.2: Description and validation of a new seamless Earth system prediction model. *Climate Dynamics*, *39*(11), 2611–2629. https://doi.org/10.1007/s00382-011-1228-5

Horel, J. D., & Wallace, J. M. (1981). Planetary-scale atmospheric phenomena associated with the Southern Oscillation. *Monthly Weather Review*, *109*(4), 813–829. https://doi.org/10.1175/1520-0493(1981)109<0813:PSAPAW>2.0.CO;2

Mantua, N. J., Hare, S. R., Zhang, Y., Wallace, J. M., & Francis, R. C. (1997). A Pacific interdecadal climate oscillation with impacts on salmon production. *Bulletin of the American Meteorological Society*, *78*(6), 1069–1079. https://doi.org/10.1175/1520-0477(1997)078<1069:APICOW>2.0.CO;2

Manubens-Gil, D., Vegas-Regidor, J., Prodhomme, C., Mula-Valls, O., & Doblas-Reyes, F. J. (2016). Seamless management of ensemble climate prediction experiments on HPC platforms. In *2016 International Conference on High Performance Computing & Simulation (HPCS)* (pp. 895–900). Innsbruck, Austria: IEEE. https://doi.org/10.1109/HPCSim.2016.7568429

Maverick, T. (2015). El niño buffers U.S. wind power dreams, Wall Street Daily. 21 September 2015. Retrieved from https://www.wallstreetdaily.com/2015/09/21/u-s-wind-power-el-nino/. (Last accessed: 31 July 2017).

Meyer, G. (2015). US clean energy suffers from lack of wind, Financial Times. 1 September 2015. Retrieved from https://www.ft.com/content/b967b6d4-5058-11e5-8642-453585f2cfcd. (Last accessed: 31 July 2017).

Monahan, A. H., & Dai, A. (2004). The spatial and temporal structure of ENSO nonlinearity. *Journal of Climate*, *17*(15), 3026–3036. https://doi.org/10.1175/1520-0442(2004)017<3026:TSATSO>2.0.CO;2

North, G. R., Bell, T. L., Cahalan, R. F., & Moeng, F. J. (1982). Sampling errors in the estimation of empirical orthogonal functions. *Monthly Weather Review*, *110*(7), 699–706. https://doi.org/10.1175/1520-0493(1982)110<0699:SEITEO>2.0.CO;2

Obama, B. (2017). The irreversible momentum of clean energy. *Science*, *355*(6321), 126–129. https://doi.org/10.1126/science.aam6284

Pegion, K., & Alexander, M. (2013). The seasonal footprinting mechanism in CFSv2: Simulation and impact on ENSO prediction. *Climate Dynamics*, *41*(5-6), 1671–1683. https://doi.org/10.1007/s00382-013-1887-5

Prodhomme, C., Batté, L., Massonnet, F., Davini, P., Bellprat, P., Guemas, V., & Doblas-Reyes, F. J. (2016). Benefits of increasing the model resolution for the seasonal forecast quality in EC-Earth. *Journal of Climate*, *29*(24), 9141–9162. https://doi.org/10.1175/JCLI-D-16-0117.1

Prodhomme, C., Doblas-Reyes, F., Bellprat, O., & Dutra, E. (2016). Impact of land-surface initialization on sub-seasonal to seasonal forecasts over Europe. *Climate Dynamics*, *47*(3-4), 919–935. https://doi.org/10.1007/s00382-015-2879-4

R Core Team (2015). *R: A language and environment for statistical computing*. Vienna, Austria: R Foundation for Statistical Computing.

Seager, R., Hoerling, M., Schubert, S., Wang, H., Lyon, B., Kumar, A., et al. (2015). Causes of the 2011–14 California drought. *Journal of Climate*, *28*(18), 6997–7024. https://doi.org/10.1175/JCLI-D-14-00860.1

St. George, S., & Wolfe, S. A. (2009). El niño stills winter winds across the southern Canadian prairies. *Geophysical Research Letters*, *36*, L23806. https://doi.org/10.1029/2009GL041282

Stuecker, M. F. (2018). Revisiting the Pacific Meridional Mode. *Scientific Reports*, *8*(1), 3216. https://doi.org/10.1038/s41598-018-21537-0

Torralba, V., Doblas-Reyes, F. J., MacLeod, D., Christel, I., & Davis, M. (2017). Seasonal climate prediction: A new source of information for the management of wind energy resources. *Journal of Applied Meteorology and Climatology*, *56*(5), 1231–1247. https://doi.org/10.1175/JAMC-D-16-0204.1

Trenberth, K. E. (1997). The definition of El Niño. *Bulletin of the American Meteorological Society*, *78*(12), 2771–2777. https://doi.org/10.1175/1520-0477(1997)078<2771:TDOENO>2.0.CO;2

Trenberth, K. E., Branstator, G. W., Karoly, D., Kumar, A., Lau, N.-C., & Ropelewski, C. (1998). Progress during TOGA in understanding and modeling global teleconnections associated with tropical sea surface temperatures. *Journal of Geophysical Research*, *103*(C7), 14,291–14,324. https://doi.org/10.1029/97JC01444

U.S. Energy Information Administration (2017). Electric power monthly, with data for May 2017.

Vimont, D. J., Wallace, J. M., & Battisti, D. S. (2003). The seasonal footprinting mechanism in the Pacific: Implications for ENSO. *Journal of Climate*, *16*(16), 2668–2675. https://doi.org/10.1175/1520-0442(2003)016<2668:TSFMIT>2.0.CO;2

Wang, S.-Y., L'Heureux, M., & Chia, H.-H. (2012). ENSO prediction one year in advance using western North Pacific sea surface temperatures. *Geophysical Research Letters*, *39*, L05702. https://doi.org/10.1029/2012GL050909

Wilks, D. S. (2005). *Statistical methods in the atmospheric sciences* (2nd ed., Vol. 100). Boston: International Geophysics, Academic Press.

Yu, J. Y., & Paek, H. (2015). Precursors of ENSO beyond the tropical Pacific. *Clivar Variations*, *13*(1), 15–20.

Supporting Information for "Investigating the effects of Pacific sea surface temperatures on the wind drought of 2015 over the United States"

Llorenç Lledó[1], Omar Bellprat[1], Francisco J. Doblas-Reyes[1,2], Albert Soret[1]

Contents of this file

1. Text S1
2. Figures S1 to S4

Introduction. This supporting information provides similar figures as seen in the main article but for other periods, variables or variability modes. Also it contains additional reasoning regarding the fourth SST variability mode, and supports the role of tropical SSTs to force the m2 anomalies.

Text S1. In the main text it has been shown that tropical SST anomalies associated with the NPM can induce a convective system and force wind reductions in the US. However, NPM does not explain all of the SST variability in the WTP region (correlation is only 0.67). The fourth SST mode (see figure S3) has also an important contribution (correlating to 0.5). Interestingly, this fourth mode does not have an extratropical pattern in the west coast of North America, but it correlates to m2 anomalies anyway (-0.35). This reinforces the idea that the extratropical anomalies associated with NPM are not essential to force the wind speed reductions. Also, the fact that NPM does not fully represents WTP SST anomalies helps understand why figure 4b) does not matches the NPM pattern.

[1]Barcelona Supercomputing Center (BSC).
[2]ICREA, Pg. Lluís Companys 23, Barcelona 08010, Spain.

0148-0227/18/$9.00

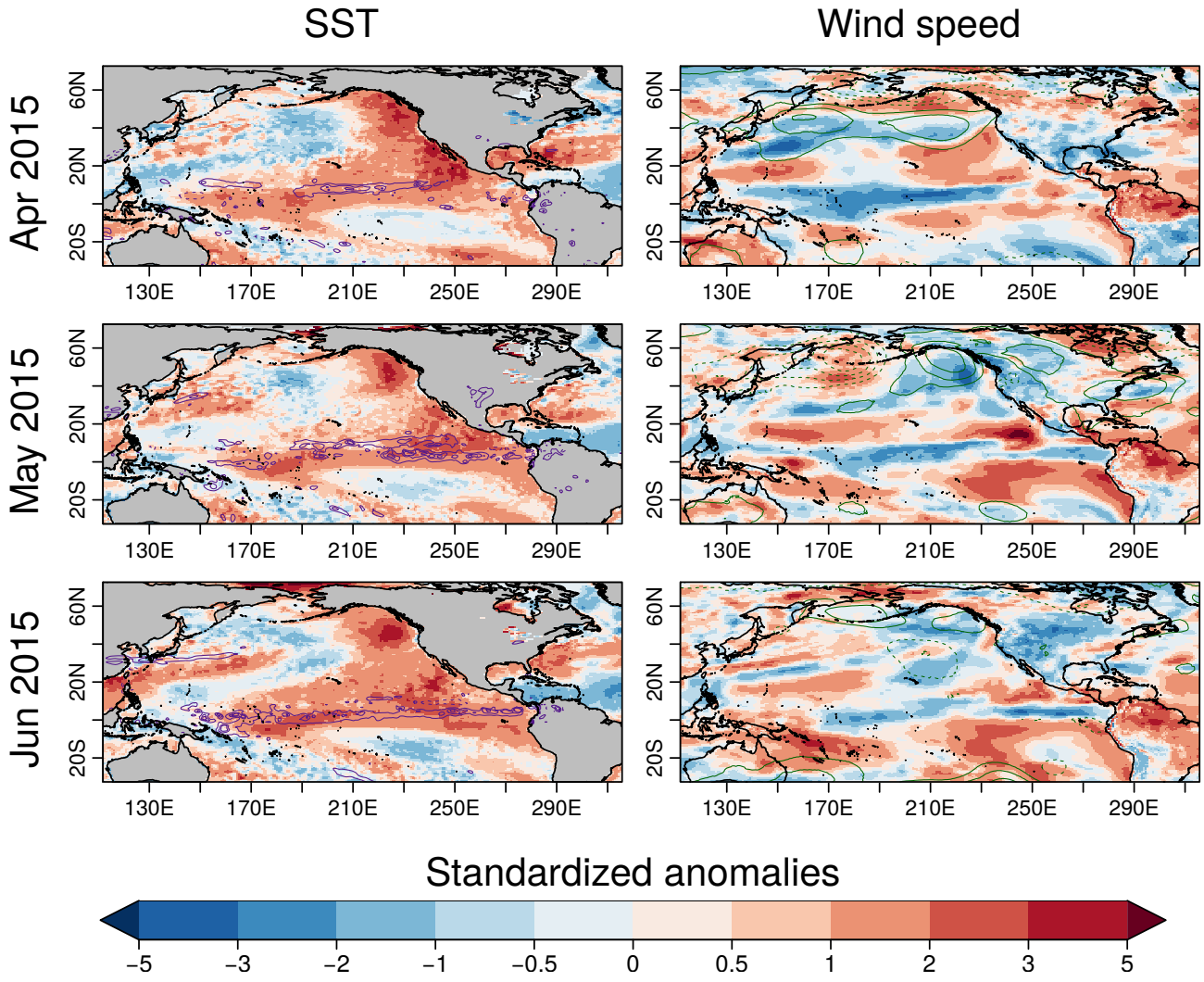

Figure S1. Same as figure 2 but for April–June.

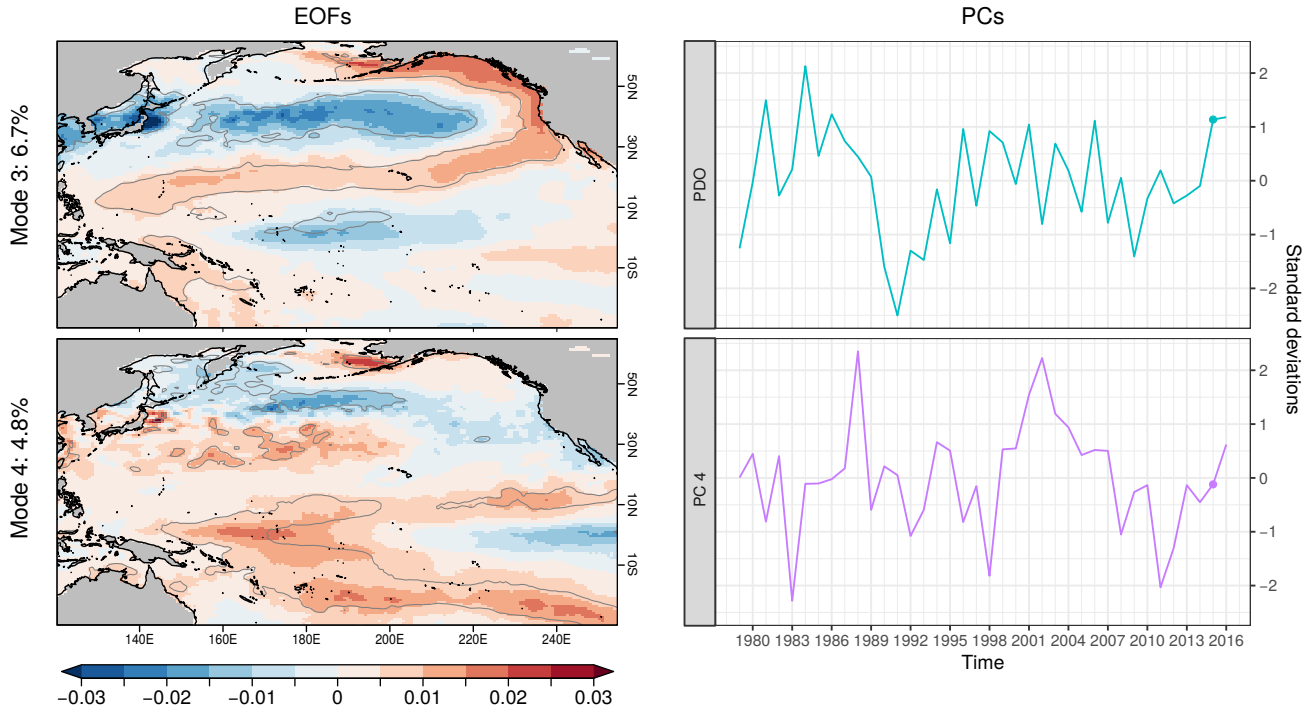

Figure S2. Same as figure 5 but for third and fourth modes.

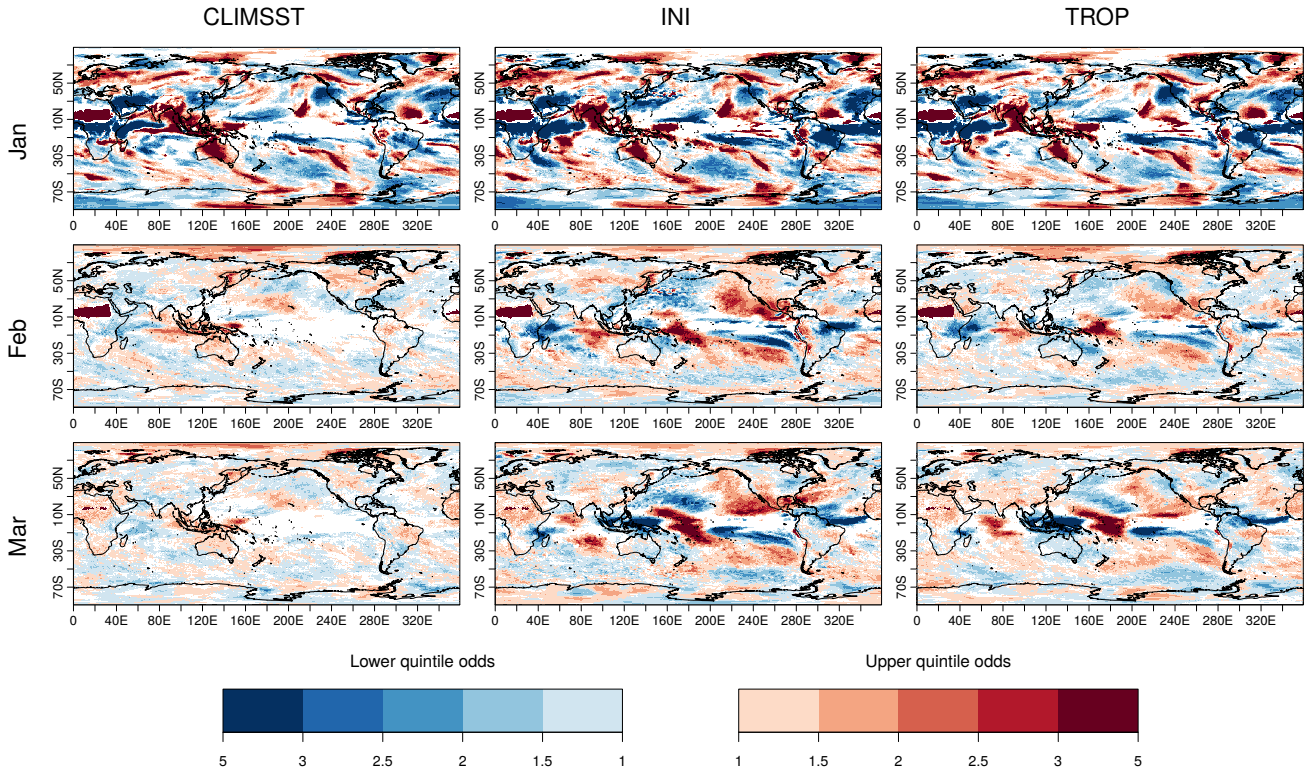

Figure S3. Same as figure 8 but for precipitation.

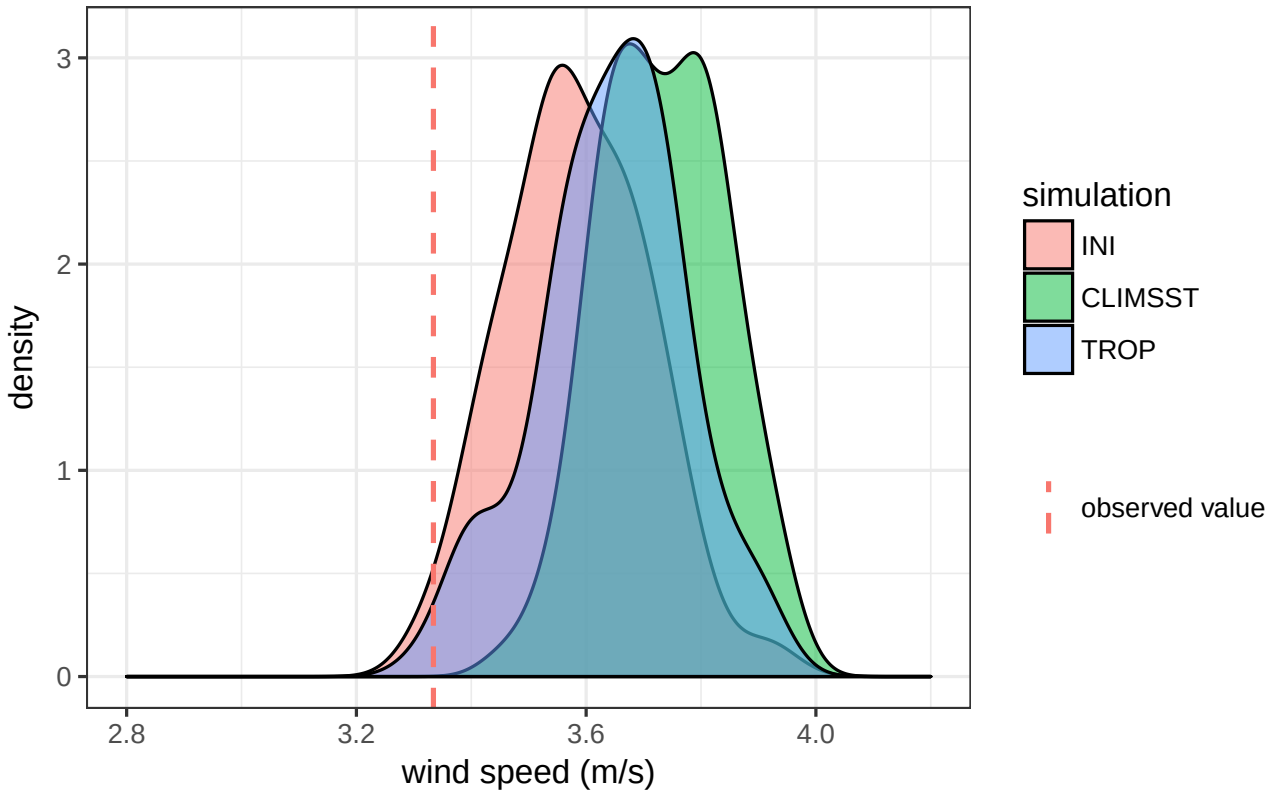

Figure S4. Same as figure 10 but for whole Q1 period.

Chapter 4

Predicting daily mean wind speed in Europe weeks ahead from MJO status

The MJO is the most outstanding oscillatory phenomena at sub-seasonal timescales. Although it occurs in the tropics, its teleconnective effects reach the extratropics through Rossby wave propagation and also through modification of the stratospheric circulation. This work analyzes the impact of strong MJO events on near-surface daily mean wind speed in Europe. As the MJO is a traveling wave the impacts depend on the phase of the oscillation. However, in this case the teleconnection transit time has a similar timescale to the MJO propagation through different phases, complicating the analyses. In a second part of the work, a new hybrid method that combines impacts of the MJO with sub-seasonal forecasts of strong MJO events is proposed. It is found that strong MJO events cannot be forecasted more than 10 days ahead with current sub-seasonal prediction systems. This limits the possibilities of employing the proposed method, but highlights the need to better study strong MJO events.

This paper deals with objectives (i) and (ii) of this dissertation.

Lledó, L. and Doblas-Reyes, F. J. (2020). Predicting daily mean wind speed in Europe weeks ahead from MJO status. *Monthly Weather Review*, 148(8):3413–3426, doi: 10.1175/mwr-d-19-0328.1

Predicting Daily Mean Wind Speed in Europe Weeks ahead from MJO Status

LLORENÇ LLEDÓ

Barcelona Supercomputing Center, Barcelona, Spain

FRANCISCO J. DOBLAS-REYES

Barcelona Supercomputing Center and ICREA, Barcelona, Spain

(Manuscript received 5 October 2019, in final form 9 April 2020)

ABSTRACT

The Madden–Julian oscillation (MJO), a prominent feature of the tropical atmospheric circulation at subseasonal time scales, is known to modulate atmospheric variability in the Euro-Atlantic region. However, current subseasonal prediction systems fail to accurately reproduce the physical processes involved in these teleconnection mechanisms. This paper explores the observed impact of strong MJO events on surface wind speed over Europe. It is found that some MJO phases are accompanied by strong wind anomalies in Europe. After showing that this teleconnective mechanism is not present in the predictions of the ECMWF monthly forecasting system, a methodology to reconstruct forecasts of daily mean wind speed in the continent weeks ahead is proposed. This method combines MJO forecasts from the S2S project database and the observed teleconnection impacts in the historical records. Although it is found that strong MJO events cannot be skillfully predicted more than 10 days ahead with current prediction systems, a theoretical experiment shows that this method can effectively transform a dynamical MJO forecast into a probabilistic wind speed prediction in Europe.

1. Introduction

The Madden–Julian oscillation (MJO) is the dominant mode of atmospheric variability at subseasonal time scales in the tropics. It consists of an enhanced convection cell traveling west to east along the equator, completing a whole lap of Earth in 30–60 days (Madden and Julian 1971, 1972; Zhang 2005). Several studies have shown that the MJO modulates many atmospheric phenomena at the intraseasonal time scales (see Zhang 2013 for a review). Extratropical circulation is specially affected through excitation of tropospheric Rossby waves but also through the stratosphere (Barnes et al. 2019). For instance Lin et al. (2009) and Cassou (2008) established a connection between the MJO and the North Atlantic Oscillation (NAO), which is the first mode of atmospheric variability over the Euro-Atlantic region. This relationship depends on the location of the enhanced convective activity (i.e., the MJO phase), but also on its intensity, propagation speed, or lifetime (Zheng and Chang 2019).

A good description of the physical processes that play a role in MJO propagation (viz., convection, moisture advections and underlying sea surface temperatures) is key to forecast the MJO evolution (Kim et al. 2019), while an adequate representation of the teleconnective mechanisms that derive from it (diabatic heating due to convection and propagation of Rossby waves through background flow) would in turn allow to anticipate its impact on the extratropics (Zheng and Chang 2019). The S2S project (Vitart et al. 2017) brings together subseasonal predictions from several operational centers and allows a systematic study of the MJO prediction skill in these systems (Vitart 2017; Lim et al. 2018), which show that the ECMWF model has a clear lead in predicting the MJO evolution. This system has a skillful prediction horizon of 36 days [defined as the day at which bivariate correlation (Lin et al. 2008) goes below 0.5]. However, Vitart (2017) also shows that all models

Denotes content that is immediately available upon publication as open access.

Supplemental information related to this paper is available at the Journals Online website: https://doi.org/10.1175/MWR-D-19-0328.s1.

Corresponding author: Llorenç Lledó, lledo@bsc.es

DOI: 10.1175/MWR-D-19-0328.1

in the S2S database fail to reproduce the teleconnection impacts in the Northern Hemisphere. Specifically, geopotential height anomalies 11 to 15 days after the MJO was in phase 3 or 7 are too weak in the models when compared to observations (Figs. 7 and 8 in Vitart 2017). Summarizing, the ECMWF model does a decent job in simulating MJO propagation, but fails to reproduce the teleconnective impacts over Europe, and this is a generalized behavior of subseasonal prediction systems.

This scenario opens the door to employ hybrid dynamical-statistical approaches (i.e., combine a dynamical forecast of the MJO state with the observed teleconnection impacts) to produce forecasts for specific sectoral applications. One socioeconomic sector that can benefit from this approach is the wind energy sector. While power producing companies, traders and grid operators use weather forecasts up to 10 days ahead routinely for its daily operations, forecasts of daily mean wind speed weeks ahead could be useful for many of them (Soret et al. 2019).

A methodology that combines a probabilistic seasonal forecast of ENSO with its past observed wind speed impacts has been proposed in Torralba (2019) and applied with success in some regions where dynamical models fail to reproduce ENSO teleconnections. However, the MJO is a traveling wave and its state has to be described with two indices: either the two components of an empirical orthogonal function (EOF) decomposition (usually known as RMM1 and RMM2; Wheeler and Hendon 2004), or a phase and an amplitude index. Therefore this method, which was devised for one single index, cannot be directly employed here, and new algorithms need to be designed.

In this work the impact of strong MJO events on wind speeds over Europe is analyzed through reanalysis stratifications as a function of the MJO phase. Then the same stratifications are performed for the ECMWF subseasonal predictions to confirm that the teleconnections are not well reproduced for wind speed. After that, a novel method to combine past observed teleconnection effects with an MJO forecast is described and analyzed.

2. Datasets and methods

a. Datasets

1) Surface wind observations

Observational estimates of surface winds (i.e., at 10 m) for the period 1981–2017 have been obtained from the fifth generation of the European Centre for Medium-Range Weather Forecasts (ECMWF) reanalysis (ERA5) [Copernicus Climate Change Service (C3S) 2017]. Some findings have also been confirmed with winds at 100 m above ground from ERA5 and at 50 m from NASA's Modern-Era Retrospective Analysis for Research and Applications-2 (MERRA2, Gelaro et al. 2017). Daily mean speeds have been computed from hourly values in both datasets. Those two reanalyses provide the best global estimates of observed surface or near-surface wind according to a comparison of several global reanalysis datasets (Ramon et al. 2019). ERA5 has been obtained on a Gaussian F320 grid (a resolution of 0.281 25° or ~28 km) while MERRA2 has a regular grid with a resolution of 0.625° × 0.5°.

2) Surface wind predictions

Subseasonal predictions of surface wind from the ECMWF monthly forecasting system (MFS) (ECMWF 2019; Vitart 2004) have been employed to evaluate the strength of the MJO teleconnection response and estimate future wind speed. Daily mean winds have been computed from 6-hourly outputs for all the available forecast times up to 46 days ahead and for the 11 ensemble members. The full hindcasts associated with the 2018 real-time forecasts—covering the 1998–2017 period—have been employed to obtain a consistent and long record of retrospective predictions. The data, which corresponds to IFS cycle CY43R3, have been obtained from ECMWF MARS on a regular Gaussian F320 grid (~28 km of horizontal resolution, which is the same resolution of ERA5).

3) MJO observations

The MJO is a propagating wave, and many methods have been proposed in the literature to describe its state. Generally speaking, two coordinates that specify its phase and amplitude are required. Here, observed MJO daily indices have been retrieved from two separate sources, both using a combined (or multivariate) EOF decomposition. First, the Real-Time Multivariate MJO indices (RMM) described in Wheeler and Hendon (2004) have been obtained from Australian Bureau of Meteorology (BoM) (http://www.bom.gov.au/climate/mjo/graphics/rmm.74toRealtime.txt). These RMM components are computed operationally from satellite outgoing longwave radiation (OLR, a proxy for convective activity) and NCEP–NCAR reanalysis (Kalnay et al. 1996) zonal winds at 850 and 200 hPa, after removing ENSO-related variability and the mean of the 120 most recent days. Second, daily indices derived fully from ERA-Interim fields (Dee et al. 2011) have been retrieved from the S2S database (Vitart 2017) in a methodology that differs slightly from the Wheeler and Hendon (2004) method (ENSO-related variability is not

removed; see Gottschalck et al. 2010 for details). While the BoM index has been widely used to monitor the MJO and evaluate its teleconnective impacts, the S2S index was adopted by the S2S project to develop and verify forecasts. The MJO phase and amplitude have been derived from RMM components in both datasets.

4) MJO PREDICTIONS

MJO retrospective predictions from the ECMWF MFS-2018 hindcasts—covering the 1998–2017 period—have been retrieved from the S2S database (Vitart et al. 2017). The MJO predictions employ the method described in Vitart (2017) and are methodologically consistent with the S2S ERA-Interim-derived MJO observations. MJO S2S forecasts have been obtained individually for each ensemble member and for the ensemble mean (i.e., computed from ensemble-mean fields). MFS has been selected among all models within the S2S database because, as explained above, it has been shown to be the best model in forecasting the MJO evolution (Vitart 2017).

b. Methods

1) STRATIFICATIONS

Wind speed conditions in Europe during strong MJO events are analyzed through stratifications of daily mean wind speed. Stratifications—also known as composite maps—consist of separate statistical analyses of a sample that is partitioned into subgroups by an external factor. In this case the sample of observed 1981–2017 daily mean wind speeds is partitioned into nine groups by the observed MJO phase and amplitude, producing a disjoint and exhaustive partition: the distribution of wind speed values is analyzed separately for those days when the MJO is in one of its eight phases with a strong amplitude (amplitude > 2; see Fig. S6 in the online supplemental material for a graphical representation of those nine groups and a short digression on the threshold selected to define strong MJO events). For each of these groups, the mean wind speed anomalies with respect to the whole sample have been computed at each grid point and expressed as a percentage. This normalization allows to plot anomalies over land and ocean (where winds and absolute anomalies are much higher) in the same scale. It also allows a fair comparison between wind speed anomalies at different heights above ground (see Figs. S1, S2), for the same reasons.

As the MJO activity tends to be stronger from October to March, the analysis focuses on this period of the year. The extratropical impact of the MJO depends on the location and strength of the tropical convection (i.e., MJO phase and amplitude), but also on the mean zonal flow in the extratropics, which modulates the propagation of Rossby waves. To account for differences in mean flow during this extended winter period, the stratifications have been produced separately for October to December (OND) and January to March (JFM). Separate stratifications for each month would have resulted in too small samples. Notice that daily anomalies have been computed with respect to OND and JFM averages instead of using a smoothed daily climatology. The impact of this simplification is small because intraseasonal variability of daily winds is much higher than the variation in climatological mean wind speed during this 3-month period. Lagged stratifications (i.e., a number of days after strong MJO events occurred) have also been studied to account for Rossby wave propagation time. The statistical significance of the stratifications has been assessed with a two-tailed Student's t test with a confidence level of 95%.

First, 1981–2017 winds from ERA5 and MERRA2 have been stratified. The sensitivity to the analyzed period has been assessed comparing the whole period (1981–2017) to a shorter period (1998–2017). The impact of the MJO index definition (i.e., BoM or S2S index) has also been considered.

Then, wind speeds from the MFS have been stratified similarly, according to the forecasted (S2S) MJO index at several lead times. The S2S MJO indices are available separately for each of the 11 ensemble members of MFS hindcasts. Only the members that predict a strong MJO event are included in the stratification. Results have been grouped for forecast days 1 to 4, 5 to 11 (week 1), 12 to 18 (week 2), and so on, following the convention in Vitart (2004). In this case the anomalies have been computed with respect to a lead-time-dependent climatology (i.e., separately for each of the forecast weeks considered). As the forecasts have an ensemble available, the sample sizes for the MFS stratification are larger than for the observational stratification, impacting the statistical significance (i.e., weaker impacts are detected as significant).

2) MOST FREQUENT TERCILE MAPS

The mean value of a sample (employed in the stratifications) is not a very meaningful statistic and overly simplifies the sample distribution properties. For instance we can have many wind speed distributions with the same mean but differing variability. To overcome this limitation, observed tercile frequencies (frequency of above-normal, normal, and below-normal wind conditions) during strong MJO events complement the mean wind stratifications. Maps of the most frequently observed tercile display the occurrence frequency of the

tercile category that has occurred more times during each strong MJO phase. To construct these maps, first the 33rd and 66th percentiles of the 1981–2017 wind speed distribution are obtained for each grid point (separately for each month). Then the number of observations that are above, below, and within these thresholds is counted for all days in each strong MJO phase. This procedure has previously been used to present probabilistic climate predictions from large ensembles in a simplified way and overcome the dangers of using ensemble-mean anomalies (Jupp et al. 2012; Torralba et al. 2016).

3) Hybrid dynamical–statistical surface wind predictions

Under the hypothesis that MJO prediction is accurate at subseasonal time scales, but that the representation of teleconnection mechanisms is weak or defective in dynamical models, a hybrid dynamical–statistical method is proposed here. The method combines dynamical MJO forecasts with past observed relationships to reproduce the impact forecasts (wind speeds in this case) in a perfect prognosis approach. The aim is to produce a simple probabilistic forecast of daily mean wind speed in the form of tercile probabilities, mimicking typical subseasonal probabilistic products derived from ensemble prediction systems. The method uses observed tercile frequencies conditioned on the observation of an MJO phase [as in section 2b(2)] as forecast probabilities. If the forecasted MJO amplitude ($\widehat{\mathrm{MJO}}_{\mathrm{ampl}}$) is less than 2, then 1/3 of probability is assigned to each category. Otherwise when a strong MJO is anticipated, past observed frequencies for each tercile during the forecasted MJO phase ($\widehat{\mathrm{MJO}}_{\mathrm{ph}}$) are used as forecast. We call this method conditional climatology. For each day d it is computed as

$$\mathrm{clim}|_{\mathrm{MJO}}(d) = \begin{cases} \mathrm{clim}(x) & \text{if } \widehat{\mathrm{MJO}}_{\mathrm{ampl}}(d) < 2 \\ \mathrm{clim}(x|\mathrm{MJO}_{\mathrm{ph}}(x) = 1 \text{ and } \mathrm{MJO}_{\mathrm{ampl}}(x) \geq 2) & \text{if } \widehat{\mathrm{MJO}}_{\mathrm{ph}}(d) = 1 \text{ and } \widehat{\mathrm{MJO}}_{\mathrm{ampl}}(d) \geq 2 \\ \vdots & \\ \mathrm{clim}(x|\mathrm{MJO}_{\mathrm{ph}}(x) = 8 \text{ and } \mathrm{MJO}_{\mathrm{ampl}}(x) \geq 2) & \text{if } \widehat{\mathrm{MJO}}_{\mathrm{ph}}(d) = 8 \text{ and } \widehat{\mathrm{MJO}}_{\mathrm{ampl}}(d) \geq 2 \end{cases}, \quad (1)$$

where x are all days in the historical observational record and a hat represents a forecasted value. In the equation above, "clim" can be any climatology statistic, such as the mean (deterministic forecast), or tercile probabilities (probabilistic forecast), as employed here.

4) Verification of probabilistic forecasts

The forecasts of tercile probabilities that are produced with the conditional climatology method have been verified employing the ranked probability skill score (RPSS) (Jolliffe and Stephenson 2012), which is specifically designed for ordered multicategorical probabilistic forecasts. For each day, the observed tercile category is determined from ERA5 and used as verification truth. The RPSS compares the scores for the conditional climatology forecasts to the scores of a climatology (i.e., 33% of probability for each tercile category independently of the MJO status), and gives the relative improvement over this baseline: positive RPSS values denote better performance than climatology, with the value of one corresponding to a perfect forecast.

When using statistical models, and to obtain fair results, it is important that the verification is made with an independent sample that has not been employed during the model construction. The leave-one-out cross-validation technique (Wilks 2011) consists in repeating the training and verification steps multiple times by setting aside one observation each time that is not used for building the model and is reserved for verification only. This allows us to estimate the model parameters with all but one observations, and is suitable for small sample sizes. Specifically for the conditional climatology method, this means that the observed category for a given day is not included in the computation of the observed tercile frequencies used as forecast for that day.

3. Results

a. Observed teleconnection impacts

To characterize wind speed anomalies over Europe during strong MJO events, the daily mean ERA5 surface wind speeds have been stratified employing MJO time series [see section 2b(1) for details]. Figure 1 shows the JFM composite maps for both BoM and S2S observed MJO indices and for two different periods, 1981–2017 and 1998–2017. For the long period and the BoM index (first column) the 733 strong MJO events recorded in JFM are related to systematic anomalies over the North Atlantic ocean and Europe (around 10% to 15%, but up to ±40% in some cases), although those anomalies are located in different areas for each of the phases.

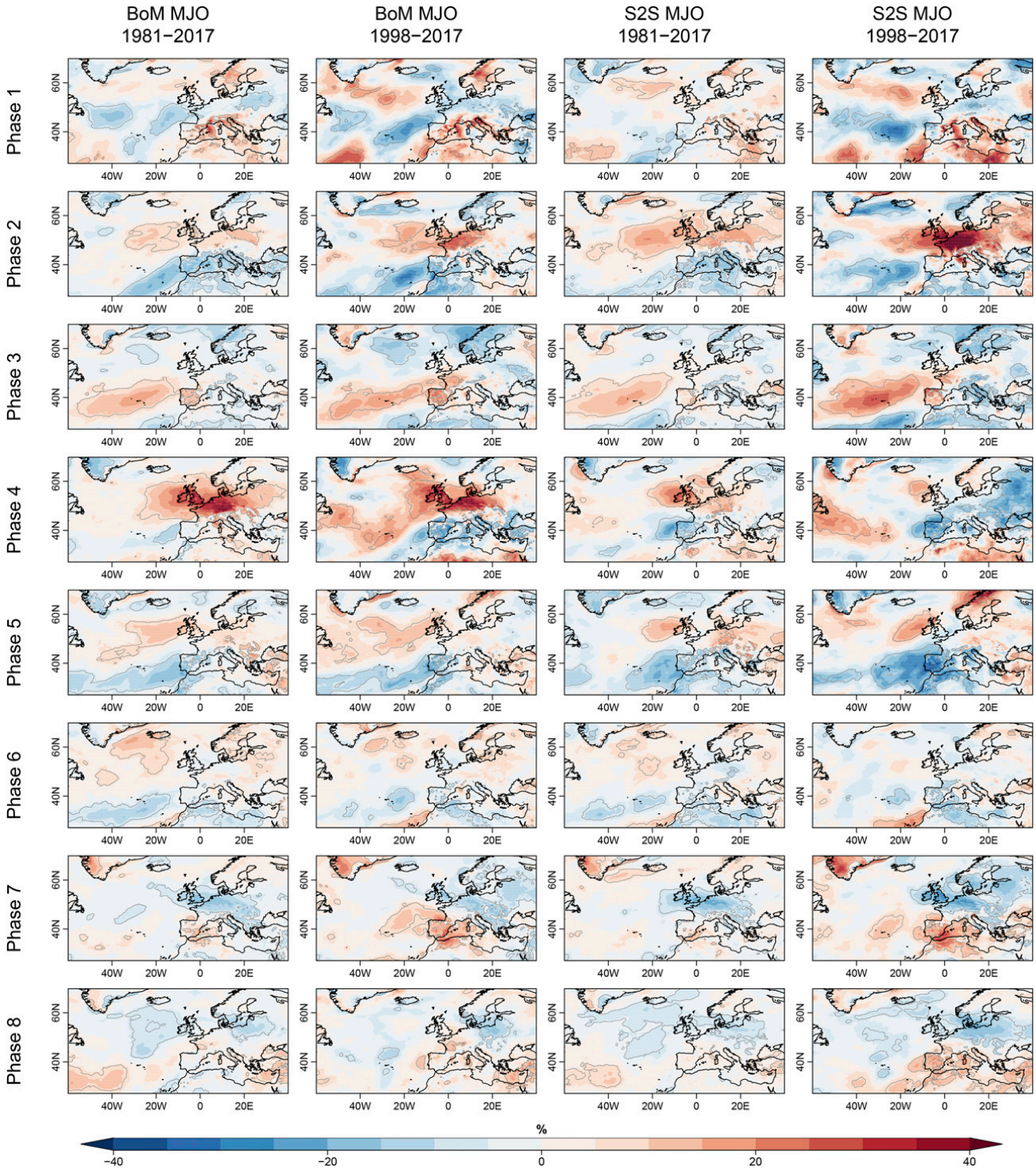

FIG. 1. JFM surface wind anomalies in Europe during strong MJO events (amplitude > 2) for each MJO phase (rows), expressed as a percentage of mean wind speed in the period. Columns show results for different periods and MJO indices: (first column),(second column) BoM MJO index and (third column),(fourth columns) S2S MJO index computed from ERA-Interim. Note that the first and third columns use a long period (1981–2017), while the second and fourth columns use a shorter period (1998–2017). Gray contours indicate statistical significance at the 95% level.

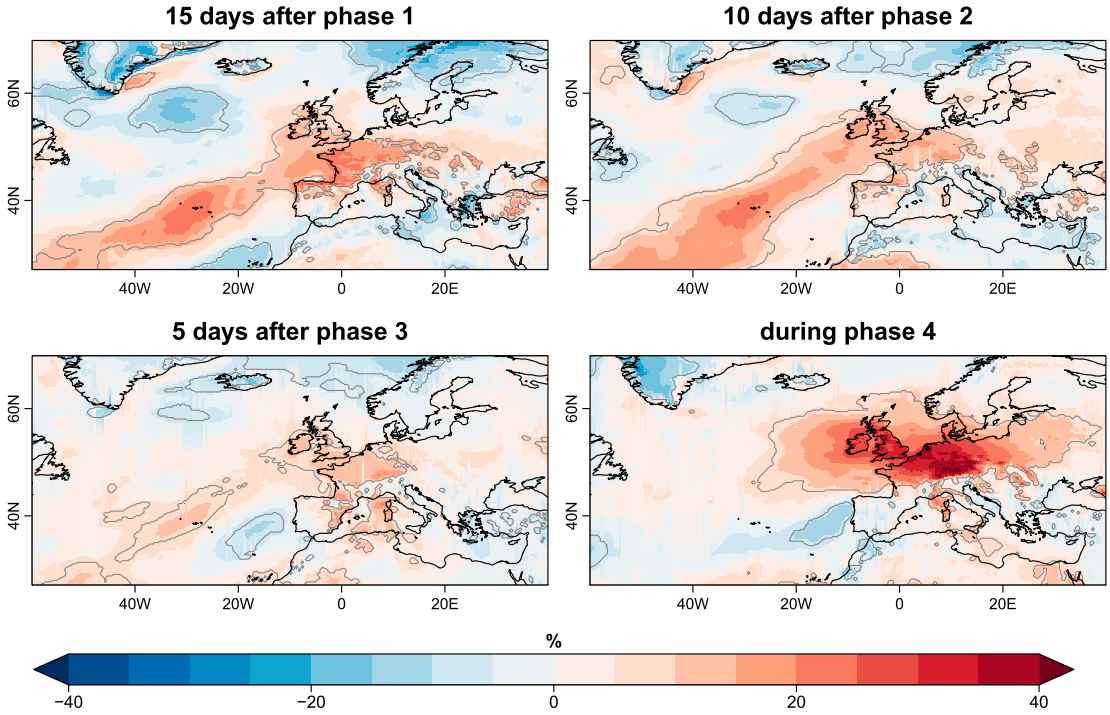

FIG. 2. JFM surface wind anomalies in Europe (top left) 15, (top right) 10, (bottom left) 5, and (bottom right) 0 days after strong MJO events (amplitude > 2) in phases 1, 2, 3, and 4, respectively, expressed as a percentage of mean wind speed in the 1981–2017 period and for the BoM MJO index. Gray contours indicate statistical significance at the 95% level.

In particular, during phase 4 (78 events), winds are 30% to 40% higher than average over the British Isles and central Europe, while during phase 7 (132 events) this region experiences weaker winds than average. Phase 1 also shows a strong signal over the western Mediterranean, with daily mean winds around 30% above average in some spots. The whole Iberian Peninsula is also affected by phases 2, 3, and 5. A similar analysis for 50- and 100-m winds—the heights at which wind turbines are typically installed— reveals the same anomaly patterns (see Figs. S1, S2). The number of strong events in each phase, and associated sea level pressure anomalies can also be seen in Figs. S1 and S2.

These results for BoM MJO index stratifications are in line with existing literature that shows that the atmospheric circulation in the Euro-Atlantic region in boreal winter is conditioned on the MJO (Lin et al. 2009; Cassou 2008). Indeed, the wind anomalies in the first column of Fig. 1 and the associated pressure patterns in Fig. S1 resemble various circulation patterns: phases 7 and 8 recall a negative NAO pattern or a Scandinavian blocking, while phases 2 to 5 bear a resemblance to positive NAO or east Atlantic patterns. Lin et al. (2009) and Cassou (2008) show that the NAO response to the MJO forcing is delayed between 5 and 15 days. The time scale of this teleconnection depends on "differing lengths of the teleconnection pathway for different MJO phases, differing propagation speeds of MJO events yielding differing teleconnection responses, and the NAE region simultaneously responding to multiple positions of MJO convection considering different lags" (Lee et al. 2019). However, lagged wind speed stratifications 5 to 15 days after strong MJO events produced weaker impacts. For instance, Fig. 2 shows lagged stratifications 15, 10, 5, and 0 days after phases 1, 2, 3, and 4, respectively. The anomalies seen during phase 4 are stronger than those seen the days after phases 1 to 3. On average, it takes around 5 days for the MJO to propagate from one phase to the next one. However, 15 days after a phase 1 strong MJO event only a small portion of days have a phase 4 strong MJO (see Fig. S7), and similarly, of all the days with a phase 4 strong MJO event only a few of them were in a phase 1 strong MJO 15 days before. This diversity of MJO events—differing MJO propagation but differing Rossby wave propagation as well (Wang et al. 2019; Zheng and Chang 2019)—difficult isolating the effects of the different lagged responses to the MJO phases.

Additionally, Fig. S3 provides a detailed analysis day by day of the lagged impacts of MJO phases for a single location near Frankfurt (a representative spot of NAO impact on wind). It can be seen how wind anomalies in

that location precede the initiation of MJO events in phase 1. This is also consistent with some research that found that the NAO can influence tropical winds in the Atlantic and African areas after some lag and initiate or amplify MJO events during phases 8 and 1 (Barnes et al. 2019; Lin et al. 2009). Indeed tropical winds have an active role in the MJO RMM computation, and sometimes large-scale circulation anomalies precede MJO convection (Liu et al. 2016; Straub 2013). Under all these circumstances, it is important to note that the stratification results presented cannot distinguish causality links between MJO activity and extratropical wind speed anomalies. Despite not knowing the exact reasons behind the strong wind anomalies that accompany strong phase 4 MJO events, that information can still be useful for statistical modeling (section 3f).

b. *Sensitivity to period and index definition*

Although the BoM index is typically used in the majority of works that study observed MJO teleconnections and impacts (e.g., Cassou 2008; Lin et al. 2009; Zhang 2013), most of the work focusing on MJO forecasting (and in particular the S2S project) employs a computation variant described in Gottschalck et al. (2010). As the present work combines both of the worlds, the observed impact has also been assessed employing the S2S ERA-Interim-derived index for the 1981–2017 period (third column in Fig. 1). Wind speed from these stratifications bears some resemblance to the results obtained with the BoM stratifications (first column). However, in general the values are smaller and the patterns have important differences at the regional scale. An analysis of the days that are classified as strong MJO events by each of the two indices has been performed (see Fig. S4), and although the bivariate correlation (Lin et al. 2008; Rashid et al. 2010) between both MJO indices is 0.90, and its amplitudes have a Pearson correlation of 0.81, the days included in each strong MJO phase category are very different for both indices, resulting in the discrepancies aforementioned.

Figure 1 also presents the stratifications for a shorter period (that will be used later in section 3d for the MFS hindcasts). We find that the results are also sensitive to the sample period, and reducing the number of years (differences between first and second columns, or between the third and fourth columns) produces some differences in pattern position and magnitude (e.g., see phase 2 in central Europe or phase 4 in the Iberian Peninsula). Conversely, the results are not sensitive to the observational wind speed dataset employed, and stratifications made with MERRA2 show almost identical results (Figs. S1, S2). These results are useful for the interpretation of the quality of the prediction-based wind speed stratification results in section 3d.

c. *Distribution of wind speed values under strong MJO events*

The stratifications presented so far show the mean wind speed anomalies associated with strong MJO events but do not inform about the full distribution of observed values during each MJO phase. To exemplify this, the whole distribution of daily mean wind speed values associated with each strong MJO phase (according to BoM index) is shown in Fig. 3 for a grid point over Frankfurt (49.88°N, 8.44°E). The selected location is a spot of high correlation between the NAO and surface wind, and therefore it is a good representative of the interactions between the NAO and the MJO. To better understand how those distributions differ from the whole-period climatology, the 10th, 33rd, 66th, and 90th percentiles of the climatology (referred as P10, P33, P66, and P90, respectively) have been used to color the distributions and compute tercile occurrence frequencies. For instance, for phase 4 most of the daily wind speed values (61%) fall above P66, with a 31% of values above P90. But for phase 1, the normal category (between P33 and P66) is the most frequent category indicating that either high or low wind speeds are less frequent under this MJO phase. This figure also shows that although the MJO can influence the wind speed over Europe, the teleconnective mechanism is not straightforward, and other elements can interact with it and determine the final wind speed values [such as the phase of the quasi-biennial oscillation (Lim et al. 2019; Zhang and Zhang 2018), the strength of the stratospheric polar vortex (Barnes et al. 2019), the ENSO phase (Lee et al. 2019), or the intensity and location of the westerly subtropical jet that guides Rossby wave propagation (Adames and Wallace 2014)].

To summarize part of the information presented in Fig. 3 in a map but still include more information on the distribution that just its mean value, the most frequent tercile maps of the wind speed have been produced for each MJO phase (see Fig. 4). The maps present the observed frequency of the most frequent tercile at each point and for each MJO phase [see section 2b(2)]. Those plots are more informative than the mean anomaly. The plots have been produced for the whole globe to highlight the connections between tropical winds (which are employed in the computation of MJO) and wind anomalies over the extratropics. Phases 4 and 5 tend to be associated with above normal-wind speed conditions in the tropics while during phases 8 and 1 the tropics are more likely to experience weak (below-normal) winds. The patterns that were described in Fig. 1 for Europe

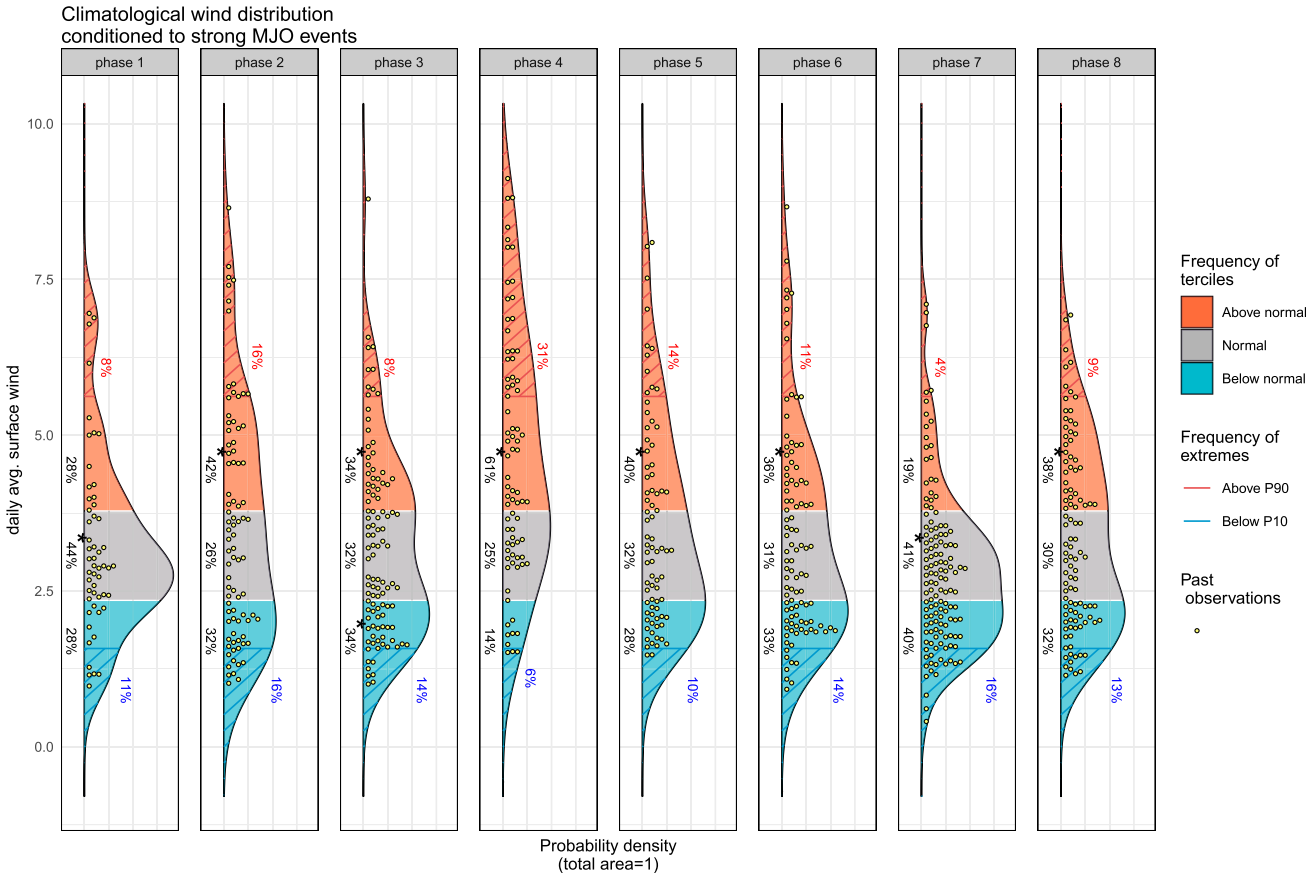

FIG. 3. Observed (ERA5, 1981–2017) daily mean wind speed distribution near Frankfurt (49.88°N, 8.44°E) for each of the eight MJO phases when amplitude is higher than 2 according to BoM index. Frequencies of occurrence of the tercile categories below-normal, normal, and above-normal conditions have been colored in red, gray, and blue, respectively, and annotated, while red (blue) stripes indicate frequency of exceeding (not reaching) the 90th percentile (10th percentile). Yellow dots indicate individual daily observations. A star indicates the most frequent tercile category.

can be seen here as well, with a high frequency of above-normal conditions during phase 4 over central Europe, or a high frequency of below-normal conditions over the Iberian Peninsula during phase 2. Important connections can be seen as well in North America and other extratropical regions, although those have not been explored further in this paper.

d. Teleconnection impacts in the subseasonal simulations

To understand the ability of ECMWF subseasonal forecasts to reproduce the observed MJO impacts over Europe, the stratifications have been applied also to the MFS forecasts at different forecast times, employing the MFS MJO forecasts from S2S. Figure 5 compares the results for forecast days 1 to 4, 5 to 11 (week 1), and 12 to 18 (week 2) with reanalysis (ERA5) winds stratified with the S2S MJO ERA-Interim index. The results are shown for phases 2, 5, and 7 only, which are the phases with stronger impacts over Europe for the S2S MJO index (see last column of Fig. 1). The impacts for the first 4 days of forecasts resemble the observed patterns, although amplitudes are weaker. With longer forecast times (weeks 1 and 2) the impacts become even weaker, that is, for those days where the model predicts a strong MJO event 1 or 2 weeks ahead, the associated wind speed predictions over Europe do not reproduce the expected teleconnection effects beyond week 2. Those results are in agreement with Vitart's (2017) Figs. 7 and 8. From this we conclude that MFS is not able to reproduce the MJO teleconnection impacts over European wind speeds more than a couple of weeks ahead.

e. Verification of subseasonal forecasts of strong MJO events

In view of the limited ability of the ECMWF subseasonal predictions to reproduce the expected wind speed impacts of MJO over Europe, the conditional climatology method described in section 2b(3) can be used to combine dynamic MJO forecasts with its

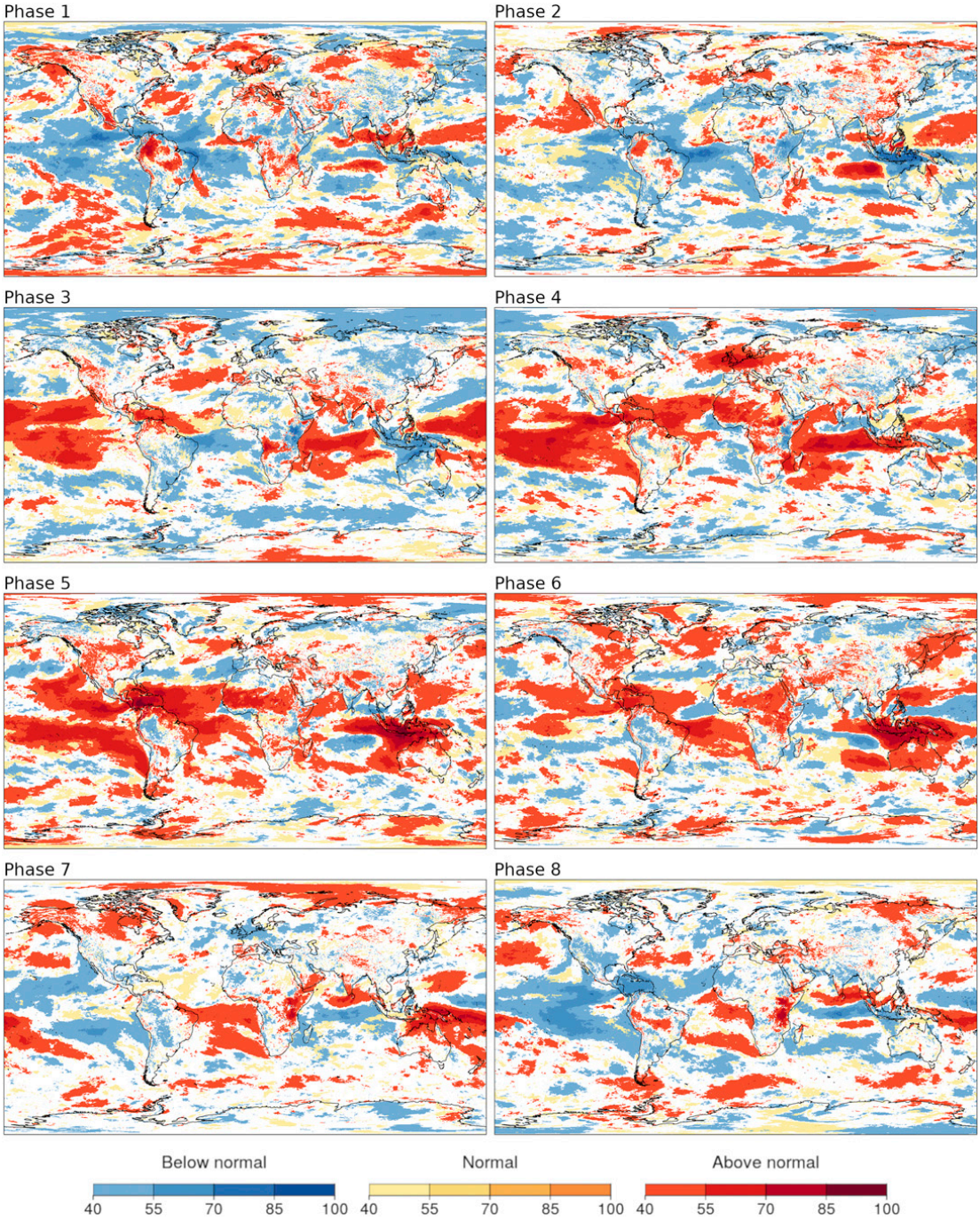

FIG. 4. Global maps of most frequently observed tercile during strong MJO events for each of its phases. The distribution of daily mean wind speed values from ERA5 in JFM 1981–2017 is analyzed according to the BoM MJO index. At each grid point and for each MJO phase, individual values of the distribution are grouped in three tercile categories (above-normal, normal, and below-normal wind speed conditions) and the frequency of each category is computed. The color indicates the most frequently observed tercile category, while color intensity indicates its associated frequency of occurrence.

observed wind speed impacts. As a first step, the quality of the MJO forecasts needs to be assessed. Many studies of MJO forecast verification employ the forecast time at which bivariate correlation goes below 0.5 (Lin et al. 2008; Lim et al. 2018; Vitart 2017) as a threshold of a skillful prediction, and for MFS they show skill up to 36 days ahead. But in order to employ MJO forecasts from the S2S database with the conditional climatology method, we need to understand how accurate the forecasts are for each of the strong MJO phases. That could

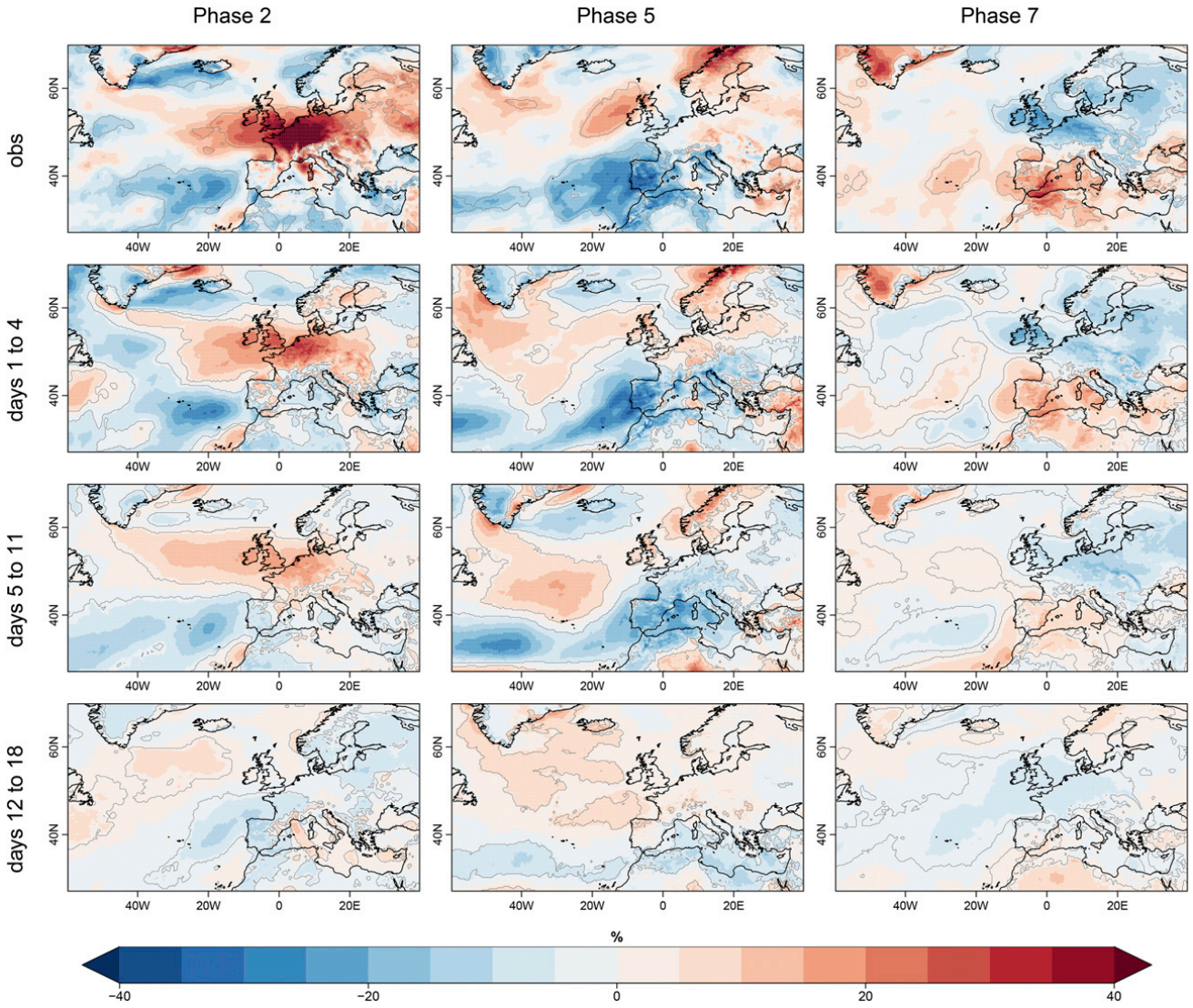

FIG. 5. Surface wind stratifications for phases (left) 2, (center) 5, and (right) 7 from ERA5 and MFS in JFM 1998–2017. (first row) Observed teleconnection impacts as seen in ERA5 (as in last column of Fig. 1). (second to fourth rows) Predicted impacts in MFS for days 1 to 4, 5 to 11 (week 1), and 12 to 18 (week 2), respectively. Gray contours indicate statistical significance at the 95% level.

be done through contingency tables for each of the phases. Instead of that, a more visual verification is proposed here, employing parallel sets plots (Kosara et al. 2006). In Fig. 6 each panel presents the verification for a different range of forecast times. The information of all the contingency tables for each forecast time group can be seen at once in the plot, but the graph also allows to understand phase errors. All the lines that connect one category on the left (forecasts) to the same category on the right (observations) are the hits. All the lines that point toward the Ampl < 2 category are false alarms, while the lines that emerge from Ampl < 2 are misses. Phase errors (lines connecting one strong MJO category to another one) have to be counted also as misses and false alarms, but this graphical separation is more meaningful than the contingency table. Correct rejections (Ampl < 2 to Ampl < 2) have been omitted in these figures, because they are much more numerous (representing an 83% of the total) and are indeed meaningless to our purposes.

For short forecast times from 1 to 4 days ahead, there are a good amount of hits for all the phases but for phase 4. The number of false alarms is quite small with the misses being especially noticeable for phase 3. When moving to longer forecast times, the number of misses grows substantially, while the false alarms are reduced. By week 1 (days 5 to 11) the number of misses is more than 40% (excluding the correct rejections in the total) and by week 3 (days 19 to 25) the number of hits is reduced to almost nothing. MJO propagation in most

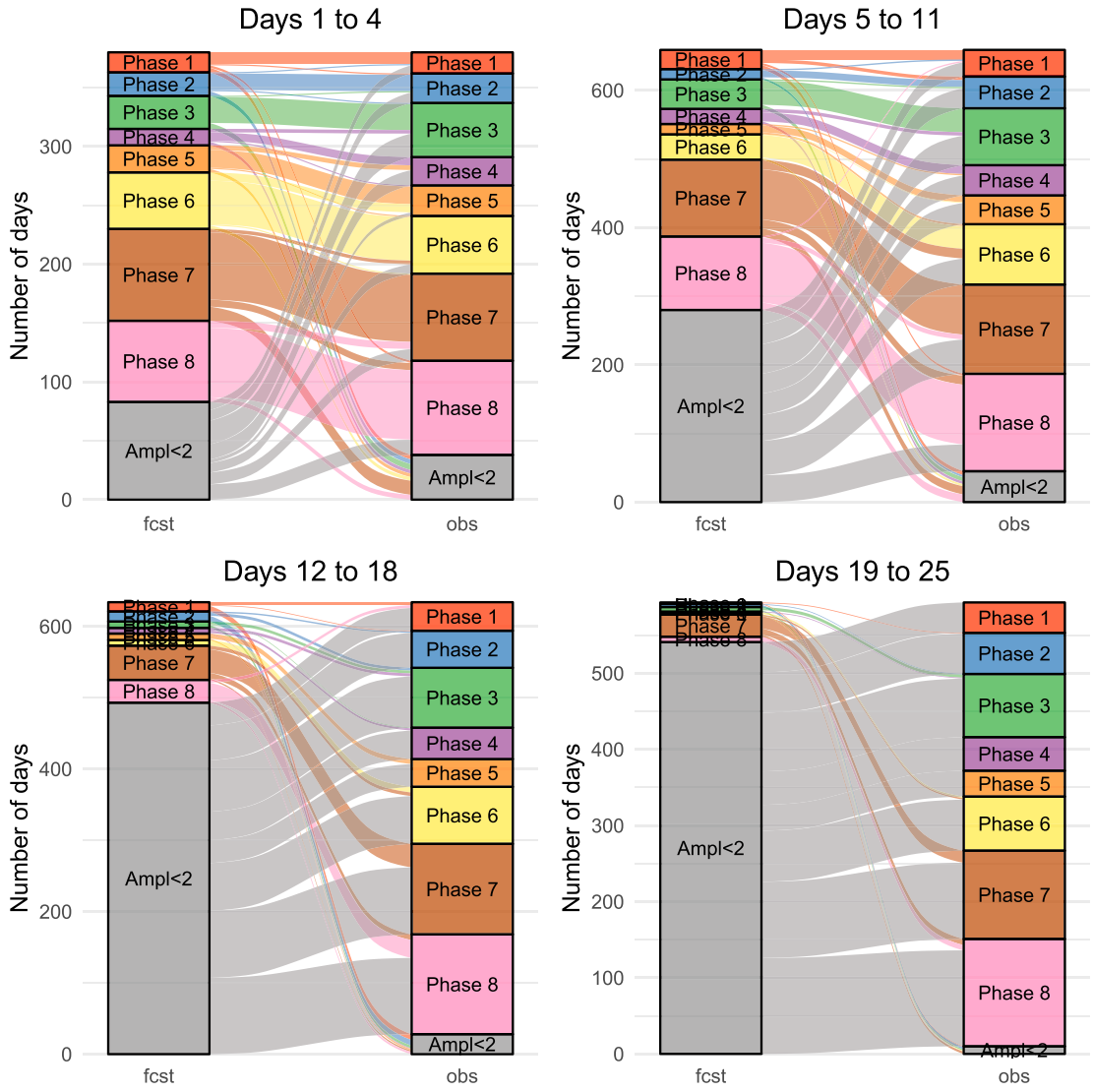

FIG. 6. Verification of ECMWF MFS 2018 categorical forecasts of strong MJO events at four different forecast time ranges: days (top left) 1–4, (top right) 5–11, (bottom left) 12–18, and (bottom right) 19–25. The forecast category is determined from the ensemble-mean S2S MJO forecast, and the observed category is determined from the S2S ERA-Interim-derived MJO index. Each panel employs a parallel sets graph to illustrate correspondence between forecasts on the left side and observations on the right side. The width of the lines is proportional to the number of days in each correspondence relationship. Correct rejections (i.e., lines connecting Ampl < 2 to Ampl < 2) have been omitted for clarity.

subseasonal forecast systems (including MFS) is known to be too slow and to have weaker amplitude than observed (Vitart 2017). These biases can lead to the aforementioned weak skill for strong MJO events. The fact that ensemble-mean fields are being employed to compute MJO forecasts can also affect the amplitudes, as there is some cancellation from individual members before computing the RMM components. However, analyzing the individual ensemble member forecasts does not produce better results (see Fig. S5). In conclusion, although MFS MJO forecasts are skillful in terms of bivariate correlation up to 36 days ahead, the MFS cannot provide a good categorical forecast of wind speed for strong MJO events unless the MJO forecasts are more realistic in their phase and amplitude.

f. Conditional climatology under perfect knowledge of MJO

The previous section has shown that for lead times of more than 10 days the number of correct forecasts of strong MJO events (i.e., the hits) is low. Therefore, employing these forecasts with the conditional climatology method would produce very marginal benefits only, because the method would be issuing climatology

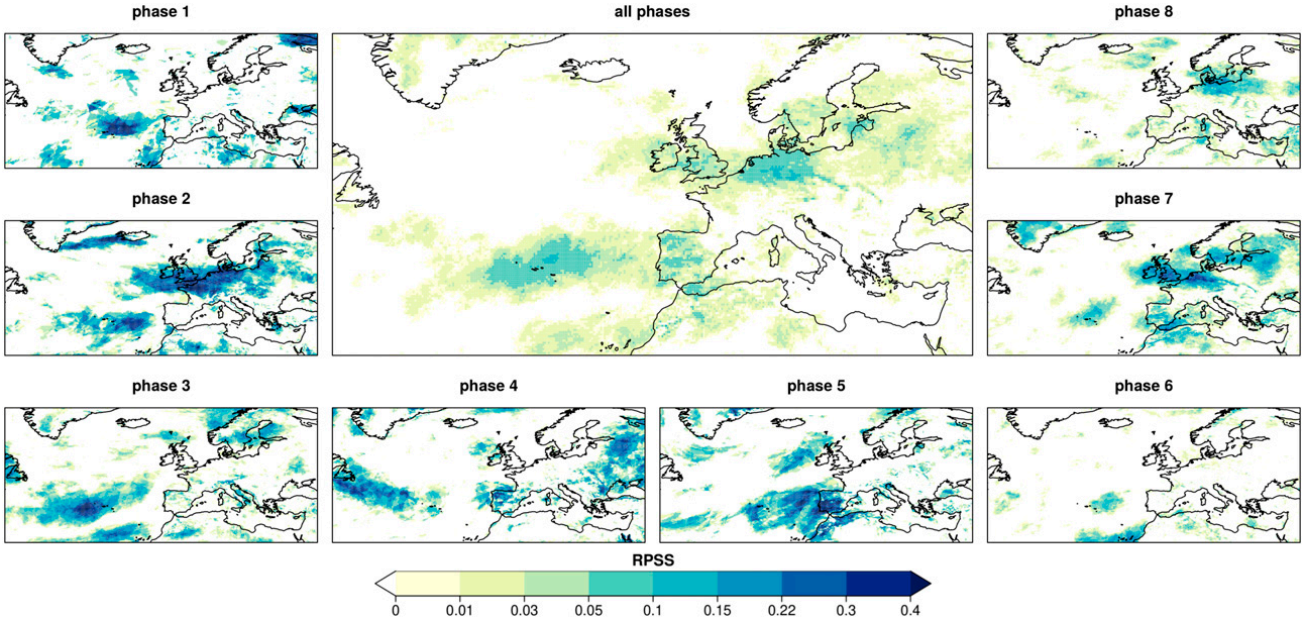

FIG. 7. Ranked probability skill scores of the conditional climatology forecasts under perfect knowledge of the MJO state, (left), (bottom),(right) verified separately for all the days in each MJO phase, and (center) for all the strong MJO events regardless of the MJO phase. Positive values indicate better performance than the benchmark, with 1 representing a perfect forecast.

probabilities for almost all the days. To illustrate the potential that this simple method can bring, it has been used here assuming perfect knowledge of MJO status to produce an upper bound of its skill. MJO forecasts are only made available for the S2S index, therefore for consistency the method is employed with observed terciles conditioned to S2S ERAI-derived MJO index for the 1998–2017 period. The method issues probabilities for tercile categories, and therefore the skill assessment employs the RPSS metric [see section 2b(4)]. Figure 7 shows the RPSS of the conditional climatology predictions for all the days under a strong MJO, and separately for each of the phases. Positive skills (i.e., better performance than climatology) can be seen for all phases in the regions where the observed tercile frequencies differ appreciably from the climatology. The skill reaches values higher than 0.35 over central Europe for phase 2 and 7 or over the Iberian Peninsula for phase 5. When looking at the skill for all days with a strong MJO, values up to 0.1 remain in many parts of Europe, with a pattern that spans the central latitudes of Europe and the Iberian Peninsula. The number of days with a strong MJO (733) is small compared to the whole JFM 1981–2017 sample, representing 22%. Then, when considering the skill for the whole period, the regular climatology dominates the forecasts and the gains that are made during the strong MJO days are diluted (not shown). However, the results show that there is a window of opportunity for employing this method during the days when the MJO is predicted to be in a strong amplitude, although better MJO forecasts for strong events would be needed for longer forecast times.

4. Conclusions

Deep convection in the tropics is connected to extratropical anomalies of surface wind speed at different time scales through Rossby wave propagation. For instance, convection associated with ENSO or the North Pacific mode influences wind speed in North America at seasonal time scales (Lledó et al. 2018). The MJO associated convection moves eastward at a pace of around 5° of longitude per day, offering an opportunity to analyze its extratropical impacts. An analysis of simultaneous wind speeds over Europe during strong MJO episodes using reanalyses has revealed that large wind anomalies do exist. Their location and strength are a function of the MJO phase, although there are considerable variations among individual events. For instance, recent studies have shown that the MJO teleconnection to Europe can vary substantially with the ENSO phase, which impacts MJO propagation speed (Lee et al. 2019; Wang et al. 2019). The relationship between the phase of strong MJO events and surface wind speed over Europe is a source of predictability that could be employed by the wind energy sector.

Stratifications of wind speed predictions from ECMWF MFS have shown that this subseasonal prediction system is not able to accurately reproduce the expected MJO teleconnection impacts in wind speed over Europe for

lead times of more than 10 days (i.e., whenever a member of the MFS anticipates a strong MJO event more than 10 days ahead the simultaneous wind speed anomalies over Europe do not resemble those observed in the past records). To overcome this limitation, which is also found in other prediction systems (Vitart 2017), a hybrid dynamical–statistical model that combines MJO dynamical forecasts with the observed impacts of the MJO has been proposed. The method employs observed frequencies of above-normal, normal, and below-normal wind speeds during strong MJO events as probabilistic forecasts whenever a strong MJO event is anticipated. This method—named conditional climatology—has been tested under perfect knowledge of the MJO state, showing that it has the potential to deliver categorical probabilistic predictions of daily mean wind speed that are better than the reference climatology in many European regions. However, although MFS can skillfully predict the MJO evolution up to 36 days ahead in terms of bivariate correlation, strong MJO events cannot be skillfully predicted more than 10 days ahead. The inability to anticipate strong MJO events poses a barrier to the effective application of this method.

In summary this research has shown that 1) strong MJO events have an effect on surface winds in Europe; 2) analyzing the most frequently observed terciles under each MJO phase provides a more robust analysis of the diversity of MJO impacts; 3) the BoM and S2S MJO indices produce significant differences in terms of strong MJO events; 4) the MFS cannot anticipate strong MJO events more than 10 days ahead; and 5) an hybrid statistical–dynamical method could deliver good performance levels weeks ahead if better predictions for strong MJO events were available. Overall, this research highlights the relevance of tropical–extratropical interactions for enhancing subseasonal predictions in the extratropics, and for anticipating surface conditions that impact climate-vulnerable sectors weeks ahead. This paper illustrates that the MJO plays a limited role in defining the daily wind speed in Europe, even if its features were much better predicted by future subseasonal forecast systems. Hence, the usefulness of subseasonal predictions for sectors vulnerable to surface wind variability requires paying attention to the multiple factors that determine the atmospheric circulation in the area at those time scales.

Acknowledgments. The research leading to these results has received funding from the European Union's Horizon 2020 research and innovation program under Grant 776787 (S2S4E) and from the Ministerio de Ciencia, Innovación y Universidades (MICINN) as part of the CLINSA project (CGL2017-85791-R). The authors acknowledge Australian Bureau of Meteorology for providing the MJO RMM historical indices, and the S2S project for providing the MJO indices from ECMWF MFS forecasts and ERA-Interim. The authors want to thank Nicolau Manubens for technical support with the startR R package, which allows processing big memory arrays by chunks in a cluster and then merges the results back together. Many analyses would have not been possible without this package. The CSTools R package was also used to produce some figures. Pierre-Antoine Bretonnière and Margarida Samsó helped downloading and formatting the surface wind datasets. The authors want to thank Frederic Vitart and Laura Ferranti for helping with the interpretation of some results, and Verónica Torralba for helping to structure the material.

REFERENCES

Adames, Á. F., and J. M. Wallace, 2014: Three-dimensional structure and evolution of the MJO and its relation to the mean flow. *J. Atmos. Sci.*, **71**, 2007–2026, https://doi.org/10.1175/JAS-D-13-0254.1.

Barnes, E. A., S. M. Samarasinghe, I. Ebert-Uphoff, and J. C. Furtado, 2019: Tropospheric and stratospheric causal pathways between the MJO and NAO. *J. Geophys. Res. Atmos.*, **124**, 9356–9371, https://doi.org/10.1029/2019jd031024.

Cassou, C., 2008: Intraseasonal interaction between the Madden–Julian Oscillation and the North Atlantic oscillation. *Nature*, **455**, 523–527, https://doi.org/10.1038/nature07286.

Copernicus Climate Change Service (C3S), 2017: ERA5: Fifth generation of ECMWF atmospheric reanalyses of the global climate. Copernicus Climate Change Service Climate Data Store (CDS), accessed 1 June 2019, https://cds.climate.copernicus.eu/cdsapp#!/home.

Dee, D. P., and Coauthors, 2011: The ERA-Interim reanalysis: Configuration and performance of the data assimilation system. *Quart. J. Roy. Meteor. Soc.*, **137**, 553–597, https://doi.org/10.1002/qj.828.

ECMWF, 2019: The ECMWF monthly forecasting system. ECMWF, accessed 15 May 2019, https://www.ecmwf.int/en/forecasts/documentation-and-support/extended-range-forecasts/ecmwf-monthly-forecasting-system.

Gelaro, R., and Coauthors, 2017: The Modern-Era Retrospective Analysis for Research and Applications, version 2 (MERRA-2). *J. Climate*, **30**, 5419–5454, https://doi.org/10.1175/JCLI-D-16-0758.1.

Gottschalck, J., and Coauthors, 2010: A framework for assessing operational Madden–Julian Oscillation forecasts. *Bull. Amer. Meteor. Soc.*, **91**, 1247–1258, https://doi.org/10.1175/2010BAMS2816.1.

Jolliffe, I. T., and D. B. Stephenson, Eds., 2012: *Forecast Verification: A Practitioner's Guide in Atmospheric Science*. 2nd ed. John Wiley & Sons, 274 pp., https://doi.org/10.1002/9781119960003.

Jupp, T. E., R. Lowe, C. A. S. Coelho, and D. B. Stephenson, 2012: On the visualization, verification and recalibration of ternary probabilistic forecasts. *Philos. Trans. Roy. Soc.*, **A370**, 1100–1120, https://doi.org/10.1098/rsta.2011.0350.

Kalnay, E., and Coauthors, 1996: The NCEP/NCAR 40-Year Reanalysis Project. *Bull. Amer. Meteor. Soc.*, **77**, 437–471, https://doi.org/10.1175/1520-0477(1996)077<0437:TNYRP>2.0.CO;2.

Kim, H., M. A. Janiga, and K. Pegion, 2019: MJO propagation processes and mean biases in the SubX and S2S reforecasts. *J. Geophys. Res. Atmos.*, **124**, 9314–9331, https://doi.org/10.1029/2019jd031139.

Kosara, R., F. Bendix, and H. Hauser, 2006: Parallel sets: Interactive exploration and visual analysis of categorical data. *IEEE Trans. Vis. Comput. Graph.*, **12**, 558–568, https://doi.org/10.1109/TVCG.2006.76.

Lee, R. W., S. J. Woolnough, A. J. Charlton-Perez, and F. Vitart, 2019: ENSO modulation of MJO teleconnections to the north Atlantic and Europe. *Geophys. Res. Lett.*, **46**, 13 535–13 545, https://doi.org/10.1029/2019GL084683.

Lim, Y., S.-W. Son, and D. Kim, 2018: MJO prediction skill of the subseasonal-to-seasonal prediction models. *J. Climate*, **31**, 4075–4094, https://doi.org/10.1175/JCLI-D-17-0545.1.

——, ——, A. G. Marshall, H. H. Hendon, and K.-H. Seo, 2019: Influence of the QBO on MJO prediction skill in the subseasonal-to-seasonal prediction models. *Climate Dyn.*, **53**, 1681–1695, https://doi.org/10.1007/s00382-019-04719-y.

Lin, H., G. Brunet, and J. Derome, 2008: Forecast skill of the Madden–Julian Oscillation in two Canadian atmospheric models. *Mon. Wea. Rev.*, **136**, 4130–4149, https://doi.org/10.1175/2008MWR2459.1.

——, ——, and ——, 2009: An observed connection between the North Atlantic Oscillation and the Madden–Julian oscillation. *J. Climate*, **22**, 364–380, https://doi.org/10.1175/2008JCLI2515.1.

Liu, P., Q. Zhang, C. Zhang, Y. Zhu, M. Khairoutdinov, H.-M. Kim, C. Schumacher, and M. Zhang, 2016: A revised real-time multivariate MJO index. *Mon. Wea. Rev.*, **144**, 627–642, https://doi.org/10.1175/MWR-D-15-0237.1.

Lledó, L., O. Bellprat, F. J. Doblas-Reyes, and A. Soret, 2018: Investigating the effects of Pacific sea surface temperatures on the wind drought of 2015 over the United States. *J. Geophys. Res. Atmos.*, **123**, 4837–4849, https://doi.org/10.1029/2017JD028019.

Madden, R. A., and P. R. Julian, 1971: Detection of a 40–50 day oscillation in the zonal wind in the tropical Pacific. *J. Atmos. Sci.*, **28**, 702–708, https://doi.org/10.1175/1520-0469(1971)028<0702:DOADOI>2.0.CO;2.

——, and ——, 1972: Description of global-scale circulation cells in the tropics with a 40–50 day period. *J. Atmos. Sci.*, **29**, 1109–1123, https://doi.org/10.1175/1520-0469(1972)029<1109:DOGSCC>2.0.CO;2.

Ramon, J., L. Lledó, V. Torralba, A. Soret, and F. J. Doblas-Reyes, 2019: What global reanalysis best represents near-surface winds? *Quart. J. Roy. Meteor. Soc.*, **145**, 3236–3251, https://doi.org/10.1002/qj.3616.

Rashid, H. A., H. H. Hendon, M. C. Wheeler, and O. Alves, 2010: Prediction of the Madden–Julian Oscillation with the POAMA dynamical prediction system. *Climate Dyn.*, **36**, 649–661, https://doi.org/10.1007/s00382-010-0754-x.

Soret, A., and Coauthors, 2019: Sub-seasonal to seasonal climate predictions for wind energy forecasting. *J. Phys. Conf. Ser.*, **1222**, 012009, https://doi.org/10.1088/1742-6596/1222/1/012009.

Straub, K. H., 2013: MJO initiation in the real-time multivariate MJO index. *J. Climate*, **26**, 1130–1151, https://doi.org/10.1175/JCLI-D-12-00074.1.

Torralba, V., 2019: Seasonal climate prediction for the wind energy sector: Methods and tools for the development of a climate service. Ph.D. thesis, Universidad Complutense de Madrid, 296 pp.

——, F. J. Doblas-Reyes, I. Jiménez, L. Lledó, N. González-Reviriego, and A. Soret, 2016: Development of a wind energy climate service based on seasonal climate prediction. *Third BSC Int. Doctoral Symp.*, Barcelona, Spain, Barcelona Supercomputing Center, 43–45, https://doi.org/10.13140/rg.2.2.18352.15362.

Vitart, F., 2004: Monthly forecasting at ECMWF. *Mon. Wea. Rev.*, **132**, 2761–2779, https://doi.org/10.1175/MWR2826.1.

——, 2017: Madden–Julian Oscillation prediction and teleconnections in the S2S database. *Quart. J. Roy. Meteor. Soc.*, **143**, 2210–2220, https://doi.org/10.1002/qj.3079.

——, and Coauthors, 2017: The Subseasonal to Seasonal (S2S) prediction project database. *Bull. Amer. Meteor. Soc.*, **98**, 163–173, https://doi.org/10.1175/BAMS-D-16-0017.1.

Wang, B., G. Chen, and F. Liu, 2019: Diversity of the Madden–Julian Oscillation. *Sci. Adv.*, **5**, eaax0220, https://doi.org/10.1126/sciadv.aax0220.

Wheeler, M. C., and H. H. Hendon, 2004: An all-season real-time multivariate MJO index: Development of an index for monitoring and prediction. *Mon. Wea. Rev.*, **132**, 1917–1932, https://doi.org/10.1175/1520-0493(2004)132<1917:AARMMI>2.0.CO;2.

Wilks, D. S., Ed., 2011: Statistical forecasting. *Statistical Methods in the Atmospheric Sciences*, Academic Press, 215–300.

Zhang, C., 2005: Madden–Julian Oscillation. *Rev. Geophys.*, **43**, RG2003, https://doi.org/10.1029/2004RG000158.

——, 2013: Madden–Julian Oscillation: Bridging weather and climate. *Bull. Amer. Meteor. Soc.*, **94**, 1849–1870, https://doi.org/10.1175/BAMS-D-12-00026.1.

——, and B. Zhang, 2018: QBO–MJO connection. *J. Geophys. Res. Atmos.*, **123**, 2957–2967, https://doi.org/10.1002/2017JD028171.

Zheng, C., and E. K. M. Chang, 2019: The role of MJO propagation, lifetime, and intensity on modulating the temporal evolution of the MJO extratropical response. *J. Geophys. Res. Atmos.*, **124**, 5352–5378, https://doi.org/10.1029/2019JD030258.

MONTHLY WEATHER REVIEW

Supplementary material for "Predicting daily mean wind speed in Europe weeks ahead from MJO status"

LLORENÇ LLEDÓ*

Barcelona Supercomputing Center

FRANCISCO J. DOBLAS-REYES
Barcelona Supercomputing Center and ICREA

1. Stratifications of wind speed at higher heights

Currently, most of the installed wind turbines have hub heights between 60 and 120 m above ground. Therefore it is important to analyze the impact of strong MJO events on wind speed at those levels. Stratifications of wind speeds at 100 m from ERA5 (figure S2) and at 50 m from MERRA2 (figure S1) have been prepared using the BoM MJO index. The results show a striking similarity between the percentage anomalies at different heights, even across different reanalysis datasets. Also, those results are very consistent with the surface anomalies reported in first column of figure 1 in the main text. Sea level pressure anomalies from ERA5 and MERRA2 (green contours in figures S2 and S1 respectively) confirm the consistency of patterns across different datasets.

2. Lagged impacts of MJO activity

Figure S3 shows surface wind stratifications for a grid point over Frankfurt from 20 days before to 20 days after strong MJO events occurred. Negative lags indicate wind speeds a number of days before a strong MJO event (i.e. wind leading the MJO) while positive lags indicate wind speed anomalies a number of days after a strong MJO event (lagged wind response to MJO activity). The selected location is a spot of high correlation between NAO and surface wind, and therefore the figure displays the interactions between NAO and MJO. Stronger wind speeds follow 5 to 15 days after phases 2/3, while weaker winds occur 5 to 10 days after phase 6. This is in agreement with higher probabilities of having a positive NAO phase after MJO phases 2/3 and higher probabilities of a negative NAO phase after MJO phase 6 as shown in Cassou (2008). The figure also shows that wind speed anomalies in Europe precede strong phase 1 MJO events. This has also been described recently in Barnes et al. (2019), where they show that the NAO and the stratospheric polar vortex can be precursors of phase 1 MJO events.

3. Differences between BoM and S2S indices at representing strong MJO events

The differences between strong MJO events according to S2S and BoM indices have been explored through a Parallel Sets graph (Kosara et al. 2006). Figure S4 shows how the fraction of days distributed in each of the strong MJO phases according to the BoM index (left) relate to the same categories but derived from the S2S index (right) for the 1981–2018 period. For all the phases, there is a notable portion of the days that are classified as strong events only by one of the two indices (all lines emerging from or arriving to the Ampl$<$2 category). This produces most of the differences seen in figure 1 of the main manuscript. Regarding the days that are classified as strong in both datasets there is a fair correspondence in the indicated phase, but a small portion of days in strong MJO events according to BoM index correspond to the previous phase according to S2S index, indicating a small systematic phase shift. An even smaller portion corresponds to the next phase.

4. Skill of MJO forecasts from individual members

Figure S5 compares the verification of MJO forecasts obtained from the ensemble mean and from the individual members. When employing individual ensemble member MJO forecasts, the number of misses decreases substantially, but at expenses of increasing the number of false alarms. The number of hits does not change substantially, and with more false alarms this would produce worse results with the conditional climatology methodology.

5. Analysis of the threshold employed to define strong MJO events

All the stratifications and analyses in this paper are sensitive to the amplitude threshold that has been used to

* *Corresponding author address:* Barcelona Supercomputing Center, c/ Jordi Girona 29 08008 Barcelona, Spain.
E-mail: lledo@bsc.es

classify MJO strong events (i.e. amplitude>2). Grouping the analysis results by phase is also arbitrary somehow. Looking at wind anomalies for both RMM components of the MJO can reveal some details that are hidden in the stratifications. Figure S6 presents the mean anomalies over Germany, France, Iberian Peninsula and British Isles (averaging all grid points within each region) in a phase space diagram. Hypothetically, the strongest MJO events (larger convection) will impart more forcing to extratropical winds. Reducing the thresholds would enlarge the sample size at the cost of including situations where the impacts were not pronounced or at least not consistent.

6. Analysis of the time evolution of strong MJO events

An analysis of the transitions between strong MJO events is presented in figure S7. The central coloured column displays all the days that belong to each strong MJO category. Then coloured lines display the corresponding category 5, 10 and 15 days after (right) and before (left). For instance we can see that 5 days before a strong phase 4 event around a half of the days belong to a strong phase 3, with some more days coming from phase 3 but not strong, and only a few were already in a strong phase 4. Going back to 10 days shows a varied mixture of origins. This variety of MJO transitions and evolutions makes the analysis of the impact on European wind speeds complex. Only a 15% of the strong MJO events had an amplitude less than one 15 days before.

References

Barnes, E. A., S. M. Samarasinghe, I. Ebert-Uphoff, and J. C. Furtado, 2019: Tropospheric and stratospheric causal pathways between the MJO and NAO. *Journal of Geophysical Research: Atmospheres*, doi:10.1029/2019jd031024, URL https://doi.org/10.1029/2019jd031024.

Cassou, C., 2008: Intraseasonal interaction between the madden–julian oscillation and the north atlantic oscillation. *Nature*, **455 (7212)**, 523–527, doi:10.1038/nature07286, URL https://doi.org/10.1038%2Fnature07286.

Kosara, R., F. Bendix, and H. Hauser, 2006: Parallel sets: interactive exploration and visual analysis of categorical data. *IEEE Transactions on Visualization and Computer Graphics*, **12 (4)**, 558–568, doi:10.1109/tvcg.2006.76, URL https://doi.org/10.1109/tvcg.2006.76.

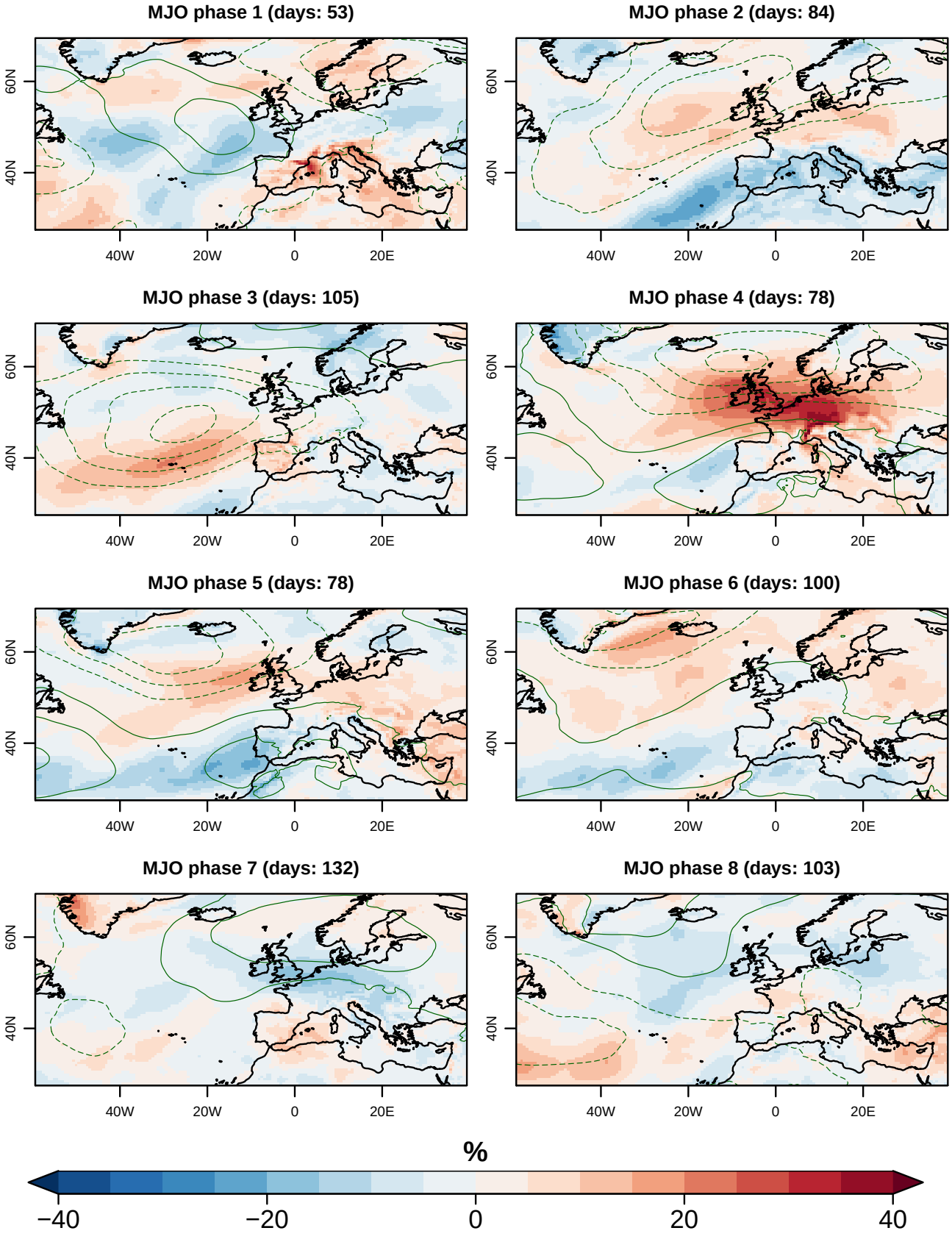

FIG. S1. Observed (MERRA2) 50m wind speed relative anomalies during strong (amplitude>2) MJO events for each MJO phase in JFM 1981–2017 according to the BoM MJO index. Green contours show associated sea level pressure absolute anomalies. Contour intervals are 2 hPa with the zero contour omitted. The number of days in each strong MJO category is specified.

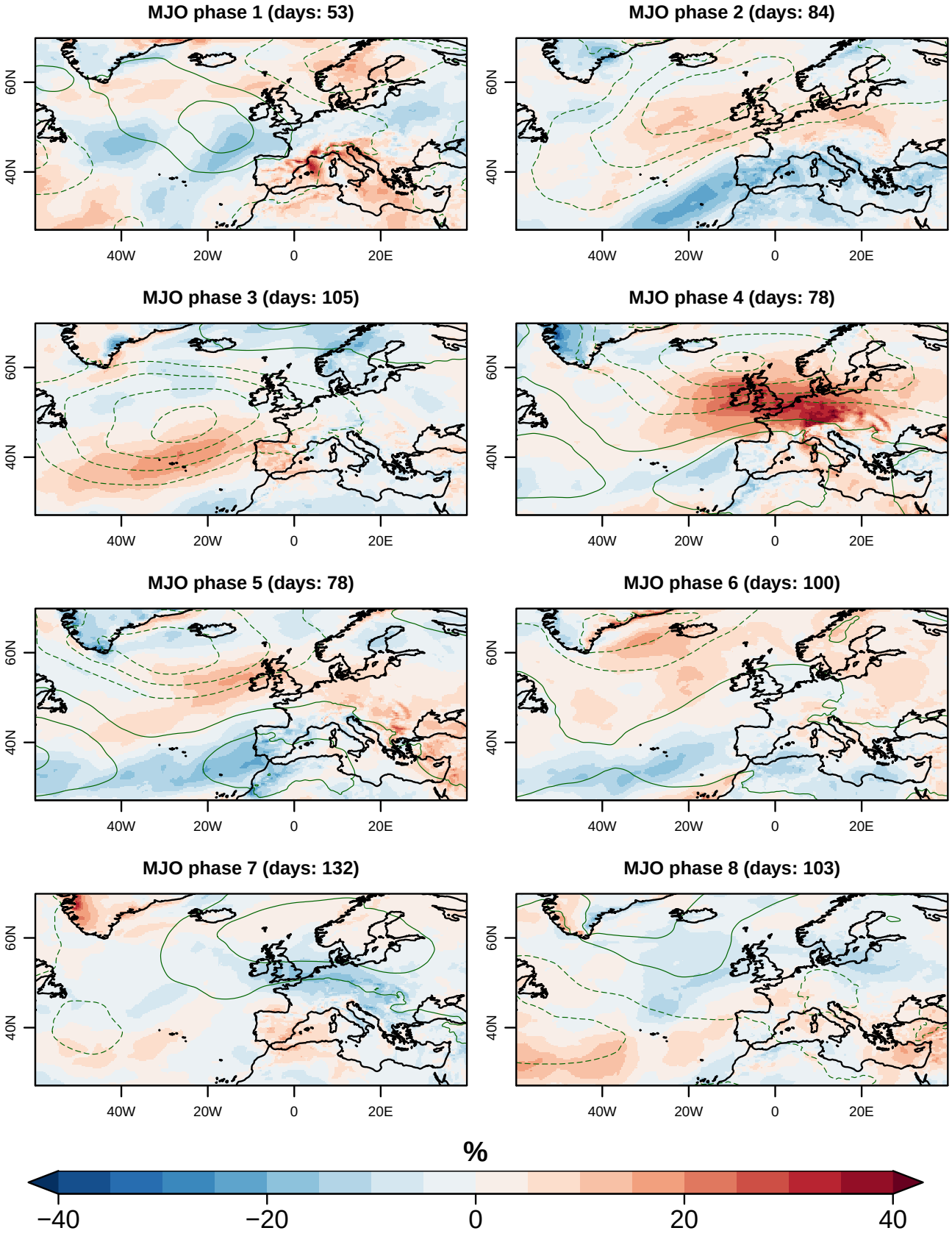

FIG. S2. Observed (ERA5) 100m wind speed relative anomalies during strong (amplitude>2) MJO events for each MJO phase in JFM 1981–2017 according to the BoM MJO index. Green contours show associated sea level pressure absolute anomalies. Contour intervals are 2 hPa with the zero contour omitted. The number of days in each strong MJO category is specified

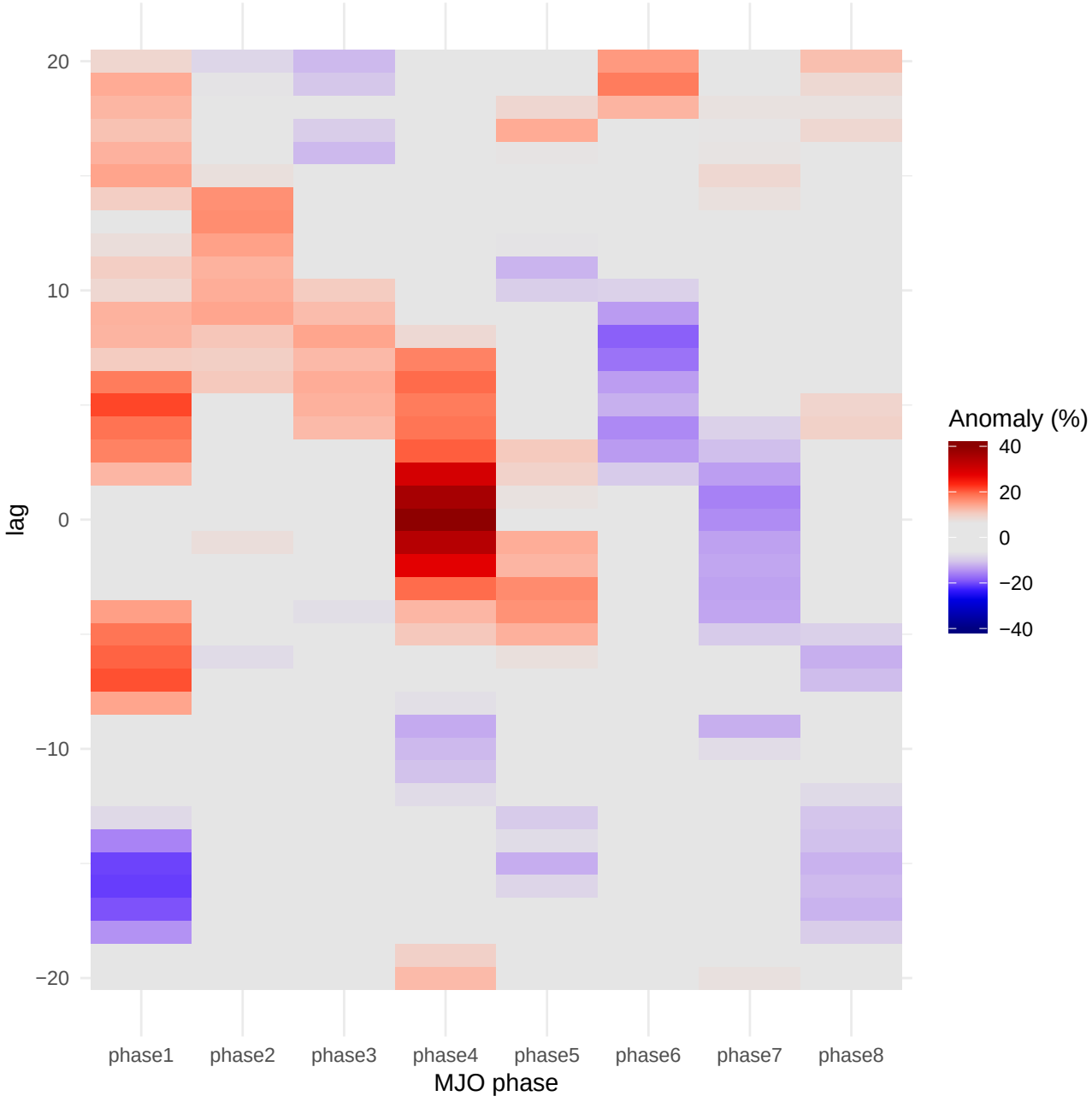

FIG. S3. Lagged impact of strong MJO events (according to BoM index) on observed (ERA5) wind speed over Frankfurt for each of the MJO phases. A positive lag indicates a wind speed anomaly a number days after a MJO strong event, while a negative lag indicates that a wind speed anomaly leads a strong MJO event by a number of days.

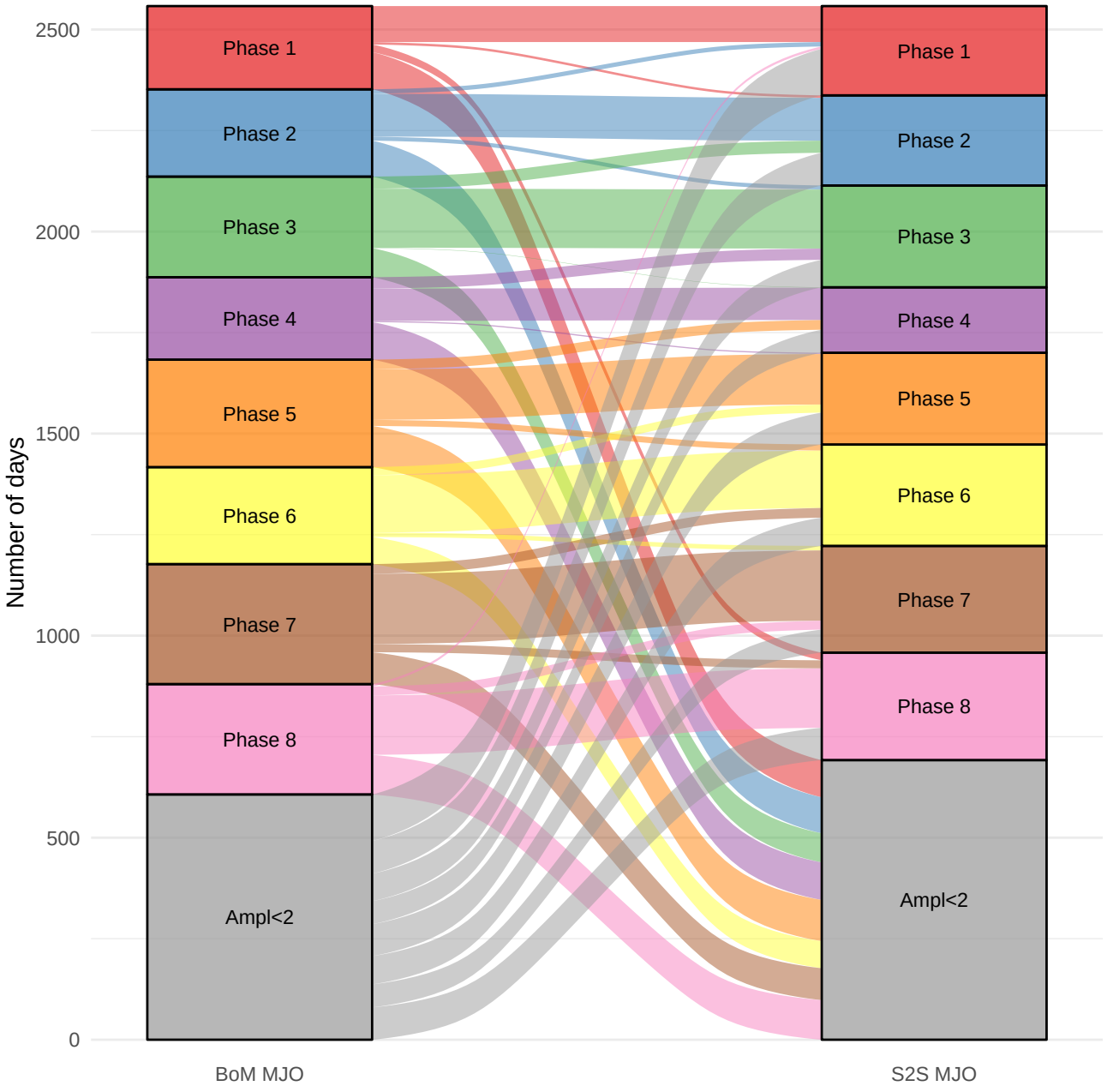

FIG. S4. Comparison between days classified as strong MJO events for each phase according to BoM (left) and S2S ERAI (right) MJO indices in the 1981–2017 period. The width of the lines is proportional to the number of days in each correspondence relationship. All the days which have amplitude less than two in both indices have been omitted.

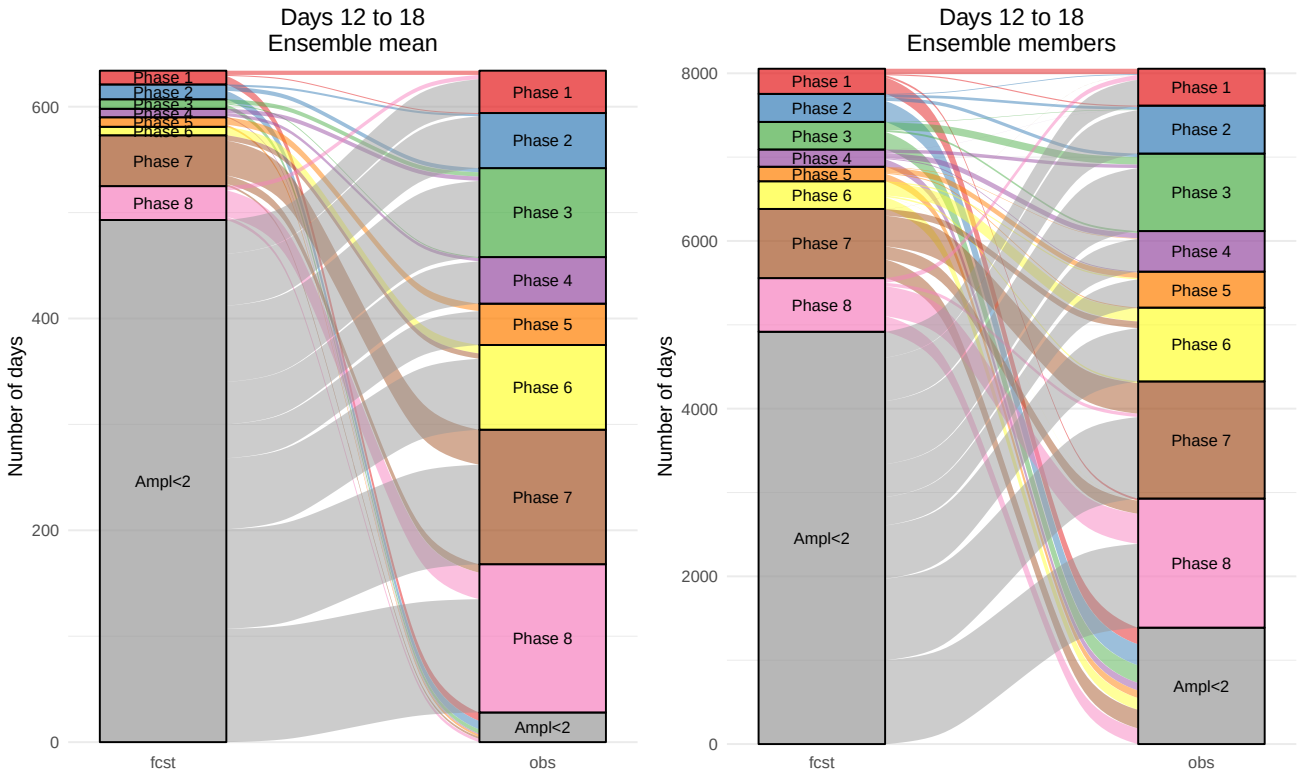

FIG. S5. Comparison of the verification of ECMWF MPS 2018 MJO forecasts for days 12 to 18 employing the ensemble mean (left panel) or individual ensemble members (right panel).

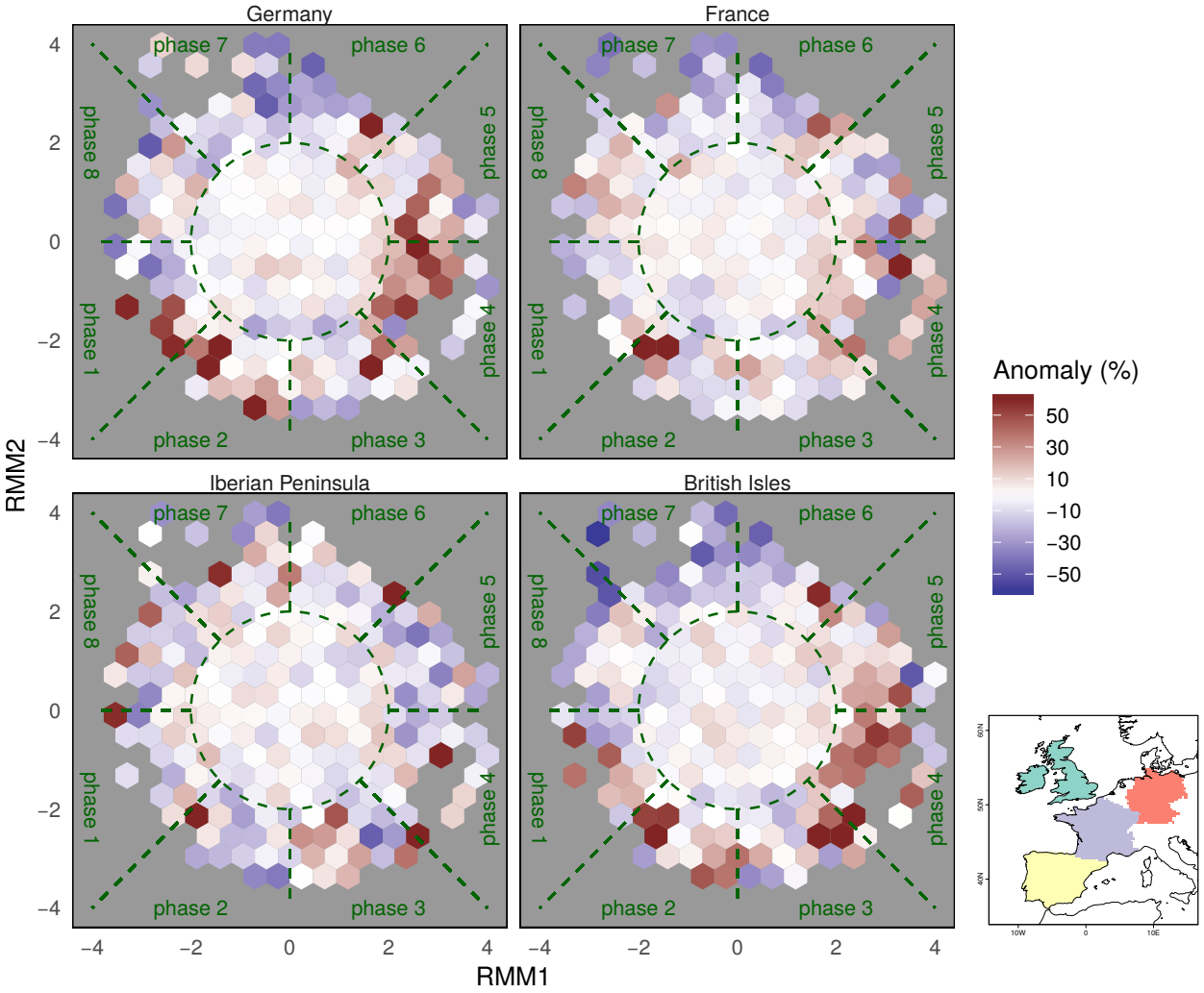

FIG. S6. Average wind speed anomalies over Germany (1st panel), France (2nd panel), Iberian Peninsula (3rd panel) and British Isles (4th panel), represented in the RMM phases space. The green dashed circle encloses amplitudes less than 2. The grid points employed for each region are depicted in the inset map.

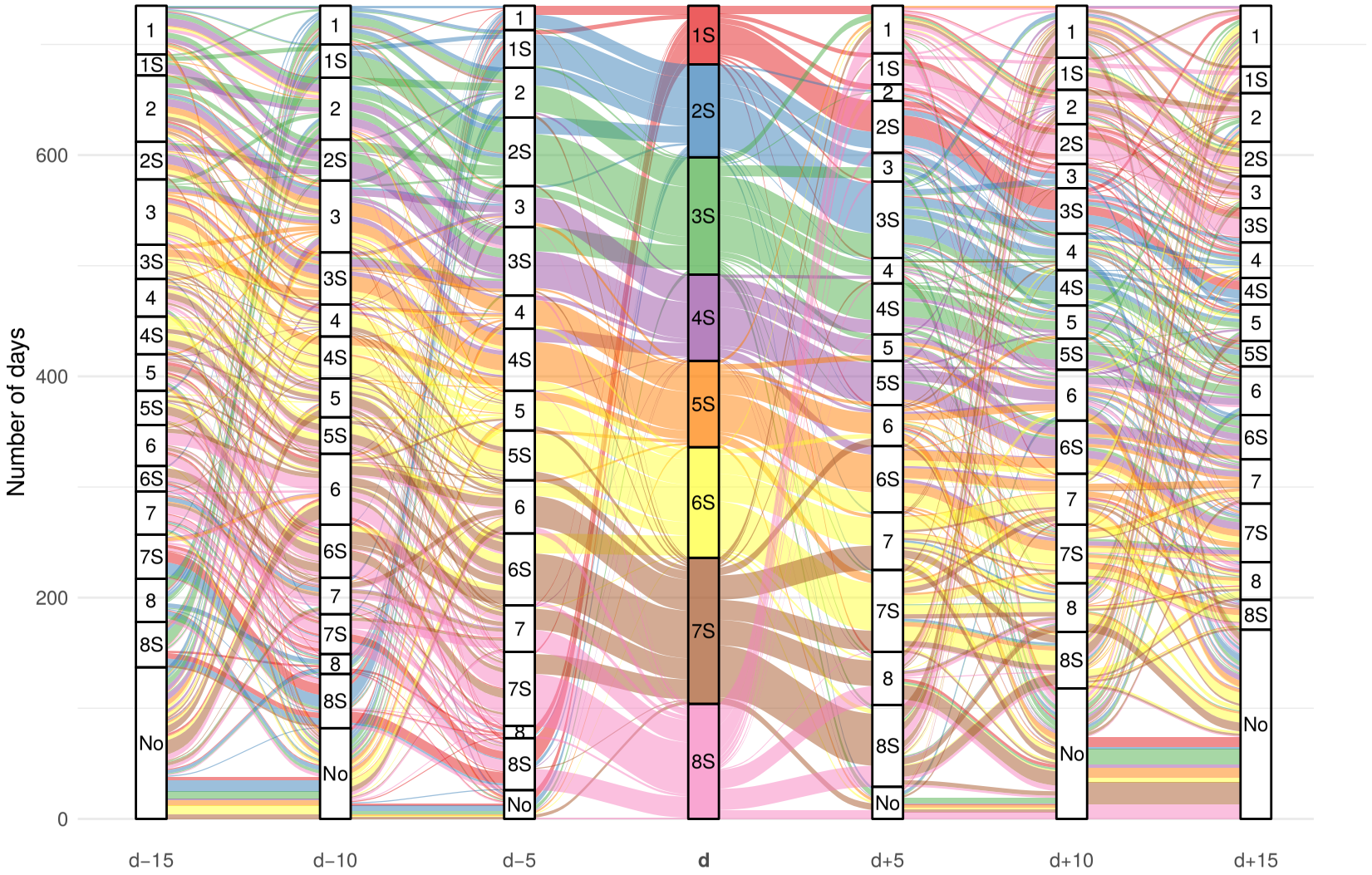

FIG. S7. Transitions of MJO category 15, 10 and 5 days before (left) and after (right) a strong MJO event occurred. The central coloured column shows the proportion of days in the JFM 1981–2017 period in each strong MJO category, and the colour lines join each day with the previous or following phase and amplitude category. Category numbers followed by an S indicate a strong MJO category (amplitude>2), while numbers without S indicates amplitudes between 1 and 2.

Chapter 5

Seasonal forecasts of wind power generation

The work in this chapter describes a methodology to produce seasonal forecasts of capacity factor from the output of a seasonal prediction system. As described in table 1.1, many potential users of climate predictions are not finally interested in wind speed forecasts but rather in other quantities that are more related to their final needs, such as wind power generation, electricity prices or wind farm revenues. In order to facilitate uptake of the predictions and fulfill the needs of those user groups it is important to build specific indicators derived from atmospheric variables that can be related to the final decisions to be made. Regarding wind power generation, the relationship between wind speed and power generated by a wind turbine is highly non-linear. Indeed, the energy contained in the wind passing through a turbine is proportional to the cube of its speed. Of course, not all of the energy contained in the wind is converted to electricity, and therefore the relationship is even further complicated. Different turbine designs produce different amounts of generation. Also big wind farms with many turbines will generate more power than small wind farms under the same meteorological conditions. Capacity factor is a normalized indicator of generation that is typically employed in the energy industry. However, producing forecasts of capacity factors from a seasonal prediction system is not straightforward. This paper describes the challenges that need to be addressed when computing seasonal predictions of capacity factor.

This paper deals with objectives (ii) and (iii) of this dissertation.

Lledó, L., Torralba, V., Soret, A., Ramon, J., and Doblas-Reyes, F. (2019). Seasonal forecasts of wind power generation. *Renewable Energy*, 143:91–100, doi: 10.1016/j.renene.2019.04.135

Renewable Energy 143 (2019) 91–100

Contents lists available at ScienceDirect

Renewable Energy

journal homepage: www.elsevier.com/locate/renene

Seasonal forecasts of wind power generation

Ll. Lledó [a, *], V. Torralba [a], A. Soret [a], J. Ramon [a], F.J. Doblas-Reyes [a, b]

[a] Barcelona Supercomputing Center (BSC), Spain
[b] ICREA, Pg. Lluís Companys 23, Barcelona 08010, Spain

ARTICLE INFO

Article history:
Received 19 December 2018
Received in revised form
5 April 2019
Accepted 25 April 2019
Available online 3 May 2019

Keywords:
Seasonal prediction
Wind power generation
Capacity factor
Climate services
Energy forecasting

ABSTRACT

The energy sector is highly dependent on climate variability for electricity generation, maintenance activities and demand. In recent years, a few climate services have appeared that provide tailored information for the energy sector. In particular, seasonal climate predictions of wind speed have proven useful to the wind power industry. However, most of the service users are ultimately interested in forecasts of electricity generation instead of wind. Although power generation depends on many factors other than wind conditions, the capacity factor is a suitable indicator to quantify the impact of wind variability on production. In this paper a methodology to produce seasonal predictions of capacity factor for a range of turbine classes is proposed for the first time. The strengths and weaknesses of the method are discussed and the forecast quality is evaluated for an application example over Europe.

1. Introduction

The energy sector is heavily impacted by atmospheric variability: energy demand and supply are conditioned by atmospheric conditions at several time scales ranging from small-scale turbulence through day-ahead weather or seasonal anomalies and up to climate change impacts [14,43]. Renewable generation from hydro, solar and wind power installations is specially sensitive to seasonal or multiannual climate oscillations and long-term trends [28,48]. Recent improvements in the field of climate prediction make it now possible to inform in advance of anomalous conditions for the months to come (i.e. seasonal prediction) [12,31]. Anticipating the future variability of energy sources beyond the first two weeks allows to take calculated, precautionary actions with potential cost savings. To foster the usage of those predictions, in 2015 the World Meteorological Organization (WMO) included energy as one of the priority areas in the Global Framework for Climate Service (GFCS) [23,52]. The GFCS set the basis for understanding user needs in terms of climate knowledge and building applications that transform climate model outputs to fulfill those specific user needs. Since then a few climate services have appeared that provide specific information for assisting decision making in the energy sector [6]. One of such examples is the RESILIENCE prototype (resilience.bsc.es), developed specifically for the wind power industry under the EUPORIAS project [7,46]. In RESILIENCE the value of seasonal forecasts of wind speed issued one to three months ahead was explored according to the needs of various stakeholders in the sector: wind farm owners, operation and maintenance (O&M) teams, energy traders and transmission system operators (TSO).

The needs of those different user profiles regarding seasonal outlooks was explored through stakeholder interviews in EUPORIAS and S2S4E projects ([16,38,41]). After analysing 22 interviews and 69 survey responses, the needs of the wind energy sector proved to be quite diverse. For example, O&M teams need to perform maintenance activities under weak winds for safety reasons. For that purpose wind forecasts are directly useful and some recent research has already shown skill for seasonal wind predictions in some regions [3,9,46]. But most of the remaining stakeholders use the wind speed forecasts as a proxy to anticipate wind power generation either at site or country level: TSOs need to schedule alternative generation sources in advance to guarantee power supply, traders want to forecast power prices, owners need to be ready for cash flow shortages in case of mince revenues, and even O&M teams try to minimize generation losses due to turbine stoppings. Therefore direct forecasts of wind power generation would be beneficial to those stakeholders, as indicated in the interviews and surveys. However, efforts to transform seasonal predictions of wind speed to generation forecasts have received little attention so far and have only been considered very preliminarily in the work of MacLeod et al. [30].

* Corresponding author.
E-mail address: lledo@bsc.es (Ll. Lledó).

https://doi.org/10.1016/j.renene.2019.04.135

While forecasts of wind power generation at lead times from minutes and hours to a few days ahead have been produced with very advanced methodologies (e.g. dynamical downscaling, machine learning or statistical downscaling [17]), a number of difficulties make the provision of generation forecasts at seasonal timescales challenging. Climate models have more complexity than weather models as they simulate and couple the different components of the climate system (atmosphere/hydrosphere/cryosphere/land surface/biosphere) and therefore demand enormous amounts of computational resources. This limits the effective temporal and spatial scales of the climate predictions that are currently available. Besides, climate predictions are affected by different sources of uncertainty than weather forecasts. Therefore some advanced methodologies that have been used with weather forecasts cannot be directly employed with climate model outputs. For instance, dynamical downscaling might be computationally prohibitive, and statistical downscaling usually requires long observational records that are scarce. Additionally, the vast differences among technologies that extract kinetic energy from the wind and convert it to electricity complicate physical approaches for computing wind power production. This paper explores all those challenges and difficulties, identifies gaps and provides reasonable choices whenever that is possible. The decisions are guided by the view of producing an indicator that can be computed from publicly available state-of-the-art seasonal prediction systems, covers the whole globe, is useful for estimating power production at wind farm level and general enough to serve any technology.

The paper is organized as follows: section 2 describes the indicator and the technological challenges. The limitations of seasonal forecasts to produce generation forecasts are presented in section 3. In section 4 the potential of the methodology is explored through an application example over Europe. Finally some conclusions are provided in section 5.

2. An indicator of wind power generation that is suitable for any kind of wind farm

2.1. Capacity factor

Wind power generation of a single wind farm depends on many factors. The most important ones are the number of installed turbines and the turbine model —which determine the maximum power that can be produced (also known as installed capacity)— altogether with the wind blowing at the site. Ideally, we are interested in an indicator as general as possible, that accounts for the impact of wind speed variations and is useful to as many stakeholders as possible. Therefore different turbine types and wind farm sizes should be accommodated. In conversations with a co-designer from the industry (an important wind power producer and project developer) the capacity factor was selected as a suitable indicator of wind power generation. The capacity factor (CF) is a widespread performance indicator in the whole energy sector that allows fair comparisons between power plants of different sizes and types. It is a typical way of assessing the relative performance or usage of any generating power plant. For a given period of time, it is defined as the ratio of total produced energy (E_{prod}) to the maximum production that could be achieved if the plant were operating at full (installed) capacity during all the time (E_{max}). Simple calculus shows that CF can also be computed as the average produced power ($\overline{P}$) normalized by the installed capacity (C_{inst}).

$$CF = \frac{E_{prod}}{E_{max}} = \frac{\overline{P}}{C_{inst}} \quad (1)$$

CF is typically expressed as a percentage, and can be also interpreted as the percentage of time that the plant would have to be working at full capacity to produce the same amount of energy actually produced. This amount of time is also known as equivalent hours, and sometimes used in the industry, although CF is more prominent.

For conventional technologies, typically the capacity factor depends on factors like the availability and cost of fuel, the electricity demand, the needs of the grid operator or the market prices, because the power output can be adjusted at discretion according to the needs of the plant operator. But in the case of renewable energies like wind or solar, the fuel cannot be directly controlled (nor stored for later usage as hydropower allows), and as the fuel has no cost, all the produced energy is fed into the grid without further considerations. So, the generation in wind and solar plants depends almost exclusively on meteorological factors such as wind or irradiation. These meteorological factors have a natural variability, and hence the power output from these plants is said to be intermittent and non-dispatchable. In this sense, capacity factor of an already installed wind farm measures how efficient the meteorological conditions have been for producing energy during a specific period.

The capacity factor is therefore independent from the number of turbines and their nameplate capacity, which is a desirable property. However it does depend on the efficiency of the specific turbine at extracting energy from the wind at different speeds (see section 2.2). The total generation of a wind farm during a period can be easily derived from its capacity factor just by multiplying it by the installed capacity and the number of hours in the period of interest.

$$E_{tot} = CF * C_{inst} * t \quad (2)$$

2.2. Computing capacity factor

There are multiple approaches to computing capacity factors. Power producers and TSOs simply obtain it directly from metering records of the energy that is fed into the grid and use equation (1). This capacity factor takes into account all energy losses in the wind farm and is therefore called net capacity factor [5]. An other approach is to estimate a theoretical capacity factor that would be achieved if there were no losses at all, i.e. all available wind was converted into energy according to turbine specifications. This is referred as gross capacity factor. The typical way of computing the gross capacity factor is using manufacturer-provided power curves that relate power output to steady 10-min winds blowing at hub height. Capacity factor can easily be derived from power curve values dividing the power output by the nominal capacity of the turbine.

It is important to understand differences between gross and net capacity factors. The main element that impacts gross generation is the flow speed that the blades receive, although other flow properties affect the turbine performance, namely wind shear, wind veer, turbulence and air density. If the flow is not steady and homogeneous through all the swept area the generation will slightly differ from the values provided in power curves [8,15,35,44]. Changes in air density (through temperature, humidity and pressure variations) also modify the available kinetic energy that goes through the swept area and can produce generation differences of up to 5% [49]. In this study we will neglect all the turbulence and shear effects and assume a standard density of 1.225 kg m^{-3}, which is the density reported in most power curves.

The list of factors affecting net generation, i.e. losses of all kinds,

is long and diverse: downtime due to maintenance or failures, grid curtailments, environmental curtailments (e.g. presence of birds or bats), electrical transport and conversion losses, icing conditions, accretion of dust or mosquitoes, blade degradation due to abrasion, control strategies, wakes from obstacles or nearby turbines, etcetera. Those losses vary greatly from one wind farm to another, and even from one period to another. Differing wind farm designs, country regulations, O&M strategies, risk appetites and other factors make big differences in the final losses. Just as a reference, total losses might be in the range of 7.8%–37% with a typical value of 18.5% [5]. In view of this diversity of losses, and for the sake of generality, an indicator of gross generation has been selected. Then each user is allowed to subtract the losses deemed necessary in order to obtain net generation estimates.

2.3. Handling a diversity of wind turbines

There are in the market several manufacturers offering a wide range of turbines, and each of them is suited for maximum efficiency at specific wind conditions. Since the advent of industrial wind turbines in the 1980's there has been a technological race to build taller turbines, with bigger rotor diameters and more powerful generators. However we are interested here solely in their efficiency in extracting energy from the wind, i.e. their normalized power curves. The international standard IEC-61400-1 [25] defines four classes of turbines suited for an average annual wind speed of 10, 8.5, 7.5 and 6 m s^{-1} at hub height respectively (see Table 1). The mean wind speed is used in these standard to estimate the extreme 50-year gust that the turbine will receive, so all turbines of this class have to withstand such gusts. Classes are further subdivided by the turbulence in the site, which also impacts structural loads.

Typically turbines of type III are lighter than type II or I for the same nameplate capacity, because they do not have to withstand heavy loads. Therefore, they can produce energy with weaker winds. Conversely, turbines of type I are heavy, and they only produce energy with stronger winds. In general turbines of the same IEC class have similar normalized power curves, and this gives a chance to provide a simplified approach to a diversity of turbine models.

From a sample of more than two-hundred turbine models, five have been selected to represent the different IEC classes. Capacity factors have been computed using those five power curves and will then be up to the users to select the one that most closely matches their turbine power curve. A first screening was carried out to select the most representative technologies. Several conditions were imposed: (a) consider only pitch-regulated turbines (i.e. the blade angle can be adjusted), (b) with nominal capacities around 2 MW, (c) available for installation at 100 m hub height (within the range 95–105 m), and (d) from the manufacturers with highest market shares in Europe: Vestas, Enercon and Siemens-Gamesa. Class IV is barely used in the industry, and Class S is for special designs not fitting any other class, so they have been discarded. Note that some turbines can be certified as Class I and II or II and III at the same time, so we selected five turbines (see Table 2 and Fig. 1).

All the selected turbines start to turn and produce energy around 3 or 4 m s^{-1} (cut-in speed). However, there are substantial differences in the wind speeds at which the five turbines reach the nominal power (rated speed). In the steeper section of the power curves, around 8 or 10 m s^{-1}, differences of capacity factor reach more than 50%. It is also important to notice differences in the cut-out speed, i.e. the speed at which the turbine has to stop turning for safety reasons and stops producing energy (cut-out speed): the Vestas turbines for class II/III and class III stop producing at 20 m s^{-1} while the others still produce energy up to 25 m s^{-1}. Cut-out values are very important for sensitivity because small variations of wind produce ramps in capacity factor from 100% to 0%. Notice that there exist class III turbines with cut-out speeds of 25 m s^{-1}, but these ones were selected to represent the widest range of differences amongst power curves.

3. Limitations of climate predictions to produce seasonal forecasts of capacity factor

Several centers produce operational climate predictions for the next months to come [20]. Typical settings cover up to six months ahead with some of the systems extending even one year ahead. These predictions are produced with coupled atmosphere/ocean/ice/land models. Although the atmosphere is very chaotic in nature and predictable only up to a few days ahead, the evolution of ocean temperatures, soil humidity, snow cover or sea ice extent evolves much slowly and in turn forces the atmosphere. This provides a chance to anticipate mean-state atmospheric anomalies [40]. To account for uncertainty, the predictions are repeated many times with slightly distinct but equally plausible initial conditions. This provides a set of ensemble members from which probabilities of occurrence of different situations can be estimated. Moreover, each prediction system is accompanied with a retrospective set of predictions for the past ten to thirty years, which is used to evaluate the quality of the predictions and adjust the biases.

These particularities of climate prediction result in huge amounts of data and expensive computational resource needs. Therefore all the producing centers carefully select the number of variables they generate, the spatial and temporal resolutions of their products as well as the number of ensemble members. Those compromises sometimes difficult the usage of the predictions for specific applications. The limitations that constrain our goal of producing capacity factor forecasts are detailed below.

3.1. Spatial resolution

At small scales, the wind field near the ground is very spatially inhomogeneous. Turbulence, topography effects and obstacles can change the wind speed at distances of only a few tenths of meters. For that reason not all the turbines in a wind farm receive the same

Table 1
Turbine classes defined in IEC-61400-1.

Class	Description	Annual average wind speed (m/s)	Turbulence intensity (%)	Extreme 50-year gust (m/s)
Ia	high wind & high turbulence	10.0	18	70
Ib	high wind & low turbulence	10.0	16	70
IIa	medium wind & high turbulence	8.5	18	59.5
IIb	medium wind & low turbulence	8.5	16	59.5
IIIa	low wind & high turbulence	7.5	18	52.5
IIIb	low wind & low turbulence	7.5	16	52.5
IV	very low wind	6.0	–	42.0
S	special	–	–	–

Table 2
Technical characteristics of the selected turbines.

Turbine model	IEC Class	Rotor diameter (m)	Rated power (MW)	Cut-in speed (m/s)	Rated speed (m/s)	Cut-out speed (m/s)
Enercon E70_2.3 MW	I	70	2.3	2	16	25
Gamesa G80_2.0 MW	I/II	80	2.0	4	17	25
Gamesa G87_2.0 MW	II	87	2.0	4	16	25
Vestas V100_2.0 MW	II/III	100	2.0	3	15	20
Vestas V110_2.0 MW	III	110	2.0	3	11.5	20

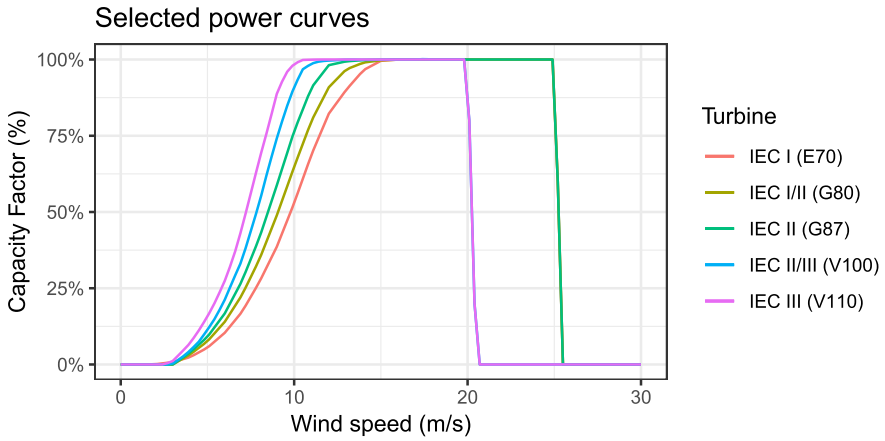

Fig. 1. Selected power curves, normalized by maximum generation. Their specifications can be seen in Table 2.

wind speed at a given time. But the global models employed for producing seasonal predictions have grid sizes much bigger ($\sim 50km$) than a typical wind farm extent, and therefore only provide one single wind speed value for all the turbines. Dynamical and statistical downscaling techniques can be used to refine the predictions [12, p.256]. Using microscale models one could adjust the wind speed to specific turbine locations [2], e.g. by computing a speed-up factor for each turbine location. However, this would require specific information on the wind turbine locations for each wind farm, which is not publicly available. Some authors have assumed a fixed distribution of speeds through the turbines to try to model this effect [42]. Other authors have used empirical power curves for the whole wind farm [18,29,37]. This approach also requires site-specific metering records of wind speed and production and cannot be employed to produce global forecasts. Although monthly or seasonal wind anomalies tend to be more homogeneous than the mean wind field and impact the whole wind farm in the same manner, power curves are sensitive to the absolute value of the wind, and therefore this effect can produce some differences in the monthly total generation of each turbine. The model employed here sticks to turbine power curves despite this limitation.

3.2. Temporal resolution

State-of-the-art seasonal prediction systems produce instantaneous outputs every six hours. Typically, those values are further aggregated to monthly or seasonal means, because predictability at seasonal timescales only arises when looking at long period averages: when averaging, the noise cancels and the forcing signal imparted by the ocean/land conditions can appear. In contrast, power curves are compiled with ten-minutal average winds as mentioned in section 2.1. As power curves are highly non-linear, using averages of wind speed to derive an average capacity factor can produce inaccurate results. Moreover instantaneous or ten-minutal wind speed distributions tend to be highly skewed [33,34]. Therefore one might wonder what is the error incurred by using six-hourly sampled (instantaneous) winds or longer-period averages from the models with ten-minutal power curves. To illustrate this problematic, quality-controlled wind speed observations from 9 tall towers have been employed (see Table 3). For each location, ten-minutal wind speeds have been compared to its six-hourly, daily, monthly and seasonal averages. Fig. 2 shows the joint probability density of ten-minutal wind speeds and those longer period averages for one of those towers near Erie, Colorado and spanning 2006 to 2010. This plot reveals how apart are all the ten-minutal averages that compose a longer period average from the average itself. For six-hourly averages most of the ten-minutal values lie close to the $y = x$ line. This means that for a given six-hourly period most of the ten-minutal values in that period are close to the six-hourly mean value, although a few of them can be quite apart. But for longer period aggregations the density peaks below the $y = x$ line, and therefore a high number of ten-minutal values are lower than the period mean, with only a few of them above, although farther away. The analysis for the other 8 towers (see supplementary material) shows similar patterns. The non-linearity of the power curve complicates this further. The work of MacLeod et al. [30] discusses this issue in detail and finds that using daily averages is fair enough to produce accurate capacity factors. Six-hourly instantaneous values have been employed here. It is worth noticing that six-hourly instantaneous values from models are not directly comparable to six-hourly instantaneous samples from site observations. Global models at coarse scales do not represent adequately mesoscalar and turbulent motions and moreover the values provide a statistical value representative of a wide area. Therefore those six-hourly model outputs are much smoother than six-hourly instantaneous samples from anemometry, and tend to be closer to six-hourly averages [21].

3.3. Available variables

Another constraint for using power curves is that wind speed

Table 3
Details of the nine tall towers employed.

Tower name	Country	Measuring height (m)	Period of record
BAO	USA	100	2007–2016
Butler Grade	USA	62	2002–2018
Cabauw	Holland	80	1986–1997 and 2001–2017
CVO	Cape Verde	30	2011–2018
FINO1	Germany	90	2004–2017
Ijmuiden	Holland	90	2011–2016
Lindenberg	Germany	98	1999–2017
NWTC M2	USA	80	1996–2017
WM01	South Africa	62	2010–2017

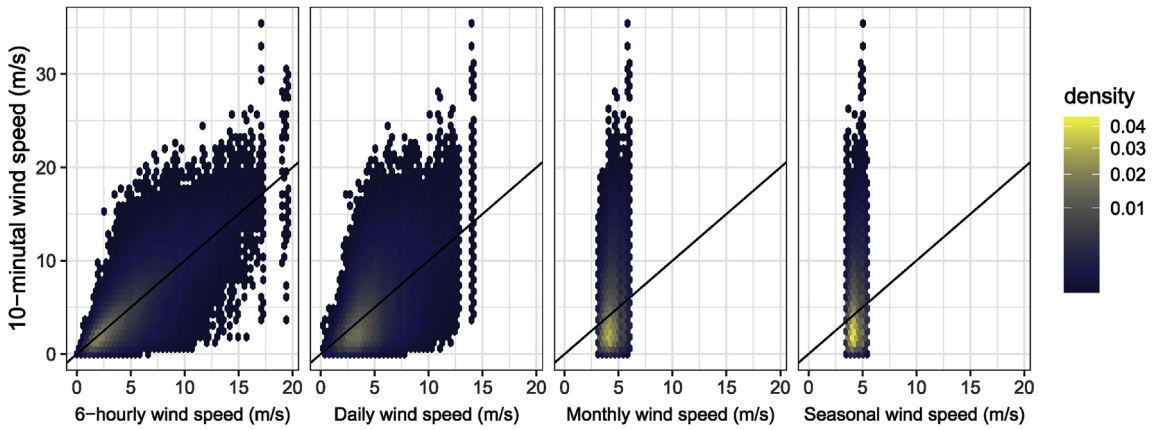

Fig. 2. Joint probability density function of ten-minutal and longer-period averages of wind speeds at Boulder Atmospheric Observatory. The black line is the $y = x$ line.

should be provided at hub height. Modern turbines have hub heights in the range of 80–120 m, although many exceptions exist, especially with old wind farms that have lower hub heights. But current seasonal prediction systems only provide 10 m winds (or its components), which are obviously weaker than at those heights above ground. Some models also provide wind at standard pressure levels, but the changing orography and the sparse vertical levels make impossible to obtain wind at 100 m above ground. To estimate hub height winds from surface winds an extrapolation method is typically used. There exist two classical approaches: the power law and the log-profile [5,37]. For simplicity, we have selected here the power law and assumed a fixed hub height of 100 m, with a shearing exponent of $\alpha = 0.143$ for land [47] and $\alpha = 0.11$ for water [24]. Both shear exponents assume neutral stability (computing stability from existing forecast fields would be difficult if not impossible). Under these assumptions, wind at 100 m is obtained as:

$$V_{100m} = V_{10m*}\left(\frac{100}{10}\right)^{\alpha} = \begin{cases} V_{10m*}1.39 & \text{over land} \\ V_{10m*}1.29 & \text{over sea} \end{cases} \quad (3)$$

Another not uncommon problem with available variables is the provision of time-averaged meridional and zonal wind components. As a result, computing the wind speed modulus from the average zonal and meridional components (using Pythagorean rule) produces much lower wind speeds than averaging the modulus directly. This limitation prevents the use of many seasonal forecast systems, for instance CFSv2 [39].

3.4. Model biases

All numerical prediction models have systematic biases due to many simplifications in the modelling of the complex behavior of the Earth system. Those biases need to be adjusted before using forecasts for decision making or feeding impact models [46]. Moreover seasonal predictions might also exhibit drift [22] (i.e. non-stationary biases that change with the lead-time of the forecast), and need to be calibrated (i.e the spread of the ensemble adjusted to obtain reliable probabilities) [50]. There exist many bias adjustment methodologies for this purpose in the literature. For adjusting and calibrating monthly wind speed forecasts, the two methodologies described in Torralba et al. [46] are simple yet very effective. The general idea is to employ a set of retrospective forecasts (also known as hindcasts) and estimate the mean bias for each start date and lead time and subtract it from the corresponding monthly average forecasts. However, when trying to apply those methodologies to six-hourly winds some issues appear: when subtracting the monthly mean bias from six-hourly values, negative values can appear. Those negative values could be set to zero, but then the method would not entirely remove the bias. An alternative approach to avoid the negative values is to use a multiplicative approach, i.e. to compute a relative bias in percentage, and use this percentage to correct wind speed. But there is also a conceptual problem with these two approaches: they are designed to produce accurate monthly average wind speeds. However the goal here is to use the full range of six-hourly values to feed a (non-linear) power curve. Therefore it is not enough to correct the mean bias. Differences in variance and skewness of the wind distribution also have an impact on CF. Fig. 3 shows how two wind speed distributions with same mean but different variance result in a very different distribution of CF values. The narrower wind distribution produced less zero capacity factor values. From the example it is clear that the whole six-hourly forecast distribution needs to be adjusted. To that end, an empirical quantile mapping methodology has been employed [4,45]. This methodology aims to correct all of the moments of the distribution (ideally). As long as the adjusted

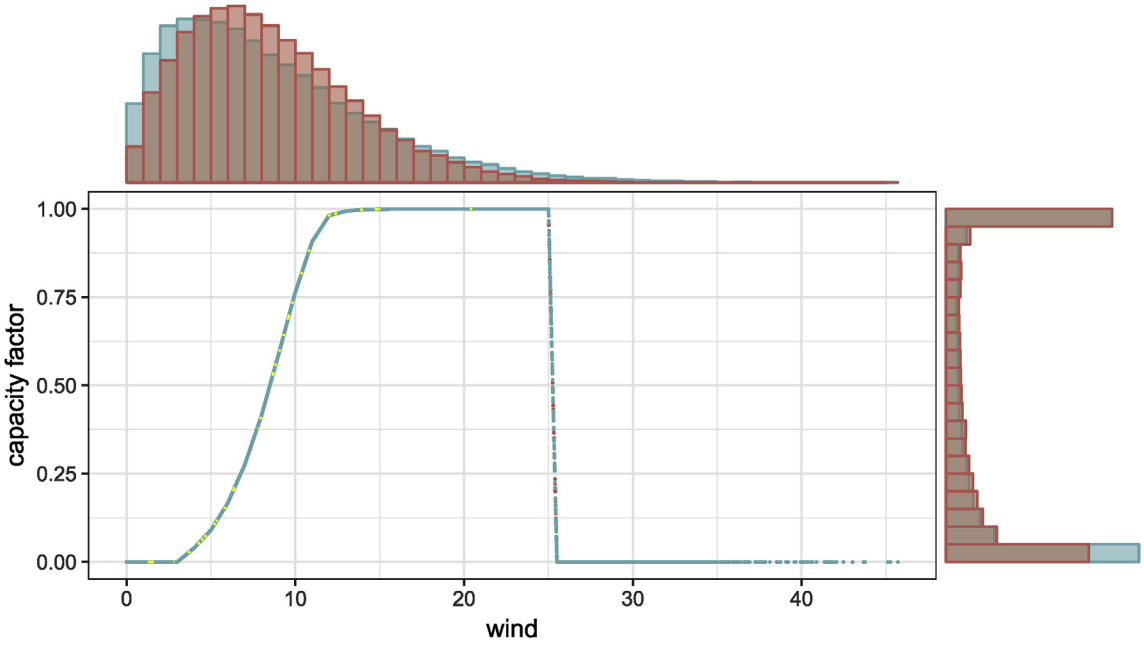

Fig. 3. Scatterplot of wind speed and corresponding capacity factor values obtained from two Weibull distributions with same mean (8.5 m/s) but different standard deviation (5 m/s in red and 6 m/s in blue), when the Gamesa G87 power curve is used for the conversion. The histograms on top are for wind, and the ones on the right for capacity factor values. (For interpretation of the references to colour in this figure legend, the reader is referred to the Web version of this article.)

distribution of six-hourly wind speed values is similar to the observed one our capacity factor forecasts will be unbiased.

For the forecasts to be successful it is still needed to have some degree of skill in predicting the 6-hourly distribution shape. Although seasonal predictions do not provide correspondence between forecast and observations at daily or sub-daily scales it is possible to obtain skill in predicting the whole distribution of six-hourly winds in a longer period. Note that quantile mapping does not correct errors in the ensemble spread, so calibration might be needed separately (this has not been done here). Also, quantile mapping is known to worsen verification scores in areas where there is not any forcing signal [53].

3.5. Accuracy of reanalysis data as observational reference

The impact model we propose to compute capacity factor is very sensitive to the absolute value of wind speed that it receives. For that reason, the accuracy of the observational dataset used to bias adjust predictions needs to be as good as possible. Seasonal predictions are typically bias adjusted with reanalysis datasets [51], due to the need of having both global coverage and long records. Those global reanalysis datasets are good at representing variability at monthly, daily or sub-daily scales [10], but they suffer from similar problems than seasonal predictions, as far as they are produced also with modelling techniques. Although some of them provide hourly outputs and at higher spatial resolutions, and even some provide winds at 50 or 100 m above ground, the long-term mean wind speeds at hub height derived from them are biased when compared with tall tower observations. Wind atlases, such as DTU's Global Wind Atlas (GWA) or the New European Wind Atlas [1,36], incorporate information from mesoscale and microscale models and even from some observational sites and provide refined estimates of mean wind speed at relevant hub heights and for a finer grid. The 1981–2015 100 m mean wind speed difference between GWA and ERA-Interim [11] is shown in Fig. 4 as a percentage. According to GWA, over most of the continents the ERA-Interim 100 m wind speed needs to be increased. In some mountainous regions the correction is very high (more than 100%). Probably the GWA winds are too high in this case, as this is one of the known limitations of the GWA methodology that have been reported in Badger et al. [1] and Beaucage et al. [2]. To incorporate the mean wind speed information from a wind atlas but not loose the temporal variability that reanalyses provide, the ERA-Interim extrapolated 100 m wind data has been multiplied by the GWA to ERAI ratio. This adjustment can indeed be understood as a refinement at each location of the shearing exponent employed in equation (3) when extrapolating wind speed to hub height.

Another issue with global reanalyses that can be corrected with a wind atlas is the representativeness problem. Wind farms tend to be located in ridges or places where the wind is higher than its surroundings, therefore using the mean wind speed of the ERA-Interim grid box, even corrected by GWA mean wind speed in the grid cell, might be inaccurate. If the coordinates of the wind farms are known then the wind atlas value for the specific location can be used, instead of an average. This has not been done here.

Despite the mentioned difficulties, estimates of capacity factor for the past years have already been produced at hourly and six-hourly resolution from several global reanalyses datasets in the literature [13,19,42].

4. Application of the methodology over Europe and verification results

To illustrate the potential of the proposed methodology, it has been applied retrospectively for the winter season (DJF) with a hindcast of ECMWF System4 seasonal predictions [32] issued on November and covering 1981/82 to 2015/16 winters. Table 4 summarizes the main characteristics of this prediction system. The employed predictions from November have an extended integration up to 13 months and a hindcast with 51 ensemble members. Winter is the season with the highest inter-annual variability in Europe and therefore most seasonal prediction applications focus in this period. An overview of the steps that have been followed to produce the CF forecasts can be seen in Fig. 5. Details on

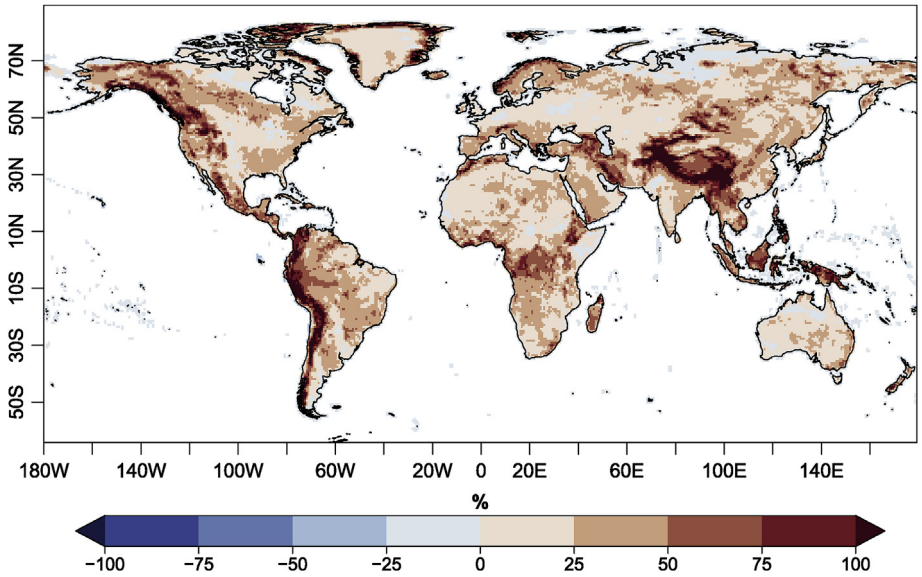

Fig. 4. Percentual difference between 100 m mean wind speeds from GWA and ERA-Interim over the period 1981–2015. ERA-Interim winds at 100 m were extrapolated from 10 m winds using a power law.

Table 4
Main characteristics of ECMWF System4 prediction system, as described in Molteni et al. [32].

System components	
Atmosphere	IFS (model cycle 36r4)
Ocean	NEMO
Land	HTESSEL
Sea ice	Prescribed from climatology
IFS configuration	
Horizontal resolution	T_L255 ($\sim 78km$)
Vertical levels	91 levels up to 0.01 hPa
NEMO configuration	
Horizontal resolution	$\sim 1 \times 1$deg
Vertical levels	42 levels
Operational configuration	
Start date	1st of each month
Issue date	8th of each month
Ensemble members	51
Integration	7 months
Extended runs	extend 15 members up to 13 months (only Feb, May, Aug & Nov)
Hindcast	
Ensemble members	15 (Jan, Mar, Apr, Jun, Jul, Sep, Oct & Dec) 51 up to 7 months and 15 up to 13 months (Feb, May, Aug & Nov)
Period	1981 to 2010

most of the steps have already been covered in the previous sections. The only step that has not received attention so far is the final presentation of the probabilistic forecast results (step 5). The information from the fifty-one ensemble members has to be summarized in an informative way to be useful for decision-making. The standard approach in the climate prediction community is to provide probabilities for three tercile-defined categories: above normal CF, normal CF and below normal CF. The thresholds that define the three categories are computed as the percentile 33 and 66 of an observational historical record.

4.1. Verification

A verification has been undertaken employing reanalysis-derived CF values as verification truth. Therefore this verification does not quantifies the quality of the impact model itself but of the whole capacity factor forecasts. Leave-one-out cross-validation has been employed to ensure that for each single forecast, the corresponding observations are not included in the bias adjustment procedure (i.e. each year is adjusted using the biases from all other years). The probabilistic nature of the seasonal predictions requires specific verification metrics [27]. The Ranked Probability Score (RPS) measures the quality of probabilistic forecasts presented in form of tercile probabilities. To gain a better understanding of the results, scores are typically compared to a baseline forecast and expressed as improvement over the baseline (known as skill scores). The Ranked Probability Skill Score (RPSS) compares the RPS of the seasonal predictions from System4 with the RPS of a climatological forecast. A climatological forecast uses observed values from previous years to derive probabilities for each tercile category

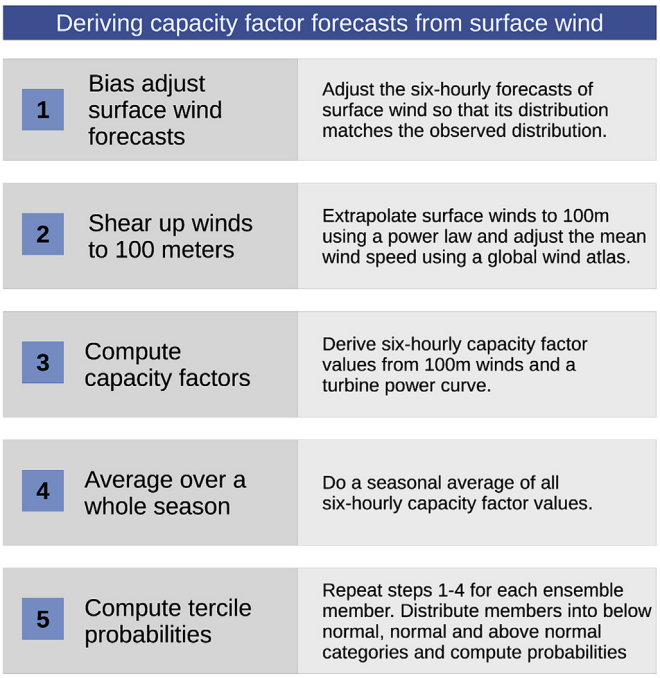

Fig. 5. Flow diagram of the steps followed to compute capacity factor forecasts.

(i.e. 1/3 of probability is always assigned to each tercile). Positive RPSS values represent an improvement over the climatology, while negative values discourage the usage of this forecasts. Fig. 6 presents RPSS values over Europe for both surface wind predictions (adjusted with the calibration method in Torralba et al. [46]) and capacity factor forecasts for IEC1, 2 and 3 classes. The skill for surface wind is modest in this region, but still positive in some spots, reaching up to a 17% of improvement over Finland. When looking at capacity factors, there is a slight increase of skill in many areas compared to surface wind. Especially in the British Isles, northern Germany, western France, and Scandinavian peninsula the seasonal predictions perform better than the climatology and offer some options to employ those forecasts for decision making.

5. Conclusions

A methodology to compute wind power generation seasonal forecasts employing manufacturer-provided power curves has been described. Several challenges related to how seasonal predictions are made available and how wind turbines generate electricity from wind speed have been addressed. A summary of those challenges and the proposed solutions follows below:

- Challenge: generation of a wind farm depends largely on the number of turbines and the total installed capacity.

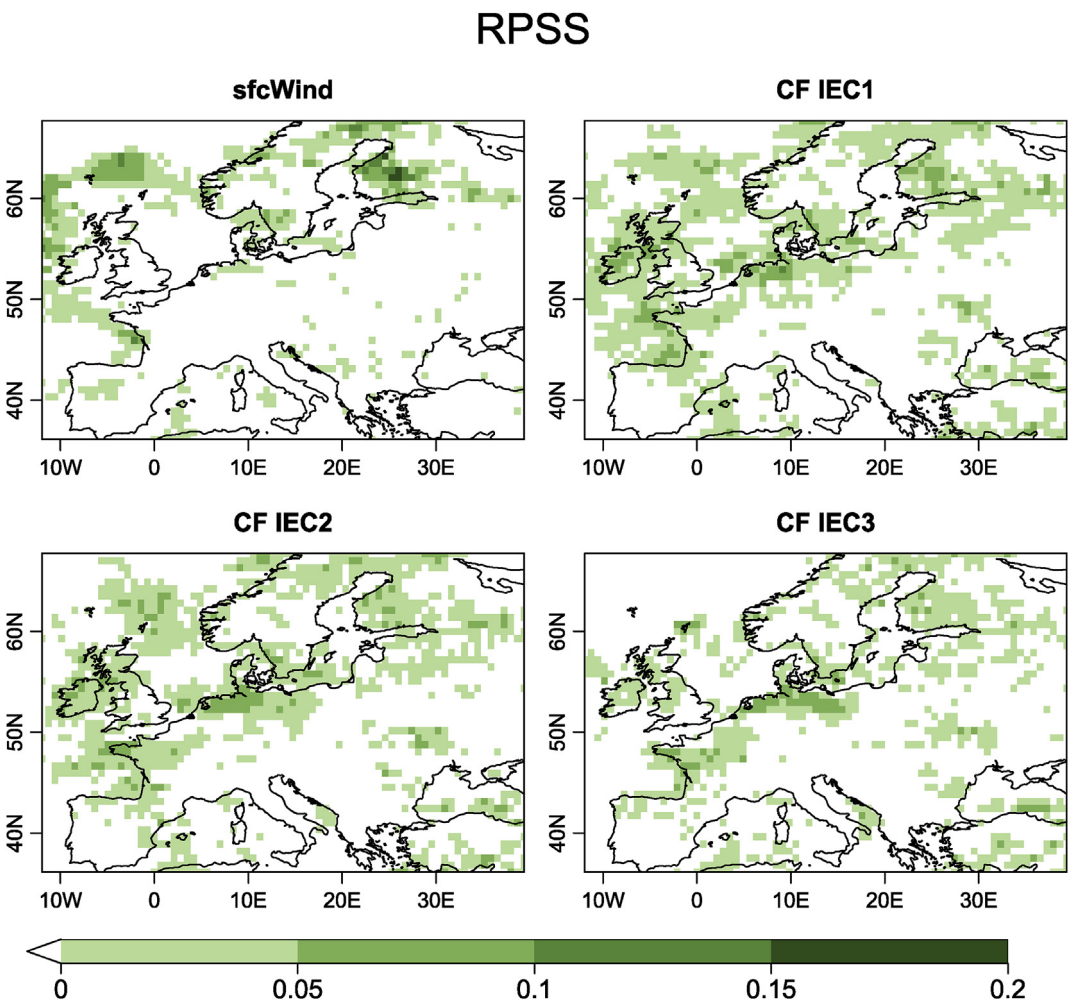

Fig. 6. Ranked Probability Skill Score of surface wind speed and capacity factor forecasts from ECMWF System4 issued in November and valid for next DJF season over Europe. The scores have been estimated from a hindcast covering 1981–2015, and employing ERA-Interim-derived capacity factors as verification truth.

Proposed solution: capacity factor provides normalized generation dividing by the installed capacity. Each user can derive total generation forecasts for a wind farm multiplying capacity factor by the installed capacity.

- Challenge: a large number of turbine models exist with differing efficiency curves.
  Proposed solution: capacity factor is computed for three different turbines representing three turbine classes suitable for low, medium and high wind speed conditions.
- Challenge: wind farm losses are highly specific to each project.
  Proposed solution: provide net capacity factor estimates and let each user subtract the losses deemed necessary.
- Challenge: Seasonal predictions are produced at a coarse scale.
  Proposed solution: Employ the predictions at the provided resolution. Statistical downscaling techniques cannot be applied without long on-site observational records. Dynamical downscaling is not feasible in terms of computational resources. Anomalies at monthly or seasonal time scales tend to be spatially smoother than short-term variability, therefore the local scale is not so relevant for seasonal predictions as might be for meteorological (e.g. day-ahead) prediction.
- Challenge: power curves are valid for 10-minutal wind speeds, while most seasonal prediction systems produce monthly mean outputs and only a few of them provide daily or 6-hourly values at most.
  Proposed solution: Employ six-hourly instantaneous values directly with the 10-minutal power curves. This effectively restricts the number of systems that can be used with this methodology.
- Challenge: power curves are valid for wind speed at hub height, but only surface wind is available from state-of-the-art seasonal prediction systems.
  Proposed solution: surface wind is adjusted at hub height with a simple power law, assuming a hub height of 100 m and fixed shearing exponents valid over land and sea under neutral stability.
- Challenge: seasonal prediction systems have biases and drift in time.
  Proposed solution: employ a lead-time dependant empirical quantile mapping bias adjustment technique. These method corrects the shape of the distribution.
- Challenge: surface wind from reanalysis models, which is employed as observation for bias adjustment, is also biased, with the extrapolation at 100 m adding even more uncertainty.
  Proposed solution: long-term mean wind speed from a high-resolution global wind atlas has been employed to adjust reanalysis winds at 100 m.

The methodology has been applied over Europe employing ECMWF System4 wind speed predictions. Those capacity factor predictions for the winter season proved to be better than using a climatological forecast in some regions, especially around the North Sea region. The method, although simple in some aspects, proved to be able to produce skillful forecasts of wind power generation one to three months ahead. Further developments could transform those generation forecasts into wind farm revenue forecasts or region/country aggregate forecasts that would be useful for TSOs and traders.

Acknowledgments

This work was funded by the H2020 project S2S4E (GA 776787), the COPERNICUS service contract CLIM4ENERGY (C3S_441_Lot2_-CEA), and the projects INDECIS and MEDSCOPE cofunded by the H2020 ERA-net ERA4CS. The research leading to these results has also received funding from the Ministerio de Ciencia, Innovación y Universidades (MICINN) as part of the CLINSA project (CGL2017-85791-R). We acknowledge NOAA/ESRL Physical Sciences Division to provide wind speed records from the Boulder Atmospheric Observatory. Cabauw data have been retrieved from CESAR database and Dr. Fred Bosveld (KNMI). Thanks to Elena Kozlova (University of Exeter) for sharing CVO data. The BMWi (Bundesministerium fuer Wirtschaft und Energie) and the PTJ (Projekttraeger Juelich) provided the FINO1 mast data. We also thank Hans Verhoef (ECN) and Dr. Frank Beyrich (DWD) for sharing Ijmuiden and Lindenberg data, respectively. We acknowledge the providers of the NWTC M2 mast data [26]. Thanks to WASA (Wind Atlas for South Africa) for providing WM01 tall tower data. Long-term mean wind speed data at hub heights was obtained from DTU Wind Energy Global Wind Atlas, funded by Danish Energy Agency EUDP 11-II, Globalt Vind Atlas J.nr. 64011-0347. Authors want to thank Pierre-Antoine Bretonnière for technical support with the datasets.

Appendix A. Supplementary data

Supplementary data to this article can be found online at https://doi.org/10.1016/j.renene.2019.04.135.

References

[1] J. Badger, H. Frank, A.N. Hahmann, G. Giebel, Wind-climate estimation based on mesoscale and microscale modeling: statistical–dynamical downscaling for wind energy applications, J. Appl. Meteorol. Climatol. 53 (8) (2014) 1901–1919.
[2] P. Beaucage, M.C. Brower, J. Tensen, Evaluation of four numerical wind flow models for wind resource mapping, Wind Energy 17 (2) (2014) 197–208.
[3] P.E. Bett, H.E. Thornton, J.F. Lockwood, A.A. Scaife, N. Golding, C. Hewitt, R. Zhu, P. Zhang, C. Li, Skill and reliability of seasonal forecasts for the Chinese energy sector, J. Appl. Meteorol. Climatol. 56 (11) (2017) 3099–3114.
[4] J. Boé, L. Terray, F. Habets, E. Martin, Statistical and dynamical downscaling of the Seine basin climate for hydro-meteorological studies, Int. J. Climatol. 27 (August 2007) (2007) 1643–1655.
[5] M.C. Brower, Wind Resource Assessment, John Wiley & Sons, Inc., Hoboken, NJ, USA, 2012.
[6] C. Buontempo, European climate services, in: A. Troccoli (Ed.), Weather & Climate Services for the Energy Industry, Springer International Publishing, Cham, 2018, pp. 27–40.
[7] C. Buontempo, H.M. Hanlon, M. Bruno Soares, I. Christel, J.-M. Soubeyroux, C. Viel, S. Calmanti, L. Bosi, P. Falloon, E.J. Palin, E. Vanvyve, V. Torralba, N. Gonzalez-Reviriego, F. Doblas-Reyes, E.C. Pope, P. Newton, F. Liggins, What have we learnt from EUPORIAS climate service prototypes? Clim. Serv. 9 (2018) 21–32.
[8] C.J. Christensen, J.B. Dragt, Accuracy of Power Curve Measurements, Technical Report 2632, Risoe National Laboratory, 1987.
[9] R.T. Clark, P.E. Bett, H.E. Thornton, A.A. Scaife, Skilful seasonal predictions for the european energy industry, Environ. Res. Lett. 12 (2) (2017), 024002.
[10] M. Decker, M.A. Brunke, Z. Wang, K. Sakaguchi, X. Zeng, M.G. Bosilovich, Evaluation of the reanalysis products from GSFC, NCEP, and ECMWF using flux tower observations, J. Clim. 25 (6) (2012) 1916–1944.
[11] D.P. Dee, S.M. Uppala, A.J. Simmons, P. Berrisford, P. Poli, S. Kobayashi, U. Andrae, M.A. Balmaseda, G. Balsamo, P. Bauer, P. Bechtold, A.C.M. Beljaars, L. van de Berg, J. Bidlot, N. Bormann, C. Delsol, R. Dragani, M. Fuentes, A.J. Geer, L. Haimberger, S.B. Healy, H. Hersbach, E.V. Hólm, L. Isaksen, P. Kållberg, M. Köhler, M. Matricardi, A.P. McNally, B.M. Monge-Sanz, J.-J. Morcrette, B.-K. Park, C. Peubey, P. de Rosnay, C. Tavolato, J.-N. Thépaut, F. Vitart, The era-interim reanalysis: configuration and performance of the data assimilation system, Q. J. R. Meteorol. Soc. 137 (656) (2011) 553–597.
[12] F.J. Doblas-Reyes, J. García-Serrano, F. Lienert, A.P. Biescas, L.R.L. Rodrigues, Seasonal climate predictability and forecasting: status and prospects, Wiley Interdiscip. Rev. Clim. Change 4 (4) (2013) 245–268.
[13] C. Draxl, A. Clifton, B.-M. Hodge, J. McCaa, The wind integration national dataset (wind) toolkit, Appl. Energy 151 (2015) 355–366.
[14] L. Dubus, S. Muralidharan, A. Troccoli, What does the energy industry require from meteorology? in: A. Troccoli (Ed.), Weather & Climate Services for the Energy Industry Springer International Publishing, 2018, pp. 41–63.
[15] D. Elliott, J. Cadogan, Effects of Wind Shear and Turbulence on Wind Turbine Power Curves, Wind Energy, 1990.
[16] EUPORIAS, Report Summarising Users' Needs for S2d Predictions, Technical Report Deliverable 12.3, EUPORIAS, 2015.
[17] A.M. Foley, P.G. Leahy, A. Marvuglia, E.J. McKeogh, Current methods and advances in forecasting of wind power generation, Renew. Energy 37 (1) (2012) 1–8.

[18] E. García-Bustamante, J.F. González-Rouco, P.A. Jiménez, J. Navarro, J.P. Montávez, A comparison of methodologies for monthly wind energy estimation, Wind Energy 12 (7) (2009) 640–659.
[19] I. Gonzalez Aparicio, A. Zucker, F. Careri, F. Monforti, T. Huld, J. Badger, Emhires Dataset. Part I: Wind Power Generation. European Meteorological Derived High Resolution Res Generation Time Series for Present and Future Scenarios, 2016.
[20] R. Graham, W. Yun, J. Kim, A. Kumar, D. Jones, L. Bettio, N. Gagnon, R. Kolli, D. Smith, Long-range forecasting and the global framework for climate services, Clim. Res. 47 (1) (2011) 47–55.
[21] J.O. Haerter, B. Eggert, C. Moseley, C. Piani, P. Berg, Statistical precipitation bias correction of gridded model data using point measurements, Geophys. Res. Lett. 42 (6) (2015) 1919–1929.
[22] L. Hermanson, H.-L. Ren, M. Vellinga, N.D. Dunstone, P. Hyder, S. Ineson, A.A. Scaife, D.M. Smith, V. Thompson, B. Tian, K.D. Williams, Different types of drifts in two seasonal forecast systems and their dependence on enso, Clim. Dyn. 51 (4) (August 2018) 1411–1426.
[23] C. Hewitt, S. Mason, D. Walland, The global framework for climate services, Nat. Clim. Change 2 (2012) 831 (EP –).
[24] S. a. Hsu, E. a. Meindl, D.B. Gilhousen, Determining the power-law wind-profile exponent under near-neutral stability conditions at sea, J. Appl. Meteorol. 33 (6) (1994) 757–765.
[25] IEC, International Standard IEC 61400-1, third ed., 2005.
[26] D. Jager, A. Andreas, Nrel National Wind Technology Center (Nwtc): M2 Tower; Boulder, colorado (Data), Technical report, National Renewable Energy Lab.(NREL), Golden, CO (United States), 1996.
[27] I. Jolliffe, D. Stephenson, Forecast Verification: A Practitioner's Guide in Atmospheric Science, Wiley, 2012.
[28] L. Lledó, O. Bellprat, F.J. Doblas-Reyes, A. Soret, Investigating the effects of pacific sea surface temperatures on the wind drought of 2015 over the United States, J. Geophys. Res. Atmos. 123 (10) (2018) 4837–4849.
[29] M. Lydia, S.S. Kumar, A.I. Selvakumar, G.E.P. Kumar, A comprehensive review on wind turbine power curve modeling techniques, Renew. Sustain. Energy Rev. 30 (2014) 452–460.
[30] D. MacLeod, V. Torralba, M. Davis, F. Doblas-Reyes, Transforming climate model output to forecasts of wind power production: how much resolution is enough? Meteorol. Appl. 25 (1) (2017) 1–10.
[31] A. Mariotti, P.M. Ruti, M. Rixen, Progress in subseasonal to seasonal prediction through a joint weather and climate community effort, npj Clim. Atmos. Sci. 1 (1) (2018).
[32] F. Molteni, T. Stockdale, M. Alonso-Balmaseda, G. Balsamo, R. Buizza, L. Ferranti, L. Magnusson, K. Mogensen, T. Palmer, F. Vitart, The New Ecmwf Seasonal Forecast System (System 4), Technical Report 656, ECMWF, 2011.
[33] A.H. Monahan, Y. He, N. McFarlane, A. Dai, The probability distribution of land surface wind speeds, J. Clim. 24 (15) (2011) 3892–3909.
[34] E.C. Morgan, M. Lackner, R.M. Vogel, L.G. Baise, Probability distributions for offshore wind speeds, Energy Convers. Manag. 52 (1) (2011) 15–26.
[35] PCWG, Power Curve Working Group Roadmap 2018, 2018.
[36] E.L. Petersen, I. Troen, H.E. Jørgensen, J. Mann, Are local wind power resources well estimated? Environ. Res. Lett. 8 (1) (2013), 011005.
[37] M. Ritter, Z. Shen, B.L. Cabrera, M. Odening, L. Deckert, Designing an index for assessing wind energy potential, Renew. Energy 83 (2015) 416–424.
[38] S2S4E, Technical Report Deliverable D2, User Needs and Decision-Making Processes that Can Benefit from S2s Forecasts, vol. 1, 2018, p. S2S4E.
[39] S. Saha, S. Moorthi, X. Wu, J. Wang, S. Nadiga, P. Tripp, D. Behringer, Y.-T. Hou, H. ya Chuang, M. Iredell, M. Ek, J. Meng, R. Yang, M.P. Mendez, H. van den Dool, Q. Zhang, W. Wang, M. Chen, E. Becker, The NCEP climate forecast system version 2, J. Clim. 27 (6) (2014) 2185–2208.
[40] J. Shukla, J.L. Kinter, Predictability of seasonal climate variations: a pedagogical review, in: T. Palmer, R. Hagedorn (Eds.), Predictability of Weather and Climate, Cambridge University Press, 2006, pp. 306–341.
[41] M.B. Soares, M. Alexander, S. Dessai, Sectoral use of climate information in europe: a synoptic overview, Clim. Serv. 9 (2018) 5–20 (Climate services in practice: what we learnt from EUPORIAS).
[42] I. Staffell, S. Pfenninger, Using bias-corrected reanalysis to simulate current and future wind power output, Energy 114 (2016) 1224–1239.
[43] I. Staffell, S. Pfenninger, The increasing impact of weather on electricity supply and demand, Energy 145 (2018) 65–78.
[44] J. Sumner, C. Masson, Influence of atmospheric stability on wind turbine power performance curves, J. Sol. Energy Eng. 128 (4) (2006) 531.
[45] M.J. Themeßl, A. Gobiet, G. Heinrich, Empirical-statistical downscaling and error correction of regional climate models and its impact on the climate change signal, Clim. Change 112 (2) (2012) 449–468.
[46] V. Torralba, F.J. Doblas-Reyes, D. MacLeod, I. Christel, M. Davis, Seasonal climate prediction: a new source of information for the management of wind energy resources, J. Appl. Meteorol. Climatol. 56 (5) (2017) 1231–1247.
[47] J.S. Touma, Dependence of the wind profile power law on stability for various locations, J. Air Pollut. Control Assoc. 27 (9) (1977) 863–866.
[48] A. Troccoli, K. Muller, P. Coppin, R. Davy, C. Russell, A.L. Hirsch, Long-term wind speed trends over Australia, J. Clim. 25 (1) (2012) 170–183.
[49] J.W. Wagenaar, P.J. Eecen, Dependence of Power Performance on Atmospheric Conditions and Possible Corrections, Technical Report ECN-M–11-033, Energy research Centre of the Netherlands, 2011.
[50] A. Weisheimer, T.N. Palmer, On the reliability of seasonal climate forecasts, J. R. Soc. Interface 11 (96) (2014).
[51] WMO, Appendix 2.2.36. Standardized verification system for long-range forecasts, Technical Report 485, in: Manual on the Global Data-Processing and Forecasting System, Annex IV to the WMO Technical Regulations, WMO, 2017.
[52] WMO, Energy Exemplar to the User Interface Platform of the Global Framework for Climate Services, 2017.
[53] T. Zhao, J.C. Bennett, Q.J. Wang, A. Schepen, A.W. Wood, D.E. Robertson, M.-H. Ramos, How suitable is quantile mapping for postprocessing gcm precipitation forecasts? J. Clim. 30 (9) (2017) 3185–3196.

Supplementary figure 1 for "Seasonal forecasts of capacity factor"

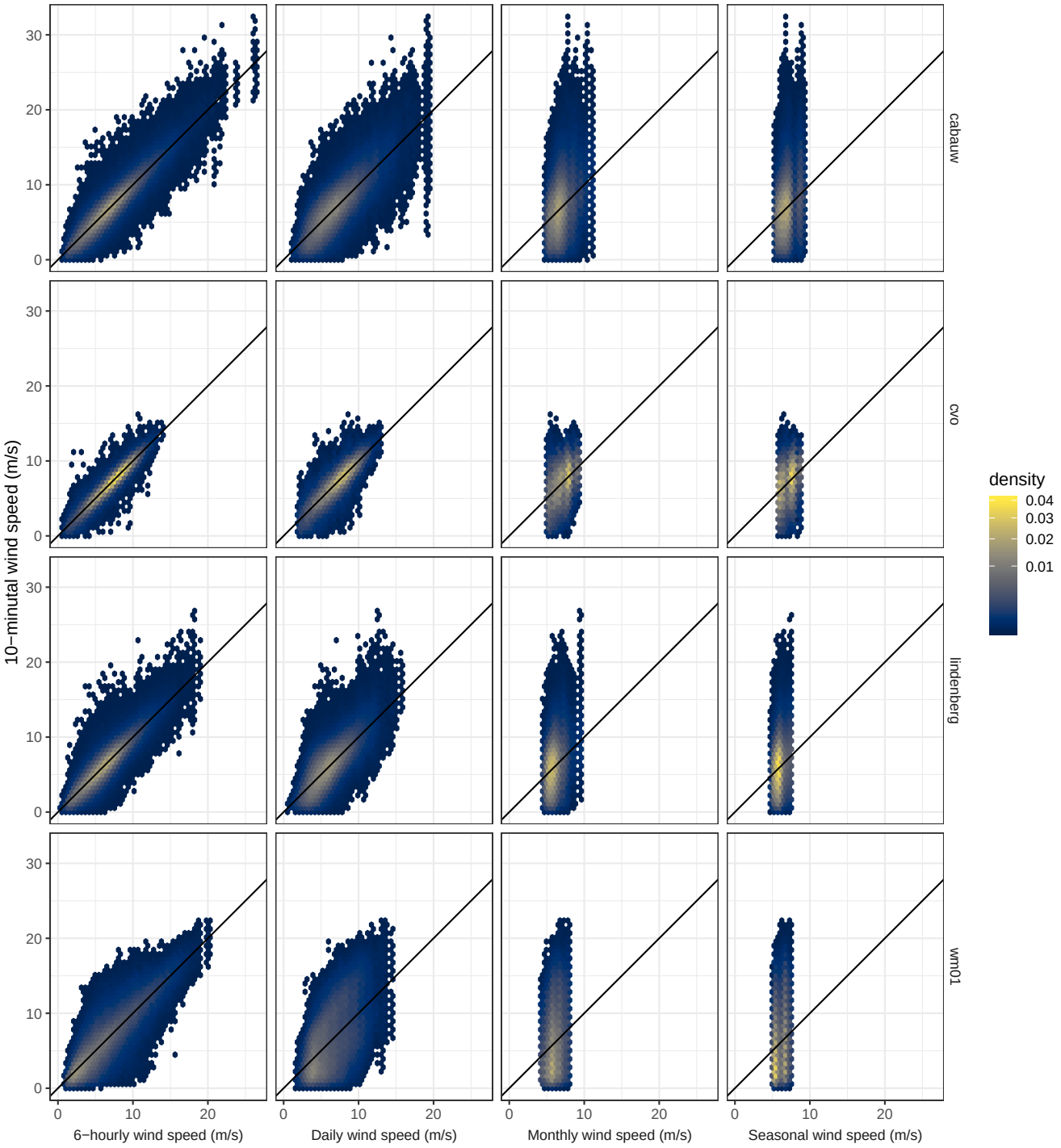

Supplementary figure 2 for "Seasonal forecasts of capacity factor"

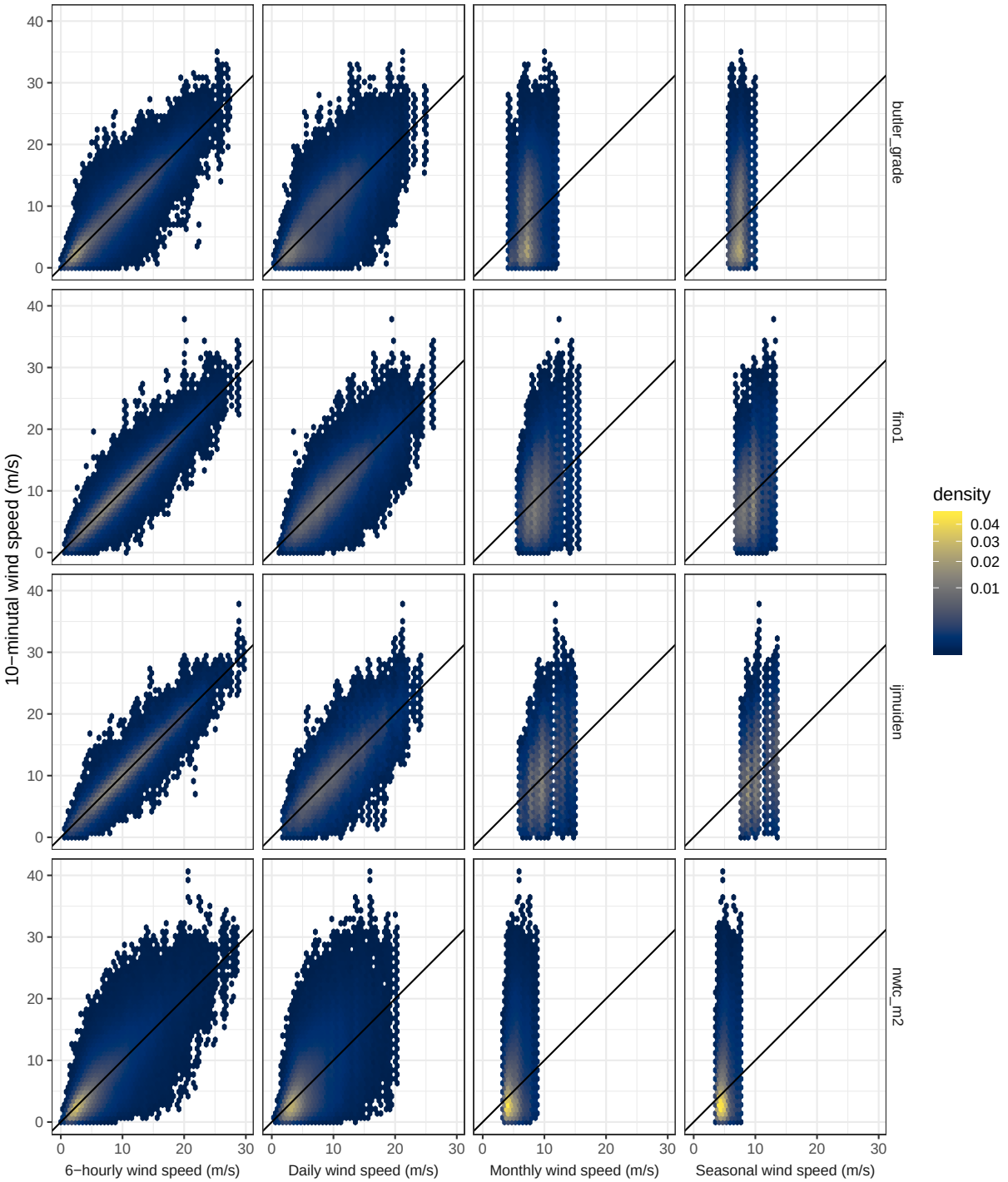

Chapter 6

Seasonal prediction of Euro-Atlantic teleconnections from multiple systems

The paper presented in this chapter analyzes the skill of five seasonal prediction systems at anticipating the values of four teleconnection indices that are relevant in the Euro-Atlantic sector. The analysis is carried out for the four seasons of the year and from zero to four months before the start of the season. The four teleconnections considered, namely the North Atlantic Oscillation (NAO), the East Atlantic (EA), the East Atlantic/Western Russia (EAWR) and the Scandinavian Pattern (SCA), can be used to describe the atmospheric circulation over Europe in a simplified way. This work might seem a bit distant from practical applications for the wind industry. However, each of those teleconnection indices is associated to specific wind speed and wind power generation anomalies in Europe (see figure 6.1 and Yang et al. (2020)). For the NAO this relationship is well known in the energy sector, and is already being used by the industry in forensic analyses to understand the performance of wind farms in the past in relation to circulation anomalies. Therefore, providing forecasts for the teleconnection indices can be a simple yet effective way to inform users of future variability of wind speed and wind power generation. Additionally, further work has revealed the potential of employing forecasts of the teleconnections altogether with observed impacts to produce downscaled predictions at the local scales (see chapter 8).

This paper deals with objectives (ii) and (iii) of this dissertation.

Lledó, L., Cionni, I., Torralba, V., Bretonnière, P.-A., and Samsó, M. (2020). Seasonal prediction of Euro-Atlantic teleconnections from multiple systems. *Environmental Research Letters*, 15(7):74009, doi: 10.1088/1748-9326/ab87d2

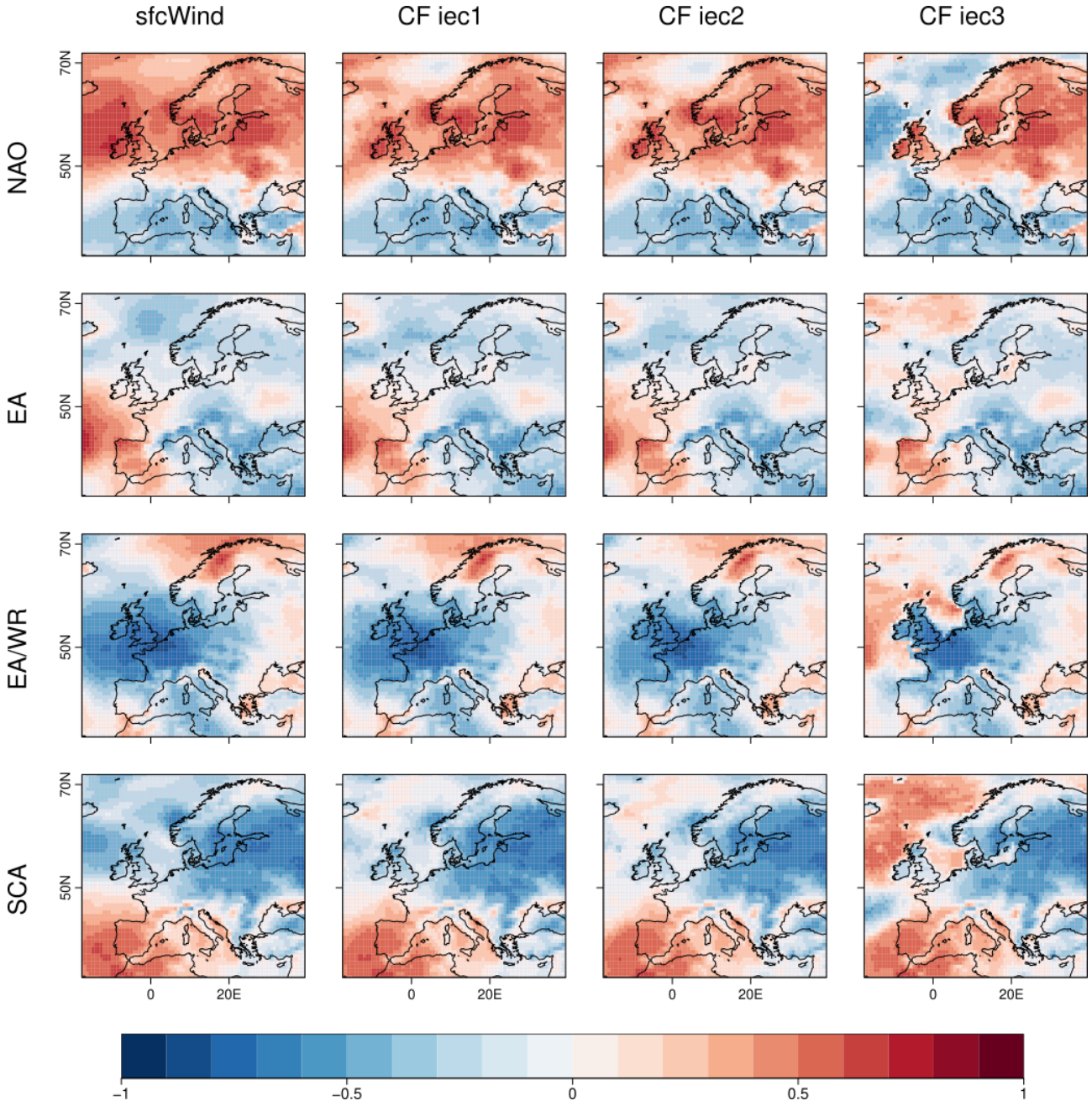

Figure 6.1: Impact of the four Euro-Atlantic teleconnection indices in January on surface wind speed and capacity factor for three different turbine types, estimated by Pearson correlation coefficients from ERA-Interim reanalysis in the 1981–2016 period. The capacity factors are derived from surface wind employing the model described in Lledó et al. (2019).

IOP Publishing Environ. Res. Lett. 15 (2020) 074009 https://doi.org/10.1088/1748-9326/ab87d2

Environmental Research Letters

PAPER

Seasonal prediction of Euro-Atlantic teleconnections from multiple systems

Llorenç Lledó[1], Irene Cionni[2], Verónica Torralba[1], Pierre-Antoine Bretonnière[1] and Margarida Samsó[1]

[1] Barcelona Supercomputing Center (BSC), Barcelona, Spain
[2] Agenzia nazionale per le nuove tecnologie, l'energia e lo sviluppo economico sostenibile (ENEA), Roma, Italy

E-mail: lledo@bsc.es

OPEN ACCESS

RECEIVED
16 December 2019

REVISED
23 March 2020

ACCEPTED FOR PUBLICATION
8 April 2020

PUBLISHED
22 June 2020

Keywords: Euro-Atlantic Teleconnections, teleconnections, seasonal prediction, multi-system predictions, climate variability

Abstract

Seasonal mean atmospheric circulation in Europe can vary substantially from year to year. This diversity of conditions impacts many socioeconomic sectors. Teleconnection indices can be used to characterize this seasonal variability, while seasonal forecasts of those indices offer the opportunity to take adaptation actions a few months in advance. For instance, the North Atlantic Oscillation has proven useful as a proxy for atmospheric effects in several sectors, and dynamical forecasts of its evolution in winter have been shown skillful. However the NAO only characterizes part of this seasonal circulation anomalies, and other teleconnections such as the East Atlantic, the East Atlantic Western Russia or the Scandinavian Pattern also play an important role in shaping atmospheric conditions in the continent throughout the year. This paper explores the quality of seasonal forecasts of these four teleconnection indices for the four seasons of the year, derived from five different seasonal prediction systems. We find that several teleconnection indices can be skillfully predicted in advance in winter, spring and summer. We also show that there is no single prediction system that performs better than the others for all seasons and teleconnections, and that a multi-system approach produces results that are as good as the best of the systems.

1. Introduction

Atmospheric circulation in Europe and the North Atlantic has a strong seasonal cycle, but it can also vary substantially from one year to another in the same season. The year-to-year climate variability can partly be attributed to the chaotic nature of the atmosphere but also to external forcings exerted by other components of the Earth system such as ocean temperature, soil moisture or sea ice extent anomalies that modify the energy budget of the atmosphere and ultimately modify the large-scale circulation (Doblas-Reyes *et al* 2013, Heinze *et al* 2019, Mariotti *et al* 2018). This interannual variability has strong impacts on several socioeconomic sectors such as energy, agriculture, tourism, insurance, water management, health or civil protection among others (Hewitt *et al* 2012, WMO 2014). Therefore seasonal forecasts that provide climate information for the next few months are very useful to take precautionary actions and adapt to anomalous climate conditions in advance (Soares *et al* 2018, White *et al* 2017, Torralba *et al* 2017, Ceglar *et al* 2018, Walz *et al* 2018, Turco *et al* 2018, Clark *et al* 2017).

Seasonal climate variability over Europe is often analyzed through atmospheric teleconnections. The rationale behind atmospheric teleconnections is to find recurrent and persistent large-scale atmospheric circulation patterns and corresponding temporally varying indices that can be used to describe monthly or seasonal climate variability and its surface impacts in a simplified way. For instance, the North Atlantic Oscillation (NAO) (Hurrell *et al* 2003, Wanner *et al* 2001), the most relevant Euro-Atlantic teleconnection, is known to affect surface temperature, precipitation and wind speed in almost all of Europe (Trigo *et al* 2002, Brayshaw *et al* 2011). However the NAO only represents around one third of the seasonal circulation variability over Europe in winter, spring and summer (in autumn represents only one sixth), while other Euro-Atlantic Teleconnections (EATC) such as the East Atlantic (EA) (Woollings *et al* 2010), the East Atlantic/Western Russia (EAWR) (Lim 2014) and the Scandinavian pattern (SCA) (Bueh and Nakamura

2007) also play an important role in modulating surface conditions (see for example Zubiate *et al* (2016), Josey *et al* (2011) or Hall and Hanna (2018)).

Several authors have recently shown that the state of the NAO during winter (DJF) can be skillfully predicted months or even more than a year ahead employing dynamical prediction systems that simulate the interactions between atmosphere, ocean, sea ice and soil moisture conditions (Scaife *et al* 2014, Smith *et al* 2014, Dunstone *et al* 2016, Johnson *et al* 2019). The use of multi-system prediction ensembles can achieve even better results (Athanasiadis *et al* 2017, Baker *et al* 2018). However, the ability of state-of-the-art seasonal forecast systems to simulate the other EATC indices has not yet been systematically explored in the literature. Only empirical predictions of the EA index derived from sea surface temperature in the preceding months have been proved useful in summer (Ossó *et al* 2017, Iglesias *et al* 2014), while a point-based sea level pressure index that resembles the EA has been studied for winter in Baker *et al* (2017). Therefore it would be highly beneficial to produce and analyse dynamical forecasts for the other EATC indices (Hall and Hanna 2018). Also, the focus of most of the previous studies has been on the winter season, while forecasts for the other seasons can be relevant as well for many seasonal climate service users. Therefore a systematic approach that can be employed throughout the year for all the EATCs and for both observations and seasonal prediction systems has been defined in this work.

Teleconnection patterns and indices can be computed in many different ways. Essentially, point-based, box-based or Empirical Orthogonal Function analysis methods are used in the literature. A typical method to define those teleconnections is through Rotated Empirical Orthogonal Function (REOF) analysis (Barnston and Livezey 1987). REOF is a dimensionality reduction technique that allows for approximating circulation anomalies as a linear combination of only a few spatial patterns:

$$Anom(t,x,y) = \sum_{i=1}^{nmodes} TCI_i(t) * TCP_i(x,y) + Residuals. \quad (1)$$

Teleconnection Patterns (TCP) and Indices (TCI) –i.e. the weights in the linear combination—are chosen so that the residual term is minimized. Over the Euro-Atlantic region, when retaining four variability modes the aforementioned teleconnections (NAO, EA, EAWR and SCA) are obtained. This methodology mimics well-known Climate Prediction Center patterns and indices as much as possible (Climate Prediction Center 2012), and does not rely on identifying the centers of action of the different teleconnections, which move from one season to another. Additionally, point-based indices are sensitive to model biases and local skill at the centers of action. Indeed Athanasiadis *et al* (2017) have already shown that the highest skills for NAO forecasts are obtained when using spatially-averaged indices.

The observed patterns and indices for these four Euro-Atlantic Teleconnections (EATC) have been obtained from ERA5 reanalysis, and forecasts of each EATC index have been derived from multiple seasonal prediction systems by projecting predicted circulation anomalies onto the observed teleconnection patterns. Employing this method, the skill of several seasonal prediction systems from the Copernicus Climate Change Service (C3S) in simulating the year-to-year variability of the NAO, EA, EAWR and SCA teleconnection indices for the four seasons of the year, and from zero to three months before the start of the season has been analysed. Section 2 describes the data and methods employed in detail, section 3 presents the results and conclusions follow in section 4.

2. Datasets and methodology

2.1. Datasets

2.1.1. Observational reference

The ERA5 reanalysis (Copernicus Climate Change Service 2019, Copernicus Climate Change Service (C3S) 2017) from the European Center for Medium-Range Weather Forecasts (ECMWF) has been employed as observational reference to define the four Euro-Atlantic teleconnection patterns and indices for the 1981–2018 period. More specifically, seasonal anomalies of geopotential height at 500 hPa with respect to the whole period have been obtained separately for each of the four seasons (DJF, MAM, JJA and SON). Although the ERA5 data has a spatial resolution of ∼0.28 degrees (or ∼30 km), in order to obtain teleconnection patterns that can be compared with the seasonal prediction systems, the data has been regrided to match the spatial resolution of the forecasts (1 x 1°, see table 1).

2.1.2. Seasonal prediction systems

Several European national meteorological centers and institutions produce operational seasonal predictions. Those are made with coupled Earth system models that simulate the evolution of atmosphere, ocean, sea ice and land surface conditions in the upcoming months. Five different seasonal prediction systems have been employed in this study, from the European Centre for Medium-Range Weather Forecasts (ECMWF), Deutscher Wetterdienst (DWD), Météo France (MF), UK Met Office (UKMO) and Centro Euro-Mediterraneo sui Cambiamenti Climatici (CMCC). The latest operational prediction systems (at the time of writing) from those centers have been employed: SEAS5 from ECMWF (Johnson *et al* 2019), Seasonal Prediction System 3 from CMCC (SPS3) (Sanna *et al* 2017), System6 from MF (MF6) (Dorel *et al* 2017), GloSea5-GC2 from UKMO (GS5GC2) (MacLachlan *et al* 2014, Williams *et al* 2015) and System2 from DWD (DWD2)

(Deutscher Wetterdienst 2019). All of the predictions have been obtained from the Climate Data Store (CDS) of the Copernicus Climate Change Service (C3S) initiative, which provides a unified access point, and a common hindcast period and spatial resolution (ECMWF 2019). The most relevant details of each one of the prediction systems employed here, such as the number of ensemble members, the hindcast period analyzed or the spatial grid are specified in table 1. Notice that the ECMWF SEAS5 predictions have been additionally obtained for a longer period and bigger ensemble from ECMWF MARS service, and used in section 3.3 to test the sensitivity of the results to the period length and the ensemble size.

The configuration of those prediction systems is similar in terms of initialization, numerical integration, parametrizations and coupling of the different Earth system components modelled. However GS5GC2 and MF6 have a lagged ensemble—produced by accumulating several integrations initialized at different instants of time during the latest month—while the other systems are initialized in burst mode the first day of the month—perturbed initial conditions and stochastic parametrizations are used to initialize and run several ensemble members in order to describe uncertainty—. The MF6 hindcast ensemble is built from 1 ensemble member initialized the first of the month plus 12 members initialized the 25th of the previous month and 12 members initialized the 20th of the previous month. Similarly, the GS5GC2 hindcast ensembles are built from 7 members initialized the first of the month, plus 7 members for the 9th, 17th and 25th of the previous month respectively (see ECMWF (2019)). The hindcast for GS5GC2 has been built by combining two versions of this system: all the System13 hindcasts available in the CDS with a few System14 runs for May to October 2016.

The 500 hPa geopotential height fields of these systems were downloaded, formatted and quality checked with an in-house developed python software suite that automatically processes the data to a common format (NetCDF). Quality controls include file integrity, time and ensemble members completeness and consistency, missing values, and physical value checks. These checks detected issues in 28 fields of 500 hPa geopotential height of the SPS3, distributed across all the period and ensemble. The issues were reported to C3S and confirmed by the data provider, and have been documented under known issue E5a in the C3S portal (https://confluence.ecmwf.int/ display/ CKB/ C3S+Seasonal+Forecasts+known+issues). The affected members and months have been not included in the analysis. Given the relatively low number of erroneous fields (28 out of 80 640), this should not produce noticeable effects on the results. However keeping the erroneous fields would produce a significant skill degradation.

2.2. Methods

2.2.1. Observed teleconnection patterns and indices

The four observed EATC patterns and indices have been computed from ERA5 500 hPa geopotential height seasonal anomalies through a Rotated Empirical Orthogonal Function (REOF) analysis (Hannachi *et al* 2007, Wilks 2019) over the Euro-Atlantic domain (90°W–60°E and 20°N–80°N). First, seasonal anomalies for each season (DJF/MAM/JJA/SON) and for the 1981–2018 period have been computed with respect to the same period mean. Then an EOF analysis has been performed, and the first four variability modes have been retained. The anomalies have been weighted by the cosine of the latitude prior to the EOF analysis to account for differences in the areas of the grid points. After that, a *Varimax* rotation has been applied to the unit length eigenvectors (or loading patterns), in order to simplify the spatial structure of the patterns but still preserve its orthogonality (Mestas-Nuñez 2000). Finally, the four obtained REOF modes have been reordered and their sign has been adjusted when needed so that the EATC patterns resemble as much as possible the positive phases of the NAO, EA, EAWR and SCA patterns as computed by NCEP's Climate Prediction Center (Climate Prediction Center 2012, Barnston and Livezey 1987, Lim 2014). Figure 1 shows the four teleconnection patterns (i.e. the rotated unit-vector loadings after readjusting for the latitudinal weights) obtained for each of the four seasons of the year. Due to the normalization, the more localized patterns such as the EA have strongest colors in the figure, while more widespread patterns such as the NAO have lighter colors. The percentage of variance that each of the EATC patterns represents can be seen in figure 3 lower left panel for each season. While NAO represents around one third of the total variance in winter, spring and summer, the other EATC patterns also contribute to describe the atmospheric circulation variability with values of up to 20% of explained variance. The residual variance that remains unexplained by the four EATCs in each season (i.e. the variance of the residual term in equation (1)) indicates the goodness of the approximation of the circulation anomalies by the four EATCs, and expressed as a percentage of the total variance it is: 23% (DJF), 36% (MAM), 33% (JJA) and 36% (SON). This is much less than when only using the first EOF to compute the NAO (always above 60%).

2.2.2. Forecasts of EATC indices

To obtain retrospective forecasts of the EATC indices, the 500 hPa geopotential height fields from the seasonal prediction system hindcasts initialized in the 1993–2016 period have been used (note that the ERA5 EATCs have been computed with a longer period

Table 1. Summary of the seasonal prediction systems employed.

Producing center	Prediction system	Data source	Analyzed period	Ensemble members	Ensemble generation	Horizontal grid
CMCC	SPS3	CDS	1993-2016	40	burst	Regular 360x180
DWD	System2	CDS	1993-2016	30	burst	Regular 360x180
UKMO	GloSea5 GC2	CDS	1993-2016	28	lagged	Regular 360x180
MF	System6	CDS	1993-2016	25	lagged	Regular 360x180
ECMWF	SEAS5	CDS	1993-2016	25	burst	Regular 360x180
ECMWF	SEAS5	MARS	1981-2016	51	burst	Regular Gaussian F160 (640x320)

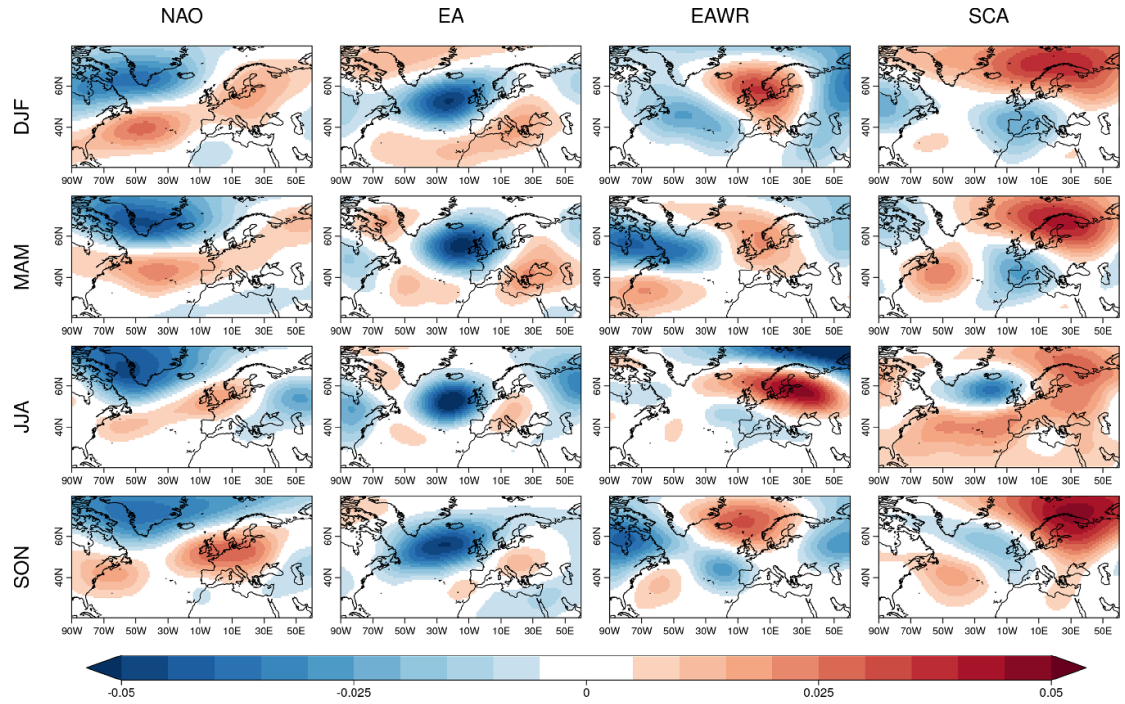

Figure 1. The loading patterns (i.e. of norm one) of the four Euro-Atlantic teleconnections obtained for each season from ERA5 geopotential height anomalies at 500 hPa in the 1981–2018 period.

to obtain more robust patterns). The seasonal mean anomalies of each system (with respect to its own climatology in the 1993–2016 period) and for each season have been projected onto the observed patterns, individually for each ensemble member. To do so, first the anomalies are weighted by the cosine of the latitude, and then the scalar product with each teleconnection pattern is computed. The projected indices have not been normalized, so that the explained variances can be computed by just doing the scalar product of each projected EATC index by itself. The total variance of each prediction system has also been computed and normalized per number of grid points, years and ensemble members, so that results can be compared with observed variance.

2.2.3. Multi-system ensemble predictions

Combining the information from several prediction systems into a single forecast can be beneficial for the forecast quality. Each prediction system represents physical processes in slightly different ways. Hence, it has been shown that the combination of all the ensemble members from different systems tends to compensate modelling errors and uncertainties from different sources (DelSole *et al* 2014). The larger ensemble size of the combination also contributes to cancel noise in the individual members and extract smaller forcing signals (Scaife *et al* 2014, Baker *et al* 2018). Two multi-system combinations have been produced here (as in Doblas-Reyes *et al* (2003) and Athanasiadis *et al* (2017)): first by pooling all the ensemble members together (MSPool) and secondly by weighting each prediction system by combining the ensemble means computed separately in each system so that all systems have equal weight in the final results (MSEW).

2.2.4. Forecast quality assessment

The quality of the EATC forecasts has been assessed employing both deterministic and probabilistic skill metrics. First the ensemble mean correlation has been used as a measure of association. The statistical

Table 2. Summary of the forecast start months employed for verification in each season and the corresponding valid periods.

Valid period	Forecast start dates
JJA 1993–2016	MAMJ 1993–2016
SON 1993–2016	JJAS 1993–2016
DJF 1993/94–2016/17	SOND 1993–2016
MAM 1994–2016	D 1993–2015
JFM 1994–2016	

significance of ensemble mean correlations has been checked with a one-tailed Student's *t*-test at a level of 95% of confidence. Additionally, the Ranked Probability Skill Score (RPSS) has been employed (as in Doblas-Reyes *et al* (2003) for NAO forecasts) to understand the improvement of tercile forecasts of EATC indices over a climatological benchmark (Jolliffe and Stephenson 2011). This score assesses the quality of a probabilistic forecast that delivers probabilities of having a below normal, normal or above normal value of an EATC index. Those categories are defined based on the 33rd and 66th percentiles (i.e. terciles) of the historical distribution of forecast values in the hindcast. The uncertainty affecting the RPSS values has been explored in terms of the Diebold-Mariano test (Diebold and Mariano 1995). This test allows to identify if the differences between a probabilistic forecast and the climatological forecast (the reference here) are statistically significant at the 95% confidence level. The Diebold-Mariano test from the SpecsVerification R package has been employed.

The assessment has been performed for all seasons, and employing the forecasts initialized at the beginning of the season and also from 1 up to 3 months before. The elapsed time between the initialization date and the start of the valid period of the forecasts is the lead time, which has been referred to as lead 0, 1, 2 and 3 to indicate the number of months of lead time. For lagged ensembles, the latest initialization date in the ensemble is employed to compute the lead (i.e. lead times are counted since the first day of the month, when all the ensembles are built). All the verifications correspond to the start dates in the 1993–2016 period. Table 2 summarizes the start dates and valid date periods employed for each season. Notice that DJF forecasts initialized in the 1993–2016 period correspond to 1993/94 to 2016/17 winters. The MAM season requires special attention: since predictions initialized in December 1992 are not available in the CDS, the 1993 start dates for January, February and March (JFM) were also discarded in order to obtain consistent results across all lead times. Therefore the verification of forecasts for spring has one year less than the other seasons. This fine-detail information is essential for reproducibility in view of the sensitivity of results to the hindcast period employed (see section 3.3).

The focus of the verification is on assessing the quality of the products as available to end users. Therefore, no correction has been applied to compensate for the differing number of ensemble members across systems, nor for the longer lead times of the older members in lagged systems.

3. Results

To illustrate how the seasonal prediction systems simulate the ERA5 EATC indices, figure 2 shows the seasonal predictions of the four EATC indices issued in November and valid for DJF (i.e. 1 month of lead time) for each of the systems in the 2000 1993–2016 period. All the systems agree in a negative NAO phase for 2009/2010 winter (first panel), although the actual observed value was well below the range of any prediction. Less well-known events such as a strong EA phase in 2013/2014 or a strong SCA phase in 2009/2010 can also be seen. As the forecasted teleconnection indices have not been normalized, a widest range can be seen for the NAO than for the other three EATCs.

3.1. Variance explained by each EATC in the prediction systems

In order to understand how well the observed teleconnection patterns describe the variability in each of the prediction systems, the explained variance of each EATC pattern as a percentage of the total variance in the system has been analysed for the 1993–2016 period. The explained variance percentages have also been computed for ERA5 in the same period. The differences between explained variance percentages in the prediction systems and in ERA5 is displayed in figure 3 for each season, lead time and EATC pattern. Additional analyses revealed that those differences are not due to sampling variability (not shown). In general, all prediction systems have less proportion of NAO variability than observed in winter, spring, and specially in summer. Something similar occurs with the EAWR pattern in autumn or the EA in winter. On the other hand the NAO has slightly more variability than observed in most prediction systems in autumn and the same occurs for the EAWR in winter and the EA in spring. Most of these differences in variability show up already from lead 0 forecasts, and do not grow with higher lead times, indicating a small role of model drift. In terms of absolute variance, all of the systems have a good agreement with the ERA5 variance (not shown), i.e. the total amount of variability in the prediction systems is comparable to that in the observational reference for the four seasons.

These biases show that variability has a different structure in the prediction systems than in the observations. This might be related to the internal variability modes of the prediction systems do not match the observed ones, i.e. there are biases in location and shape of the EATC patterns directly obtained from the prediction systems (e.g. see Walz *et al* (2018) for a

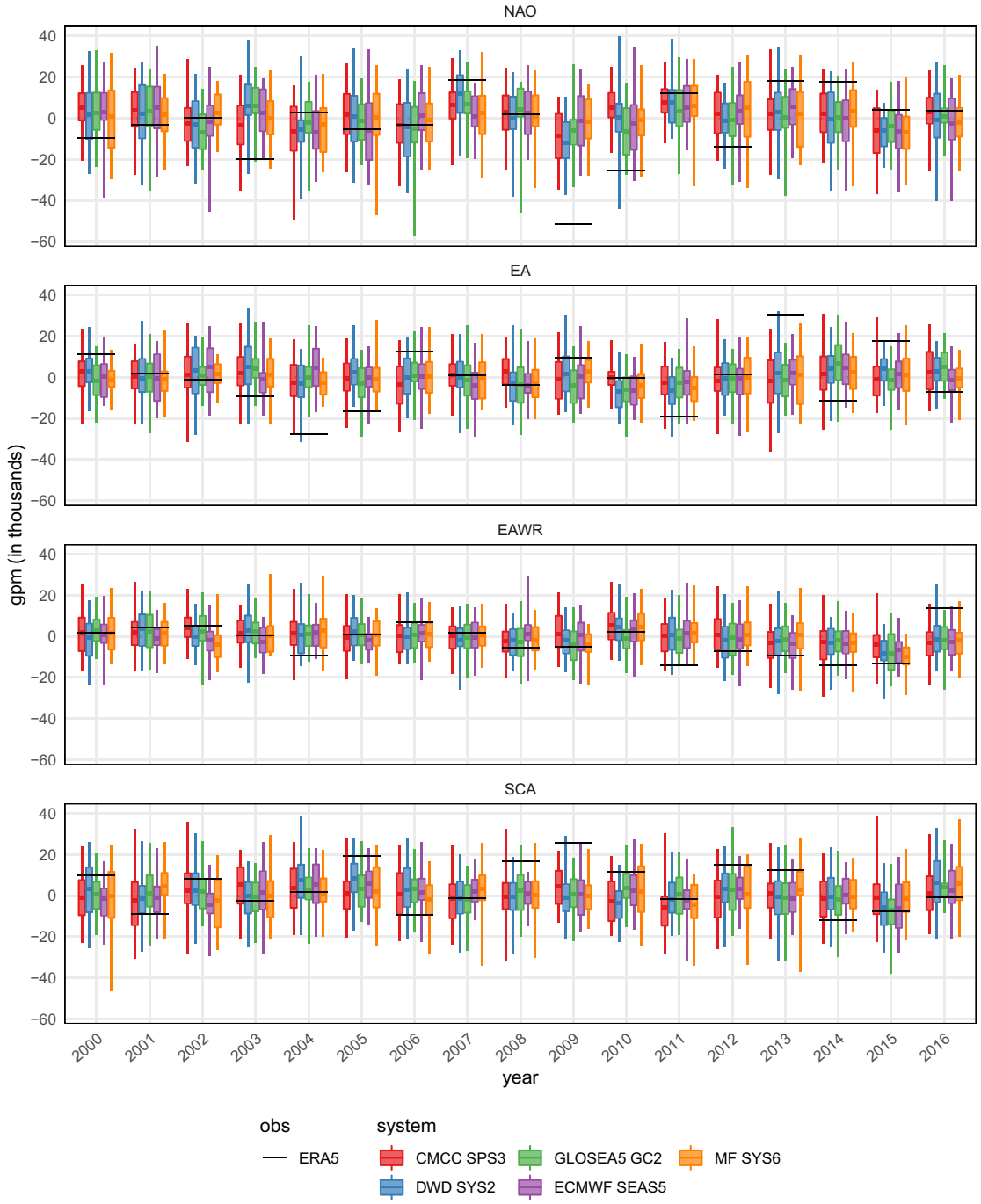

Figure 2. Retrospective forecasts of the four EATC indices issued in November and valid for DJF (i.e. one month of lead time) for each of the prediction systems in the 2000–2016 period. Each boxplot shows the maximum and minimum forecast value (whiskers), the first and third quartiles (box) and the ensemble mean (color line). The black line denotes the observed value according to ERA5. The year labels correspond to the forecast start date (i.e. November). The vertical axe represents geopotential meters, so that when those non-normalized EATC indices are multiplied by the loadings, an approximation of the original anomalies is obtained.

comparison of the internal variability modes of a seasonal prediction system and a reanalysis in winter).

3.2. Forecast quality of EATC predictions

The ensemble mean correlation has been widely used to verify ensemble predictions of the NAO. The process of averaging the teleconnection index predictions from several individual members produces the effect of cancelling the noise present in each single realization and allows extracting any forcing signal that is common to the different members. Figure 4 summarizes the ensemble mean correlation results for all systems, seasons, lead-times and teleconnections in a graphical way. A first sight reveals important differences between seasons, while there is a good degree of agreement between different prediction systems on which teleconnections have a positive and statistically significant correlation. In winter (top left)

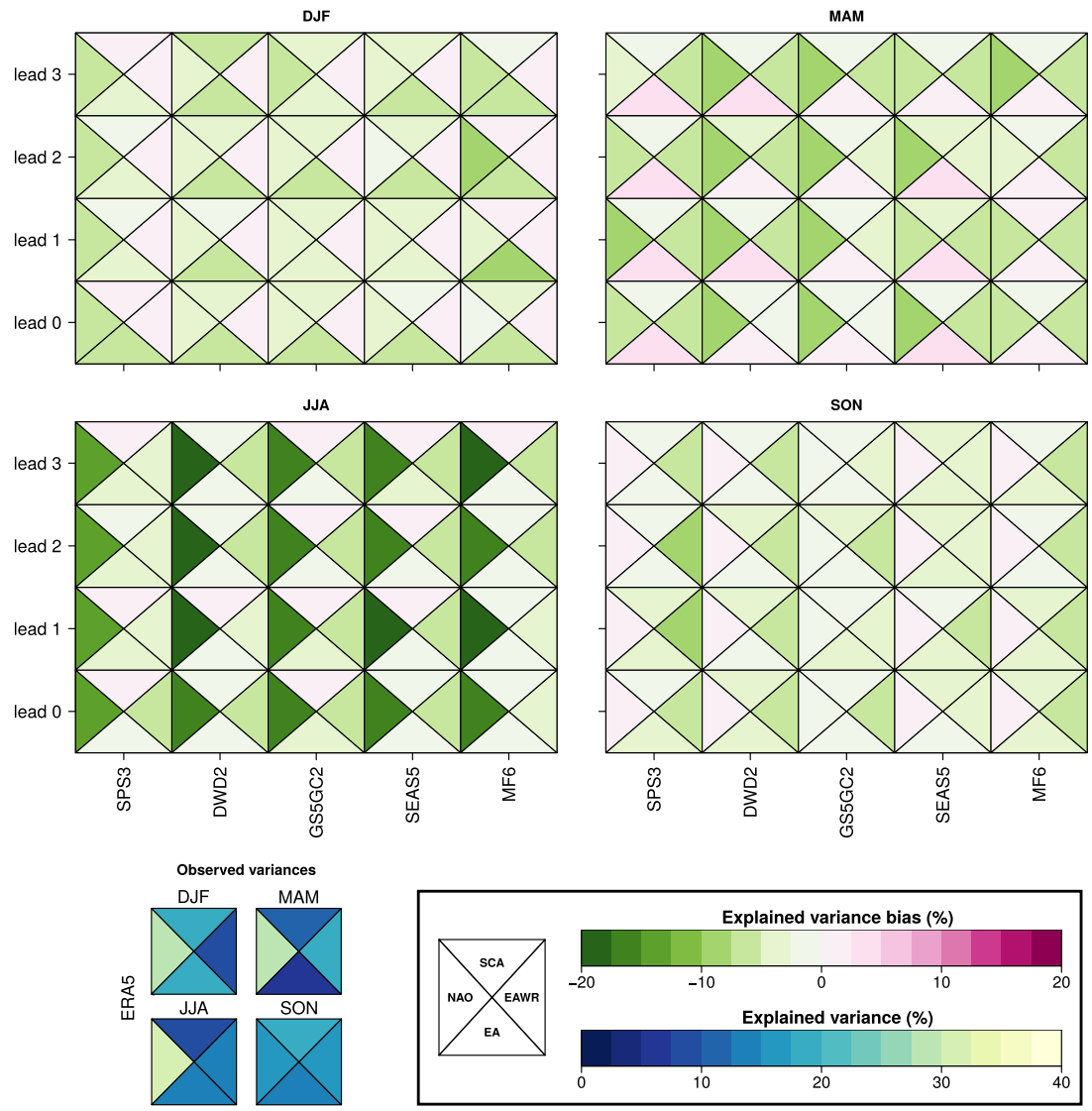

Figure 3. Biases in the percentage of the total variance explained by each EATC for each prediction system, lead time and season with respect to the explained variance in ERA5 (bottom-left panel) for the same period (1993–2016).

all systems show positive correlations for the NAO and SCA at the start of the season, while SEAS5 and MF6 systems still show significant correlations in the forecasts issued in September (lead 3). The EA also has positive and significant correlations for some systems at lead 0. In spring (top right) and at lead 0, all the teleconnections have positive correlations in almost all of the systems. However, at longer lead times the correlation values become weaker and statistically non-significant. In summer (bottom left) the NAO and SCA indices show very good correlation levels for all lead times and almost all systems. The EA and EAWR correlations are only statistically significant at lead 0 for SEAS5 and DWD2 respectively. Autumn shows the worst results overall. The EA shows statistically significant correlations only in lead 0 but for almost all systems. Surprisingly, the SCA shows also positive and significant correlation levels at lead 3 for SPS3, SEAS5 and MF6 systems, but not for any other smaller lead time.

Most of the non-significant correlations are still positive. This might be a sign that although small, those correlations are not just random outcomes (which should be distributed evenly into positive and negative values), but rather that the signal-to-noise ratio is too low in those cases for the significance test to be able to detect it. This is consistent with some works that have shown the difficulties to provide skillful seasonal climate predictions in the Euro-Atlantic region as a consequence of the excessive role that internal variability plays in prediction systems in that region (Scaife and Smith 2018). This issue has been further explored in the following section.

The results for winter NAO predictions are in line with previous published research (Scaife *et al* 2014, Baker *et al* 2018, Athanasiadis *et al* 2017, Johnson *et al* 2019), taking into account the different methodologies employed and also the high variability of verification metrics due to the verification period employed (see section 3.3 below).

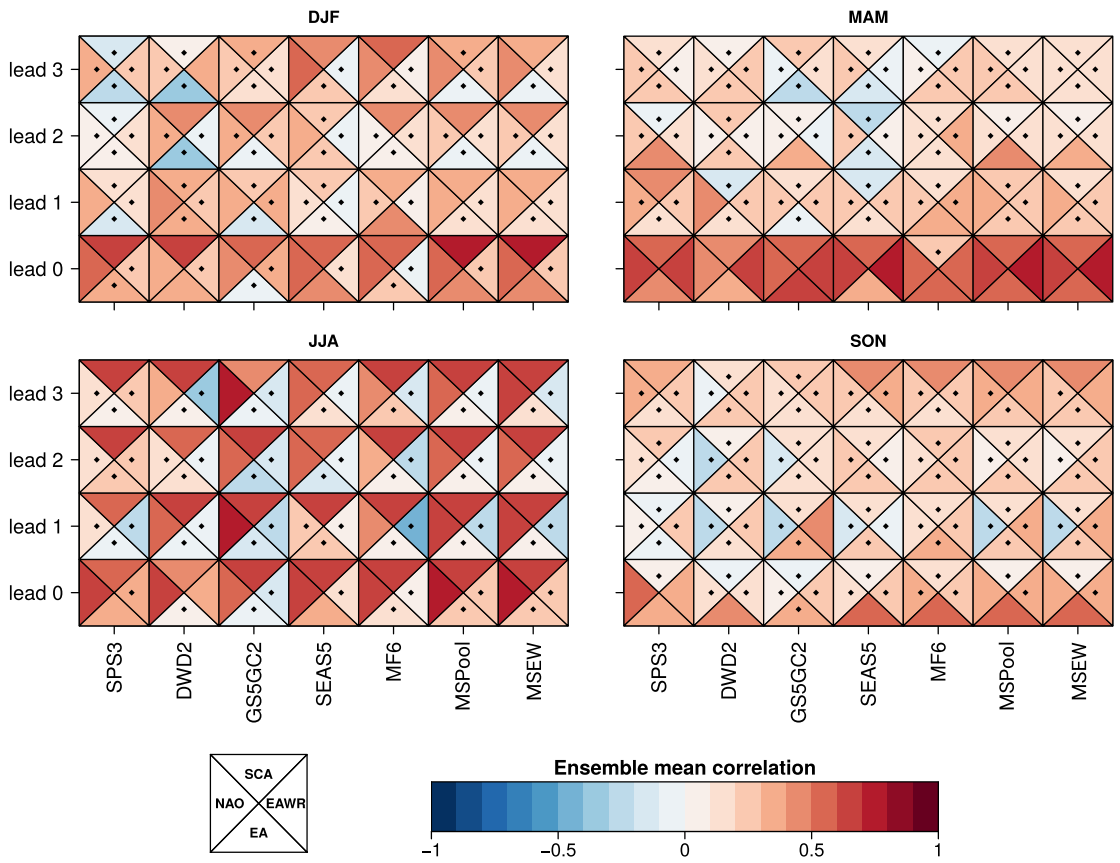

Figure 4. Correlation between the ensemble mean of the EATC forecasts and the corresponding observed (ERA5) values for each system, lead time and season in the 1993–2016 hindcast period. Black dots indicate cases were the correlation is not found statistically significant at the 95% of confidence level.

Multi-system predictions that combine the members from several prediction systems (MSPool and MSEW; see section 2.2.3) tend to perform very good in terms of ensemble mean correlation. This is partly due to an increase of the ensemble size by around five times compared to the individual systems, but also thanks to the cancelling of modelling errors from different systems. Although many times there is a single model that does better for a given teleconnection index, overall the multi-system shows more stable results through the lead-times and indices and is always very close or above the best system. The two multi-system methods produced almost identical performance. For that reason and for simplicity, the RPSS has been only computed for the MSPool method.

The RPSS corresponding to the EATC indices for all seasons, lead-times, and systems has been plotted similarly in figure 5. The plot shows very similar results to the ensemble mean correlations, in general terms, although the absolute values of RPSS are much lower than those of correlation. Some differences in terms of statistical significance of the results can be seen. For example, figure 5 (bottom-left) shows that the NAO RPSS in JJA is not significant in SEAS5 and MF6 beyond lead 0, however, correlation values were statistically significant in all the lead times and seasons (figure 4). On the other hand, RPSS for the EA index in DJF (lead 0) in the MF6 system is significant while correlation is not.

Both employed metrics analyze different aspects of the predictions and therefore cannot be numerically compared. The RPSS is in general a more restrictive quality measure than ensemble mean correlation. For instance, Kumar (2009) showed that randomly-generated forecasts with similar levels of signal-to-noise ratio reach higher ensemble mean correlations than RPSS values. Also, ensemble calibration techniques such as variance inflation (Doblas-Reyes *et al* 2005, Torralba *et al* 2017) could be employed to adjust the EATC forecasts and obtain more reliable predictions. This would translate in better RPSS values, although the ensemble mean correlation would not change. These considerations show that it is necessary to consider more than one metric to derive meaningful conclusions.

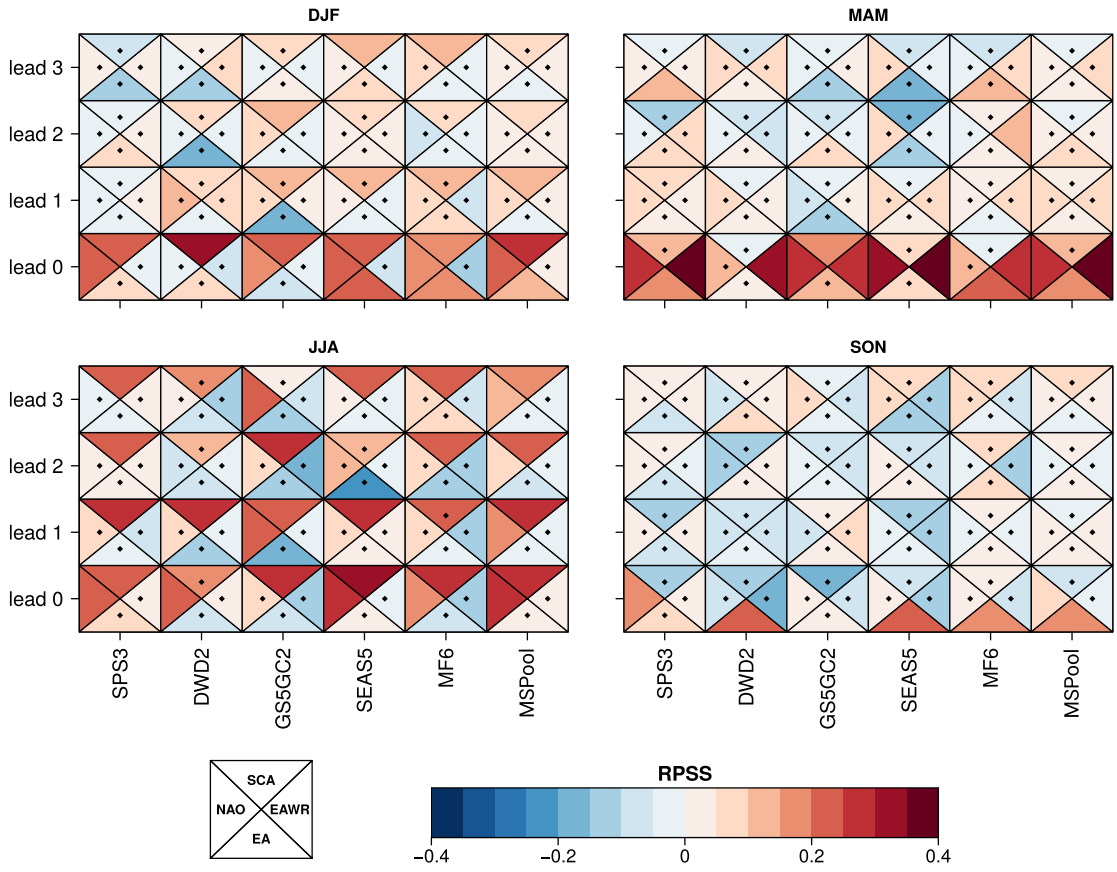

Figure 5. Ranked probability skill score of EATC tercile forecasts for each system, lead time and season in the 1993–2016 hindcast period. Black dots indicate cases were the RPSS is not found statistically significant at the 95% of confidence level.

3.3. Sensitivity of ensemble mean correlation to hindcast period and number of members

Previous research has found that ensemble mean correlation of NAO is sensitive to hindcast length and ensemble size (Baker *et al* 2018, Siegert *et al* 2016, Kumar 2009). To further verify this for the other EATCs, the ECMWF SEAS5 hindcast from MARS have been employed. This hindcast has a longer period (1981–2018) than the C3S hindcast, and for the November initialization it has 51 ensemble members. By subsetting the number of years and the number of members included in the verification, we can evaluate the sensitivity of the correlation and RPSS results to the ensemble size and the hindcast length. For each EATC index, a collection of 10 000 random subsets of 25 members out of the 51 available are used to draw a distribution of verification results. In the same way, a collection of 10 000 subsets of 25 years out of the 38 available is used to produce one distribution of verification values for each EATC. Figure 6 shows the results in violin plots (which enhance typical boxplots with information from the whole distribution). The variability is very large both for correlations (top panels) and for RPSS (bottom panels), with ranges of values of more than 0.5 points in correlation, and 0.2 points in RPSS. The spread of the distributions is very similar among different EATCs, indicating that this uncertainty is not intrinsically related to NAO variability but is a general issue of seasonal predictability over Europe. The variability when subsetting the period (right panels) is a bit larger than the variability when subsetting the members (left panels), for all the EATCs. The mean value of the distributions (not shown) is slightly higher when the period is subsetted. The effect of adding more years is to get a more reliable estimate of skill, but adding more members will tend to produce higher skill scores due to a higher cancellation of noise in bigger ensembles. From this analysis it is clear that the verification of both deterministic and probabilistic EATC forecasts requires large ensembles and large hindcast periods. As a consequence, all the results presented in previous sections, although very useful to characterize the EATC prediction skill in the current operational seasonal prediction systems, have to be cautiously interpreted.

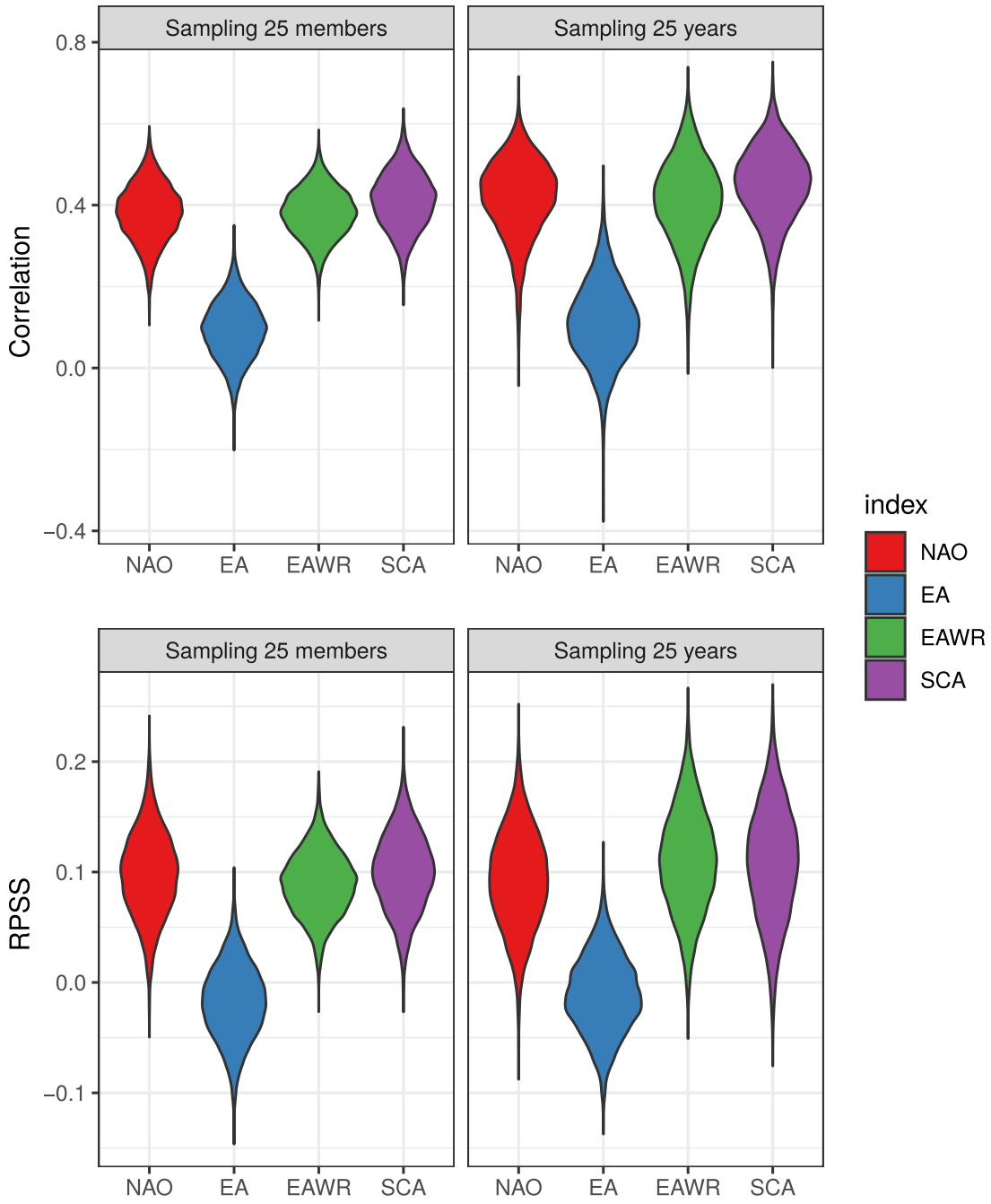

Figure 6. Sensitivity of ensemble mean correlation and RPSS for each EATC to the hindcast years and the number of ensemble members included in the verification. The SEAS5 hindcast for MARS (covering 1981–2018 with 51 members) has been subsetted 10 000 times to produce a distribution of values.

4. Conclusions

A method to produce seasonal forecasts of NAO, EA, EAWR and SCA indices for the four seasons and from five different seasonal prediction systems available in the C3S CDS has been developed. Retrospective predictions of those indices for the 1993–2016 period have been verified. A few conclusions can be drawn from the results:

- Prediction skill is not limited to NAO: atmospheric variability shaped like EA, EAWR and SCA patterns can also be simulated by the seasonal prediction systems.
- Prediction skill is not limited to winter: spring and summer have also similar levels of skill for some teleconnections, while autumn shows only modest scores (probably due to a lower signal-to-noise ratio).
- There is a good degree of agreement between systems in which EATCs can be predicted for each season with different lead times. This might highlight inherent predictability of the teleconnections.
- Multi-system predictions of EATC perform almost as well or sometimes even better than the best

system. There is not a single system that produces the best forecasts for all the teleconnections, lead times and seasons. Therefore a multi-system simplifies the application of the method in order to implement an operational climate service.
- Initiatives such as C3S are very helpful to produce such multi-system predictions.
- Both deterministic and probabilistic verification metrics show a strong sensitivity to the ensemble size and hindcast length.

These results open the door to produce an operational climate service that provides forecasts of those teleconnection indices all year round. The forecasts could be used directly as proxies or also be employed to derive forecasts of sectorial indicators or to produce downscaled predictions as in Baker *et al* (2017).

Acknowledgment

The research leading to these results has received funding from the European Union's Horizon 2020 research and innovation programme under grant agreement n° 776787 (S2S4E).

The authors acknowledge the Copernicus Climate Change Service (C3S) for providing seasonal predictions from several European meteorological centers and the ECMWF for producing the ERA5 reanalysis. All the analyses have been done with R employing the packages s2dverification and SpecsVerification.

Data availability

The data that support the findings of this study are openly available at the Climate Data Store of the Copernicus Climate Change service. The ERA5 data is available at https://doi.org/10.24381/cds.6860a573, and the seasonal predictions can be accessed at https://cds.climate.copernicus.eu.

ORCID iDs

Llorenç Lledó https://orcid.org/0000-0002-8628-6876
Verónica Torralba https://orcid.org/0000-0002-8941-1548

References

Athanasiadis P J, Bellucci A, Scaife A A, Hermanson L, Materia S, Sanna A, Borrelli A, MacLachlan C and Gualdi S 2017 A multisystem view of wintertime NAO seasonal predictions *J. Clim.* **30** 1461–75

Baker L H, Shaffrey L C and Scaife A A 2017 Improved seasonal prediction of UK regional precipitation using atmospheric circulation *Int. J. Climatol.* **38** e437–e453

Baker L H, Shaffrey L C, Sutton R T, Weisheimer A and Scaife A A 2018 An intercomparison of skill and overconfidence/underconfidence of the wintertime north atlantic oscillation in multimodel seasonal forecasts. *Geophys. Res. Lett.* **45** 7808–17

Barnston A G and Livezey R E 1987 Classification, seasonality and persistence of low-frequency atmospheric circulation patterns *Mon. Weather Rev.* **115** 1083–126

Brayshaw D J, Troccoli A, Fordham R, and Methven J 2011 The impact of large scale atmospheric circulation patterns on wind power generation and its potential predictability: a case study over the UK *Renew. Energy* **36** 2087–96

Bueh C and Nakamura H 2007 Scandinavian pattern and its climatic impact *Q. J. R. Meteorol. Soc.* **133** 2117–31

Ceglar A, Toreti A, Prodhomme C, Zampieri M, Turco M and Doblas-Reyes F J 2018 Land-surface initialisation improves seasonal climate prediction skill for maize yield forecast *Sci. Rep.* **8** 1

Clark R T, Bett P E, Thornton H E, and Scaife A A 2017 Skilful seasonal predictions for the European energy industry *Environ. Res. Lett.* **12** 024002

Climate Prediction Center 2012 Northern hemisphere teleconnection patterns (www.cpc.ncep.noaa.gov/data/teledoc/telecontents.shtml) (Accessed: 14 November 2019)

Copernicus Climate Change Service 2019 Era5 monthly averaged data on pressure levels from 1979 to present (https://cds.climate.copernicus.eu/doi/10.24381/cds.6860a573)

Copernicus Climate Change Service (C3S) 2017 ERA5: fifth generation of ECMWF atmospheric reanalyses of the global climate. Copernicus climate change service climate data store (CDS), ECMWF (https://cds.climate.copernicus.eu/cdsapp#!/home) (Accessed: 14 November 2019)

DelSole T, Nattala J and Tippett M K 2014. Skill improvement from increased ensemble size and model diversity *Geophys. Res. Lett.* **41** 7331–42

Deutscher Wetterdienst 2019 Seasonal forecasting with the german climate forecast system (www.dwd.de/EN/ourservices/seasonals_forecasts/project_description.html?nn=641552&lsbId=619784) (Accessed: 14 November 2019)

Diebold F X and Mariano R S 1995. Comparing predictive accuracy. *J. Business Econ. Stat.* **13** 253–63

Doblas-Reyers F J, Hagedorn R, and Palmer T N 2005 The rationale behind the success of multi-model ensembles in seasonal forecasting—II calibration and combination *Tellus* A **57** 234–52

Doblas-Reyes F J, García-Serrano J, Lienert F, Biescas A P and Rodrigues L R L 2013 Seasonal climate predictability and forecasting: status and prospects *Wiley Interdiscip. Rev.: Clim. Change* **4** 245–68

Doblas-Reyes F J, Pavan V, and Stephenson D B 2003 The skill of multi-model seasonal forecasts of the wintertime north atlantic oscillation *Clim. Dyn.* **21** 501–14

Dorel L, Ardilouze C, Déqué M, Batté L and Guérémy J-F 2017 Documentation of the meteo-france pre-operational seasonal forecasting system (https://seasonal.meteo.fr/sites/data/Documentation/doc_modele/Model_MF-S6_C3S_technical_en.pdf) (Accessed: 14 November 2019)

Dunstone N, Smith D, Scaife A, Hermanson L, Eade R, Robinson N, Andrews M and Knight J 2016. Skilful predictions of the winter north atlantic oscillation one year ahead *Nat. Geosci.* **9** 809–14

ECMWF 2019 Seasonal forecasts and the copernicus climate change service (https://confluence.ecmwf.int//display/COPSRV/Seasonal+forecasts+and+the+Copernicus+Climate+Change+Service) (Accessed: 14 November 2019)

Hall R J and Hanna E 2018 North atlantic circulation indices: links with summer and winter UK temperature and precipitation and implications for seasonal forecasting *Int. J. Climatol.* **38** e660–e677

Hannachi A, Jolliffe I T and Stephenson D B 2007 Empirical orthogonal functions and related techniques in atmospheric science: A review *Int. J. Climatol.* **27** 1119–52

Heinze C *et al* 2019 ESD reviews: climate feedbacks in the earth system and prospects for their evaluation *Earth Syst. Dyn.* **10** 379–452

Hewitt C, Mason S and Walland D 2012 The global framework for climate services *Nat. Clim. Change* **2** 831–2

Hurrell J W, Kushnir Y, Ottersen G and Visbeck M 2003 *An overview of the North Atlantic oscillation The North Atlantic Oscillation: Climatic Significance and Environmental Impact* (Washington, DC: American Geophysical Union) pp 1–35

Iglesias I, Lorenzo M N and Taboada J J 2014 Seasonal predictability of the east atlantic pattern from sea surface temperatures *PLoS ONE* **9** e86439

Johnson S J *et al* 2019 SEAS5: the new ECMWF seasonal forecast system *Geosci. Model Dev.* **12** 1087–117

Jolliffe I T and Stephenson D B ed 2011 *Forecast Verification* (New York: Wiley) (https://doi.org/10.1002/9781119960003)

Josey S A, Somot S and Tsimplis M 2011 Impacts of atmospheric modes of variability on mediterranean sea surface heat exchange *J. Geophys. Res.* **116** C2

Kumar A 2009 Finite samples and uncertainty estimates for skill measures for seasonal prediction *Mon. Weather Rev.* **137** 2622–31

Lim Y-K 2014 The East Atlantic/West Russia (EA/WR) teleconnection in the North Atlantic: climate impact and relation to rossby wave propagation *Clim. Dyn.* **44** 3211–22

MacLachlan C *et al* 2014 Global seasonal forecast system version 5 (GloSea5): a high-resolution seasonal forecast system *Q. J. R. Meteorol. Soc.* **141** 1072–84

Mariotti A, Ruti P M and Rixen M 2018 Progress in subseasonal to seasonal prediction through a joint weather and climate community effort *NPJ Clim. Atmos. Sci.* **1** 1

Mestas-Nuñez A M 2000 Orthogonality properties of rotated empirical modes *Int. J. Climatol.* **20** 1509–16

Ossó A, Sutton R, Shaffrey L and Dong B 2017 Observational evidence of european summer weather patterns predictable from spring *Proc. Natl Acad. Sci.* **115** 59–63

Sanna A, Borelli A, Athanasiadis P, Materia S, Storto A, Navarra A, Tibaldi S and Gualdi S 2017 RP0285—CMCC-SPS3: The CMCC Seasonal Prediction System 3 *Technical report* Centro Euro-Mediterraneo sui Cambiamenti Climaticci

Scaife A A *et al* 2014 Skillful long-range prediction of European and North American winters *Geophys. Res. Lett.* **41** 2514–19

Scaife A A and Smith D 2018 A signal-to-noise paradox in climate science *NPJ Clim. Atmos. Sci.* **1** 1

Siegert S, Stephenson D B, Sansom P G, Scaife A A, Eade R and Arribas A 2016 A bayesian framework for verification and recalibration of ensemble forecasts: How uncertain is NAO predictability? *J. Clim.* **29** 995–1012

Smith D M, Scaife A A, Eade R and Knight J R 2014 Seasonal to decadal prediction of the winter north atlantic oscillation: emerging capability and future prospects *Q. J. R. Meteorol. Soc.* **142** 611–17

Soares M B, Daly M and Dessai S 2018 Assessing the value of seasonal climate forecasts for decision-making *Wiley Interdiscip. Rev.: Clim. Change* **9** e523

Torralba V, Doblas-Reyes F J, MacLeod D, Christel I and Davis M 2017 Seasonal climate prediction: A new source of information for the management of wind energy resources *J. Appl. Meteorol. Climatol.* **56** 1231–47

Trigo R, Osborn T and Corte-Real J 2002 The north atlantic oscillation influence on europe: climate impacts and associated physical mechanisms *Climate Research* **20** 9–17

Turco M, Jerez S, Doblas-Reyes F J, AghaKouchak A, Llasat M C and Provenzale A 2018 Skilful forecasting of global fire activity using seasonal climate predictions *Nat. Commun.* **9** 1

Walz M A, Donat M G and Leckebusch G C 2018 Large-scale drivers and seasonal predictability of extreme wind speeds over the North Atlantic and Europe *J. Geophys. Res.: Atmos.* **123** 11518–35

Wanner H, Brönnimann S, Casty C, Gyalistras D, Luterbacher J, Schmutz C, Stephenson D B and Xoplaki E 2001 North atlantic oscillation – concepts and studies *Surv. Geophys.* **22** 321–81

White C J *et al* 2017 Potential applications of subseasonal-to-seasonal (s2s) predictions *Meteorol. Appl.* **24** 315–25

Wilks D S 2019 Principal component (EOF) analysis *Statistical Methods in the Atmospheric Sciences* (Amsterdam: Elsevier) pp 617–68

Williams K D *et al* 2015 The met office global coupled model 2.0 (GC2) configuration *Geosci. Model Dev.* **8** 1509–24

WMO 2014 Implementation Plan of the Global Framework for Climate Services (GFCS)

Woollings T, Hannachi A and Hoskins B 2010 Variability of the north atlantic eddy-driven jet stream *Q. J. R. Meteorol. Soc.* **136** 856–68

Zubiate L, McDermott F, Sweeney C and O'Malley M 2016 Spatial variability in winter NAO-wind speed relationships in Western Europe linked to concomitant states of the East Atlantic and Scandinavian patterns *Q. J. R. Meteorol. Soc.* **143** 552–62

Chapter 7

The weather roulette: a game to communicate the usefulness of probabilistic climate predictions

Probabilistic forecasts are difficult to handle for the vast majority of users. Most of the decisions that users typically make are yes/no measures (e.g. implement an adaptation or protection measure or not). While there is scientific literature that proposes optimal strategies to make those decisions based on probabilities of the different situations that can occur, in the case of long-range forecasts it is difficult to realize the value of those predictions. The benefits of adopting a strategy based on probabilistic forecasts is usually not perceived unless the strategy is maintained for several years and is evaluated only after many outcomes have been realized. The weather roulette is a conceptual experiment that relates some widely-known gambling concepts such as odds or return of investment to more awkward aspects such as verification metrics typically employed in climate prediction science. The paper in this chapter presents an implementation of the weather roulette that employs tercile probabilities from a seasonal prediction system. The results are shown in a mobile phone app, that can be used to teach users the concepts of probabilistic forecasts, its value and its verification.

This paper deals with objective (iii) of this dissertation.

Terrado, M., Lledó, L., Bojovic, D., Clair, A. L. S., Soret, A., Doblas-Reyes, F. J., Manzanas, R., San-Martín, D., and Christel, I. (2019). The weather roulette: A game to communicate the usefulness of probabilistic climate predictions. *Bulletin of the American Meteorological Society*, 100(10):1909–1921, doi: 10.1175/bams-d-18-0214.1

THE WEATHER ROULETTE

A Game to Communicate the Usefulness of Probabilistic Climate Predictions

Marta Terrado, Llorenç Lledó, Dragana Bojovic, Asun Lera St. Clair, Albert Soret, Francisco J. Doblas-Reyes, Rodrigo Manzanas, Daniel San-Martín, and Isadora Christel

We apply a game to communicate the usefulness of climate predictions to users, showing that in skillful areas economic benefits are obtained in the long term.

Seasonal-to-decadal climate predictions try to anticipate the most likely climate conditions for the next few months up to a decade into the future (Doblas-Reyes et al. 2013; Meehl et al. 2014). Sitting between weather forecasts (from the next few hours up to a few days ahead) and climate change projections (from a few decades up to centuries), climate predictions have the potential to inform different climate-sensitive sectors (e.g., energy, agriculture, water management, health, insurance, tourism) in adapting their short- to medium-term practices and plans to climate variability and change (Thomson et al. 2006; Jewson et al. 2009; Torralba et al. 2017; Turco et al. 2017). Climate-sensitive sectors can benefit from understanding climate predictions and how they can be used to make better informed decisions and thus gain strategic advance toward other competitors. However, despite their potential advantages and the recent efforts to develop underpinning science for climate predictions, so far there has been limited uptake of these tools by users (McNie 2007; Feldman and Ingram 2009).

Main barriers hindering users' uptake of climate predictions include (i) the lack of a common and widely accepted terminology between climate scientists and user communities, (ii) the difficulty to deal with probabilistic rather than deterministic outcomes, (iii) their lower skill (i.e., the quality of the prediction based on its performance in the past) compared to the skill of weather forecasts, and (iv) the need to move from a short- to a long-term approach for the assessment of benefits in the business sector, since the benefits from adopting climate predictions can only be perceived in the long term. Adding to these barriers, there is also little evidence of the use of climate predictions for operational applications (Coelho and Costa 2010), often ascribed

AFFILIATIONS: Terrado, Lledó, Bojovic, St. Clair, Soret, and Christel—Department of Earth Sciences, Barcelona Supercomputing Center, Barcelona, Spain; Doblas-Reyes—Department of Earth Sciences, Barcelona Supercomputing Center, and Institut Català de Recerca i Estudis Avançats, Barcelona, Spain; Manzanas and San-Martín—Predictia Intelligent Data Solutions SL, Santander, Spain
CORRESPONDING AUTHOR: Marta Terrado, marta.terrado@bsc.es

The abstract for this article can be found in this issue, following the table of contents.
DOI:10.1175/BAMS-D-18-0214.1

In final form 3 July 2019

to the users' difficulty to integrate predictions into existing decision support systems. In this sense, there is a need to improve the way in which actionable climate information is made salient and relevant to different users.

An important step toward encouraging the adoption of climate predictions for supporting decision-making consists in quantifying and communicating the potential economic value, either in terms of increased outcome, avoided cost, or vulnerability reduction. Different methods can be found in the literature, ranging from quantitative studies that focus on the technical aspects of forecasts to more qualitative and user-centered approaches (Bruno-Soares et al. 2018).

Games are a powerful way to facilitate a more thorough analysis of complex issues, transferring scientific information into understandable and tailored knowledge that is tacitly connected to the target audience (van Pelt et al. 2015). Therefore, game-based learning has seen promising results in different areas, including the field of climate science (Ramos et al. 2013; Vincent et al. 2017; van Pelt et al. 2015; Arnal et al. 2016; Crochemore et al. 2016). These works have used games to demonstrate the potential utility of probabilistic forecasts for taking better risk-based decisions, while also suggesting that greater attention needs to be paid to the communication of uncertainties. Although uncertainties constitute an added value of probabilistic over deterministic forecasts, they also present challenges for both forecasters and users of forecasts (Arnal et al. 2016). Indeed, forecast skill is one of these sources of uncertainty that needs additional communication efforts to be presented in a way that is well understood by users (Taylor et al. 2015). In this line Hagedorn and Smith (2009) developed the Weather Roulette (WR) conceptual framework, a simple and easy to understand approach for communicating the value of probabilistic weather forecasts.

The WR was first applied to communicate the value of probabilistic weather forecasts for the next few days (Palmer et al. 2005; Hagedorn and Smith 2009). However, the approach has recently been extended to multiannual hurricane predictions (Caron et al. 2018), and to seasonal predictions of temperature extremes (Lazenby et al. 2014). The WR approach interprets probabilistic predictions in terms of economic value, translating metrics commonly used by the scientific community (e.g., ignorance skill score) to other metrics more easily understood in the private sector such as return on investment.

In this paper, we provide an example of how gamification can overcome communication and understanding barriers for the uptake of probabilistic climate predictions. In a simplified context, we use a betting game based on the WR approach to demonstrate the efficiency of climate predictions compared to climatology (past observations). This is supported through the translation of skill scores into economic terms, which provides a different approach to communicate forecast uncertainty to users and allows comparing the potential economic value of climate predictions in skillful regions with regions of limited skill. Understanding the usefulness of climate predictions could provide the basis for a better integration of knowledge about climate anomalies into operational and managerial processes.

The Weather Roulette approach: From theory to practical implementation. To illustrate the practical application of the game, in the context of the European Provision of Regional Impacts Assessments on Seasonal and Decadal Time Scales (EUPORIAS) and the Subseasonal to Seasonal Climate Forecasting for Energy (S2S4E) projects, we developed the WR mobile app (Predictia 2019), which is specifically addressed to the wind energy sector—an industry with an increasing awareness of the need to understand climate risk (Lledó et al. 2018). Traditionally, climatology has been used for wind resource assessment on the ever less reliable assumption that what happened in the past will be representative of future conditions (Carta et al. 2013; Lledó 2017). However, recent advances in climate prediction have already shown that probabilistic forecasting, once tailored to the specific needs of users, could provide opportunities for better informed investments, improving risk assessments, and indicating the climate exposure of energy assets. Therefore, there are a number of wind energy companies that could become early adopters of climate predictions (Terrado et al. 2017).

The WR mobile app has been implemented as a communication and engagement tool that shows the potential benefits of climate predictions over climatology in the long term. The app has the aim to engage relevant users within energy companies to consider the uptake of climate predictions and foster interaction with climate scientists to create more complex and customized climate services that inform their decision-making (European Commission 2015; see sidebar).

THE WEATHER ROULETTE GAME FOR CLIMATE PREDICTION.

Data for the Weather Roulette. The WR is defined here as a game where a player chooses between two forecast options, aiming

to select the one that predicts better in which category (i.e., a range of values) the observed value will fall. There are different possible categorizations. For the WR mobile app described in this paper, we have used tercile categories based on the historical climatology (above normal, normal, and below normal), which is a standard categorization for presenting seasonal predictions (Jupp et al. 2012). Other category settings more relevant to specific user decisions could be defined instead, such as quintile categories or even asymmetrical categories (i.e., below the 10th percentile, a central category between the 10th and 90th percentile, and above the 90th percentile).

The two forecast options considered in the WR game are option 1, which corresponds to the use of seasonal climate predictions, and option 2, corresponding to the use of climatological predictions (see description below). Observational data have also been used for comparison with predicted data.

Option 1—Climate predictions (calibrated ECMWF System 4 prediction system). Global information on seasonal variations of the wind resource are obtained from the RESILIENCE prototype (http://resilience.bsc.es), an interactive climate service interface for wind industry users developed as part of the European funded projects EUPORIAS (FP7; http://euporias.eu/) and CLIM4ENERGY [Copernicus Climate Change Service (C3S); http://clim4energy.climate.copernicus.eu/]. RESILIENCE uses the calibrated predictions coming from the 51-member ensemble version of the ECMWF System 4 seasonal forecasting system (Molteni et al. 2011). Winter wind predictions have both higher skill and variability in the Northern Hemisphere, and provide a good test case. Therefore, we focus exclusively on winter (DJF) predictions of surface (10 m) wind speed, initialized on 1 November for a period of 33 past years, from 1981 to 2013, at those locations with installed wind power capacity (n = 2,023) obtained from the windpower.net database. The technique of variance inflation (von Storch and Zwiers 2001) is selected for calibration and applied as in Doblas-Reyes et al. (2005); the reader is referred to Manzanas et al. (2019) for further details on the effect of calibration of seasonal forecasts. The percentage of probability for the different categories to occur is computed as the percentage of ensemble members falling within each category.

Option 2—Climatological predictions (probabilities derived from historical observations). The observed frequencies of occurrence of different categories in the historical records (ERA-Interim reanalysis) have been used as forecast probabilities. As already mentioned, climatology has been traditionally the preferred choice for the wind energy sector when assessing risks, and therefore has been set as the baseline to bet against.

CLIMATE PREDICTION: WHAT WE SHOULD KNOW

The atmosphere is chaotic in nature and therefore becomes unpredictable after a few days. This is why weather forecasts only provide useful information up to a few days ahead. However, the atmosphere is forced by other components of the Earth system, namely, the ocean, land, and sea ice components that evolve much slower and are predictable at longer time scales. Climate predictions, which take into account these forcings, can be used to compute the likelihood of a certain outcome (e.g., having above-normal, normal, or below-normal wind speed conditions for the next season). This probabilistic nature often does not align with the expectations of users, who are more interested in a yes/no answer to whether they should implement or not a particular action. Therefore, the integration of probabilistic predictions into actionable decision-making constitutes an important challenge.

Besides its probabilistic nature, there are other aspects of climate predictions that should be considered and that, potentially, further limit their usability. Any probabilistic prediction should be accompanied by an estimate of its past performance, known as forecast verification, which can guide users about the expected performance of future predictions (Weisheimer and Palmer 2014). Forecast verification should address the accuracy—how close the forecast probabilities are to the observed frequencies; the utility—the economic or other advantages of the probabilistic forecasts; and the skill—how the probabilistic forecasts compare with a reference forecast (Jolliffe and Stephenson 2012). However, as the predictability of weather forecasts comes from initial atmospheric conditions, their skill is normally high at the beginning of the forecast period and experiences a fast decrease after a few days, whereas the skill of climate predictions is lower than that of weather forecasts and is kept more stable and decreases at a slower pace as lead time increases (White et al. 2017). The generally low skill exhibited by climate predictions in extratropical regions such as Europe has resulted in their limited practical applications (Doblas-Reyes et al. 2013; Manzanas et al. 2014). Apart from the region, useful skill also depends on the time of the year (e.g., the season), which further lowers the perceived reliability in these predictions (Bruno-Soares and Dessai 2016). It is also paramount to understand that a single prediction is not representative of the long-term performance of climate predictions, even in an area where the model has skill for the period of interest.

Observational data. Reanalysis data from ERA-Interim (Dee et al. 2011) have been employed as truth for comparison with predicted data (forecast verification).

Skill of climate predictions. Different quality metrics are available for this task, often quantifying different characteristics of forecast performance. Here, two skill scores are calculated taking climatology as reference: the ignorance skill score (ISS; or logarithmic score; Good 1952) and the ranked probability skill score (RPSS; Wilks 2011). Both scores have been computed at the selected locations using the retrospective climate predictions and observational data described in the "Data for the Weather Roulette" section. The ISS has been considered because it possesses geometric symmetry and a correspondence with the WR approach. Therefore, it has a clear interpretation in terms of gambling returns, being easily communicated as an effective interest rate. On the other hand, RPSS is a widely used skill score in atmospheric science (Jolliffe and Stephenson 2012), and therefore, there is an increasing interest in bringing it closer to the user community. ISS is defined as an average of logarithms of the probabilities assigned to the observed outcome. It only takes into account the probabilities assigned to the observed or winning category; hence, it is technically defined as a local score (Mason 2008; Jolliffe and Stephenson 2012). Conversely, RPSS is not local; rather, it uses the probabilities assigned to all categories and the distance to the observed category to compute the verification, taking into account how big the probabilities predicted for the nonobserved categories are. Both ISS and RPSS range from 1 to minus infinity. Values above zero indicate that the verified seasonal forecasts perform better than a simple, constant prediction based on climatology.

The Weather Roulette game. The WR game [see Hagedorn and Smith (2009) for an extensive description of the method] is defined as a bet between two different forecast options: seasonal climate predictions and climatological predictions. The roulette slots represent the possible outcome categories that can contain the observation. An initial capital (c_0) is set, and every time all the capital is reinvested in the next round, with one round for each year. To start, the initial capital is spread in the different slots proportionally to the percentage probabilities predicted by each of the options (climate predictions and climatological predictions). The winning slot is then determined as the slot where the real observations fall. Then, for each option, payments are received proportionally to the bets in the winning category. The odds (i.e., the payoff to stake ratio) are inverse to the climatological probabilities for that category. The bet invested in the other categories is lost.

The code used to apply the WR game to the locations and years selected in this work was developed in R language (R Core Team 2015). The data described in the "Data for the Weather Roulette" section were used to run the code.

Translating skill scores into economic value. The WR can be played both for individual years (one round) and for the 33-yr period considered (33 rounds). Results are expressed in well-known economic measures (Table 1): (i) the return ratio for each individual round (r_t) calculated as the ratio between the capital obtained after and before playing the WR; (ii) the average or overall return ratio (R) for the 33 rounds, corresponding to the geometric average of r_t; (iii) the effective interest rate obtained for the full period played (IR, in %), which gives the annualized proportion of money earned each year over a given time period; and (iv) the return on investment (ROI), also for the full 33-yr period.

The added value of using climate predictions corresponds to the difference between the gains resulting from using climate predictions and the gains resulting from directly using a climatological constant prediction. Return ratios (r_t and R) larger than 1 indicate

Table 1. Definition and calculation of economic metrics used in the Weather Roulette approach.

Economic metric	Calculation
Initial capital (c_0)	Arbitrary value to be defined by the player
Number of rounds (n)	n = 33 (the number of DJF seasons in 1981–2013 period)
Final capital (c_n)	$c_n(\text{EUR}) = c_0 r_1 r_2 r_3 \ldots r_n = c_0(R)^n$
Return ratio for each individual round (r_t)	$r_t = c_t / c_{t-1}$
Average return ratio for the whole period played (R)	$R = (r_1 r_2 r_3 \ldots r_n)^{1/n}$
Effective interest rate obtained for the full period played (IR)	IR (%) = $(R - 1) \times 100$
Return on investment for the full period played (ROI)	ROI = $(c_n - c_0)/c_0$

gains. For instance, a value of 1.5 corresponds to a return of half the bet on top of that bet. A value of 1 indicates a neutral return (no gain and no loss) and values below one indicate losses. Note that for climatology, the return ratio is always 1, as the invested amount in the winning category is proportional to the climatological probabilities while the odds are inversely proportional to it. A positive IR indicates a net gain over the years, whereas net losses are indicated by negative IR values. The ROI indicates the net gains associated to an initial investment (c_0). These economic measures allow the immediate comparison of different prediction systems, and show which of the systems produce higher net gains after a certain period of time.

The Weather Roulette app. The WR game can be played from an interactive interface where the app simulates how much a player would have won or lost using either seasonal climate predictions or climatological predictions for decision-making. This allows for a comparison of the performance of both forecasts considering tercile categories for wind speed based on the historical climatology. At the beginning of the game, the user is presented with a global map with the distribution of the skill (ISS) and can select a particular location to start playing (Fig. 1a). For the selected location, the player can decide either to play for a single year among the period 1981–2013, or for all years (the game runs a forecast consecutively for each of the 33 years of the period). Together with the level of skill, the player is shown the probabilities predicted by the seasonal climate prediction for each of the tercile categories (Fig. 1b). Based on this information the player decides its preferred option to play the game. When playing for all years the skill value is shown and the preferred initial capital can be set by the player (Fig. 1c). Note that in the case of climatology all three categories are equally probable, with a probability of 1/3 each. After playing for a single year, the app returns the value of the return ratio (r_t) for that particular year. When the game is played for all years, the app returns the value of the effective IR and the ROI after the 33 years. The winning forecast option (seasonal forecasts or climatological forecasts) is reported at the end of the game and results obtained for both options are compared.

RESULTS. *Skill of seasonal wind predictions.* Global maps of ISS and RPSS have been calculated to assess the skill of winter wind speed predictions (Fig. 2a). Although the skill of seasonal predictions is in general low at extratropical latitudes (Manzanas et al. 2014), some positive skill is found in certain regions

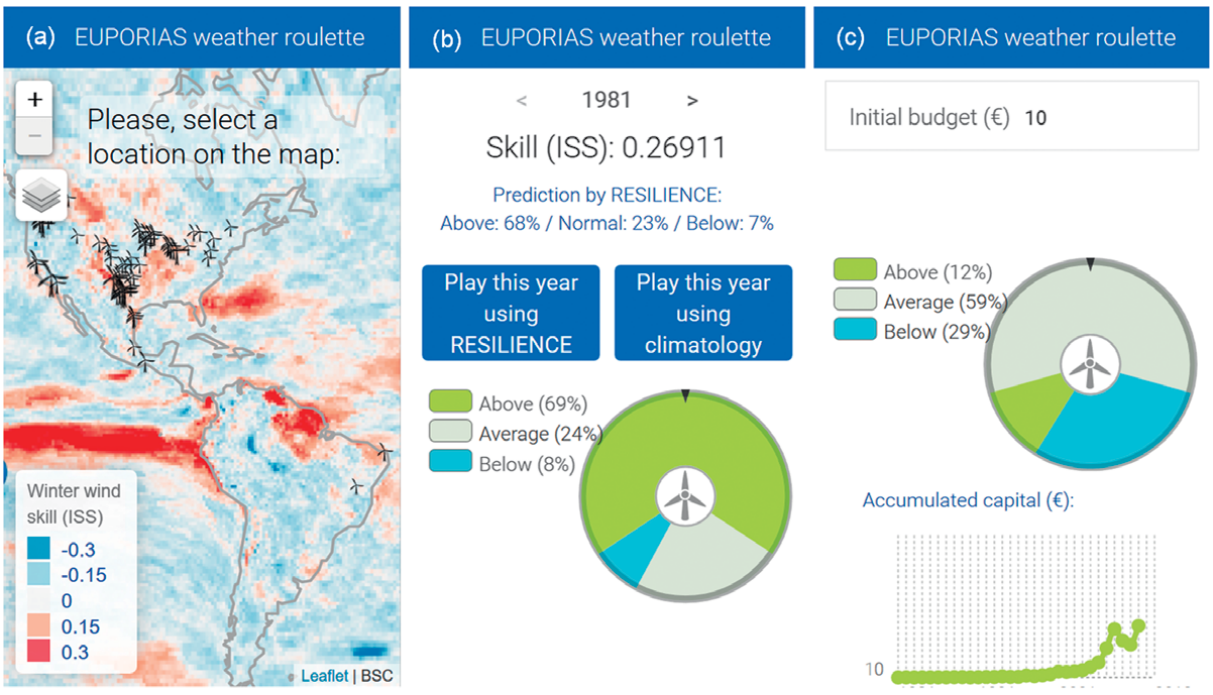

Fig. 1. The WR app: (a) global map of skill (ISS) with the option to select a particular location, (b) option to play for a single year choosing either the seasonal climate prediction or the climatology, and (c) result of the game after playing all years with the seasonal climate prediction. After playing the roulette for a selected year (b) and for all years (c), the screen displays a message informing the player of the winning option, and the return ratio or the return on investment. The black triangle in the roulette shows the tercile where the observation falls.

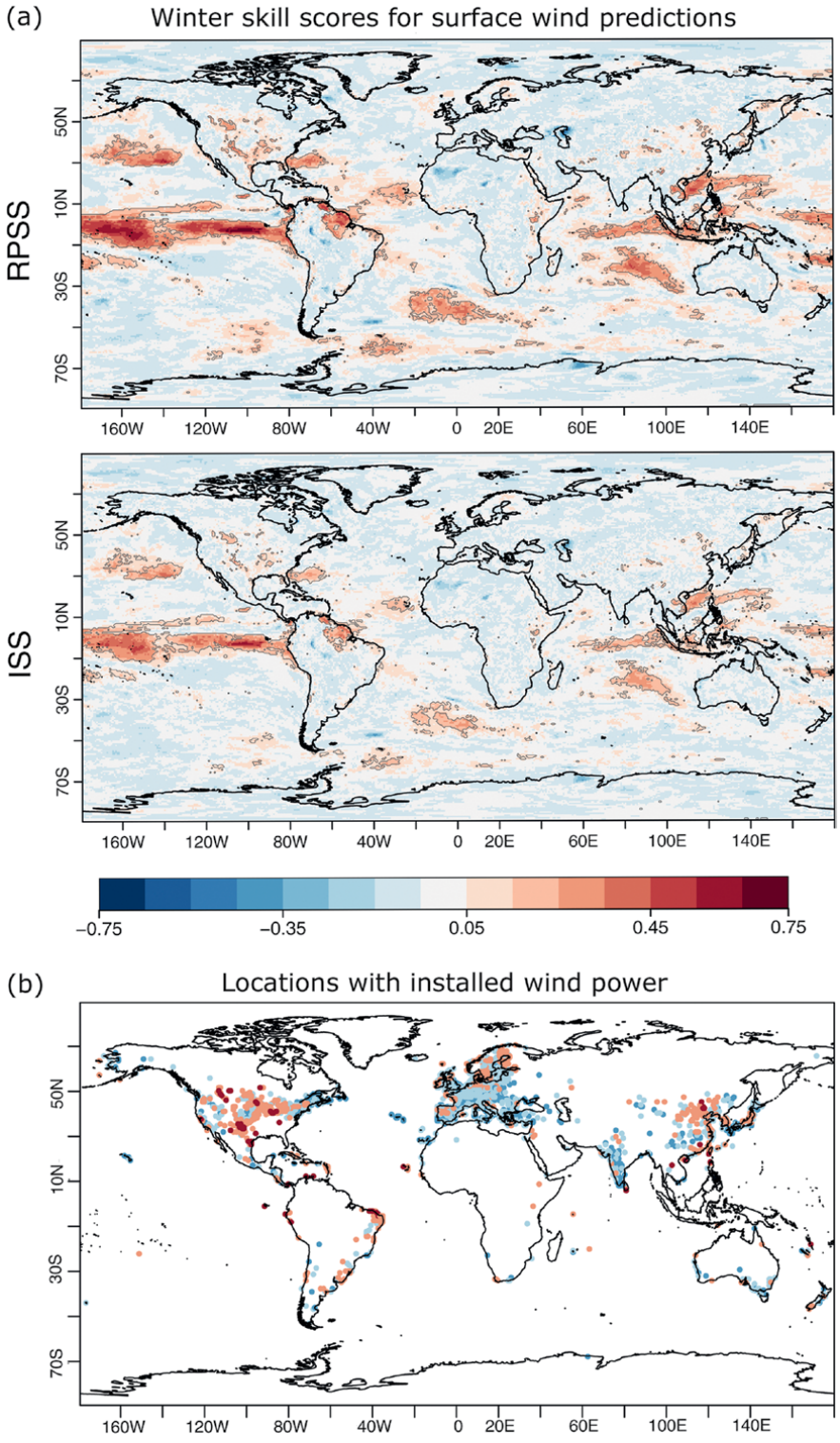

Fig. 2. (a) Skill scores (RPSS and ISS) for tercile categories of winter (DJF) surface (10 m) wind speed, as given by the calibrated seasonal forecasts from ECMWF S4 for the period 1981–2013 (ERA-Interim has been considered as reference). Red (blue) areas show higher (lower) performance than a climatological prediction. Gray contours enclose statistically significant values with a 95% of confidence level. (b) Considered locations with installed wind power divided in locations with negative RPSS (blue) and locations with positive RPSS (red). Light colors indicate nonsignificant RPSS values.

of Europe such as the North Sea or Scandinavia. However, there is a significant number of wind farms in Europe (Fig. 2b), with a nonnegligible amount of installed wind power in regions with low or negative skill such as in southern Europe (Torralba et al. 2017). Wind speed has positive skill in some North American regions. From the 2,023 locations with installed wind power, 473 were located in skillful areas (RPSS > 0). RPSS values tend to be higher than ISS values in most locations. This is due to the nature of the metrics themselves (see Fig. 3 for more detail). Statistical significance of skill score values has been assessed according to Bradley et al. (2008), employing a confidence level of 95%. Skill scores lower than 0.15 are nonsignificant at this confidence level.

Relationship between skill scores and economic indices. Hagedorn and Smith (2009) showed that the average return ratio (R) is a mathematical transformation of the ignorance score (IS) used to calculate the ISS. For the particular case presented here, $R = 3 \times 2^{(-IS)}$. Wind farms with $R > 1$, which is equivalent to the condition IS < 1.58, will produce a return superior to the climatology, meaning that a player choosing climate predictions will win in the WR game.

Although RPSS and ISS do not measure exactly the same thing, they are highly correlated in the case of the wind farms selected in this work (R^2 = 0.840). Thus, in skillful areas (with RPSS > 0 and ISS > 0), higher RPSS and ISS values lead to higher gains in

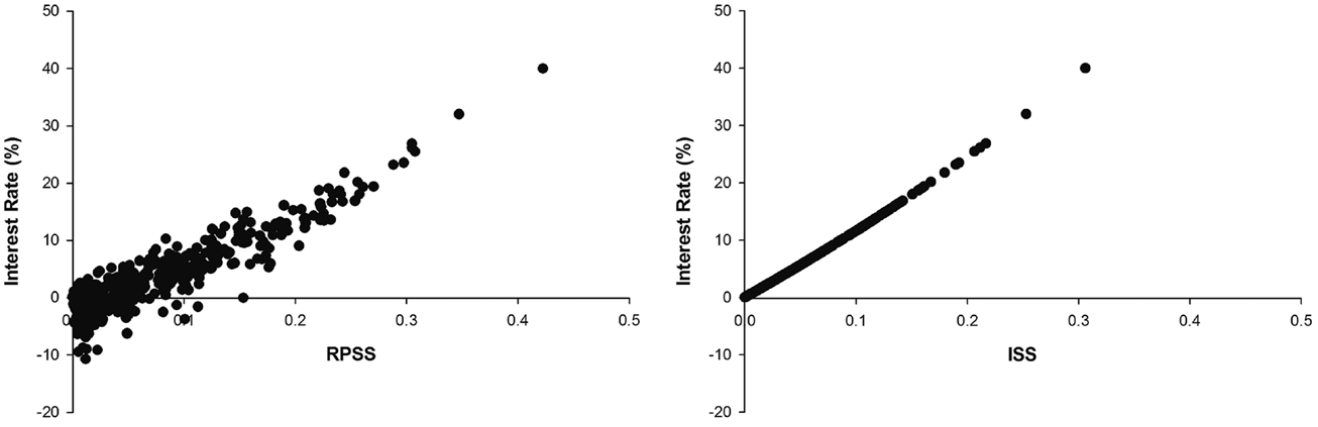

Fig. 3. Interest rate after 33 years at locations in skillful areas: (left) RPSS > 0 and (right) ISS > 0.

the WR (Fig. 3). Unlike ISS, for which positive values are always associated to long-term benefits, for some locations with RPSS values close to zero (0–0.15), either gains or losses can be experienced in terms of IR and ROI. This means that in this RPSS range some climate predictions are not better than climatology despite the positive RPSS value.

Translating skill scores into economic value. The application of the WR to each of the selected locations allows calculating the added value of using seasonal climate predictions compared to using the climatology. Figure 4 shows both the return ratios for each year (r_t, represented by black dots) as well as the average return ratio after 33 years (R, represented by a solid line) at nine different locations. The dashed line in Fig. 4 plots corresponds to $R = 1$. Above this line, predictions perform better than climatology and below they perform worse. A sample of locations from areas with different levels of skill is shown in Fig. 4: locations where RPSS and ISS are both negative (upper row), locations where RPSS is nonsignificant (i.e., ranging from 0 to 0.15) but ISS can have either positive or negative values (middle row), and locations where RPSS and ISS are both positive, with RPSS values above 0.15 (lower row).

In all cases, r_t values can be found indistinctly above or below the dashed line, indicating that a better performance of either climate predictions or climatology depends on the particular year of interest (Fig. 4). However, for those locations with negative values for both RPSS and ISS, the solid line is majorly found below the dashed line. The R values for the three selected locations with negative skill are below 1 (0.80–0.83), and both the IR and ROI report economic losses, meaning that at these locations using climate predictions does not provide any added value over using climatology (Fig. 4, upper row). For locations with RPSS between 0 and 0.15, the solid line can indistinctly appear above or below the dashed line, with a trend to approach the dashed line at the end of the 33-yr period. The R values for these selected locations are around 1 (0.99–1.05) and both economic losses and gains are reported depending on the sign of the ISS value (Fig. 4, middle row). Note that negative IR and ROI values are obtained when ISS < 0. Finally, for locations with positive ISS values and RPSS above 0.15, the solid line is majorly found above the dashed line. These locations have R values above 1 (1.25–1.40) and report economic gains, shown by the positive IR and ROI values (Fig. 4, lower row).

Results in Fig. 4 show how the ROI at the location in Greece (X37407; upper row), which has no skill, is −0.99. This means that the initial bet decreases by almost 100% after 33 years of playing the WR. The case of the locations in Denmark and eastern United States (X24592 and X36231; middle row) illustrates situations where, although the skill is nonsignificant (RPSS < 0.15), using climate predictions is still better than using climatology. However, in other locations with similar skill, such as the one in Canada (X28027; middle row), the WR reports losses at the end of the 33-yr period, meaning that in this case it would have been better to use the climatology. The location in southern United States (X39788; lower row), which exhibits a good skill, has an ROI of 66,049. This means that the initial bet increases by 6,604,900% after 33 years. Figure 5 shows the ROI at skillful locations (where RPSS > 0). Whereas this figure shows some locations with losses (corresponding to 0 < RPSS < 0.15), benefits are obtained in many locations, the highest being in North America and around the tropics.

DISCUSSION. Potential users of climate predictions are far from being a homogeneous group: they belong to different socioeconomic sectors and have

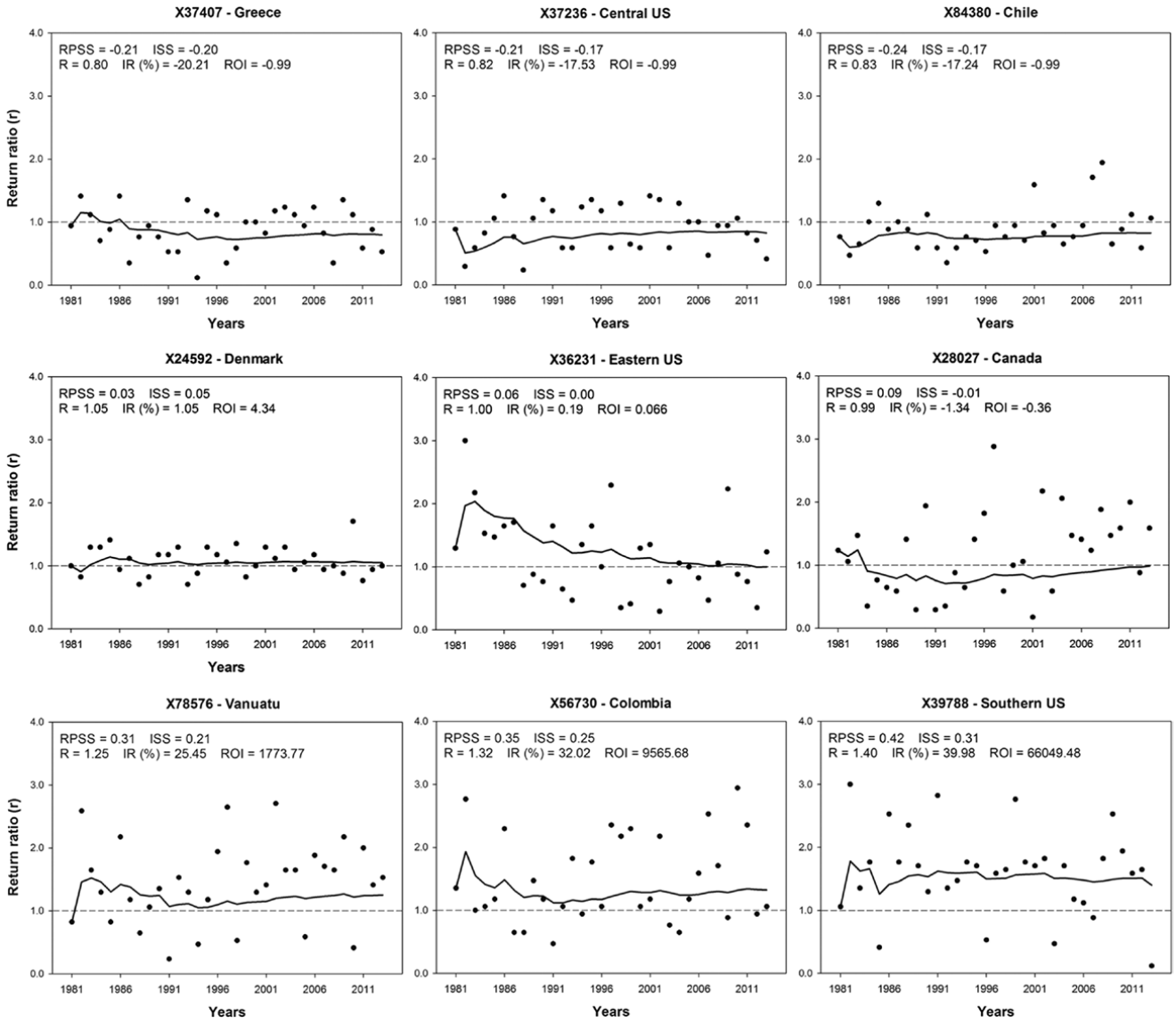

Fig. 4. Example of results from the WR at locations with different levels of skill: (top) RPSS < 0 (Greece–central United States–Chile), (middle) 0 < RPSS < 0.15 (Denmark–eastern United States–Canada), and (bottom) RPSS > 0.15 (Vanuatu–Colombia–southern United States). Black dots show the return ratio (r_t) for each of the 33 years (1981–2013). The solid line is the evolution of the average return ratio (R) [i.e., the geometric average of all the previous individual return ratios (r_t)]. The final R value is used to calculate the effective interest rate (IR) and the return on investment (ROI) with an initial investment of EUR 10. Over the dashed line (R > 1), climate predictions outperform climatology, whereas climatology performs better below the dashed line.

different backgrounds ranging from highly technical users to those with a business background. Therefore, the communication of climate predictions and their associated uncertainties to different audiences requires a transdisciplinary approach able to illustrate the benefits of using climate predictions through alternative approaches such as games. This communication task is normally undertaken by climate knowledge brokers and science communicators working at the interface between the science and user communities. They work to improve coherence and smooth the collaboration between providers and users of climate predictions, which is essential to build trust in such predictions (Bruno-Soares and Dessai 2016). By using the WR approach, we address some of the barriers that have been identified to the uptake of climate predictions.

One of the barriers is related to the uncertainty of an event happening according to a particular forecast, also known as first-order uncertainty (Taylor et al. 2015). There is a mismatch between model outcomes (probabilistic) and users' decision-making approaches (deterministic). From our experience in user engagement, the predicted probability of the most likely category is highly relevant to many users, who often associate higher predicted probabilities to more

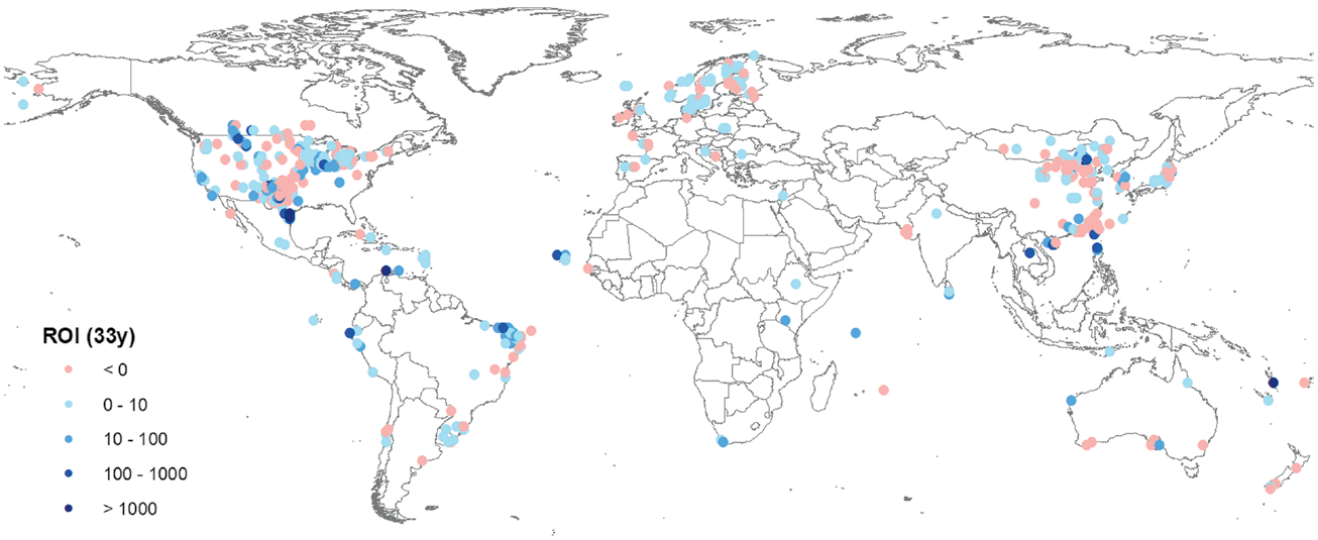

Fig. 5. Return on investment (ROI) at skillful locations (RPSS > 0) for DJF after 33 years.

trustworthy predictions or willingness to take action. Therefore, requests for high predicted probabilities as a method to reduce uncertainty are often found in the descriptions of user needs. However, establishing an appropriate threshold for those probabilities is not straightforward. This requires that users know which are the probability thresholds that maximize their benefits for each relationship between the costs of implementing an action and the losses that users would have incurred if no action had been taken (MacLeod et al. 2015). In addition, although some users may feel comfortable with a predicted probability for the most likely category above 50%, this only occurs occasionally. Indeed, for the locations selected for this study, the predicted most likely tercile probability was above 50% only the 23% of the times (Fig. 6).

Besides the first-order uncertainty, there is a second-order uncertainty related to the quality of the forecast that is more complex to convey to users. The scientific community deals with this uncertainty through the calculation of various metrics, such as skill scores (Taylor et al. 2015). By translating the skill of climate predictions into economic value, we illustrate how the application of climate predictions in areas with skill brings accumulated benefits in the long term. However, for particular years, predictions based on climatology can perform better than climate predictions, even if they are for an area with skill (see Fig. 4). It is important that potential users are aware of this and understand that one single prediction is not representative of the general performance of climate predictions. Early adopters of climate predictions have to accept that they might need to wait a few years to see the benefits of adopting such predictions for decision-making. This is an important point, especially given the short-term thinking of many companies as well

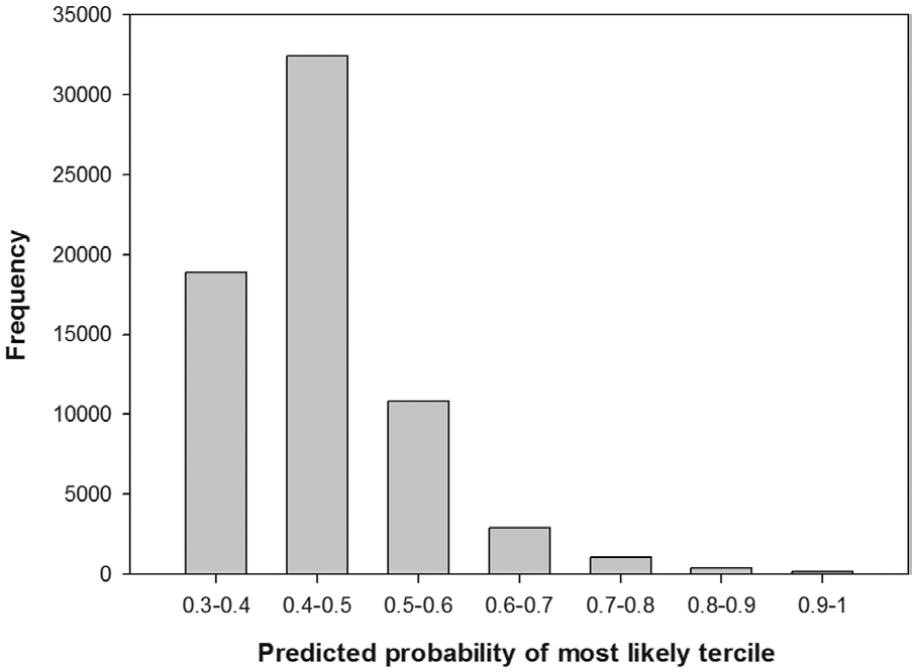

Fig. 6. Frequency of the predicted probability of the most likely category of wind speed for the locations with installed wind power.

as their incentives to avoid risks. In practice, it is unlikely that a user continues using probabilistic forecasts after two years in a row of losses, unless the user understands and has confidence in obtaining benefits in the long term. In this sense, the fact that the WR presents results for several subsequent years helps users to switch from the traditional gain and fail perspective for particular events to a long-term strategy where adjusted probabilities are included in the risk assessments, as a source of information for decision-making.

The evaluation of forecast performance plays a central role in the interpretation and use of forecast systems. Thus, an appropriate communication is needed to make the user aware of the spatiotemporal dependence of skill, and also of its dependence on the type of variable considered (wind speed, temperature, precipitation, etc.). Creating an effective communication strategy requires handling user expectations and looking for windows of opportunity to the application of climate predictions. In this regard, potential users playing the WR app in a location in the south of Europe would easily get the impression that winter wind predictions do not provide any added value over climatology, unless they are aware this is an area of limited skill for this variable. Conversely, the high positive skill in some North American regions can have important implications for the uptake of seasonal climate predictions by the wind energy sector, since the region is characterized by a high installed wind power capacity.

In this study, we show how ISS and RPSS skill scores can be easily explained through the use of the economic metrics such as interest rate and return on investment. This translation into economic terms addresses the terminology gap between climate scientists and users regarding second-order uncertainty. Results of the WR game show that positive ISS and RPSS values are generally associated to obtaining economic benefits in the long term (Figs. 3 and 4). However, for RPSS, there is a range between 0 and 0.15 where either gains or losses are possible (as shown in Fig. 4, middle row). Despite the uncertainty of obtaining long-term economic benefits with low RPSS values, this score deserves special attention, since it is widely used among the climate community (Torralba et al. 2017; Lledó et al. 2018; Manzanas et al. 2019).

An advantage of using RPSS is that the score does not only take into consideration whether or not the prediction system is able to predict a higher probability for the winning (observed) category, but also how big the probabilities are for the nonobserved categories. This is important for real-world applications, when losses and costs of any response action depend on the observed category, and highlights the importance of selecting a verification metric that is relevant to the user's gains and losses. For instance, economic implications will be different if a high probability for above-normal winds is forecasted and normal winds are observed than when below-normal winds are observed. The reason is that the protecting actions that the user takes might still work with normal winds but might be damaging when below-normal winds occur. Moreover, failing to predict the observed category in the wind energy sector would usually cause higher damages than the benefits of succeeding to predict it (Vigo et al. 2018).

We illustrate that the RPSS standard forecast quality measure has a slightly different relation to long-term user benefit than ISS. In all cases, the results highlight that statistically significant skill is not absolutely necessary for a user to obtain a long-term gain. This agrees with the broader discussion that reliance on thresholds of statistical significance can be misleading (Amrhein et al. 2019). Actually, it should be communicated to users that statistical significance, while hugely valuable in a scientific context, tries to respond to questions on specific aspects of the forecast that are not directly linked to the user benefit (Mason 2008; Amrhein et al. 2019). As a result, users should not base their decisions exclusively on the basis of the statistical significance of the results.

CONCLUSIONS. The WR mobile app conveys with an interactive game the different aspects presented in this paper as barriers to the adoption of climate predictions. The terminology gap is overcome through the translation of technical concepts into economic concepts that users are more familiar with. The difficulty to understand the uncertainty of probabilistic outcomes is dealt by allowing players to choose between the climate prediction or climatology for single years after showing them the predicted probabilities. This helps players understand that it is not only the predicted probabilities that matter, but also other factors related to the quality of the climate prediction. Finally, limitations to the understanding of the concept of skill, which needs a long-term perspective, are overcome by informing players on the skill of climate predictions at the selected location and allowing them to play the WR for the entire period. This enables players to see the long-term benefits of integrating climate predictions in their decision-making in skillful areas.

The app has been designed as a simple interface with a limited number of decisions left for the player

(selection of a geographical location, selection of the preferred forecast option and definition of the initial bet). More complexity could be added to make the game more interactive (e.g., add data for other seasons, allow the possibility to reinvest only a part of the bet), but it would make user interaction also more complex, especially for those unfamiliar with the type of concepts that are communicated. Future efforts should include some experimental designs to assess users' understanding of the concepts conveyed by the game before and after playing it. This would allow us to quantify the users' learning curve.

The way the WR approach has been applied in this study (setting a random initial capital that is fully reinvested, or considering three tercile categories) is a simplification, and the calculated ROIs cannot be directly translated into real ROIs for a particular company, unless the company agrees in taking the challenge of carrying out a real exercise of including climate predictions in their regular decision-making. This is unlikely due to the high sensitivity of real data on gains and losses. However, even if nonreal economic values are used, it still provides a more intuitive translation of climate-based skill scores into potential economic benefits. We expect that this game could encourage energy users to adopt climate predictions in skillful areas, since revenues will be higher than using the climatology. These predictions, after being tailored to specific decision-making contexts, can be integrated in many decision-making processes, including operations and management strategies, resource allocation for optimum task scheduling, or grid management taking into account renewable energy supply and demand.

Although the WR app is primarily directed to improve the communication of climate services based on seasonal predictions for the wind energy sector, it is a tool that can be useful to illustrate the potential value of using climate predictions in other socioeconomic sectors. A transdisciplinary approach, which implies transcending the disciplinary boundaries and involving actors from outside academia, requires the use of a common language between the climate science and user communities that is necessary to achieve a real coproduction of climate services. In this sense, the WR constitutes a transdisciplinary effort to communicate the usefulness and value of climate predictions in economic terms to different types of users.

The outcomes of this study can be interesting not only in the context of the many projects and initiatives working in the field of climate services and the interface between science and applications, but also for climate scientists that aim to transfer the knowledge arising from their research to potential communities of users.

ACKNOWLEDGMENTS. The research leading to these results has received funding from the EU FP7 Programme under Grant Agreement 308291 (EUPORIAS), the EU H2020 Programme under Grant Agreements 776787 (S2S4E) and 776613 (EUCP), and the Ministerio de Economía y Competitividad (MINECO) as part of the CLINSA Project CGL2017-85791-R. It is also part of the Copernicus Climate Change Service (C3S) (Framework Agreement C3S_441_Lot2_CEA), a program being implemented by the European Centre for Medium-Range Weather Forecasts (ECMWF) on behalf of the European Commission. The authors want to thank Amaia Aizpurua for her valuable technical help.

REFERENCES

Amrhein, V., S. Greenland, and B. McShane, 2019: Scientists rise up against statistical significance. *Nature*, **567**, 305–307, https://doi.org/10.1038/d41586-019-00857-9.

Arnal, L., M.-H. Ramos, E. Coughlan, H. L. Cloke, E. Stephens, F. Wetterhall, S.-J. van Andel, and F. Pappenberger, 2016: Willingness-to-pay for a probabilistic flood forecast: A risk-based decision-making game. *Hydrol. Earth Syst. Sci.*, **20**, 3109–3128, https://doi.org/10.5194/hess-20-3109-2016.

Bradley, A. A., S. S. Schwartz, and T. Hashino, 2008: Sampling uncertainty and confidence intervals for the Brier score and Brier skill score. *Wea. Forecasting*, **23**, 992–1006, https://doi.org/10.1175/2007WAF2007049.1.

Bruno-Soares, M., and S. Dessai, 2016: Barriers and enablers to the use of seasonal climate forecasts amongst organisations in Europe. *Climatic Change*, **137**, 89–103, https://doi.org/10.1007/s10584-016-1671-8.

——, M. Daly, and S. Dessai, 2018: Assessing the value of seasonal climate forecasts for decision-making. *Wiley Interdiscip. Rev.: Climate Change*, **9**, e523, https://doi.org/10.1002/wcc.523.

Caron, L. P., L. Hermanson, A. Dobbin, J. Imbers, L. Lledó, and G. A. Vecchi, 2018: How skillful are the multiannual forecasts of Atlantic hurricane activity? *Bull. Amer. Meteor. Soc.*, **99**, 403–413, https://doi.org/10.1175/BAMS-D-17-0025.1.

Carta, J. A., S. Velázquez, and P. Cabrera, 2013: A review of measure-correlate-predict (MCP) methods used to estimate long-term wind characteristics at a target site. *Renewable Sustainable Energy Rev.*, **27**, 362–400, https://doi.org/10.1016/j.rser.2013.07.004.

Coelho, C. A. S., and S. M. S. Costa, 2010: Challenges for integrating seasonal climate forecasts in user applications. *Curr. Opin. Environ. Sustainability*, **2**, 317–325, https://doi.org/10.1016/j.cosust.2010.09.002.

Crochemore, L., M.-H. Ramos, F. Pappenberger, S.-J. van Andel, and A. W. Wood, 2016: An experiment on risk-based decision-making in water management using monthly probabilistic forecasts. *Bull. Amer. Meteor. Soc.*, **97**, 541–551, https://doi.org/10.1175/BAMS-D-14-00270.1.

Dee, D. P., and Coauthors, 2011: The ERA-Interim reanalysis: Configuration and performance of the data assimilation system. *Quart. J. Roy. Meteor. Soc.*, **137**, 553–597, https://doi.org/10.1002/qj.828.

Doblas-Reyes, F. J., R. Hagedorn, and R. N. Palmer, 2005: The rationale behind the success of multi-model ensembles in seasonal forecasting—II. Calibration and combination. *Tellus*, **57A**, 234–252, https://doi.org/10.3402/tellusa.v57i3.14658.

——, J. García-Serrano, F. Lienert, A. P. Biescas, and L. R. Rodrigues, 2013: Seasonal climate predictability and forecasting: Status and prospects. *Wiley Interdiscip. Rev.: Climate Change*, **4**, 245–268, https://doi.org/10.1002/wcc.217.

European Commission, 2015: A European research and innovation roadmap for climate services. European Commission Directorate-General for Research and Innovation Rep., 56 pp., https://doi.org/10.2777/702151.

Feldman, D. L., and H. M. Ingram, 2009: Making science useful to decision makers: Climate forecasts, water management, and knowledge networks. *Wea. Climate Soc.*, **1**, 9–21, https://doi.org/10.1175/2009WCAS1007.1.

Good, I. J., 1952: Rational decisions. *J. Roy. Stat. Soc.*, **14A**, 107–114.

Hagedorn, R., and L. A. Smith, 2009: Communicating the value of probabilistic forecasts with Weather Roulette. *Meteor. Appl.*, **16**, 143–155, https://doi.org/10.1002/met.92.

Jewson, S., E. Bellone, S. Khare, T. Lepple, M. Lonfat, A. O. Shay, J. Penzer, and K. Coughlin, 2009: Five year prediction of the number of hurricanes that make United States landfall. *Hurricanes and Climate Change*, J. B. Elsner and T. H. Jagger, Eds., Springer, 73–99, https://doi.org/10.1007/978-0-387-09410-6_5.

Jolliffe, I. T., and D. B. Stephenson, 2012: *Forecast Verification: A Practitioner's Guide in Atmospheric Science.* John Wiley and Sons, 288 pp.

Jupp, T. E., R. Lowe, C. Coelho, and D. B. Stephenson, 2012: On the visualization, verification and recalibration of ternary probabilistic forecasts. *Philos. Trans. Roy. Soc.*, **370A**, 20110350, https://doi.org/10.1098/rsta.2011.0350.

Lazenby, M. J., W. A. Landman, R. M. Garland, and D. G. DeWitt, 2014: Seasonal temperature prediction skill over southern Africa and human health. *Meteor. Appl.*, **21**, 963–974, https://doi.org/10.1002/met.1449.

Lledó, L., 2017: Seasonal predictions for wind energy: Anticipating quarterly winds and revenues one month ahead. WindTech International, www.windtech-international.com/editorial-features/seasonal-predictions-for-wind-energy.

——, O. Bellprat, F. J. Doblas-Reyes, and A. Soret, 2018: Investigating the effects of Pacific sea surface temperatures on the wind drought of 2015 over the United States. *J. Geophys. Res. Atmos.*, **123**, 4837–4849, https://doi.org/10.1029/2017JD028019.

MacLeod, D. A., A. Jones, F. Di Giuseppe, C. Caminade, and A. P. Morse, 2015: Demonstration of successful malaria forecasts for Botswana using an operational seasonal climate model. *Environ. Res. Lett.*, **10**, 044005, https://doi.org/10.1088/1748-9326/10/4/044005.

Manzanas, R., M. D. Frías, A. S. Cofiño, and J. M. Gutiérrez, 2014: Validation of 40 year multimodel seasonal precipitation forecasts: The role of ENSO on the global skill. *J. Geophys. Res. Atmos.*, **119**, 1708–1719, https://doi.org/10.1002/2013JD020680.

——, J. M. Gutiérrez, J. Bhend, S. Hemri, F. J. Doblas-Reyes, V. Torralba, E. Penabad, and A. Brookshaw, 2019: Bias adjustment and ensemble recalibration methods for seasonal forecasting: A comprehensive intercomparison using the C3S dataset. *Climate Dyn.*, **53**, 1287–1305, https://doi.org/10.1007/s00382-019-04640-4.

Mason, S. J., 2008: Understanding forecast verification statistics. *Meteor. Appl.*, **15**, 31–40, https://doi.org/10.1002/met.51.

McNie, E. C., 2007: Reconciling the supply of scientific information with user demands: An analysis of the problem and review of the literature. *Environ. Sci. Policy*, **10**, 17–38, https://doi.org/10.1016/j.envsci.2006.10.004.

Meehl, G. A., and Coauthors, 2014: Decadal climate prediction: An update from the trenches. *Bull. Amer. Meteor. Soc.*, **95**, 243–267, https://doi.org/10.1175/BAMS-D-12-00241.1.

Molteni, F., and Coauthors, 2011: The new ECMWF seasonal forecast system (system 4). ECMWF Tech. Memo. 656, 51 pp.

Predictia, 2019: Weather Roulette. Predictia, https://play.google.com/store/apps/details?id=es.predictia.weatherroulette.

Palmer, T. N., G. J. Shutts, R. Hagedorn, F. J. Doblas-Reyes, T. Jung, and M. Leutbecher, 2005: Representing model uncertainty in weather and climate prediction.

Annu. Rev. Earth Planet. Sci., **33**, 163–193, https://doi.org/10.1146/annurev.earth.33.092203.122552.

Ramos, M. H., S. J. van Andel, and F. Pappenberger, 2013: Do probabilistic forecasts lead to better decisions? *Hydrol. Earth Syst. Sci.*, **17**, 2219–2232, https://doi.org/10.5194/hess-17-2219-2013.

R Core Team, 2015: R: A language and environment for statistical computing. R Foundation, www.r-project.org/.

Taylor, A. L., S. Dessai, and W. Bruine de Bruin, 2015: Communicating uncertainty in seasonal and interannual climate forecasts in Europe. *Philos. Trans. Roy. Soc.*, **373A**, 20140454, https://doi.org/10.1098/rsta.2014.0454.

Terrado, M., N. González-Reviriego, L. Lledó, V. Torralba, A. Soret, and F. J. Doblas-Reyes, 2017: Climate services for affordable wind energy. *WMO Bull.*, **66**, 48–53.

Thomson, M. C., F. J. Doblas-Reyes, S. J. Mason, R. Hagedorn, S. J. Connor, T. Phindela, and T. N. Palmer, 2006: Malaria early warnings based on seasonal climate forecasts from multi model ensembles. *Nature*, **439**, 576–579, https://doi.org/10.1038/nature04503.

Torralba, V., F. J. Doblas-Reyes, D. MacLeod, I. Christel, and M. Davis, 2017: Seasonal climate prediction: A new source of information for the management of wind energy resources. *J. Appl. Meteor. Climatol.*, **56**, 1231–1247, https://doi.org/10.1175/JAMC-D-16-0204.1.

Turco, M., A. Ceglar, C. Prodhomme, A. Soret, A. Toreti, and F. J. Doblas-Reyes, 2017: Summer drought predictability over Europe: Empirical versus dynamical forecasts. *Environ. Res. Lett.*, **12**, 084006, https://doi.org/10.1088/1748-9326/aa7859.

van Pelt, S. C., M. Haasnoot, B. Arts, F. Ludwig, R. Swart, and R. Biesbroek, 2015: Communicating climate (change) uncertainties: Simulation games as boundary objects. *Environ. Sci. Policy*, **45**, 41–52, https://doi.org/10.1016/j.envsci.2014.09.004.

Vigo, I., and Coauthors, 2018: User needs and decision-making processes that can benefit from S2S forecasts. S2S4E Tech. Rep. D2.2, 92 pp.

Vincent, K., A. J. Dougill, J. L. Dixon, L. C. Stringer, and T. Cull, 2017: Identifying climate services needs for national planning: Insights from Malawi. *Climate Policy*, **17**, 189–202, https://doi.org/10.1080/14693062.2015.1075374.

von Storch, H., and F. W. Zwiers, 2001: *Statistical Analysis in Climate Research*. Cambridge University Press, 496 pp.

Weisheimer, A., and T. N. Palmer, 2014: On the reliability of seasonal climate forecasts. *J. Roy. Soc. Interface*, **11**, 20131162, https://doi.org/10.1098/rsif.2013.1162.

White, C. J., and Coauthors, 2017: Potential applications of subseasonal-to-seasonal (S2S) predictions. *Meteor. Appl.*, **24**, 315–325, https://doi.org/10.1002/met.1654.

Wilks, D. S., 2011: *Statistical Methods in the Atmospheric Sciences*. 3rd ed. Elsevier, 676 pp.

Chapter 8

Conclusions and future directions

8.1 Conclusions

8.1.1 Impact of atmospheric variability on wind power generation at sub-seasonal and seasonal timescales

Describing the impact that atmospheric variability has on wind speed and wind power generation is a first step towards better understanding the links between the energy system and the Earth's climate. This goal has been addressed through the study of some well-known climate oscillations at sub-seasonal and seasonal time scales. Chapter 3 investigates the impact of the ENSO and the NPM seasonal oscillations on the wind resource in North America. Historical records show that during the first quarter of the year the ENSO state dominates the inter-annual variability of wind speed in North America, but the state of the NPM also plays a relevant role. While ENSO events impart anomalies in the center and north of the continent, NPM events have an impact on the southwest.

Similarly, chapter 4 investigates the wind speed anomalies over Europe during strong MJO events. Each of the eight phases of this sub-seasonal oscillation have a different signature on the near-surface wind speed in Europe. Analyzing the most frequently observed terciles under each MJO phase provides a robust analysis of the diversity of MJO impacts, which are modulated not only by MJO phase and intensity but also by many other factors.

Although not explicitly included in chapter 6 publication, the role of four Euro-Atlantic teleconnections in shaping wind speed conditions and wind power generation over Europe has been presented in figure 6.1. The results show that in many regions of Europe not only the state of the NAO is important, but the status of the EA, EAWR and SCA can also substantially modify wind power generation.

8.1.2 Case studies and attribution experiments

Showing practical examples of how much climate oscillations can affect wind power generation helps to increase awareness of the need of employing climate predictions and of making wind resource assessments better climate-informed. Additionally, attribution experiments are a powerful tool for detecting the contribution of specific components of the Earth system in setting and maintaining anomalous wind speed episodes. The US wind drought of 2015 is one of those episodes where a climate anomaly impacted the whole wind power industry in the country. In chapter 3, an attribution experiment revealed that the North American wind drought of the first quarter of 2015 can be attributed to a strongly positive phase of the NPM.

8.1.3 Enhancing sub-seasonal and seasonal predictions of wind speed through dynamical forecasts of teleconnection indices

Developing new techniques for enhancing available sub-seasonal and seasonal predictions can be very valuable, specially in a context of limited skill of the prediction systems in the extratropics. In chapter 4, the weaknesses of the ECMWF

sub-seasonal prediction system to reproduce the teleconnective impacts of the MJO in Europe have been highlighted. To overcome this limitation a hybrid dynamical-statistical prediction strategy has been proposed and tested. The conditional climatology technique consists in forecasting strong MJO events weeks ahead with a dynamical prediction system and then use the climatological wind speed conditions for the forecasted phase of the MJO as a new forecast. The technique proves useful in a theoretical framework, but the ECMWF sub-seasonal predictions can not anticipate strong MJO events more than 10 days ahead, limiting the applicability of this method.

In a similar fashion, chapter 6 presents seasonal predictions of four teleconnection indices that are relevant in the Euro-Atlantic domain. The results show that prediction skill is not limited to the NAO (which has been extensively studied in the literature) and that the EA, EAWR and SCA teleconnection indices can also be anticipated by five seasonal prediction systems in winter, spring and summer, while in autumn only modest scores are obtained. The degree of agreement between systems in which teleconnections can be predicted for each season and lead time highlights inherent predictability of the teleconnections. Those teleconnection index forecasts can be either directly employed to communicate with potential users or combined with statistical models of surface impacts to produce hybrid forecasts.

8.1.4 Tailoring forecasts to the user needs

The derivation of indicators that summarize the impact of atmospheric variables on a sectoral application is an essential part of producing an effective climate service. While climate prediction systems deliver forecasts of surface wind speed, many end users are ultimately interested in anticipating wind power generation at farm, region or country level. Chapter 5 presents and discusses a methodology to compute forecasts of capacity factor that can be used to anticipate wind power generation at site level. While total power generation of a wind farm depends on many aspects such as the number of turbines, its rated power or the losses due to wakes, curtailments or electricity transport, the gross capacity factor is an indicator that considers only the effects of wind speed conditions on generation potential. To account for technological differences, capacity factor forecasts have been computed for three different turbine types. The proposed methodology overcomes several limitations of current seasonal prediction systems, such as coarse spatial scales, a restrained set of variables, a low time frequency, and the presence of biases. The method, although simple in some aspects, proves to be able to produce skillful forecasts of wind power generation one to three months ahead when employed with the ECMWF System4 predictions.

8.1.5 Facilitating uptake of climate predictions

Probabilistic climate predictions are difficult to uptake by potential users due to the complex aspects of the science behind it. Chapter 7 presents an interactive game that helps players overcoming the barriers to the adoption of climate predictions. The player has to choose to bet money according to either climatological probabilities or to seasonal forecast probabilities. This highlights that it is not only the predicted probabilities that matter, but also other factors related to the quality of the climate prediction. The terminology gap is addressed by translating technical concepts into economic concepts that users are more familiar with. The possibility of playing many years in a row as consecutive rounds puts the concept of skill in a long-term perspective where the benefits of adopting one or another strategy are only perceived after several rounds. The fuzzy separation between forecast quality assessment and the economic value of climate predictions is diluted in this simplified setting and although gains and losses in the game are not related to a specific company decision-making scenario, the weather roulette provides an intuitive translation of skill scores into potential economic benefits.

8.2 Future directions

The work presented in this PhD dissertation paves the way for the development of new climate services for the wind power industry. The advances presented in chapter 5 are currently being implemented operationally in the S2S4E

H2020 research project to produce seasonal and sub-seasonal forecasts of capacity factor over Europe at grid point level. The work presented in chapter 6 opens the door to a year-round climate service that informs of the state of the four Euro-Atlantic teleconnections studied. This could be of interest not only to the energy industry but also to a wider audience. Chapter 3 has shown that monitoring the state and evolution of the NPM can be beneficial for anticipating wind anomalies in North America as a complement to ENSO forecasts that are currently available from many sources. However the predictability of the NPM has not been assessed thoroughly in the literature yet.

Other pieces of this work are not mature enough to be translated yet into direct improvements for the development of climate services and will require further efforts. For instance, the work presented in chapter 4 shows that sub-seasonal prediction systems are still far from being able to anticipate strong MJO events weeks ahead. Therefore the conditional climatology method cannot be implemented to anticipate daily mean wind speed in Europe. However, the concept itself can be useful in other contexts and with other teleconnections. Also, this research has pointed out the difficulties that are caused by the diverse MJO index definitions employed for monitoring and impact studies and for prediction, which are specially relevant for strong MJO events. Finally, recent research suggests that the diversity of MJO events can be better dealt with when considering the simultaneous state of ENSO and the QBO (Lee et al., 2019; Lim et al., 2019). All those topics deserve further exploration.

In terms of analyzing the impact of climate oscillations on wind energy, only a few of them have been analyzed in this dissertation. The impact of other sub-seasonal and seasonal phenomena such as the Indian Ocean Dipole (IOD), the QBO or the occurrence of sudden stratospheric warmings on near-surface wind speed still remain to be investigated systematically. This is also specially true for decadal oscillations such as the AMV or the PDO. Indeed, recent research has suggested that long-term trends of surface wind speed previously attributed to roughness changes could be due to the effect of decadal oscillations (Zeng et al., 2019). In this sense, the added value of initialized decadal predictions over long-term climate change projections for the energy industry is still uncharted terrain.

Another challenge that has not been addressed in this work is that of adjusting climate predictions to the local scale. Absolute values of wind speed can vary considerably in short distances and climate prediction systems cannot represent this fine-scale information appropriately. One of the difficulties to overcome this problem is the availability of long enough on-site observations of wind speed at hub heights to validate methodologies. The Tall Tower Dataset (Ramon et al., 2020) has recently been compiled and quality controlled, which provides an adequate observational reference. With this data at hand, a research effort is currently being conducted at the Barcelona Supercomputing Center to combine the Euro-Atlantic teleconnection forecasts presented in chapter 6 with these local observations to obtain downscaled predictions.

Last but not least, several episodes of anomalous wind speed conditions that have impacted wind power generation in the last years, and the influence of specific teleconnection states such as a strong IOD phase in autumn 2019 should be investigated. Although attribution experiments are costly, they shed light on the role of specific Earth system processes on producing damaging effects for socio-economic sectors.

Bibliography

Barnston, A. G., Kumar, A., Goddard, L., and Hoerling, M. P. (2005). Improving seasonal prediction practices through attribution of climate variability. *Bulletin of the American Meteorological Society*, 86(1):59–72, doi: 10.1175/bams-86-1-59.

Bessec, M. and Fouquau, J. (2008). The non-linear link between electricity consumption and temperature in Europe: A threshold panel approach. *Energy Economics*, 30(5):2705–2721, doi: 10.1016/j.eneco.2008.02.003.

Bessembinder, J., Terrado, M., Hewitt, C., Garrett, N., Kotova, L., Buonocore, M., and Groenland, R. (2019). Need for a common typology of climate services. *Climate Services*, 16:100135, doi: 10.1016/j.cliser.2019.100135.

Bloomfield, H. C., Brayshaw, D. J., Shaffrey, L. C., Coker, P. J., and Thornton, H. E. (2016). Quantifying the increasing sensitivity of power systems to climate variability. *Environmental Research Letters*, 11(12):124025, doi: 10.1088/1748-9326/11/12/124025.

Boer, G. J., Smith, D. M., Cassou, C., Doblas-Reyes, F., Danabasoglu, G., Kirtman, B., Kushnir, Y., Kimoto, M., Meehl, G. A., Msadek, R., Mueller, W. A., Taylor, K. E., Zwiers, F., Rixen, M., Ruprich-Robert, Y., and Eade, R. (2016). The decadal climate prediction project (DCPP) contribution to CMIP6. *Geoscientific Model Development*, 9(10):3751–3777, doi: 10.5194/gmd-9-3751-2016.

Brayshaw, D. J., Troccoli, A., Fordham, R., and Methven, J. (2011). The impact of large scale atmospheric circulation patterns on wind power generation and its potential predictability: A case study over the UK. *Renewable Energy*, 36(8):2087–2096, doi: 10.1016/j.renene.2011.01.025.

Brower, M., Barton, M., Lledó, L., and Dubois, J. (2013). A study of wind speed variability using global reanalysis data. Technical report, AWS Truepower, https://aws-dewi.ul.com/assets/A-Study-of-Wind-Speed-Variability-Using-Global-Reanalysis-Data1.pdf.

Brower, M. C. (2012). *Wind Resource Assessment*. John Wiley & Sons, Inc., doi: 10.1002/9781118249864.

Buontempo, C. (2018). European climate services. In *Weather & Climate Services for the Energy Industry*, pages 27–40. Springer International Publishing, doi: 10.1007/978-3-319-68418-5_3.

Buontempo, C., Hewitt, C. D., Doblas-Reyes, F. J., and Dessai, S. (2014). Climate service development, delivery and use in Europe at monthly to inter-annual timescales. *Climate Risk Management*, 6:1–5, doi: 10.1016/j.crm.2014.10.002.

Chardon, J., Favre, A.-C., and Hingray, B. (2016). Effects of spatial aggregation on the accuracy of statistically downscaled precipitation predictions. *Journal of Hydrometeorology*, 17(5):1561–1578, doi: 10.1175/jhm-d-15-0031.1.

Christel, I., Hemment, D., Bojovic, D., Cucchietti, F., Calvo, L., Stefaner, M., and Buontempo, C. (2018). Introducing design in the development of effective climate services. *Climate Services*, 9:111–121, doi: 10.1016/j.cliser.2017.06.002.

Crippa, M., Oreggioni, G., Guizzardi, D., Muntean, M., Schaaf, E., Lo Vullo, E., Solazzo, E., Monforti-Ferrario, F., Olivier, J., Vignati, E., European Commission, and Joint Research Centre (2019). *Fossil CO2 and GHG emissions of all world countries: 2019 report*. European Commission, ISBN: 9789276111009, http://publications.europa.eu/publication/manifestation_identifier/PUB_KJNA29849ENN.

De Felice, M., Busch, S., Kanellopoulos, K., Kavvadias, K., and Hidalgo Gonzalez, I. (2020). Power system flexibility in a variable climate. Report EUR 30184 EN, Publications Office of the European Union, doi: 10.2760/75312.

Doblas-Reyes, F. J., García-Serrano, J., Lienert, F., Biescas, A. P., and Rodrigues, L. R. L. (2013). Seasonal climate predictability and forecasting: status and prospects. *Wiley Interdisciplinary Reviews: Climate Change*, 4(4):245–268, doi: 10.1002/wcc.217.

Draxl, C., Clifton, A., Hodge, B.-M., and McCaa, J. (2015). The wind integration national dataset (WIND) toolkit. *Applied Energy*, 151:355–366, doi: 10.1016/j.apenergy.2015.03.121.

Dubus, L., Muralidharan, S., and Troccoli, A. (2018). What does the energy industry require from meteorology? In *Weather & Climate Services for the Energy Industry*, pages 41–63. Springer International Publishing, doi: 10.1007/978-3-319-68418-5_4.

Ebinger, J. (2011). *Climate impacts on energy systems : key issues for energy sector adaptation*. World Bank, Washington, D.C, ISBN: 978-0-8213-8697-2.

European Commission (2019). The European Green Deal. Technical Report COM(2019) 640 final, European Commission, Brussels, https://ec.europa.eu/info/sites/info/files/european-green-deal-communication_en.pdf.

Giebel, G. and Kariniotakis, G. (2017). Wind power forecasting—a review of the state of the art. In *Renewable Energy Forecasting*, pages 59–109. Elsevier, doi: 10.1016/b978-0-08-100504-0.00003-2.

Gonzalez, P. L. M., Brayshaw, D. J., and Zappa, G. (2019). The contribution of North Atlantic atmospheric circulation shifts to future wind speed projections for wind power over Europe. *Climate Dynamics*, 53(7-8):4095–4113, doi: 10.1007/s00382-019-04776-3.

González-Aparicio, I., Monforti, F., Volker, P., Zucker, A., Careri, F., Huld, T., and Badger, J. (2017). Simulating European wind power generation applying statistical downscaling to reanalysis data. *Applied Energy*, 199:155–168, doi: 10.1016/j.apenergy.2017.04.066.

Hewitt, C., Buontempo, C., and Newton, P. (2013). Using climate predictions to better serve society's needs. *Eos, Transactions American Geophysical Union*, 94(11):105–107, doi: 10.1002/2013eo110002.

Intergovernmental Panel on Climate Change (2014). *Climate Change 2013 - The Physical Science Basis: Working Group I Contribution to the Fifth Assessment Report of the Intergovernmental Panel on Climate Change*. Cambridge University Press, doi: 10.1017/CBO9781107415324.

Johnson, S. J., Stockdale, T. N., Ferranti, L., Balmaseda, M. A., Molteni, F., Magnusson, L., Tietsche, S., Decremer, D., Weisheimer, A., Balsamo, G., Keeley, S. P. E., Mogensen, K., Zuo, H., and Monge-Sanz, B. M. (2019). SEAS5: the new ECMWF seasonal forecast system. *Geoscientific Model Development*, 12(3):1087–1117, doi: 10.5194/gmd-12-1087-2019.

Jolliffe, I. T. and Stephenson, D. B., editors (2011). *Forecast Verification*. John Wiley & Sons, Ltd, doi: 10.1002/9781119960003.

Jonkeren, O., Rietveld, P., van Ommeren, J., and te Linde, A. (2013). Climate change and economic consequences for inland waterway transport in Europe. *Regional Environmental Change*, doi: 10.1007/s10113-013-0441-7.

Kaldellis, J. K. and Zafirakis, D. (2011). The wind energy (r)evolution: A short review of a long history. *Renewable Energy*, 36(7):1887–1901, doi: 10.1016/j.renene.2011.01.002.

Katz, R. W. and Murphy, A. H., editors (1997). *Economic Value of Weather and Climate Forecasts*. Cambridge University Press, doi: 10.1017/cbo9780511608278.

Kirtman, B. and Power, S. (2013). Near-term climate change: Projections and predictability. In on Climate Change, I. P., editor, *Climate Change 2013 - The Physical Science Basis*, pages 953–1028. Cambridge University Press, doi: 10.1017/cbo9781107415324.023.

Kumar, A., Ceron, J.-P., Coelho, C., Ferranti, L., Graham, R., Jones, D., Merryfield, W., Muñoz, A., Pai, S., and Rodriguez, E. (2020). Guidance on operational practices for objective seasonal forecasting. WMO-No. 1246, WMO, ISBN: 978-92-63-11246-9.

Lee, R. W., Woolnough, S. J., Charlton-Perez, A. J., and Vitart, F. (2019). ENSO modulation of MJO teleconnections to the North Atlantic and Europe. *Geophysical Research Letters*, 46(22):13535–13545, doi: 10.1029/2019gl084683.

Lim, Y., Son, S.-W., Marshall, A. G., Hendon, H. H., and Seo, K.-H. (2019). Influence of the QBO on MJO prediction skill in the subseasonal-to-seasonal prediction models. *Climate Dynamics*, 53(3-4):1681–1695, doi: 10.1007/s00382-019-04719-y.

Liu, Z. and Alexander, M. (2007). Atmospheric bridge, oceanic tunnel, and global climatic teleconnections. *Reviews of Geophysics*, 45(2), doi: 10.1029/2005rg000172.

Lledó, L., Bellprat, O., Doblas-Reyes, F. J., and Soret, A. (2018). Investigating the effects of Pacific sea surface temperatures on the wind drought of 2015 over the United States. *Journal of Geophysical Research: Atmospheres*, 123(10):4837–4849, doi: 10.1029/2017jd028019.

Lledó, L., Cionni, I., Torralba, V., Bretonnière, P.-A., and Samsó, M. (2020). Seasonal prediction of Euro-Atlantic teleconnections from multiple systems. *Environmental Research Letters*, 15(7):74009, doi: 10.1088/1748-9326/ab87d2.

Lledó, L. and Doblas-Reyes, F. J. (2020). Predicting daily mean wind speed in Europe weeks ahead from MJO status. *Monthly Weather Review*, 148(8):3413–3426, doi: 10.1175/mwr-d-19-0328.1.

Lledó, L., Torralba, V., Soret, A., Ramon, J., and Doblas-Reyes, F. (2019). Seasonal forecasts of wind power generation. *Renewable Energy*, 143:91–100, doi: 10.1016/j.renene.2019.04.135.

Makkonen, L. (1998). Modeling power line icing in freezing precipitation. *Atmospheric Research*, 46(1-2):131–142, doi: 10.1016/s0169-8095(97)00056-2.

Makkonen, L., Laakso, T., Marjaniemi, M., and Finstad, K. J. (2001). Modelling and prevention of ice accretion on wind turbines. *Wind Engineering*, 25(1):3–21, doi: 10.1260/0309524011495791.

Manzanas, R., Gutiérrez, J. M., Bhend, J., Hemri, S., Doblas-Reyes, F. J., Torralba, V., Penabad, E., and Brookshaw, A. (2019). Bias adjustment and ensemble recalibration methods for seasonal forecasting: a comprehensive intercomparison using the C3S dataset. *Climate Dynamics*, 53(3-4):1287–1305, doi: 10.1007/s00382-019-04640-4.

Mariotti, A., Ruti, P. M., and Rixen, M. (2018). Progress in subseasonal to seasonal prediction through a joint weather and climate community effort. *npj Climate and Atmospheric Science*, 1(1), doi: 10.1038/s41612-018-0014-z.

Mason, S. (2018). Guidance on verification of operational seasonal climate forecasts. WMO-No. 1220, WMO, ISBN: 978-92-63-11220-0.

Meehl, G. A., Goddard, L., Murphy, J., Stouffer, R. J., Boer, G., Danabasoglu, G., Dixon, K., Giorgetta, M. A., Greene, A. M., Hawkins, E., Hegerl, G., Karoly, D., Keenlyside, N., Kimoto, M., Kirtman, B., Navarra, A., Pulwarty, R., Smith, D., Stammer, D., and Stockdale, T. (2009). Decadal prediction. *Bulletin of the American Meteorological Society*, 90(10):1467–1486, doi: 10.1175/2009bams2778.1.

Merryfield, W. J., Baehr, J., Batté, L., Becker, E. J., Butler, A. H., Coelho, C. A. S., Danabasoglu, G., Dirmeyer, P. A., Doblas-Reyes, F. J., Domeisen, D. I. V., Ferranti, L., Ilynia, T., Kumar, A., Müller, W. A., Rixen, M., Robertson, A. W., Smith, D. M., Takaya, Y., Tuma, M., Vitart, F., White, C. J., Alvarez, M. S., Ardilouze, C., Attard, H., Baggett, C., Balmaseda, M. A., Beraki, A. F., Bhattacharjee, P. S., Bilbao, R., de Andrade, F. M., DeFlorio, M. J., Díaz, L. B., Ehsan, M. A., Fragkoulidis, G., Grainger, S., Green, B. W., Hell, M. C., Infanti, J. M., Isensee, K., Kataoka, T., Kirtman,

B. P., Klingaman, N. P., Lee, J.-Y., Mayer, K., McKay, R., Mecking, J. V., Miller, D. E., Neddermann, N., Ng, C. H. J., Ossó, A., Pankatz, K., Peatman, S., Pegion, K., Perlwitz, J., Recalde-Coronel, G. C., Reintges, A., Renkl, C., Solaraju-Murali, B., Spring, A., Stan, C., Sun, Y. Q., Tozer, C. R., Vigaud, N., Woolnough, S., and Yeager, S. (2020). Current and emerging developments in subseasonal to decadal prediction. *Bulletin of the American Meteorological Society*, doi: 10.1175/bams-d-19-0037.1.

Navarro, J. C. A., Ortega, P., García-Serrano, J., Guemas, V., Tourigny, E., Cruz-García, R., Massonnet, F., and Doblas-Reyes, F. J. (2019). December 2016: Linking the lowest arctic sea-ice extent on record with the lowest European precipitation event on record. *Bulletin of the American Meteorological Society*, 100(1):S43–S48, doi: 10.1175/bams-d-18-0097.1.

Peña, A., Floors, R., Sathe, A., Gryning, S.-E., Wagner, R., Courtney, M. S., Larsén, X. G., Hahmann, A. N., and Hasager, C. B. (2015). Ten years of boundary-layer and wind-power meteorology at Høvsøre, Denmark. *Boundary-Layer Meteorology*, 158(1):1–26, doi: 10.1007/s10546-015-0079-8.

Prodhomme, C., Doblas-Reyes, F., Bellprat, O., and Dutra, E. (2015). Impact of land-surface initialization on sub-seasonal to seasonal forecasts over Europe. *Climate Dynamics*, 47(3-4):919–935, doi: 10.1007/s00382-015-2879-4.

Ramon, J., Lledó, L., Pérez-Zanón, N., Soret, A., and Doblas-Reyes, F. J. (2020). The tall tower dataset: a unique initiative to boost wind energy research. *Earth System Science Data*, 12(1):429–439, doi: 10.5194/essd-12-429-2020.

Ramon, J., Lledó, L., Torralba, V., Soret, A., and Doblas-Reyes, F. J. (2019). What global reanalysis best represents near-surface winds? *Quarterly Journal of the Royal Meteorological Society*, 145(724):3236–3251, doi: 10.1002/qj.3616.

Richter, P. H. and Scholz, H.-J. (1984). Chaos in classical mechanics: The double pendulum. In *Stochastic Phenomena and Chaotic Behaviour in Complex Systems*, pages 86–97. Springer Berlin Heidelberg, doi: 10.1007/978-3-642-69591-9_9.

Schwitalla, T., Warrach-Sagi, K., Wulfmeyer, V., and Resch, M. (2020). Near-global-scale high-resolution seasonal simulations with WRF-noah-MP v.3.8.1. *Geoscientific Model Development*, 13(4):1959–1974, doi: 10.5194/gmd-13-1959-2020.

Smith, D. M., Eade, R., Scaife, A. A., Caron, L.-P., Danabasoglu, G., DelSole, T. M., Delworth, T., Doblas-Reyes, F. J., Dunstone, N. J., Hermanson, L., Kharin, V., Kimoto, M., Merryfield, W. J., Mochizuki, T., Müller, W. A., Pohlmann, H., Yeager, S., and Yang, X. (2019). Robust skill of decadal climate predictions. *npj Climate and Atmospheric Science*, 2(1), doi: 10.1038/s41612-019-0071-y.

Son, C. and Kim, T. (2020). Development of an icing simulation code for rotating wind turbines. *Journal of Wind Engineering and Industrial Aerodynamics*, 203:104239, doi: 10.1016/j.jweia.2020.104239.

Stan, C., Straus, D. M., Frederiksen, J. S., Lin, H., Maloney, E. D., and Schumacher, C. (2017). Review of tropical-extratropical teleconnections on intraseasonal time scales. *Reviews of Geophysics*, 55(4):902–937, doi: 10.1002/2016rg000538.

Terrado, M., Lledó, L., Bojovic, D., Clair, A. L. S., Soret, A., Doblas-Reyes, F. J., Manzanas, R., San-Martín, D., and Christel, I. (2019). The weather roulette: A game to communicate the usefulness of probabilistic climate predictions. *Bulletin of the American Meteorological Society*, 100(10):1909–1921, doi: 10.1175/bams-d-18-0214.1.

Tobin, I., Jerez, S., Vautard, R., Thais, F., van Meijgaard, E., Prein, A., Déqué, M., Kotlarski, S., Maule, C. F., Nikulin, G., Noël, T., and Teichmann, C. (2016). Climate change impacts on the power generation potential of a European mid-century wind farms scenario. *Environmental Research Letters*, 11(3):034013, doi: 10.1088/1748-9326/11/3/034013.

Torralba, V., Doblas-Reyes, F. J., MacLeod, D., Christel, I., and Davis, M. (2017). Sea-

sonal climate prediction: A new source of information for the management of wind energy resources. *Journal of Applied Meteorology and Climatology*, 56(5):1231–1247, doi: 10.1175/jamc-d-16-0204.1.

Valor, E., Meneu, V., and Caselles, V. (2001). Daily air temperature and electricity load in Spain. *Journal of Applied Meteorology*, 40(8):1413–1421, doi: 10.1175/1520-0450(2001)040<1413:dtael>2.0.co;2.

van Vliet, M. T. H., Wiberg, D., Leduc, S., and Riahi, K. (2016). Power-generation system vulnerability and adaptation to changes in climate and water resources. *Nature Climate Change*, 6(4):375–380, doi: 10.1038/nclimate2903.

Yang, W., Foster, K., Lledó, L., Torralba, V., Cortesi, N., Schaller, N., Cionni, I., De Felice, M., Brayshaw, D., and Bloomfield, H. (2020). Modes of variability in Europe and their impact on energy indicators. Deliverable 3.2, 2nd version, S2S4E project, https://s2s4e.eu/sites/default/files/2020-06/s2s4e_d32.pdf.

Yirtici, O., Tuncer, I. H., and Ozgen, S. (2016). Ice accretion prediction on wind turbines and consequent power losses. *Journal of Physics: Conference Series*, 753:022022, doi: 10.1088/1742-6596/753/2/022022.

Zeng, Z., Ziegler, A. D., Searchinger, T., Yang, L., Chen, A., Ju, K., Piao, S., Li, L. Z. X., Ciais, P., Chen, D., Liu, J., Azorin-Molina, C., Chappell, A., Medvigy, D., and Wood, E. F. (2019). A reversal in global terrestrial stilling and its implications for wind energy production. *Nature Climate Change*, 9(12):979–985, doi: 10.1038/s41558-019-0622-6.